



**Comparison of Various Titanium Dioxide for the Photocatalytic  
Degradation of Dyes**

**Miki Kanna**

**A Thesis Submitted in Fulfillment of the Requirements  
for the Degree of Doctor of Philosophy in Chemistry**

**Prince of Songkla University**

**2008**

**Copyright of Prince of Songkla University**

**Thesis Title**            Comparison of Various Titanium Dioxide for the Photocatalytic  
   Degradation of Dyes  
**Author**                    Miss Miki Kanna  
**Major Program**        Chemistry

---

**Major Advisor**

.....  
(Assoc. Prof. Dr. Sumpun Wongnawa)

**Co-advisors**

.....  
(Asst. Prof. Dr. Chaveng Pakawatchai)

.....  
(Asst. Prof. Dr. Orawan Sirichote)

**Examining Committee :**

.....Chairperson  
(Assoc. Prof. Dr. Lek Sikong)

.....Committee  
(Assoc. Prof. Dr. Sumpun Wongnawa)

.....Committee  
(Asst. Prof. Dr. Chaveng Pakawatchai)

.....Committee  
(Assoc. Prof. Dr. Supasarote Muensit)

.....Committee  
(Dr. Anob Kantacha)

The Graduate School, Prince of Songkla University, has approved this thesis as fulfillment of the requirements for the Doctor of Philosophy Degree in Chemistry

.....  
(Assoc. Prof. Dr. Krerchai Thongnoo)  
Dean of Graduate School

ชื่อวิทยานิพนธ์	การศึกษาเปรียบเทียบไทเทเนียมไดออกไซด์ชนิดต่าง ๆ ในการสลาย สีข้อมด้วยปฏิกิริยาโฟโตคะตะไลติก
ผู้เขียน	นางสาวมิกิ กัณณะ
สาขาวิชา	เคมี
ปีการศึกษา	2551

### บทคัดย่อ

การเตรียมไทเทเนียมไดออกไซด์ (TiO<sub>2</sub>) ในงานนี้มี 2 วิธี วิธีแรกเป็นการเตรียมผงไทเทเนียมไดออกไซด์โดยปราศจากการเผาที่มีปริมาณผสมของไทเทเนียมไดออกไซด์อสังขฐานอนาเทส และ รูไทล์ ต่างกัน ด้วยกระบวนการโซล-เจล โดยใช้กรดเป็นคะตะลิสต์ ศึกษาสมบัติทางกายภาพและทางเคมีของไทเทเนียมไดออกไซด์ที่เตรียมได้โดยใช้เทคนิค XRD, SEM, Brunauer-Emmett-Teller (BET), Fourier-transformed infrared (FT-IR), X-ray energy-dispersive (EDX) และ UV-Vis พบว่าเมื่อเตรียมโดยไม่เติมกรดและเมื่อเติมกรดไฮโดรคลอริก กรดไนตริกและกรดอะซิติกปริมาณเล็กน้อยเป็นคะตะลิสต์ จะได้ไทเทเนียมไดออกไซด์อสังขฐานที่มีผลึกแบบอนาเทสและรูไทล์ปนอยู่ด้วย ในขณะที่เมื่อใช้กรดซัลฟิวริกหรือฟอสฟอริกเป็นคะตะลิสต์ จะได้ไทเทเนียมไดออกไซด์อสังขฐานที่มีผลึกแบบอนาเทสปนอยู่เล็กน้อย รวมทั้งมีการเสนอกลไกอธิบายการเกิดผลึกไทเทเนียมไดออกไซด์ขนาดนาโนจากหน่วยพื้นฐานของไทเทเนียมไดออกไซด์ด้วย นอกจากนี้ยังได้ศึกษาความสามารถในการเป็นโฟโตคะตะลิสต์ของไทเทเนียมไดออกไซด์ที่เตรียมได้โดยใช้สลายสีข้อม 3 ชนิด คือ เมทิลีนบลู คริสตัลไวโอเลต และคองโกเรด และเปรียบเทียบกับ Degussa P25 ซึ่งเป็นไทเทเนียมไดออกไซด์ที่นิยมใช้เป็นโฟโตคะตะลิสต์ พบว่าไทเทเนียมไดออกไซด์ที่เตรียมขึ้นสามารถสลายสีข้อมได้ นอกจากนี้ไทเทเนียมไดออกไซด์ที่สังเคราะห์ขึ้นบางตัวก็ให้ผลดีใกล้เคียง กับ Degussa P25

วิธีที่สองเป็นการเตรียมสาร titanium amino-alkoxide เพื่อใช้เป็นสารตั้งต้นสำหรับการเตรียมไทเทเนียมไดออกไซด์แบบฟิล์มและอนุภาคระดับนาโน ปฏิกิริยาที่ใช้ในการเตรียม titanium amino-alkoxide หรือ [Ti(OR)<sub>4-n</sub>(L)<sub>n</sub>] โดย R= Et, Pr<sup>i</sup> และ L = bdmmap, tdmmap คือปฏิกิริยาระหว่าง HOCH(CH<sub>2</sub>NMe<sub>2</sub>)<sub>2</sub> (Hbdmap) และ HOC(CH<sub>2</sub>NMe<sub>2</sub>)<sub>3</sub> (Htdmap) กับ [Ti(OR)<sub>4</sub>] ได้สารใหม่ คือ [Ti(OEt)<sub>3</sub>(bdmap)]<sub>2</sub> โดยนำมาใช้เป็นสารตั้งต้นสำหรับเตรียมฟิล์ม ด้วยวิธี AACVD (Aerosol-Assisted Chemical Vapour Deposition) ที่อุณหภูมิ 440 องศาเซลเซียส ได้ฟิล์ม

ไทเทเนียมไดออกไซด์อสัณฐานเคลือบบนแก้ว และการเตรียมอนุภาคระดับนาโน โดยการให้ความร้อนในภาชนะที่ปิดสนิท ที่อุณหภูมิ 700 องศาเซลเซียส พบว่าได้อนุภาคระดับนาโนของ  $\text{TiO}_2@C$  ซึ่งมีเส้นผ่าศูนย์กลางประมาณ 350 นาโนเมตร ส่วนคาร์บอนที่เคลือบมีความหนาประมาณ 75 นาโนเมตร

<b>Thesis Title</b>	Comparison of Various Titanium Dioxide for the Photocatalytic Degradation of Dyes
<b>Author</b>	Miss Miki Kanna
<b>Major Program</b>	Chemistry
<b>Academic Year</b>	2008

### ABSTRACT

Titanium dioxide ( $\text{TiO}_2$ ) has been prepared by 2 methods. The first method is a preparation of mixing various amorphous-anatase-rutile contents  $\text{TiO}_2$  powders by acid-catalyzed sol-gel method at  $80^\circ\text{C}$  without calcinations. The physico-chemical properties of the powders were investigated by powder XRD, SEM, Brunauer-Emmett-Teller (BET), Fourier-transformed infrared (FT-IR), X-ray energy-dispersive (EDX), and UV-vis techniques. The results showed that the products were mixtures of mainly amorphous  $\text{TiO}_2$  with small amount of anatase and rutile phases when prepared by without using acid catalyst and by adding small amount of acid catalyst (hydrochloric acid, nitric acid, and acetic acid). However, when either sulfuric acid or phosphoric acid was used the products obtained were mainly amorphous  $\text{TiO}_2$  with small amount of anatase. Mechanism of growth from basic units to nanocrystalline was also proposed. Three dyes, methylene blue, crystal violet, and congo red were used in the photocatalytic studies. Positive photocatalytic activities of these products were found and some could be compared favorably with degussa P25.

The second method is a preparation of  $\text{TiO}_2$  films and nanoparticles by using a new precursor, titanium amino-alkoxides. Reaction of the  $\text{HOCH}(\text{CH}_2\text{NMe}_2)_2$  (Hbdmap) and  $\text{HOC}(\text{CH}_2\text{NMe}_2)_3$  (Htdmap) with  $[\text{Ti}(\text{OR})_4]$  yields a series of  $[\text{Ti}(\text{OR})_{4-n}(\text{L})_n]$  ( $\text{R} = \text{Et}, \text{Pr}^i$ ;  $\text{L} = \text{bdmap}, \text{tdmap}$ ) was studied. New compound:  $[\text{Ti}(\text{OEt})_3(\text{bdmap})]_2$  has been used as a precursor in AACVD (Aerosol-Assisted Chemical Vapour Deposition) to generate amorphous  $\text{TiO}_2$  films on glass at  $440^\circ\text{C}$ , and  $\text{TiO}_2@\text{C}$  nanoparticles of approximate diameter 350 nm with a carbon coating of width *ca.* 75 nm on heating in a sealed container at  $700^\circ\text{C}$ .

## ACKNOWLEDGEMENTS

I am greatly indebted to my advisor, Assoc. Prof. Dr. Sumpun Wongnawa who suggested this research problem, for his numerous suggestions, encouragement and criticism without which I would have been unable to complete this work.

I wish also to express my thanks to my co-advisors, Asst. Prof. Dr. Chaveng Pakawatchai and Asst. Prof. Dr. Orawan Sirichote, for their advice and assistance. I am also grateful to Assoc. Prof. Dr. Lek Sikong, Assoc. Prof. Dr. Supasarote Muensit, and Dr. Anob Kantacha, the examining committee for their kind comments and correction to the report.

Sincere thanks go to Prof. Kieran C. Molloy (Department of Chemistry, University of Bath, UK) for his valuable guidance, suggestion and understanding which kept me going while so far away from home.

Thanks are also due to all members of the academic and technical staff of both Prince of Songkla University and University of Bath who have helped me in various ways throughout this research.

For the financial supports I wish to thank the Thailand Research Fund through the Royal Golden Jubilee Ph.D. Program (Grant No.PHD/0126/2546), the Center for Innovation in Chemistry: Postgraduate Education and Research Program in Chemistry (PERCH-CIC), Commission on Higher Education, Ministry of Education, and the Graduate School-PSU through the Thesis Research Fund.

My acknowledgements are extended to all of my collaborators who helped create an enjoyable atmosphere to be working in and for their many helpful in many countless ways throughout the years.

And last but not least, I am profoundly grateful to my parents and my sister for their love and support which have made this all possible.

Miki Kanna

## **THE RELEVANCE OF THE RESEARCH WORK TO THAILAND**

Treatment of colored wastewater from textile or dye industry is a serious problem that attracts the attention of many researchers. A certain amount of dyestuff is lost during the process in the textile industry which causes environmental problems. Heterogeneous photocatalysis has attracted much attention due to its potential applications in air clean-up and water purification.  $\text{TiO}_2$  is generally used a photocatalyst for environmental application due to chemical stability, strong oxidizing power, nontoxicity, and inexpensive. However, many researchers have focused on the synthesis of  $\text{TiO}_2$  by annealing to improve its photocatalytic activity and its applicability to wastewater treatment. The purpose of this work is to study a method to prepare the  $\text{TiO}_2$  powder without calcinations at high temperature. The photocatalyst of powder could be used to degrade methylene blue, crystal violet, and congo red, a model dye compound, in wastewater. We deem that this work could be used in Thailand as a cheaper material for the destruction of dye pollutants in the textile industries before releasing wastewater into the natural system.

# CONTENTS

	<b>Page</b>
บทคัดย่อ	iii
ABSTRACT	v
ACKNOWLEDGEMENTS	vi
THE RELEVANCE OF THE RESEARCH WORK TO THAILAND	vii
CONTENTS	viii
LIST OF TABLES	x
LIST OF ILLUSTRATIONS	xi
LIST OF SCHEMES	xviii
ABBREVIATIONS AND SYMBOLS	xix
CHAPTER 1 INTRODUCTION	1
1.1 Introduction	1
1.2 Review of literatures	2
1.2.1 Titanium dioxide	2
1.2.2 Dye and treatment of dye pollutant	12
1.3 Objectives	21
CHAPTER 2 EXPERIMENTAL	22
2.1 Synthesis of nanocrystalline TiO <sub>2</sub> powders	22
2.1.1 Materials	22
2.1.2 Method	23
2.1.3 Photocatalytic study	26
2.2 Synthesis of titanium amino-alkoxides: precursors for the formation of TiO <sub>2</sub> materials	29
2.2.1 Materials	29
2.2.2 General procedures	30
2.2.3 Syntheses	30
2.2.4 Thermal decomposition [Ti(OEt) <sub>3</sub> (bdmap)] <sub>2</sub>	33



## CONTENTS (Continued)

	<b>Page</b>
2.2.5 CVD study	34
2.2.6 Photocatalytic study	34
CHAPTER 3 RESULTS AND DISCUSSION	36
3.1 Synthesis of nanocrystalline TiO <sub>2</sub> powders	36
3.1.1 Physical properties of the synthesized TiO <sub>2</sub> powders	36
3.1.2 The possible mechanism for anatase and rutile TiO <sub>2</sub> formation	49
3.1.3 Photocatalytic study	53
3.2 Synthesis of titanium amino-alkoxides: precursors for the formation of TiO <sub>2</sub> materials	99
3.2.1 Synthesis	99
3.2.2 Crystallography	102
3.2.3 Thermal decomposition of [Ti(OEt) <sub>3</sub> (bdmap)] <sub>2</sub>	108
3.2.4 Photocatalytic study	114
REFERENCES	119
APPENDICES	136
VITAE	184

## LIST OF TABLES

Table		Page
1	Some bulk properties of the three main polymorphs of titanium dioxide (Carp, <i>et al.</i> , 2004).	4
2	Characteristic of dyes	16
3	Comparison of TiO <sub>2</sub> powders prepared under various acid catalyzed conditions.	36
4	Assignment of the FT-IR bands of titanium dioxide samples (Figure 15)	41
5	Specific surface area of TiO <sub>2</sub> powders.	42
6	The absorption edges and band gap energies of titanium dioxide powders.	48
7	Selected bond lengths [ $\text{\AA}$ ] and angles [ $^{\circ}$ ] for $[\text{Ti}(\text{OEt})_3(\text{bdmap})]_2$ .	104
8	Selected bond lengths [ $\text{\AA}$ ] and angles [ $^{\circ}$ ] for $[(\text{bdmap})\text{TiO}]_2$ .	106
9	Crystallographic data for $\text{Ti}(\text{OEt})_3(\text{bdmap})$ and $[(\text{bdmap})_2\text{TiO}]_2$	107

## LIST OF ILLUSTRATIONS

<b>Figure</b>		<b>Page</b>
1	Crystal structures of anatase (a), rutile (b), and brookite (c).	3
2	TiO <sub>2</sub> pigment manufactured by the sulfate process (Büchner, <i>et al.</i> , 1989: 526).	6
3	TiO <sub>2</sub> pigment manufactured by the chloride process (Büchner, <i>et al.</i> , 1989: 528).	6
4	An overview of products prepared by sol-gel methods.	8
5	Illustration showing the elementary processes involved in the CVD of a metal-organic molecule (adapted from <a href="http://www.chemsoc.org/chembytes/ezone/images/2002/ashton_jun02.htm">www.chemsoc.org/chembytes/ezone/images/2002/ashton_jun02.htm</a> ).	10
6	Structures of <b>I</b> : Hbdmap (bis-(dimethylamino)propanol) and <b>II</b> : Htdmap (tris-(dimethylamino)propanol).	12
7	Structure of Methylene blue (a), Congo red (b), and Crystal violet (c).	16
8	Schematic representation of the semiconductor showing the electron/hole pair formed in the conduction band and the valence band, respectively.	18
9	Flow chart of the synthesis of titanium dioxide powders	25
10	The wooden compartment for photocatalytic experiment (a) outer and (b) inner.	27
11	An overview of the Swagelok used for thermal decomposition.	33
12	XRD patterns of the synthesized TiO <sub>2</sub> powders (a) Ti-no-acid, (b) Ti-HCl, (c) Ti-HNO <sub>3</sub> , (d) Ti-H <sub>2</sub> SO <sub>4</sub> , (e) Ti-CH <sub>3</sub> COOH, and (f) Ti-H <sub>3</sub> PO <sub>4</sub> . A denotes anatase and R denotes rutile	37
13	The standard addition calibration graphs of Ti-no-acid, Ti-HCl, Ti-HNO <sub>3</sub> , and Ti-CH <sub>3</sub> COOH.	38
14	The standard addition calibration graphs of Ti-H <sub>2</sub> SO <sub>4</sub> and Ti-H <sub>3</sub> PO <sub>4</sub> .	39
15	FT-IR spectra of the synthesized TiO <sub>2</sub> powders: (a) Ti-no-acid, (b) Ti-HCl, (c) Ti-HNO <sub>3</sub> , (d) Ti-H <sub>2</sub> SO <sub>4</sub> , (e) Ti-CH <sub>3</sub> COOH, and (f) Ti-H <sub>3</sub> PO <sub>4</sub> .	40

## LIST OF ILLUSTRATIONS (Continued)

<b>Figure</b>		<b>Page</b>
16	SEM images of the synthesized TiO <sub>2</sub> powders: (a) Ti-no-acid, (b) Ti-HCl, (c) Ti-HNO <sub>3</sub> , (d) Ti-H <sub>2</sub> SO <sub>4</sub> , (e) Ti-CH <sub>3</sub> COOH, and (f) Ti-H <sub>3</sub> PO <sub>4</sub> .	43
17	SEM images of TiO <sub>2</sub> reported by Yu, <i>et al.</i> , (2003).	44
18	EDX spectra of the synthesized TiO <sub>2</sub> powders: (a) Ti-no-acid, Ti-HCl, Ti-HNO <sub>3</sub> , Ti-CH <sub>3</sub> COOH, (b) Ti-H <sub>2</sub> SO <sub>4</sub> , and (c) Ti-H <sub>3</sub> PO <sub>4</sub> .	45
19	Diffuse reflectance UV-Vis spectra of the synthesized TiO <sub>2</sub> powders: (a) Ti-no-acid, (b) Ti-HCl, (c) Ti-HNO <sub>3</sub> , (d) Ti-H <sub>2</sub> SO <sub>4</sub> , (e) Ti-CH <sub>3</sub> COOH, and (f) Ti-H <sub>3</sub> PO <sub>4</sub> .	47
20	Diffuse reflectance UV-Vis spectra of the commercial TiO <sub>2</sub> powders.	48
21	Formation of growth units from <i>cis</i> -[Ti(OH) <sub>2</sub> (H <sub>2</sub> O) <sub>4</sub> ] <sup>2+</sup> ion.	51
22	Bonding mode of SO <sub>4</sub> <sup>2-</sup> anion as, (A) monodentate, (B) bidentate, and (C) tridentate ligand (● indicates OH position).	52
23	Possible pathway to inhibit the formation of rutile by SO <sub>4</sub> <sup>2-</sup> .	52
24	Spectrum of UV-light source used in this work (Random, <i>et al.</i> , 2004).	54
25	Pathway of dye degradation by TiO <sub>2</sub> .	54
26	Decolorization of MB solution at 1×10 <sup>-5</sup> M as a function of time in the presence of synthesized TiO <sub>2</sub> : (a) Ti-no-acid, (b) Ti-HCl, (c) Ti-HNO <sub>3</sub> , (d) Ti-H <sub>2</sub> SO <sub>4</sub> , (e) Ti-CH <sub>3</sub> COOH, and (f) Ti-H <sub>3</sub> PO <sub>4</sub> .	55
27	Decolorization of MB solution at 1×10 <sup>-5</sup> M as a function of time in the presence of commercial TiO <sub>2</sub> : (a) Degussa P25, (b) anatase (Carlo Erba), and (c) rutile (R706, TOA).	56
28	Decolorization of CR solution at 1×10 <sup>-5</sup> M as a function of time in the presence of synthesized TiO <sub>2</sub> : (a) Ti-no-acid, (b) Ti-HCl, (c) Ti-HNO <sub>3</sub> , (d) Ti-H <sub>2</sub> SO <sub>4</sub> , (e) Ti-CH <sub>3</sub> COOH, and (f) Ti-H <sub>3</sub> PO <sub>4</sub> .	57

## LIST OF ILLUSTRATIONS (Continued)

Figure		Page
29	Decolorization of CR solution at $1 \times 10^{-5}$ M as a function of time in the presence of commercial TiO <sub>2</sub> : (a) Degussa P25, (b) anatase (Carlo Erba), and (c) rutile (R706, TOA).	58
30	Decolorization of CV solution at $1 \times 10^{-5}$ M as a function of time in the presence of synthesized TiO <sub>2</sub> : (a) Ti-no-acid, (b) Ti-HCl, (c) Ti-HNO <sub>3</sub> , (d) Ti-H <sub>2</sub> SO <sub>4</sub> , (e) Ti-CH <sub>3</sub> COOH, and (f) Ti-H <sub>3</sub> PO <sub>4</sub> .	59
31	Decolorization of CV solution at $1 \times 10^{-5}$ M as a function of time in the presence of commercial TiO <sub>2</sub> : (a) Degussa P25, (b) anatase (Carlo Erba), and (c) rutile (R706, TOA).	60
32	Effect of the initial concentration of MB solution as a function of time in the presence of synthesized TiO <sub>2</sub> : (a) Ti-no-acid, (b) Ti-HCl, (c) Ti-HNO <sub>3</sub> , (d) Ti-H <sub>2</sub> SO <sub>4</sub> , (e) Ti-CH <sub>3</sub> COOH, and (f) Ti-H <sub>3</sub> PO <sub>4</sub> .	62
33	Effect of the initial concentration of MB solution as a function of time in the presence of commercial TiO <sub>2</sub> : (a) Degussa P25, (b) anatase (Carlo Erba), and (c) rutile (R706, TOA).	63
34	Effect of the initial concentration of CR solution as a function of time in the presence of synthesized TiO <sub>2</sub> : (a) Ti-no-acid, (b) Ti-HCl, (c) Ti-HNO <sub>3</sub> , (d) Ti-H <sub>2</sub> SO <sub>4</sub> , (e) Ti-CH <sub>3</sub> COOH, and (f) Ti-H <sub>3</sub> PO <sub>4</sub> .	64
35	Effect of the initial concentration of CR solution as a function of time in the presence of commercial TiO <sub>2</sub> : (a) Degussa P25, (b) anatase (Carlo Erba), and (c) rutile (R706, TOA).	65
36	Effect of the initial concentration of CV solution as a function of time in the presence of synthesized TiO <sub>2</sub> : (a) Ti-no-acid, (b) Ti-HCl, (c) Ti-HNO <sub>3</sub> , (d) Ti-H <sub>2</sub> SO <sub>4</sub> , (e) Ti-CH <sub>3</sub> COOH, and (f) Ti-H <sub>3</sub> PO <sub>4</sub> .	66
37	Effect of the initial concentration of CV solution as a function of time in the presence of commercial TiO <sub>2</sub> : (a) Degussa P25, (b) anatase (Carlo Erba), and (c) rutile (R706, TOA).	67

## LIST OF ILLUSTRATIONS (Continued)

Figure		Page
38	Decolorization of MB solution ( $2.5 \times 10^{-5}$ M) with (a) Ti-no acid, (b) Ti-HCl, (c) Ti-HNO <sub>3</sub> , (d) Ti-H <sub>2</sub> SO <sub>4</sub> , (e) Ti-CH <sub>3</sub> COOH, (f) Ti-H <sub>3</sub> PO <sub>4</sub> , (g) Degussa P25, (h) Anatase (Carlo Erba), and (i) Rutile (R706).	70
39	Decolorization of CV solution ( $2.5 \times 10^{-5}$ M) with (a) Ti-no acid, (b) Ti-HCl, (c) Ti-HNO <sub>3</sub> , (d) Ti-H <sub>2</sub> SO <sub>4</sub> , (e) Ti-CH <sub>3</sub> COOH, (f) Ti-H <sub>3</sub> PO <sub>4</sub> , (g) Degussa P25, (h) Anatase (Carlo Erba), and (i) Rutile (R706).	71
40	Decolorization of CR solution ( $2.5 \times 10^{-5}$ M) with (a) Ti-no acid, (b) Ti-HCl, (c) Ti-HNO <sub>3</sub> , (d) Ti-H <sub>2</sub> SO <sub>4</sub> , (e) Ti-CH <sub>3</sub> COOH, (f) Ti-H <sub>3</sub> PO <sub>4</sub> , (g) Degussa P25, (h) Anatase (Carlo Erba), and (i) Rutile (R706).	72
41	Effect of addition of hydrogen peroxide in absence of light on MB degradation as a function of time in the presence of synthesized TiO <sub>2</sub> : (a) Ti-no-acid, (b) Ti-HCl, (c) Ti-HNO <sub>3</sub> , (d) Ti-H <sub>2</sub> SO <sub>4</sub> , (e) Ti-CH <sub>3</sub> COOH, and (f) Ti-H <sub>3</sub> PO <sub>4</sub> .	76
42	Effect of addition of hydrogen peroxide in absence of light on MB degradation as a function of time in the presence of commercial TiO <sub>2</sub> : (a) Degussa P25, (b) Anatase (Carlo Erba), and (c) Rutile (R706, TOA).	77
43	Effect of addition of hydrogen peroxide in absence of light on CR degradation as a function of time in the presence of synthesized TiO <sub>2</sub> : (a) Ti-no-acid, (b) Ti-HCl, (c) Ti-HNO <sub>3</sub> , (d) Ti-H <sub>2</sub> SO <sub>4</sub> , (e) Ti-CH <sub>3</sub> COOH, and (f) Ti-H <sub>3</sub> PO <sub>4</sub> .	78

## LIST OF ILLUSTRATIONS (Continued)

<b>Figure</b>		<b>Page</b>
44	Effect of addition of hydrogen peroxide in absence of light on CR degradation as a function of time in the presence of commercial TiO <sub>2</sub> : (a) Degussa P25, (b) Anatase (Carlo Erba), and (c) Rutile (R706, TOA)	79
45	Effect of addition of hydrogen peroxide in absence of light on CV degradation as a function of time in the presence of synthesized TiO <sub>2</sub> : (a) Ti-no-acid, (b) Ti-HCl, (c) Ti-HNO <sub>3</sub> , (d) Ti-H <sub>2</sub> SO <sub>4</sub> , (e) Ti-CH <sub>3</sub> COOH, and (f) Ti-H <sub>3</sub> PO <sub>4</sub> .	80
46	Effect of addition of hydrogen peroxide in absence of light on CV degradation as a function of time in the presence of commercial TiO <sub>2</sub> : (a) Degussa P25, (b) Anatase (Carlo Erba), and (c) Rutile (R706, TOA).	81
47	Effect of hydrogen peroxide on MB solution ( $1 \times 10^{-5}$ M) as a function on time in the presence of 0.5 g/L synthesized TiO <sub>2</sub> : (a) Ti-no-acid, (b) Ti-HCl, (c) Ti-HNO <sub>3</sub> , (d) Ti-H <sub>2</sub> SO <sub>4</sub> , (e) Ti-CH <sub>3</sub> COOH, and (f) Ti-H <sub>3</sub> PO <sub>4</sub> . (□ denotes + TiO <sub>2</sub> + H <sub>2</sub> O <sub>2</sub> + light, ■ denotes +TiO <sub>2</sub> + H <sub>2</sub> O <sub>2</sub> - light, and ▲ denotes +TiO <sub>2</sub> + light)	86
48	Effect of hydrogen peroxide on MB solution ( $1 \times 10^{-5}$ M) as a function on time in the presence of 0.5 g/L commercial TiO <sub>2</sub> : (a) Degussa P25, (b) Anatase (Carlo Erba), and (c) Rutile (R706, TOA). (□ denotes + TiO <sub>2</sub> + H <sub>2</sub> O <sub>2</sub> + light, ■ denotes +TiO <sub>2</sub> + H <sub>2</sub> O <sub>2</sub> - light, and ▲ denotes +TiO <sub>2</sub> + light)	87
49	Effect of hydrogen peroxide on CR solution ( $1 \times 10^{-5}$ M) as a function on time in the presence of 0.5 g/L synthesized TiO <sub>2</sub> : (a) Ti-no-acid, (b) Ti-HCl, (c) Ti-HNO <sub>3</sub> , (d) Ti-H <sub>2</sub> SO <sub>4</sub> , (e) Ti-CH <sub>3</sub> COOH, and (f) Ti-H <sub>3</sub> PO <sub>4</sub> . (□ denotes + TiO <sub>2</sub> + H <sub>2</sub> O <sub>2</sub> + light, ■ denotes +TiO <sub>2</sub> + H <sub>2</sub> O <sub>2</sub> - light, and ▲ denotes +TiO <sub>2</sub> + light)	88

## LIST OF ILLUSTRATIONS (Continued)

Figure		Page
50	Effect of hydrogen peroxide on CR solution ( $1 \times 10^{-5}$ M) as a function on time in the presence of 0.5 g/L commercial TiO <sub>2</sub> : (a) Degussa P25, (b) Anatase (Carlo Erba), and (c) Rutile (R706, TOA). (□ denotes + TiO <sub>2</sub> + H <sub>2</sub> O <sub>2</sub> + light, ■ denotes +TiO <sub>2</sub> + H <sub>2</sub> O <sub>2</sub> - light, and ▲ denotes +TiO <sub>2</sub> + light)	89
51	Effect of hydrogen peroxide on CV solution ( $1 \times 10^{-5}$ M) as a function on time in the presence of 0.5 g/L synthesized TiO <sub>2</sub> : (a) Ti-no-acid, (b) Ti-HCl, (c) Ti-HNO <sub>3</sub> , (d) Ti-H <sub>2</sub> SO <sub>4</sub> , (e) Ti-CH <sub>3</sub> COOH, and (f) Ti-H <sub>3</sub> PO <sub>4</sub> . (□ denotes + TiO <sub>2</sub> + H <sub>2</sub> O <sub>2</sub> + light, ■ denotes +TiO <sub>2</sub> + H <sub>2</sub> O <sub>2</sub> - light, and ▲ denotes +TiO <sub>2</sub> + light)	90
52	Effect of hydrogen peroxide on CV solution ( $1 \times 10^{-5}$ M) as a function on time in the presence of 0.5 g/L commercial TiO <sub>2</sub> : (a) Degussa P25, (b) Anatase (Carlo Erba), and (c) Rutile (R706, TOA). (□ denotes + TiO <sub>2</sub> + H <sub>2</sub> O <sub>2</sub> + light, ■ denotes +TiO <sub>2</sub> + H <sub>2</sub> O <sub>2</sub> - light, and ▲ denotes +TiO <sub>2</sub> + light)	91
53	The suggested mechanisms for the degradation of congo red initiated by e <sub>aq</sub> <sup>-</sup> (a) and •OH (b) (Mu, <i>et al.</i> , 2007).	97
54	Postulated role of O <sub>2</sub> played in the degradation of aromatic compounds (Mu, <i>et al.</i> , 2007).	98
55	The asymmetric unit of [Ti(OEt) <sub>3</sub> (bdmap)] <sub>2</sub> showing the labelling scheme used; thermal ellipsoids are at the 30% probability level. Only one of two essentially identical molecules which make up the asymmetric unit is shown for clarity and discussed in the text.	103



## LIST OF ILLUSTRATIONS (Continued)

Figure		Page
56	The asymmetric unit of [(bdmap)TiO] <sub>2</sub> showing the labelling scheme used; thermal ellipsoids are at the 30% probability level. The NMe <sub>2</sub> group based on N(4) is disordered over two sites (65:35); only the major component of the disorder is shown for clarity.	105
57	XRD of the powder obtained by RAPET of [Ti(OEt) <sub>3</sub> (bdmap)] <sub>2</sub> at 700°C; indexing is consistent with anatase TiO <sub>2</sub> (PDF 84-1286)	108
58	SEM of the powder obtained by RAPET of [Ti(OEt) <sub>3</sub> (bdmap)] <sub>2</sub> at 700°C. Larger spheres are carbon while the smaller spheres are carbon-coated TiO <sub>2</sub> . Bar = 1 μm.	110
59	EDX of (top) the large elliptical particles (59a) and (bottom) the smaller spherical particle (59b) produced by RAPET of [Ti(OEt) <sub>3</sub> (bdmap)] <sub>2</sub> at 700°C.	111
60	TEM of the small particles obtained by RAPET of [Ti(OEt) <sub>3</sub> (bdmap)] <sub>2</sub> at 700°C showing the dense inner TiO <sub>2</sub> core and amorphous carbon coating. Bar = 100 nm.	112
61	Two views of the film deposited from [Ti(OEt) <sub>3</sub> (bdmap)] <sub>2</sub> by AACVD at 440°C showing (a) film thickness and (b) texture. Bar = 1 μm.	113
62	EDX of the film deposited from [Ti(OEt) <sub>3</sub> (bdmap)] <sub>2</sub> by AACVD at 440°C; gold peaks are due to a sample coating to dissipate charge.	114
63	Decolorization (%) as a function of irradiation time of MB solution (2.5 × 10 <sup>-5</sup> M) when using (a) film and (b) after annealing film at 440, 550 and 600°C.	115
64	Decolorization (%) of MB solution (2.5 × 10 <sup>-5</sup> M) with (a) Nanoparticle and (b) compare with three commercial TiO <sub>2</sub> .	116

## LIST OF SCHEMES

Scheme		Page
1	Tentative pathway to degrade dye by the synthesized TiO <sub>2</sub> with H <sub>2</sub> O <sub>2</sub> in the dark. Ti <sup>4+</sup> <sub>(s)</sub> , Ti <sup>3+</sup> <sub>(s)</sub> , and e <sup>-</sup> <sub>DB</sub> represent metal ions and an electron available from dangling bond, respectively, at the solid surface.	75
2	Schematic diagram of H <sub>2</sub> O <sub>2</sub> adsorption structure on the surface of anatase and rutile TiO <sub>2</sub> (Hirakawa, <i>et al.</i> , 2007).	83
3	Plausible process in the photocatalytic reduction of H <sub>2</sub> O <sub>2</sub> starting from three different adsorption structures (Hirakawa, <i>et al.</i> , 2007).	84
4	Summary for the proposed formation mechanism of •O <sub>2</sub> <sup>-</sup> and •OH on anatase and rutile TiO <sub>2</sub> crystal. (a) without H <sub>2</sub> O <sub>2</sub> and (b) with H <sub>2</sub> O <sub>2</sub> (Hirakawa, <i>et al.</i> , 2007).	85
5	Photocatalytic degradation pathway of methylene blue (Houas, <i>et al.</i> , 2001).	93
6	Electronic reorganization during the passage of methylene blue adsorbed to the sulfoxide form (Houas, <i>et al.</i> , 2001).	94
7	A mechanism for the formation of intermediate products involving electron transfer reactions in the photocatalytic system (Saqib and Muneer, 2003).	95
8	A mechanism for the formation of intermediate products involving reaction with hydroxyl radicals formed in the photocatalytic system (Saqib and Muneer, 2003).	96

## ABBREVIATIONS AND SYMBOLS

s	=	singlet
d	=	doublet
t	=	triplet
m	=	multiplet
br s	=	broad singlet
br	=	broad
eV	=	Electron volt
g	=	Gram
hr	=	Hour
nm	=	Nanometer
min	=	Minute
mL	=	Milliliter
mol/L	=	Mole per liter
ppm	=	Part per million
°C	=	Degree celcius
$\lambda_{\max}$	=	Maximum wavelength
CR	=	Congo red
CV	=	Crystal violet
MB	=	Methylene blue
Hbdmap	=	Bis-(dimethylamino)propanal
Htdmap	=	Tris-(dimethylamino)propanal
OEt	=	Ethoxide
OPr <sup>i</sup>	=	Isopropoxide
CDCl <sub>3</sub>	=	Deuteriochloroform
CVD	=	Chemical vapour deposition
AACVD	=	Aerosol-assisted chemical vapour deposition
TiO <sub>2</sub> @C	=	Core shell structure consists of TiO <sub>2</sub>

## ABBREVIATIONS AND SYMBOLS (Continued)

JCPDS	=	Joint Committee on Powder Diffraction Standards
BET	=	Brunauer-Emmett-Teller
EDX	=	Energy dispersive X-ray
FTIR	=	Fourier transform infrared
SEM	=	Scanning electron microscope
TGA	=	Thermogravimetric analyzer
UV-Vis	=	Ultraviolet-Visible
NMR	=	Nuclear magnetic resonance
XRD	=	X-ray diffraction

# CHAPTER 1

## INTRODUCTION

### 1.1 Introduction

Titanium dioxide ( $\text{TiO}_2$ ) is one of the most important of the ceramic metal oxides with diverse applications ranging from catalysis to material chemistry. Titanium dioxide (or titania) has been widely studied for applications in a variety of problems of environmental interest in addition to water and air purifications. It has considerable advantages over other similar photocatalysts due to its good characteristic in terms of chemical stability, endurance, thin film transparency, and lower production costs (Hoffmann, *et al.*, 1995; Fox and Dulay, 1993). Many researchers have focused on the preparation of various phase of  $\text{TiO}_2$  powder to improve its photocatalytic activity and its applicability to environmental treatment. Good catalytic property is governed by two major opposing physical properties: crystallinity and surface area of the catalysts. The high crystallinity helps prolong the recombination rate of the photoexcited electron and positive hole, hence, strong reducing of oxidizing power of the catalyst. The high surface area helps facilitate adsorption of the target molecules onto the surface of the catalyst; as higher number of molecules are adsorbed the faster the rate of reaction (Ohtani, *et al.*, 1997). Among the two properties, crystallinity and surface area, one has to decide and choose one over the other since both cannot be had simultaneously from the syntheses. It has been reported that the different methods for the syntheses of  $\text{TiO}_2$  result in products with different structures (anatase or rutile), crystallinity, and contaminants. As a consequence, the surface properties of  $\text{TiO}_2$  strongly depend on the preparation techniques (Zhang, *et al.*, 1999; Reddy, *et al.*, 2001). In preparing oxide materials, the sol-gel method can exhibit a number of advantages over conventional methods.

In our earlier work (Random, *et al.*, 2004) we found that the amorphous form, previously thought rather inactive, with small amount of crystalline anatase form also showed photocatalytic properties. This amorphous form could be synthesized by a

simple precipitation method to produce  $\text{TiO}_2$ , however, the subsequent calcination was excluded. Since no calcination was employed, the product powder was mostly present in an amorphous form with some hydrated water molecules. Its surface area was also significantly higher than that of commercially available anatase/rutile or P25 due to its amorphous morphology.

This work focused on the preparation of  $\text{TiO}_2$  powder in various amorphous-anatase-rutile contents by using sol-gel method under different acids as hydrolysis catalysts without annealing at high temperature. Hopefully, this method simplification leads to lower production costs, energy saving and no pollution.

In addition, this work encompasses the synthesis of a titanium amino-alkoxides: precursors for the formation of both  $\text{TiO}_2$  films and nanoparticles.

## **1.2 Review of literatures**

### **1.2.1 Titanium dioxide**

#### **(1) General background**

Titanium dioxide ( $\text{TiO}_2$ ) belongs to the family of transition metal oxides. In the beginning of the 20<sup>th</sup> century, industrial production started with titanium dioxide replacing toxic lead oxides as pigments for white paint. At present, the annual production of  $\text{TiO}_2$  exceeds 4 million tons. It is used as a white pigment in paints (51% of total production), plastic (19%), and paper (17%), which represent the major end-use sectors of  $\text{TiO}_2$ . The consumption of  $\text{TiO}_2$  as a pigment increased in the last few years in a number of minor end-use sectors such as textiles, food (it is approved in food-contact applications and as food coloring) under a EU legislation on the safety of the food additives, leather, pharmaceuticals (tablet coatings, toothpastes, and as a UV absorber in sunscreen cream with high sun protection factors and other cosmetic products), and various titanate pigments (mixed oxides such as  $\text{ZnTiO}_3$ ,  $\text{ZrTiO}_4$ , *etc.*) (Carp, *et al.*, 2004)

## (2) Crystal structures and properties

Titanium dioxide exists naturally in three distinct crystallographic modifications, namely, anatase, rutile, and brookite (Figure 1). The structures of rutile, anatase and brookite can be discussed in terms of  $(\text{TiO}_6^{2-})$  octahedrals. The three crystal structures differ by the distortion of each octahedral and by the assembly patterns of the octahedral chains. Anatase can be regarded to be built up from octahedrals that are connected by their vertices, in rutile the edges are connected, and in brookite both vertices and edges are connected. Some of the most important bulk properties of  $\text{TiO}_2$  are given in Table 1.

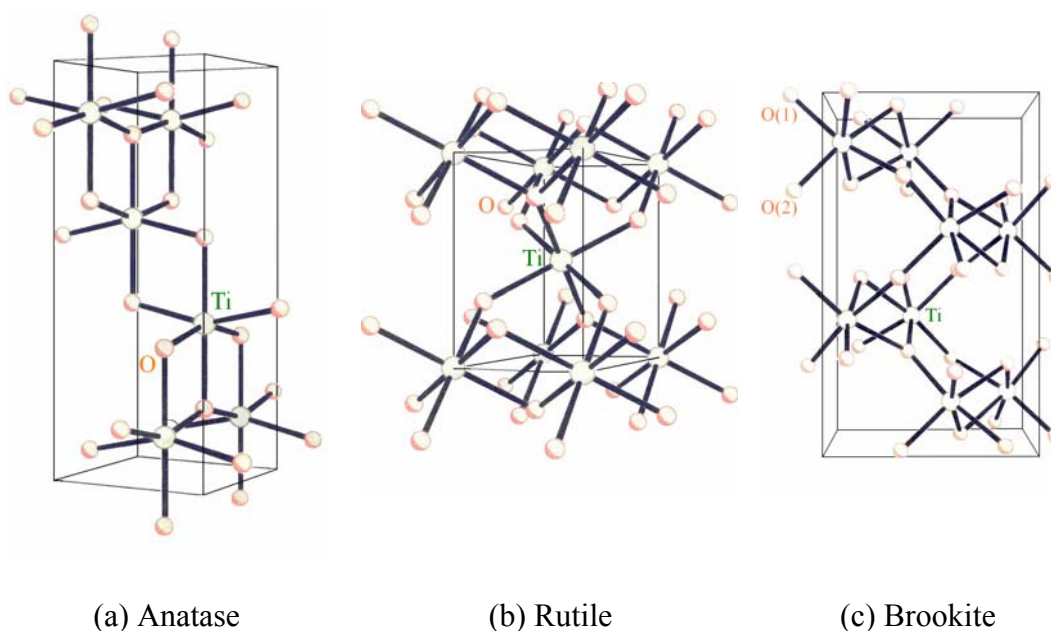


**Figure 1.** Crystal structures of anatase (a), rutile (b), and brookite (c).

Titania is widely used as a white pigment for paint, coating ink, paper, plastic, cosmetic products, catalyst supports, photoconductors, dielectric materials and so on because of its whiteness, outstanding hiding property and non-toxicity. The brookite form cannot be used in industries because of its instability at room temperature. The anatase form has the problems of poor light and heat resistance and of gradually decreasing whiteness due to weathering. The anatase form also has drawbacks for applications involving adsorption technology owing to its low

surface energy. The rutile form has outdoor applicability because of its good light resistance and can be applied to surfaces by the use of adsorption technology without advanced skills or sophisticated equipment (Hadjiivanov and Klissurski, 1996; Wang, *et al.*, 2001; Yanqing, *et al.*, 2001).

**Table 1.** Some bulk properties of the three main polymorphs of titanium dioxide. (Carp, *et al.*, 2004)

Crystal structure	System	Point group- Space group	Lattice constants (nm)			
			a	b	c	c/a
Rutile	Tetragonal	$D_{4h}^{14} - P_4/mmm$	0.4584	-	0.2953	0.644
Anatase	Tetragonal	$D_{4h}^{19} - I_4_1/amd$	0.3733	-	0.937	2.51
Brookite	Orthorhombic	$D_{2h}^{15} - Pbca$	0.5456	0.9182	0.5143	0.943
Density (kg/m <sup>3</sup> )						
Rutile	4240					
Anatase	3830					
Brookite	4170					
Melting Point (°C)						
Rutile	1840±10					
Anatase	Change to rutile					
Brookite	Change to rutile					
Dielectric properties						
	Frequency (Hz)	Temperature (K)	Dielectric constant			
Rutile, perpendicular to optical c-axis	10 <sup>8</sup>	290-295	86			
Rutile, parallel to optical c-axis	-	290-295	170			
Rutile, along c-axis	10 <sup>7</sup>	303	100			
Anatase, average	10 <sup>4</sup>	298	55			
Refractive index						
	n <sub>g</sub>	n <sub>p</sub>				
Rutile	2.9467	2.6506				
Anatase	2.5688	2.6584				
Brookite	2.809	2.677				



### (3) Synthesis of titanium dioxide

Titanium dioxide can be prepared in the form of powder, crystal, or thin film. Both powder and film can be built up from crystallites ranging from a few nanometers to several micrometers (Carp, *et al.*, 2004).

Generally, TiO<sub>2</sub> may be manufactured by either the sulfate process or the chloride process. The economics of the two processes are very much dependent upon the raw material available. The starting materials for titanium dioxide production are ilmenite and titaniferous slag in the case of the sulfate process and leucoxene, rutile, synthetic rutile, and in the future possibly also anatase for the chloride process (Büchner, *et al.*, 1989).

In sulfate process (Figure 2), ilmenite dissolved in sulfuric acid is hydrolyzed at temperatures higher than 95°C, then calcined at 800-1000°C and pulverized to produce the TiO<sub>2</sub> powder. During this calcination and pulverization process, impurities are introduced which lead to the low quality of the final TiO<sub>2</sub> powder (Nam, *et al.*, 1998; Wang, *et al.*, 2000). In the chloride process (Figure 3), TiCl<sub>4</sub> is produced by reacting natural rutile ore with HCl gas at a high temperature; then TiO<sub>2</sub> powder with a high-purity rutile structure (more than 99.9 %) is obtained by reacting the TiCl<sub>4</sub> with oxygen gas at temperatures higher than 1000°C. TiO<sub>2</sub> powder formed by this method is fine but rough. Furthermore, this method requires extra protection devices because of the use of corrosive HCl and Cl<sub>2</sub> gas. This leads to higher production costs. The application of TiO<sub>2</sub> powder obtained by these methods is limited since the particle shape, size and distribution cannot be controlled (Nam, *et al.*, 1998; Wang, *et al.*, 2000).

On a laboratory scale, titanium dioxide has been prepared by various methods, such as precipitation, solvothermal, sol-gel, microemulsion, combustion synthesis, electrochemical synthesis, chemical vapour deposition (CVD), physical vapour deposition (PVD), spray pyrolysis deposition (SPD), and so on (Carp, *et al.*, 2004). The different preparation route and the experiment conditions of titanium dioxide result in products with different structures, morphology, particle size and contaminants (Hadjiivanov, *et al.*, 1996).

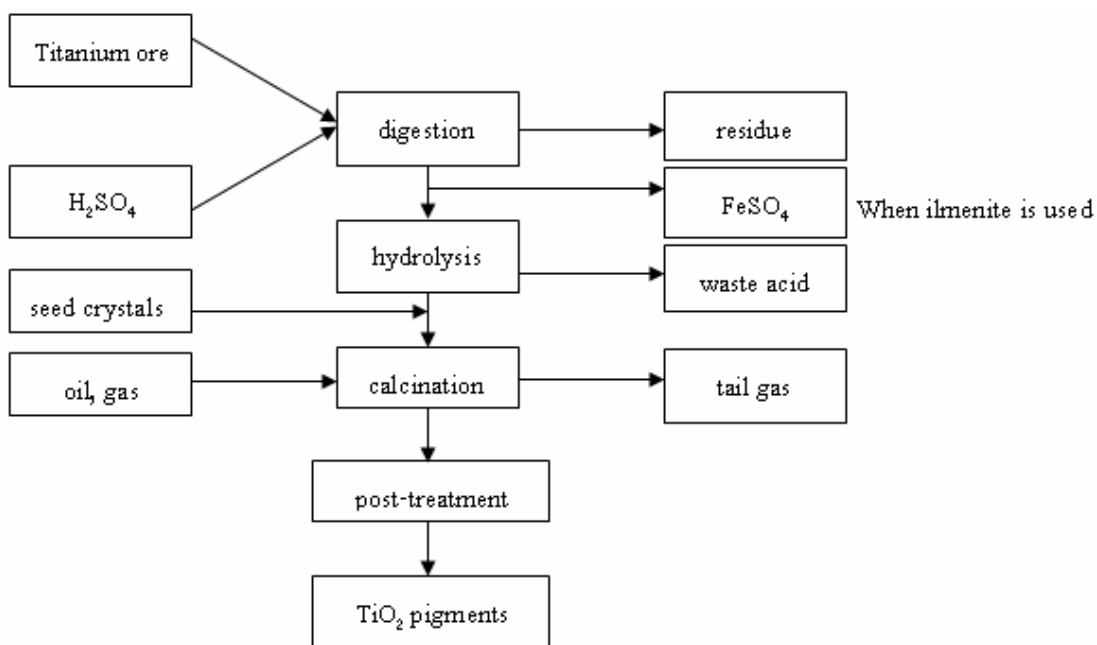


**Figure 2.** TiO<sub>2</sub> pigment manufactured by the sulfate process (Büchner, *et al.*, 1989).

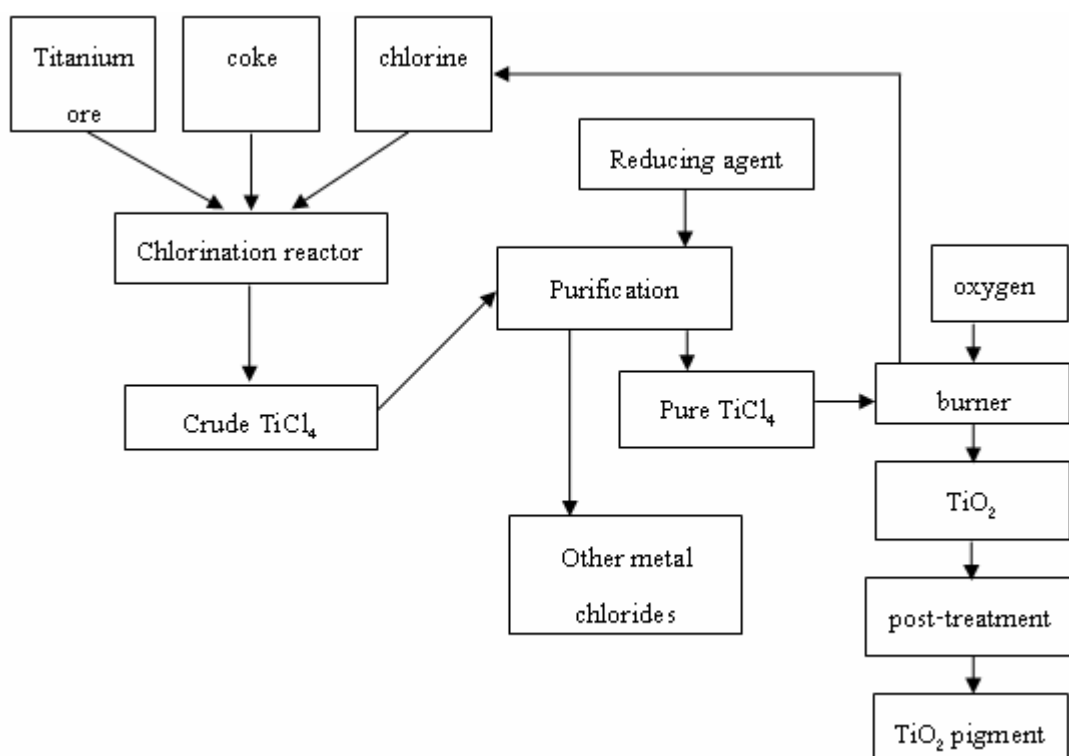


**Figure 3.** TiO<sub>2</sub> pigment manufactured by the chloride process (Büchner, *et al.*, 1989).

This work used the sol-gel and chemical vapour deposition methods to prepare titanium dioxide in form of powder and thin films, respectively.

#### **(a) Sol-gel method**

The sol-gel method involves the transition of system from a liquid “sol” into solid “gel” phase. An overview of the sol-gel products is presented in Figure 4. The starting materials in the preparation of the “sol” are usually inorganic metal salts or metal organic compounds. In a typical sol-gel method, the precursor is subjected to a series of hydrolysis and polymerization (condensation) reactions to form a colloidal suspension or a “sol”. Further processing of the “sol” enables one to make ceramic materials in different forms. Thin films can be prepared on a piece of substrate by spin coating or dip coating. When the “sol” is cast into a mold, a wet “gel” will form. With further drying and heat-treatment, the “gel” is converted into dense ceramic or glass articles. If the liquid in a wet “gel” is removed under a supercritical condition, a highly porous and extremely low density material called “aerogel” is obtained. As the viscosity of a “sol” is adjusted into a proper viscosity range, ceramic fibers can be drawn from the “sol”. Ultra-fine and uniform ceramic powders are formed by precipitation, spray pyrolysis, or emulsion techniques (Chemat Technology, Inc., 1998).

In preparing oxide materials, the sol-gel method offers many advantages in easily control and strongly influenced by the synthesis conditions. The homogeneous property of the products prepared by this method is very satisfactory (Ding and Liu, 1997; Suresh, *et al.*, 1998). Moreover, in these method precursor materials are metallic halide or alkoxide that favor the building of a solid network in a gel which eventually become a stable solid (Sanchez, *et al.*, 1996).

In sol-gel processes, titania is usually prepared by the hydrolysis and polycondensation reactions of titanium alkoxide. It is well known that titanium alkoxide hydrolyze vigorously in water, and many catalysts typically various simple acids, e.g., nitric acid, hydrochloric acid, acetic acid, sulfuric acid (Ding and Liu, 1997; Baolong, *et al.*, 2003; Samantaray, *et al.*, 2003; Zaban, *et al.*, 2000; Yamazaki, *et al.*, 2001), and acetic acid, have been applied to lower the reaction rates. The use of

phosphoric acid, however, has not been reported. Furthermore, this work used titanium tetrachloride ( $\text{TiCl}_4$ ) as precursor for preparation  $\text{TiO}_2$  powders due to inorganic compounds are more economical than alkoxides (Zhang, *et al.*, 1999).

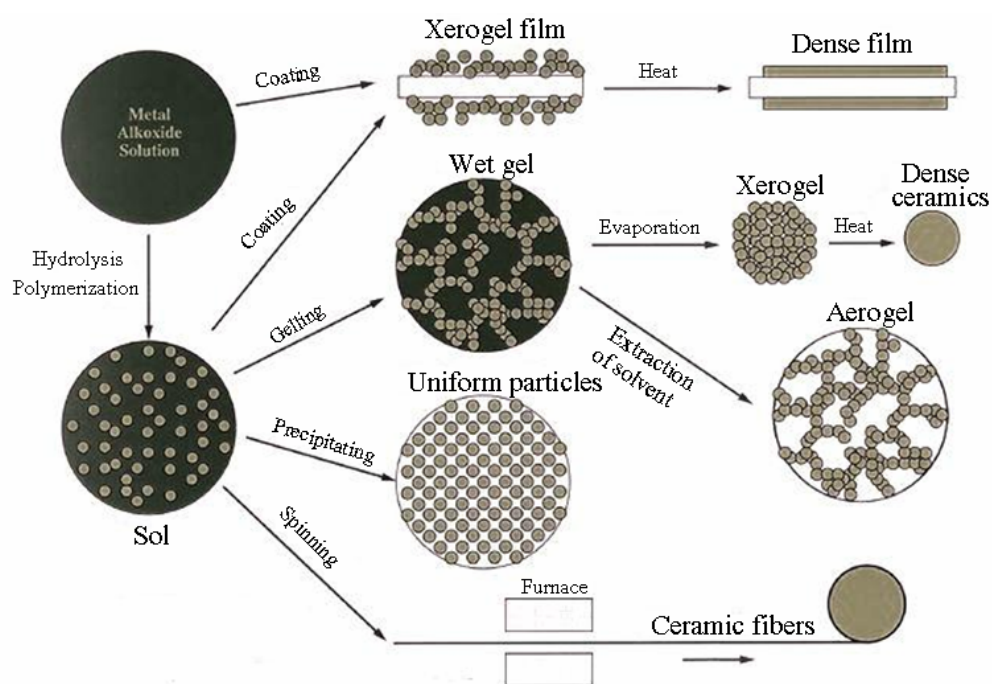


**Figure 4.** An overview of products prepared by sol-gel methods (Chemat Technology, Inc., 1998).

As is well known, Degussa P25 is the most popular and well accepted photocatalysts due to its efficiency and has often been used for the degradation of pollutants in water or air. It has found that the mixture phase of anatase and rutile was an important factor for the photoactivity of  $\text{TiO}_2$  as we can see from Degussa P25, which consist of anatase 80% and rutile 20%. In addition, it has been found that a mixture of anatase and rutile  $\text{TiO}_2$  nanoparticles has a much higher photocatalytic activity than pure anatase or pure rutile  $\text{TiO}_2$  nanoparticles (Ding and Liu, 1997; Zhang and Gao, 2001). Therefore, it is interesting to synthesize  $\text{TiO}_2$  that exhibits high photoactivity by a good combination of anatase-rutile mixture phase and surface area.

Most of the literature works usually used the precalcined titanium dioxide at around 300-400°C to induce crystallization of the anatase form. It has been reported that the different methods for the syntheses of titanium dioxide result in products with different structures (anatase or rutile), crystallinity, and contaminants. As a consequence, the surface properties of TiO<sub>2</sub> strongly depend on the preparation techniques (Zhang, *et al.*, 1999; Reddy, *et al.*, 2001). There have been some work reported the synthesis of mixture phase TiO<sub>2</sub>, for example, Gopal, *et al.*, (1997) prepared crystalline TiO<sub>2</sub> powder either rutile or anatase from titanium isopropoxide at temperature below 100°C. The precipitate sizes were between 50 and 100 nm. Wang, *et al.*, (2000) prepared a mixture of anatase and rutile-type TiO<sub>2</sub> from polyperoxotitanic acid gel obtained by addition of Ti(OBu<sup>n</sup>)<sub>4</sub> to H<sub>2</sub>O<sub>2</sub> solution. The gel was heat-treated in air at temperatures ranging from 150°C to 750°C. Zhang, *et al.*, (1999) obtained nanocrystalline TiO<sub>2</sub> in anatase or mixed phases from controlling the hydrolysis of TiCl<sub>4</sub>. The addition of small amount (NH<sub>4</sub>)<sub>2</sub>SO<sub>4</sub> promotes occurrence of anatase phase, however, these were not studied for photocatalytic activity.

In this work, samples of TiO<sub>2</sub> powder were synthesized by the sol-gel method using TiCl<sub>4</sub> as a starting material at temperature below 100°C and using different acids as hydrolysis catalysts such as hydrochloric acid, nitric acid, sulfuric acid, acetic acid, and phosphoric acid.

### **(b) Chemical vapour deposition (CVD) method**

CVD is a widely used versatile technique to coat large surface areas in a short span of time. In industry, this technique is often employed in a continuous process to produce ceramic and semiconductor films. The family of CVD is extensive and split out according to from metals to composite oxides, are formed from a chemical reaction or decomposition of a precursor in the gas phase. (Carp, *et al.*, 2004)

The basic principles of CVD can be summarized shortly as follows. Chemical vapour deposition (CVD) is a process where one or more precursors are transported (1) in the vapor phase, often in a carrier gas, to the reactor chamber where they adsorb (2) and react (3) to liberate the supporting ligands which

are subsequently desorbed (6) and transported out of the reactor (7). The metal atoms then diffuse (4) to form a stable nucleus, where subsequent growth occurs (5). Under certain circumstances gas reactions can also happen. All these processes occur on a heated substrate which decomposes the precursor, as depicted in the Figure 5.

The CVD process of creating a film has to be reproducible and controllable. As a result, the intrinsic properties, such as the purity, composition, thickness, adhesion, microstructure and surface morphology have to be reproducible for the same reactor conditions.

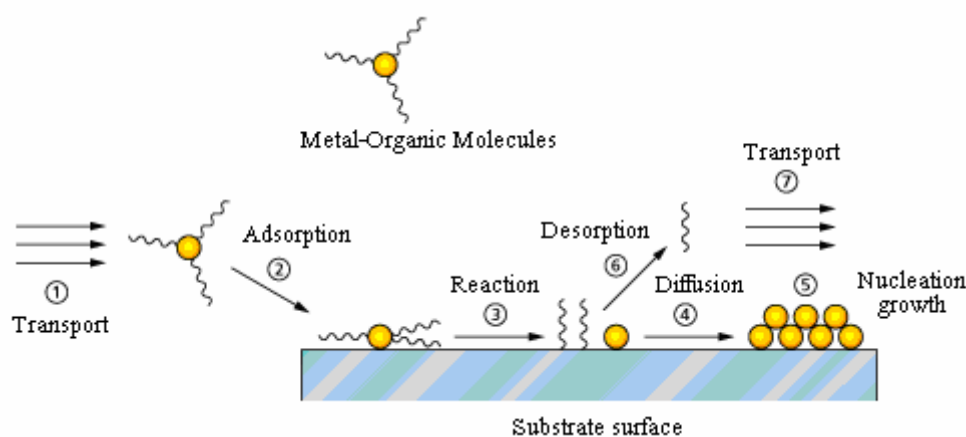


**Figure 5.** Illustration showing the elementary processes involved in the CVD of a metal-organic molecule (adapted from [www.chemsoc.org/chembytes/ezone/images/2002/ashton\\_jun02.htm](http://www.chemsoc.org/chembytes/ezone/images/2002/ashton_jun02.htm)).

Thin films of titania can be produced by metal-organic chemical vapour deposition (MOCVD) and atomic layer deposition (ALD) techniques, which offer the advantage over other techniques of being able to coat large areas and with good aspect ratios over complex geometries. Central to the MOCVD / ALD methodology is the availability and choice of precursor, which can play a significant role in controlling ease of handling, volatility, deposition temperature, film composition and morphology *etc.* Conventional precursors for  $\text{TiO}_2$  are  $\text{TiCl}_4$  (Akhtar, *et al.*, 1994) or a homoleptic alkoxide  $[\text{Ti}(\text{OR})_4]$  ( $\text{R} = \text{Me}$  (Pore, *et al.*, 2004), Et (Kim, *et al.*, 2004), or, most commonly,  $\text{OPr}^i$  (Evans, *et al.*, 2006; Simcock, 2006; Sonnenfeld, *et al.*, 2006 and Duminica, *et al.*, 2006) along with a source of oxygen

(H<sub>2</sub>O, ROH are common), but TiCl<sub>4</sub> suffers from the introduction of chlorine contaminant into the film (Aarik, *et al.*, 2000) while the alkoxides are relatively air- and moisture-sensitive making them unattractive both from a handling perspective and susceptible to pre-reaction in a dual-source MOCVD reaction. Other precursors which have been reported include the use of simple volatile Ti(NMe<sub>2</sub>)<sub>4</sub> (used with H<sub>2</sub>O<sub>2</sub>) (Pheamhom, *et al.*, 2006) and more complex precursors such as [Ti<sub>6</sub>(O)<sub>6</sub>(O<sub>2</sub>CR)<sub>6</sub>] (R = Bu, Bz) (Piszczek, *et al.*, 2005), however most variations attempts to mitigate the sensitivity of titanium alkoxides by the use of chelating ligands which saturate the coordination sphere of the metal. Pre-eminent among these ligands are the β-diketonates, which have been used extensively in conjunction with alkoxides, e.g. [Ti(OPr<sup>i</sup>)<sub>2</sub>(thd)<sub>2</sub>] (thd = 2, 2, 6, 6-tetramethylheptane-3, 5-dionate) (Roeder, *et al.*, 1996); more recently, related β-ketoesters e.g. [Ti(OPr<sup>i</sup>)<sub>2</sub>(tbaoac)<sub>2</sub>] (Htbaoac = t-butylacetoacetate) (Bhakta, *et al.*, 2004) and related malonates have been reported. The latter, when coupled with amido ligands i.e. [Ti(NMe<sub>2</sub>)<sub>2</sub>(dpml)<sub>2</sub>] (Hdpml = di-isopropylmalonate) (Baunemann, *et al.*, 2006) have generated precursors with a mixed O,N ligand sphere for ALD applications.

The use of chelating aminoalkoxides R<sub>2</sub>N(CH<sub>2</sub>)<sub>n</sub>OH in CVD precursor chemistry has been reported recently (Hollingsworth, *et al.*, 2006). Titanium derivatives of amino ethanols [n = 2; R = Me (Hdmae), Et (Hdeae)] and propanols [n = 3, R = Me (Hdmap)] have been known for some time, and several e.g. [Ti(OPr<sup>i</sup>)<sub>3</sub>(dmap)], [Ti(OPr<sup>i</sup>)<sub>2</sub>(dmae)<sub>2</sub>], (Jones, *et al.*, 1998) [Ti(OPr<sup>i</sup>)(dmae)<sub>3</sub>], [Ti(dmae)<sub>4</sub>].(Lee, *et al.*, 1999) have been used in the CVD of TiO<sub>2</sub> and / or related binary oxide films. Indeed, the use of Ti(dmae)<sub>n</sub> precursors has been claimed to lead to more uniform growth of TiO<sub>2</sub> films. (Lee, *et al.*, 1999)

The use of the more functionalised ligands bis-(dimethylamino)propanol (**I**: Hbdmap) and tris-(dimethylamino)propanol (**II**: Htdmap) have not been considered. The structures of Hbdmap and Htdmap are shown in Figure 6. Their use is of interest, firstly because of their enhanced ability to coordinate the metal centre from which the precursors may gain greater stability and secondly because unused donor sites have the potential to be further utilised for

secondary metal binding. The synthesis and characterisation of a series of compounds  $[\text{Ti}(\text{OR})_x(\text{L})_{4-x}]$  ( $\text{R} = \text{Et}, \text{Pr}^i$ ;  $\text{L} = \text{bdmap}, \text{tdmap}$ ) will also be reported in this work.

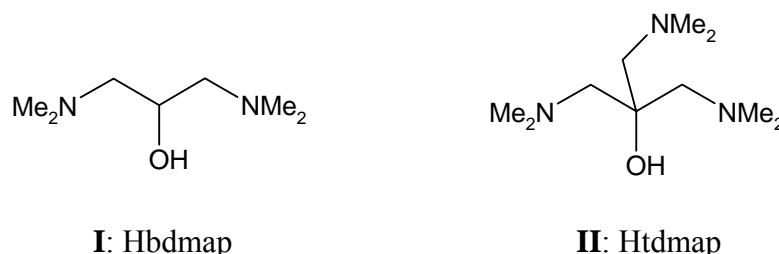


**Figure 6.** Structures of **I:** Hbdmap (bis-(dimethylamino)propanol) and **II:** Htdmap (tris-(dimethylamino)propanol).

## 1.2.2 Dye and treatment of dye pollutant

### 1.2.2.1 Dye

A dye can generally be described as a colored substance that has an affinity to the substrate to which it is being applied. The dye is generally applied in an aqueous solution, and may require a mordant to improve the fastness of the dye on the fiber.

The first human-made (synthetic) organic dye, mauveine, was discovered by William Henry Perkin in 1856. Many thousands of synthetic dyes have since been prepared. Synthetic dyes quickly replaced the traditional natural dyes. They cost less, they offered a vast range of new colors, and they imparted better properties upon the dyed materials.

Chemical classification by the nature of their chromophore, dyes are divided into (<http://en.wikipedia.org/wiki/Dye>):

- (1) Category; Acridine dyes, derivatives of acridine
- (2) Category; Anthraquinone dyes, derivatives of anthraquinone
- (3) Arylmethane dyes
  - 3.1 Category; Diarylmethane dyes, based on diphenyl methane
  - 3.2 Category; Triarylmethane dyes, derivatives of triphenyl methane



- (4) Category; Azo dyes, based on  $-N=N-$  azo structure
- (5) Cyanine dyes, derivatives of phthalocyanine
- (6) Diazonium dyes, based on diazonium salts
- (7) Nitro dyes, based on a  $-NO_2$  nitro functional group
- (8) Nitroso dyes, based on a  $-N=O$  nitroso functional group
- (9) Phthalocyanine dyes, derivatives of phthalocyanine
- (10) Quinone-imine dyes, derivatives of quinone
  - 10.1 Category; Azin dyes
    - Category; Erythrosin dyes
    - Category; Safranin dyes, derivatives of safranin
  - 10.2 Indamins
  - 10.3 Category; Indophenol dyes, derivatives of indophenol
  - 10.4 Category; Oxazin dyes, derivatives of oxazin
  - 10.5 Oxazone dyes, derivatives of oxazone
  - 10.6 Category; Thiazin dyes, derivatives of thiazin
- (11) Category; Thiazole dyes, derivatives of thiazole
- (12) Xanthene dyes, derived from xanthene
  - 12.1 Fluorene dyes, derivatives of fluorine
    - Pyronin dyes
  - 12.2 Category; Fluorone dyes, based on fluorine
    - Category; Rhodamine dyes, derivatives of rhodamine

Three types of dyes (Methylene blue, Congo red, and Crystal violet) were used as model of dye pollutants in this research.

#### **(a) Methylene Blue**

Methylene blue, MB, is a brightly colored, blue cationic thiazine dye. The structural formula and characteristic data of MB (3,7-bis(dimethylamino)phenothiazin-5-ium chloride) are shown in Figure 7(a) and Table 2, respectively. The uses of MB include being an antidote for cyanide poisoning in humans, antiseptic in veterinary medicine and, most commonly, in vitro diagnostic in

biology, cytology, hematology and histology (Mills and Wang, 1999). At room temperature it appears as a solid, odorless, dark green powder that yields a blue solution when dissolved in water.

Methylene blue has been used in several research articles. Mills and Wang (1999) studied the photobleaching of MB in an aqueous solution in the absence and presence of oxygen. Xu, *et al.*, (1999) reported the influence of particles size of TiO<sub>2</sub> on the photocatalytic degradation of MB in a suspended aqueous solution. Houas, *et al.*, (2001) investigated the TiO<sub>2</sub>/UV photocatalytic degradation of methylene blue (MB) in water. Epling and Lin (2002) studied the photoassisted bleaching of MB utilizing TiO<sub>2</sub> and visible light. Awati, *et al.*, (2003) studied the photocatalytic decomposition of MB using nanocrystalline anatase titania prepared by ultrasonic technique. Random, *et al.*, (2004) reported the bleaching of methylene blue by hydrated titanium dioxide.

### **(b) Congo Red**

The conjugated diazo dye Congo red was first synthesized in 1884 and found commercial success because of its ability to dye cotton by simple immersion. In the textile industry such dyes are known as direct dye. Congo red, as a textile dye, has been replaced by other dyes more resistant to fading and repeated washing. However, it is still widely used as a pH indicator and as a histological stain. (Bumpus, *et al.*, 1999) The structural formula and characteristic of Congo red dye (sodium 3,3'-[1,1'-biphenyl]-4,4'-diyl(azo) bis(4-aminonaphthalenesulfonate)) are shown in Figure 7(b) and Table 2, respectively.

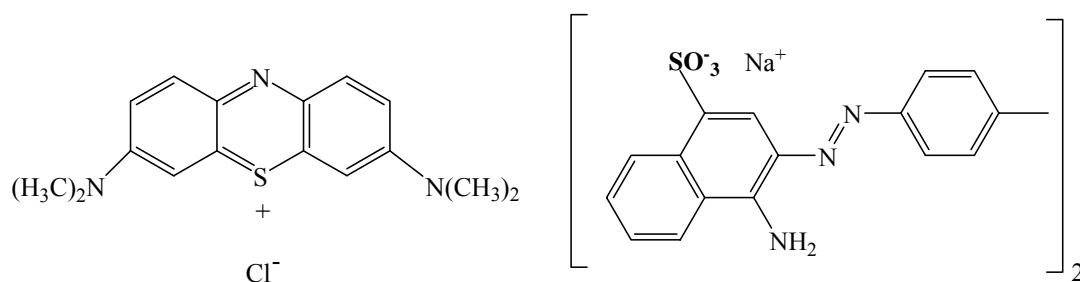
Congo red has also been used in several research articles such as Bumpus, *et al.*, (1999) who demonstrated the use of TiO<sub>2</sub>-mediated photocatalysis for remediation of water contaminated with the azo dye congo red. Hachem, *et al.*, (2001) studied the decolourization of Congo red by using P25 Degussa as catalyst. Wahi, *et al.*, (2005) reported the photodegradation of Congo red catalyzed by nanosized TiO<sub>2</sub>. Bonancêa, *et al.*, (2006) optimized SERS-active (by the presence of nanostructured silver) substrate was employed to study the photodegradation of congo

red (CR). Bejarano-Pérez and Suárez-Herrera (2007) compared between the photocatalytic and sonophotocatalytic oxidation process of congo red using titanium dioxide as a catalyst.

### **(c) Crystal Violet**

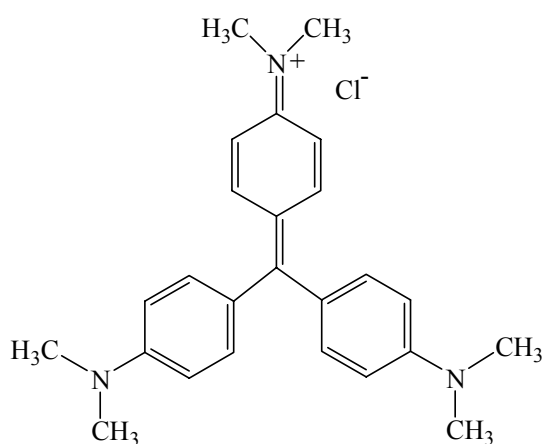
Crystal violet or Gentian violet is a triphenylmethane dye. It is extensively used in textile dyeing, paper printing, as a biological stain and as a dermatological agent. Gentian violet is a mutagen, a mitotic poison and clastogen and has been used for many years in veterinary medicine and as an additive to poultry feed to inhibit propagation of mold, intestinal parasites and fungus. Gentian violet is carcinogenic in mice at several different organ sites. Because of its low cost, its effectiveness as an antifungal agent for commercial poultry feed, and its ready availability, the general public may be exposed to the dye and its metabolites through the consumption of treated poultry products. Therefore, there are both environmental and health concerns on this particular dye (Saqib and Muneer, 2003; Sahoo, *et al.*, 2005). The structural formula and characteristic of crystal violet (hexamethylparasaniline chloride) are shown in Figure 7(c) and Table 2, respectively.

Crystal violet has also been used in several research articles. Hachem, *et al.*, (2001) studied the photocatalytic degradation of crystal violet by using P25 Degussa as catalyst. Saqib and Muneer, (2003) demonstrated the use of TiO<sub>2</sub>-mediated photocatalytic degradation of a triphenylmethane dye (gentian violet), in aqueous suspensions. Sahoo, *et al.*, (2005) studied the photocatalytic degradation of crystal violet on silver ion doped TiO<sub>2</sub>.



(a) Methylene blue

(b) Congo red



(c) Crystal violet

**Figure 7.** Structure of Methylene blue (a), Congo red (b), and Crystal violet (c).**Table 2.** Characteristic of dyes.

Dye	Formula	Abbreviation	Type of dye	Class of dye
Methylene blue	$C_{16}H_{18}ClN_3S$	MB	Thiazine	Cationic*
Congo red	$C_{32}H_{22}N_6Na_2O_6S_2$	CR	Diazo	Direct**
Crystal violet	$C_{25}H_{30}N_3Cl$	CV	Thiophenyl	Cationic**

\* Epling and Lin, 2002

\*\* Hachem, *et al.*, 2001

### 1.2.2.2 Methods for the treatment of dye pollutants

Different types of dyes are used in many industries such as textile, paint, ink, plastics, and cosmetics. A certain amount of them are lost in the process of their manufacturing and utilization and often cause environmental problems (Tanaka, *et al.*, 2000).

Depending on the chromogenes, chromophores, and auxochromes, dyes exhibit different physical and chemical properties, such as water solubility, color, brightness, fastness, and light absorption characteristics. Many dyes pose environmental hazards because their degradation may produce toxic intermediates. For example, those dyes with substructures of nitrobenzene, benzidine and quaternary amines have carcinogenicity and toxicity. With increasing awareness of water-resource protection to ensure a safe drinking supply, dye-containing wastewater originated from dye manufacturing industries and dyeing industries needs to be treated before being discharged (Epling and Lin, 2002).

A variety of physical, chemical and biological methods are presently available for treatment of textile wastewater. Biological treatment is a proven technology and is cost-effective. However, it has been reported that the majority of dyes are only adsorbed on the sludge and are not degraded. Physical methods such as ion-exchange, adsorption, air stripping, *etc.*, are also ineffective on pollutants which are not readily adsorbable or volatile, and have the further disadvantage that they simply transfer the pollutants to another phase rather than destroying them (Sauer, *et al.*, 2002).

Over the last two decades photocatalytic process has been shown to be potentially advantageous and useful for the treatment of wastewater pollutants. This process has several advantages over competing processes such as: (1) complete mineralization, (2) no waste-solids disposal problem, and (3) only mild temperature and pressure conditions are necessary (Mahmoodi, *et al.*, 2005).

### Principles of heterogeneous photocatalysis

The basic principles of heterogeneous photocatalysis can be summarized as follows. In a semiconductor exists an occupied series of levels of highest energy (the valence band: VB), followed by a finite energy gap between this level and a corresponding series of unoccupied levels, known as the conduction band (CB). The magnitude of this energy gap (band gap,  $E_g$ ) for a bulk solid is analogous to the HOMO-LUMO separation for a small molecule (Chandler, *et al.*, 1993).

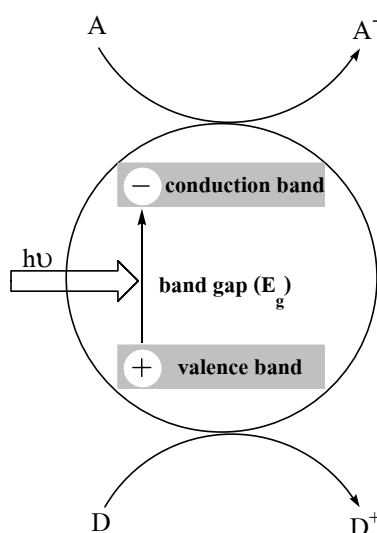


**Figure 8.** Schematic representation of the semiconductor showing the electron/hole pair formed in the conduction band and the valence band, respectively.

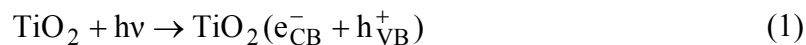
When a photon with energy of  $h\nu$  matches or exceeds the band gap energy,  $E_g$ , of the semiconductor, and electron ( $e_{CB}^-$ ), is promoted from the valence band, VB, into the conduction band, CB, leaving a hole,  $h_{VB}^+$  behind. The  $e_{CB}^-$  and the  $h_{VB}^+$  can recombine on the surface or in the bulk of the particle in a few nanoseconds (and the energy dissipated as heat) or can be trapped in surface states where they can react with donor (D) or acceptor (A) species adsorbed or close to the surface of the particle. Thereby, subsequent anodic and cathodic redox reactions can

be initiated (Figure 8). The energy level at the bottom of the CB is actually the reduction potential of photoelectrons and the energy level at the top of the VB determines the oxidizing ability of photoholes, each value reflecting the ability of the system to promote reduction and oxidations (Litter, 1999).

Some oxide and chalcogenides have enough bandgap energies to be excited by UV or visible light, and the redox potentials of the edges of the valence band and conduction band can promote a series of oxidative or reductive reactions. From the available semiconductors, ZnO is generally unstable in illuminated aqueous solutions, especially at low pH values, and WO<sub>3</sub>, although useful in the visible range, is generally less photocatalytically active than TiO<sub>2</sub>. Among others, CdS, ZnS and iron oxides have been also tested. However, and without any doubt, TiO<sub>2</sub> is extensively used as photocatalyst due to its optical and electronic properties, chemical stability, non-toxicity, and low cost.

The heterogeneous photocatalytic process is a complex sequence of reactions that can be expressed by the following equations:

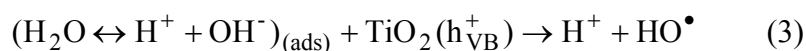
1. Absorption of efficient photons ( $h\nu \geq E_g = 3.2 \text{ eV}$ ) by titania



2. Oxygen ionosorption (first step of oxygen reduction; oxygen's oxidation degree passes from 0 to -1/2)



3. Neutralization of OH<sup>-</sup> groups by photoholes which produces HO<sup>•</sup> radicals



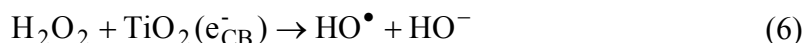
4. Neutralization of O<sub>2</sub><sup>•-</sup> by protons



5. Transient hydrogen peroxide formation and dismutation of oxygen



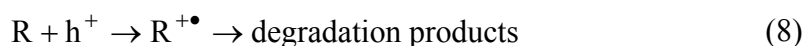
6. Decomposition of  $\text{H}_2\text{O}_2$  and second reduction of oxygen



7. Oxidation of the organic reactant via successive attacks by  $\text{HO}^\bullet$  radicals



8. Direct oxidation by reaction with holes



As an example of the last process, holes can react directly with carboxylic acids generation  $\text{CO}_2$



Many studies have shown that heterogeneous photocatalytic oxidation processes can be used for removing coloring material from dye effluent. Zhang, *et al.*, (1998) demonstrated the  $\text{TiO}_2$ -assisted photodegradation of dye pollutants under illumination by visible light. Kiriakidou, *et al.*, (1999) reported the effect of operational parameters and  $\text{TiO}_2$ -doping on the photocatalytic degradation of Acid Orange 7 (AO7). Zhu, *et al.*, (2000) studied the photocatalytic degradation of azo dyes by supported  $\text{TiO}_2$  + UV in aqueous solution. Hachem, *et al.*, (2001) studied the photocatalytic degradation of various dyes (Orange II, Orange G, Congo Red, Indigo Carmine, Crystal Violet, Malachite Green, Remazol Blue and Methyl Yellow), using P25 Degussa as catalyst. Epling and Lin (2002) demonstrated the photoassisted bleaching of dyes utilizing  $\text{TiO}_2$  and visible light. Sauer, *et al.*, (2002) studied the kinetics of photocatalytic degradation of reactive dyes in a  $\text{TiO}_2$  slurry reactor. Fernándeza, *et al.*, (2002) reported photo-discolouration of Orange II solutions at different concentrations carried out in a 1l concentric reactor irradiated with a 254 nm



mercury lamp (125 W) in the presence of Degussa TiO<sub>2</sub> P-25 dispersions. Daneshvar, *et al.*, (2003) studied the photocatalytic degradation of azo dye acid red 14 in water and investigated the effect of operational parameters. Xie and Yuan (2003) reported the photocatalytic activity and recycle application of titanium dioxide sol for X-3B photodegradation. Karkmaz, *et al.*, (2004) studied the photocatalytic degradation of amaranth, an alimentary dye in an irradiated titanium dioxide aqueous suspension. Qamar, *et al.*, (2005) reported the photocatalytic degradation of two selected dye derivatives, chromotrope 2B and amido black 10B, in aqueous suspensions of titanium dioxide.

### 1.3 Objectives

The objectives of this research are as follows:

#### Part 1: Studying TiO<sub>2</sub> in powder form

(1) Several samples of TiO<sub>2</sub> powder will be prepared by the sol-gel method using different acids as hydrolysis catalyst and TiCl<sub>4</sub> as precursor. The acids to be used are hydrochloric acid, nitric acid, acetic acid, sulfuric acid, and phosphoric acid.

(2) Samples obtained in (1) will be investigated by many physical methods, such as, XRD, BET, and spectrophotometric methods.

(3) Sample obtained in (1) will be studied further for the photocatalytic activity and compare the results with commercial TiO<sub>2</sub> samples (P25, anatase and rutile). Three dyes are used in this test: methylene blue, crystal violet, and congo red.

#### Part 2: Studying TiO<sub>2</sub> in film form and nanoparticles

(1) Samples of TiO<sub>2</sub> film and nanoparticles will be prepared from the chelating amino alkoxides of the form [Ti(OR)<sub>x</sub>(L)<sub>4-x</sub>] (R = Et, Pr<sup>i</sup>; L = bdmap, tdmmap).

(2) Samples obtained in (1) will be studied further for the photocatalytic activities using methylene blue as a dye model.

## CHAPTER 2

### EXPERIMENTAL

#### 2.1 Synthesis of nanocrystalline TiO<sub>2</sub> powders

##### 2.1.1 Materials

- (1) Acetic acid, CH<sub>3</sub>COOH; A.R., code no. A8401, Lab-scan, Ireland.
- (2) Ammonium hydroxide (Ammonia solution) 28.0-30.0%, NH<sub>4</sub>OH; A.R., code no. 9721-03, J.T. Baker, U.S.A.
- (3) Hydrochloric acid, HCl; A.R., code no. 1.00317.2500, Merck, Germany.
- (4) Nitric acid, HNO<sub>3</sub>; A.R., code no. 9601-06, J.T. Baker, U.S.A.
- (5) Phosphoric acid, H<sub>3</sub>PO<sub>4</sub>; code no. 406002, Carlo Erba, Italy.
- (6) Silver nitrate, AgNO<sub>3</sub>; A.R., code no. 102333J, BDH, England.
- (7) Sulfuric acid, H<sub>2</sub>SO<sub>4</sub>; A.R., code no.9681-03, J.T. Baker.
- (8) Titanium tetrachloride, TiCl<sub>4</sub>; A.R., code no. 8.12382.1000, Merck, Germany.
- (9) Titanium dioxide (Anatase); A.R., code no.488257, Carlo Erba, Italy.
- (10) Titanium dioxide (P25); code no. D-60287, Degussa AG, Frankfurt, Germany.
- (11) Titanium dioxide (Rutile: R706); Dupont, U.S.A.

## 2.1.2 Method

### 2.1.2.1 Preparation of TiO<sub>2</sub> powder

A flow chart for the synthesis of titanium dioxide is shown in Figure 9. Detailed procedure for the preparation is as follows: titanium tetrachloride (TiCl<sub>4</sub>) 20 mL was added slowly to 200 mL of cold distilled water which had been cooled in an ice-water bath at least 10 minutes prior to the addition. The solution was then mixed with small amount of each corresponding acid (acts as hydrolysis catalyst) in a three necked round bottom flask and refluxed 80°C for 1 hr under vigorous stirring. The solution was then treated with ammonia solution until the pH value was 7 and maintained at the same temperature for 24 hrs. The white precipitate formed was filtered and then washed with distilled water until free of chloride ion (AgNO<sub>3</sub> test). The product was dried overnight and ground to fine powder. The product were assigned as Ti-HCl, Ti-HNO<sub>3</sub>, Ti-H<sub>2</sub>SO<sub>4</sub>, Ti-CH<sub>3</sub>COOH, and Ti-H<sub>3</sub>PO<sub>4</sub>, corresponding to the preparation method of each by adding HCl, HNO<sub>3</sub>, H<sub>2</sub>SO<sub>4</sub>, CH<sub>3</sub>COOH, and H<sub>3</sub>PO<sub>4</sub> acids, respectively, plus another sample designated as Ti-no-acid since it was prepared in the absence of acid catalyst.

### 2.1.2.2 Products characterization

The XRD patterns were obtained via the Philips PW 3710 powder diffractometer using Cu K $\alpha$  radiation and equipped with a Ni filter. Diffraction patterns of both anatase and rutile phases were compared with reference in the JCPDS Powder Diffraction Files (21-1272, 21-1276). From the line broadening of the corresponding X-ray diffraction peaks and using the Scherrer's formula, the crystallite size was estimated by

$$L = \frac{K\lambda}{\beta \cos \theta} \quad (1)$$

where,  $L$  is the average crystallite size in nm,  $\lambda$  is the wavelength of the X-ray radiation (0.154056 nm for copper lamp),  $K$  is a constant usually taken as 0.9,  $\beta$  is the line width at half-maximum height in radians, and  $\theta$  is the diffraction angles (Zielińska, *et al.*, 2001; Sivalingam, *et al.*, 2003).

The infrared spectra were recorded using Fourier-transformed infrared (FT-IR) spectrophotometer (EQUINOX55, Bruker, Germany) in diffused reflectance mode at 400-4000  $\text{cm}^{-1}$  with KBr as blank. The SEM micrographs were performed on gold-coated samples using a Jeol apparatus (JSM-5800 LV) equipped with a Link analyzer (ISIS 300) for X-ray energy-dispersive analysis (EDX). The Brunauer-Emmett-Teller (BET) surface area of  $\text{TiO}_2$  powders were determined by means of Coulter SA 3100 (U.S.A) using nitrogen adsorption at  $-196^\circ\text{C}$ .

The band gap energies of titanium dioxide samples were determined using UV-Vis spectrophotometer (Shimadzu UV-2401, Japan). The spectra were recorded in diffused reflectance mode with  $\text{BaSO}_4$  as a reference. The band gap energies ( $E_g$ ) of the catalyst were calculated by the Planck's equation:

$$E_g = h \frac{c}{\lambda} = \frac{1240}{\lambda} \quad (2)$$

where  $E_g$  is the band gap energy (eV),  $h$  is the Planck's constant,  $c$  is the light velocity (m/s), and  $\lambda$  is the wavelength (nm).

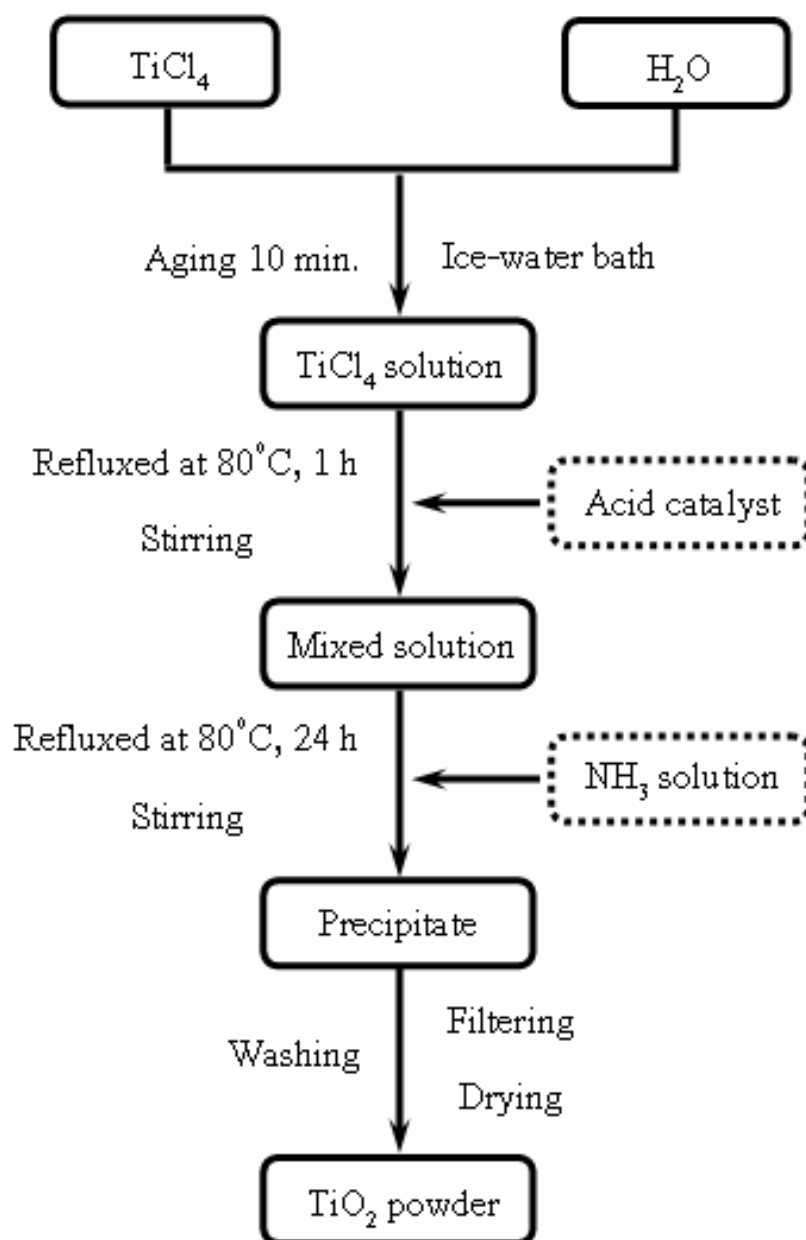


**Figure 9.** Flow chart of the synthesis of titanium dioxide powders.

### 2.1.3 Photocatalytic study

#### 2.1.3.1 Materials

- (1) Congo red,  $C_{32}H_{22}N_6Na_2O_6S_2$ ; Microscopical stain, code no. 30422, BDH, England.
- (2) Crystal violet, C.I. 42555, code no. 34024, BDH, England.
- (3) Methylene blue,  $C_{16}H_{18}N_3ClS_2 \cdot 2H_2O$ ; Laboratory Reagent, code no. 1137-25G, UNILAB, Australia.
- (4) Hydrogen peroxide,  $H_2O_2$ ; A.R., code no. 307701005, Carlo Erba, Italy.

#### 2.1.3.2 Procedures

##### (1) Test for photocatalytic activity of the samples

A solution (450 mL) containing  $1 \times 10^{-5}$  mol of dye per liter of water, a stirring bar, and 0.225 g of  $TiO_2$  were placed in the beaker. Prior to the illumination, the suspension was stirred for 30 min to allow the dye adsorption onto the solid surface. The UV irradiation was carried out using the fluorescence black light tube (20 w, F20T12-BLB, G.E., U.S.A.) as previously reported (Randorn, *et al.*, 2004) but with newly designed wooden compartment that can accommodate up to 5 tubes of black light. The picture of a wooden compartment was shown in Fig. 10. At specific time intervals, 5 mL of the sample was sampled and centrifuged (EBA 20 Hettich, Germany) to remove titanium dioxide particles. The change in absorbance of dye solution was measured using an UV-Vis Spectrophotometer (Specord S100, Germany) at  $\lambda_{max}$  665, 590, and 500 nm for methylene blue (MB), crystal violet (CV), and congo red (CR), respectively. Controlled experiments with either light and  $TiO_2$  were performed to demonstrate that decolorization of the dyes was dependent on the

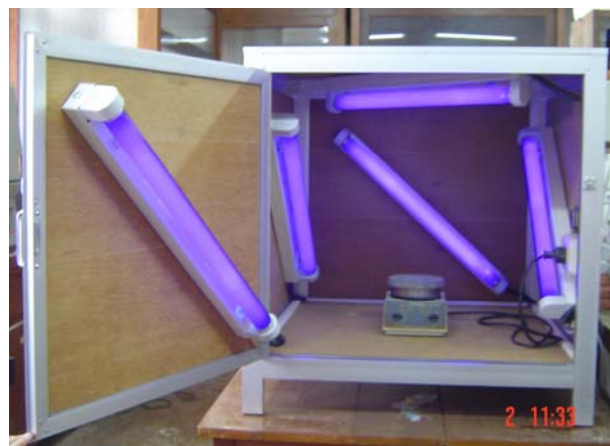
presence of both light and  $\text{TiO}_2$ . During adsorption in the darkness, the beaker was wrapped with aluminum foil to shield it from the ambient light.

## (2) The initial dye concentration

The effect of initial dye concentrations on the photocatalytic activity of titanium dioxide was investigated with three dyes. The dye concentrations were  $1 \times 10^{-5}$ ,  $1.75 \times 10^{-5}$ , and  $2.5 \times 10^{-5}$  mol/L. In each case, the  $\text{TiO}_2$  powder (0.225 g) was mixed in the known concentration of dye solution under continuous stirring and kept for 30 min in the dark to equilibrate. The UV-lights were turned on to irradiate the suspension. At irradiation time intervals (1, 2, 3, 4, and 5 hr), samples were taken, centrifuged to remove  $\text{TiO}_2$  particles. After centrifugation the absorbance at  $\lambda_{\text{max}}$  665 nm for methylene blue, 590 nm for crystal violet, and 500 nm for congo red was determined.



(a) Outer compartment



(b) Inner compartment

**Figure 10.** The wooden compartment for photocatalytic experiment (a) outer and (b) inner.

### (3) Effect of hydrogen peroxide

In the studies on the effect of addition of hydrogen peroxide on dye degradation, a starting solution was prepared from a dye solution (500 mL) containing a known concentration of dye with added small volume of 1 mol/L (5 mL) of hydrogen peroxide. From the starting solution, 450 mL was taken and 0.225 g of TiO<sub>2</sub> was added. It was allowed to equilibrate for 30 min in the darkness and kept at the maintained condition. The beaker was wrapped with aluminum foil to shield against the ambient light.

#### (a) In the absence of light

The suspension prepared above was sampled after an appropriate time (1, 2, 3, 4, and 5 hr). TiO<sub>2</sub> particles were removed by centrifugation. The absorbance of the dye solution was determined at  $\lambda_{\max}$  665, 590, and 500 nm for methylene blue, crystal violet, and congo red, respectively. Two controlled experiments were also run simultaneously, one containing only dye and hydrogen peroxide while the other only dye and TiO<sub>2</sub>.

#### (b) In the presence of light

In this experiment, the same set up as above was employed but after being equilibrated for 30 min in the dark the aluminum foil was removed. The lamps were switched on to initiate the reaction. The suspension was sampled after an appropriate illumination time (1, 2, 3, 4, and 5 hr). TiO<sub>2</sub> particles were removed by centrifugation. Two controlled experiments were also run simultaneously, one containing only dye and hydrogen peroxide while the other only dye and TiO<sub>2</sub>. The absorbance of the dye solution was determined at  $\lambda_{\max}$  665 nm for methylene blue, 590 nm for crystal violet, and 500 nm for congo red.



## 2.2 Synthesis of titanium amino-alkoxides: precursors for the formation of TiO<sub>2</sub> materials

### 2.2.1 Materials

- (1) Epichlorohydrin, C<sub>3</sub>H<sub>5</sub>ClO; A.R., CAS No. 106-89-9, Aldrich, UK.
- (2) 40% Dimethylamine, (CH<sub>3</sub>)<sub>2</sub>NH, A.R., CAS No. 124-40-3, SIGMA-Aldich, UK.
- (3) Sodium hydroxide, NaOH, A. R., CAS No.1310-73-2, Aldrich, UK.
- (4) Dichloromethane, CH<sub>2</sub>Cl<sub>2</sub>, Laboratory reagent grade, CAS No. 75-09-2, Fisher Scientific, UK.
- (5) Magnesium sulfate-dried, Laboratory reagent grade, CAS No. 7487-88-9, Fisher Scientific, UK.
- (6) Titanium (IV) i-propoxide, Ti(OCH(CH<sub>3</sub>)<sub>2</sub>)<sub>4</sub>, CAS No. 20527-3, Aldrich, UK.
- (7) Titanium (IV) ethoxide, Ti(OC<sub>2</sub>H<sub>5</sub>)<sub>4</sub>, CAS No. 3087-36-3, Aldrich, UK.
- (8) Titanium (IV) ethoxide, Ti(OCH<sub>2</sub>CH<sub>3</sub>)<sub>4</sub>, A.R., CAS No. 8087-36-3, Alfa Aesar, UK.
- (9) 3-Chloro-2-chloromethyl-1-propene, (CH<sub>2</sub>=C(CH<sub>2</sub>Cl)<sub>2</sub>), CAS No. 1871-57-4, Aldrich, UK.
- (10) 3-Chloroperbenzoic acid, ClC<sub>6</sub>H<sub>4</sub>CO<sub>3</sub>H, CAS No. 937-14-4, Aldrich, UK.
- (11) Chloroform, CHCl<sub>3</sub>, CAS No. 67-66-3, Aldrich, UK.

### 2.2.2 General procedures

Elemental analyses were performed using an Exeter Analytical CE 440 analyser.  $^1\text{H}$  and  $^{13}\text{C}$  NMR spectra were recorded on a Bruker Advance 300 MHz FT-NMR spectrometer as saturated solution at room temperature; chemical shifts are in ppm with respect to  $\text{Me}_4\text{Si}$ ; coupling constants are in Hz. SEM was carried out on a JEOL JSM-6310 microscope equipped with Oxford Instruments ISIS EDXS attachment while TEM used a JEOL 1200EX machine. XRD was performed using a Bruker D8 Diffractometer on which coupled  $\theta$ - $2\theta$  scans were carried out.

Crystal structure data were collected on a Nonius Kappa CCD diffractometer at 150(2) K using Mo- $\text{K}\alpha$  radiation ( $\lambda = 0.71073 \text{ \AA}$ ).

### 2.2.3 Syntheses

All reactions were carried out under an inert atmosphere. Solvents were dried and degassed under an argon atmosphere over activated alumina columns using an Innovative Technology solvent purification system (SPS)

(1) Hbdmap (Campbell, *et al.*, 1949) and Htdmap (Müller and Schätzle, 2004) were prepared by literature methods.

- Synthesis of Hbdmap: One mole (92.5 g) of epichlorohydrin was added at the rate of 3-4 drops per second, with vigorous stirring, to 800 g of 40% dimethylamine solution. The reaction was exothermic and the inside temperature had risen to  $70^\circ\text{C}$  by the time addition was completed. The reaction mixture was stirred at  $90^\circ\text{C}$  for 6 hrs and then allowed to stand overnight. The mixture was chilled in an ice-bath and saturated with sodium hydroxide; the yellow organic layer which separated was dried over sodium hydroxide. Distillation through a short Vigreux column yielded 96.9 g or 66% of a colourless oil.

- Synthesis of Htdmap: A 500 mL two-necked flask fitted with a dropping funnel and thermometer was charged with 120 mL of a 40% aqueous

solution of dimethylamine (0.95 mol). 1-chloro-2,3-epoxy-2-chloromethylpropane (10.1g, 72 mmol) was slowly added dropwise under stirring whereupon the temperature of the cloudy solution rose from 14 to 40°C. The dropping funnel was replaced by a reflux condenser and the solution was refluxed for 6 hr at 90°C which was accompanied by gas evolution (mostly HNMe<sub>2</sub>). After standing overnight, the solution was cooled in an ice bath and 30 g of NaOH was slowly added in small portions which resulted in further gas evolution and phase separation. After addition of chloroform the phases were separated and the aqueous phase was washed with several small portions of chloroform until a total of 250 mL of chloroform was used. The combined organic phases were dried over MgSO<sub>4</sub> and solvent was evaporated in vacuo (1 mbar) leaving 20.3 g of an orange liquid. Distillation at 1 mbar yielded 13.9 g (68 mmol, 95%) of colourless.

(2) Synthesis of [Ti(OEt)<sub>3</sub>(bdmap)]: [Ti(OEt)<sub>4</sub>] (1.59 g, 6.9 mmol) was dissolved in dry hexane (10 mL) and Hbdmap (1.02 g, 6.9 mmol) was added. After stirring overnight, the mixture was heated at 50°C with stirring for 2 hrs. All volatiles were removed under vacuum, giving 2.17 g (96%) of a white solid. This was subsequently dissolved in dry dichloromethane (5 mL) and placed in the freezer at -12°C where colourless crystals appeared. Analysis: Found (calc. for TiO<sub>4</sub>N<sub>2</sub>C<sub>13</sub>H<sub>32</sub>): C 45.9 (47.6); H 9.7 (9.8); N 8.3 (8.5)%. <sup>1</sup>H-NMR (CDCl<sub>3</sub>): 4.40 (1H, br sh OCH), 4.30 (6H, br s, OCH<sub>2</sub>), 2.45 (4H, br s, NCH<sub>2</sub>) 2.25 (12H, s, NCH<sub>3</sub>), 1.20 (9H, t, CCH<sub>3</sub>) <sup>13</sup>C-NMR (CDCl<sub>3</sub>): 75.2 (br, OCH), 69.3 (br, OCH<sub>2</sub>), 65.0 (br, NCH<sub>2</sub>), 45.7 (NCH<sub>3</sub>), 18.7 (br, CCH<sub>3</sub>).

(3) Synthesis of [Ti(O<sup>i</sup>Pr)<sub>3</sub>(bdmap)]: [Ti(O<sup>i</sup>Pr)<sub>4</sub>] (1.83 g, 6.3 mmol) was dissolved in dry hexane (10 mL) and Hbdmap (0.92 g, 6.3 mmol) was added. After stirring overnight, the mixture was heated at 50°C with stirring for 2 hrs. All volatiles were removed under vacuum, giving 2.02 g (87%) colourless clear oil. Analysis: Found (calc. for TiO<sub>4</sub>N<sub>2</sub>C<sub>16</sub>H<sub>38</sub>): C 49.9 (51.9); H 10.0 (10.3) ; N 7.7 (7.6)%. <sup>1</sup>H-NMR (CDCl<sub>3</sub>): 4.60 (3H, septet, CHO), 4.38 (1H, m, CHCH<sub>2</sub>), 2.47 (2H, m, NCH<sub>2</sub>),

2.33 (2H, m, NCH<sub>2</sub>), 2.28 (12H, s, NCH<sub>3</sub>), 1.20 (18H, d, CCH<sub>3</sub>) <sup>13</sup>C-NMR (CDCl<sub>3</sub>): 75.1 (OC of Pr<sup>i</sup>), 74.9 (OCH of bdmmap), 64.8 (CH<sub>2</sub>N), 45.8 (NCH<sub>3</sub>), 25.5 (CCH<sub>3</sub>).

(4) Synthesis of [Ti(OEt)<sub>3</sub>(tdmap)]: [Ti(OEt)<sub>4</sub>] (1.18 g, 5.2 mmol) was dissolved in dry hexane (10 mL) and Htdmap (1.05 g, 5.2 mmol) was added. After stirring overnight, the mixture was heated at 50°C with stirring for 2 hrs. All volatiles were removed under vacuum, giving 1.95 g (98%) creamy solid. This was subsequently dissolved in dry hexane (5 mL) and placed in the freezer at -12°C where white crystals appeared; these were found to be soft, diffracting poorly. Analysis: Found (calc. for TiO<sub>4</sub>N<sub>3</sub>C<sub>16</sub>H<sub>39</sub>): C 48.6 (49.9); H 10.0 (10.2) ; N 10.7 (10.9)%. <sup>1</sup>H-NMR (CDCl<sub>3</sub>): 4.30 (6H, br s, OCH<sub>2</sub>), 2.45 (6H, s, CH<sub>2</sub>N), 2.30 (12H, s, NCH<sub>3</sub>), 2.25 (6H, s, NCH<sub>3</sub>) 1.15 (9H, t, CCH<sub>3</sub>) <sup>13</sup>C-NMR (CDCl<sub>3</sub>): 84.0 (OC), 69.0 (OCH<sub>2</sub>), 66.2, 63.9 (2:1, NCH<sub>2</sub>), 47.9, 47.0 (2:1, NCH<sub>3</sub>), 18.9 (CCH<sub>3</sub>); minor signals also observed at 62.7, 44.6 ppm.

(5) Synthesis of [Ti(O<sup>i</sup>Pr)<sub>3</sub>(tdmap)]: [Ti(O<sup>i</sup>Pr)<sub>4</sub>] (1.35 g, 4.6 mmol) was dissolved in dry hexane (10 mL) and Htdmap (0.94 g, 4.6 mmol) was added. After stirring overnight, the mixture was heated at 50°C with stirring for 2 hrs. All volatiles were removed under vacuum, giving 1.87 g (95%) colourless clear oil. Analysis: Found (calc. for TiO<sub>4</sub>N<sub>3</sub>C<sub>19</sub>H<sub>45</sub>): C 49.4 (53.4); H 10.1 (10.6)% ; N 8.9 (9.8)%. <sup>1</sup>H-NMR (CDCl<sub>3</sub>): 4.60 (3H, septet, OCH), 2.45 (6H, s, CH<sub>2</sub>N), 2.30 (18H, s, NCH<sub>3</sub>), 1.15 (18H, d, CCH<sub>3</sub>) <sup>13</sup>C-NMR (CDCl<sub>3</sub>): 83.9 (OC), 74.8 (OCH), 66.0 (CH<sub>2</sub>N), 47.5 (NCH<sub>3</sub>), 24.8 (CCH<sub>3</sub>).

(6) Synthesis of [Ti(OEt)<sub>2</sub>(bdmap)<sub>2</sub>]: [Ti(OEt)<sub>4</sub>] (0.78 g, 3.4 mmol) was dissolved in dry hexane (10 mL) and Hbdmap (0.99 g, 6.8 mmol) was added. After stirring overnight, the mixture was heated at 50°C with stirring for 2 hrs. All volatiles were removed under vacuum, giving 1.36 g (47%) colourless oil [Ti(OEt)<sub>2</sub>(bdmap)]. Crystals of the hydrolysis product [(bdmap)<sub>2</sub>TiO]<sub>2</sub> appeared on standing over a few days. [Ti(OEt)<sub>2</sub>(bdmap)<sub>2</sub>] : <sup>1</sup>H-NMR (CDCl<sub>3</sub>): 4.50 (2H, br s, OCH), 4.32 (4H, br s, OCH<sub>2</sub>), 2.45 (8H, br s, CH<sub>2</sub>N), 2.25 (24H, br s, NCH<sub>3</sub>), 1.15 (6H, br s, CCH<sub>3</sub>). <sup>13</sup>C-

NMR (CDCl<sub>3</sub>): 77.5 (OCH), 69.1 (OCH<sub>2</sub>), 65.1, 64.8 (3:1, NCH<sub>2</sub>), 45.8 (NCH<sub>3</sub>), 18.7 (CCH<sub>3</sub>).

(7) Synthesis of [Ti(O<sup>i</sup>Pr)<sub>2</sub>(bdmap)<sub>2</sub>]: [Ti(O<sup>i</sup>Pr)<sub>4</sub>] (1.07 g, 3.6 mmol) was dissolved in dry hexane (10 mL) and Hbdmap (1.03 g, 7.1 mmol) was added. After stirring overnight, the mixture was heated at 50°C with stirring for 2 hrs. All volatiles were removed under vacuum, giving 1.52 g (94%) colourless clear oil. Analysis: Found (calc. for TiO<sub>4</sub>N<sub>4</sub>C<sub>20</sub>H<sub>48</sub>): C 49.1(52.7); H 10.0 (10.6)% ; N 12.0 (12.3)%. <sup>1</sup>H-NMR (CDCl<sub>3</sub>): 4.60 (2H, m, CHO), 4.40 (2H, m, CHCH<sub>2</sub>), 2.25 (32H, overlapping m, NCH<sub>3</sub> and CH<sub>2</sub>N), 1.15 (12H, d, CCH<sub>3</sub>). <sup>13</sup>C-NMR (CDCl<sub>3</sub>): 77.8, 75.0 (CHO of OPr<sup>i</sup> and bdmap), 65.2, 64.9, 62.9 (ca. 1:2:1, CH<sub>2</sub>N), 45.8, 45.5, 44.9 (ca. 2:1:1, NCH<sub>3</sub>), 25.5 (CCH<sub>3</sub>).

#### 2.2.4 Thermal decomposition of [Ti(OEt)<sub>3</sub>(bdmap)]

The experiment follows the procedure outlined by Gedanken (Pol, *et al.*, 2004). A 0.5 g of [Ti(OEt)<sub>3</sub>(bdmap)] was introduced into the Swagelok cell at room temperature in a nitrogen filled glove box. The filled cell was closed tightly with the two plugs and placed inside an iron pipe in the middle of a tube furnace. The temperature was raised at a rate of 10°C per minute to 700°C and held at that temperature for 1 hr. The Swagelok fitting was gradually cooled (1.5°C per minute) to room temperature (25°C). 0.12 g of a dark black powder was collected.

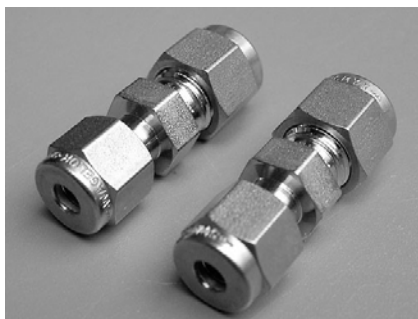


**Figure 11.** An overview of the Swagelok used for thermal decomposition.

### 2.2.5 CVD study

Films were grown using AACVD on glass microscope slides ( $76 \times 26 \times 1.0$  mm) under an inert atmosphere at 1 bar pressure, using a horizontal, cold-wall reactor. The reactor has been described in appendix A. The slides were cleaned prior to use by washing successively with water/detergent and acetone.  $[\text{Ti}(\text{OEt})_3(\text{bdmap})]_2$  (ca. 0.2 g) was dissolved in dry toluene (20 mL) and an aerosol generated using a domestic household humidifier. The aerosol was transported to the reactor using argon carrier gas ( $1.2 \text{ Lmin}^{-1}$ ). The glass substrate temperature was held at  $440^\circ\text{C}$ . The run time was 60 min.

### 2.2.6 Photocatalytic study

#### (1) Photoactivity of $\text{TiO}_2@\text{C}$ nanoparticles

The photocatalytic activities of the  $\text{TiO}_2@\text{C}$  nanoparticles were also evaluated by the degradation of methylene blue in an aqueous solution under UV light. An aqueous solution of MB ( $2.5 \times 10^{-5}$  M) and  $\text{TiO}_2$  were placed in the beaker (0.5 g of  $\text{TiO}_2$  per liter of MB solution). Prior to the illumination, the suspension was stirred for 30 min to allow for the dye adsorption onto the  $\text{TiO}_2$  surface. In all studies, the mixture was magnetically stirred, before and during illumination. At specific time intervals, 2 mL of the sample was sampled and centrifuged to remove  $\text{TiO}_2$  particles. The absorbance of MB in each degraded sample was observed from its characteristic at  $\lambda_{\text{max}}$  665 nm using a UV-Vis spectrophotometer. Controlled experiments without light and without  $\text{TiO}_2$  were performed to demonstrate that degradation of the dye was dependent on the presence of light and  $\text{TiO}_2$ . In addition, the photocatalytic activity between the  $\text{TiO}_2@\text{C}$  nanoparticles and the commercial  $\text{TiO}_2$  Degussa P25 from Degussa (Germany), Anatase from Carlo Erba (Italy), and Rutile from Dupont (U.S.A.) were also compared.

**(2) Photoactivity of thin films**

In the photocatalytic studies, the film slide was placed in a Petri dish (4 inch diameter) containing 50 ml of methylene blue solution ( $2.5 \times 10^{-5}$  M). Prior to the illumination, the system was kept for 30 min to allow for the dye adsorption onto the TiO<sub>2</sub> film. At given irradiation time intervals (every 1 hr), 2 mL of MB solution sample was collected. Controlled experiments without TiO<sub>2</sub> thin film coated and only MB solution were performed.

**(3) Calculation of decolorization**

The decolorization of dye solutions was calculated as follows:

$$\text{Decolorization} = (A_0 - A_t) / A_0 \times 100\%$$

$A_0$  and  $A_t$  are the maximum absorbance in visible area of the dye solution before and after irradiation

## CHAPTER 3

### RESULTS AND DISCUSSION

#### 3.1 Synthesis of nanocrystalline TiO<sub>2</sub> powders

##### 3.1.1 Physical properties of the synthesized TiO<sub>2</sub> powders

The X-ray diffraction patterns in Figure 12 illustrate the effect of type of acids (hydrolysis catalysts) on the phase formation of TiO<sub>2</sub>. The compositions of the synthesized Ti-no-acid, Ti-HCl, Ti-HNO<sub>3</sub>, and Ti-CH<sub>3</sub>COOH were mixtures of mainly amorphous TiO<sub>2</sub> with small amount of anatase and rutile phases. For the Ti-H<sub>2</sub>SO<sub>4</sub> and Ti-H<sub>3</sub>PO<sub>4</sub> (Figure 12(d) and 12(f)), the peaks are broad indicating low crystallinity of anatase phase. The possible mechanism for anatase and rutile phases formation will be discussed in Section 3.1.2. Summary of results obtained from the X-ray diffraction patterns are shown in Table 3.

**Table 3.** Comparison of TiO<sub>2</sub> powders prepared under various acid catalyzed conditions.

Samples	Crystallite size <sup>a</sup> (nm)	Crystallinity <sup>b</sup> (%)
Ti-no-acid	4.1 (A), 12.8 (R)	11 (A), 10 (R)
Ti-HCl	4.2 (A), 13.8 (R)	13 (A), 6 (R)
Ti-HNO <sub>3</sub>	4.7 (A), 13.6 (R)	15 (A), 13 (R)
Ti-H <sub>2</sub> SO <sub>4</sub>	4.1 (A)	15 (A)
Ti-CH <sub>3</sub> COOH	4.0 (A), 13.2 (R)	12 (A), 8 (R)
Ti-H <sub>3</sub> PO <sub>4</sub>	3.8 (A)	14 (A)
Anatase (Carlo Erba)	16.3 (A)	100 (A)
Rutile:R706 (Dupont)	42.7 (R)	100 (R)
P25 (Degussa)	10.2 (A), 42.7 (R)	80 (A), 20 (R) <sup>c</sup>

<sup>a</sup> Calculated from XRD data using Scherrer's formula. A denotes anatase and R denotes rutile.

<sup>b</sup> Determined by XRD using standard addition method, the rest is amorphous phase.

<sup>c</sup> Stylidi, *et al.*, 2004.



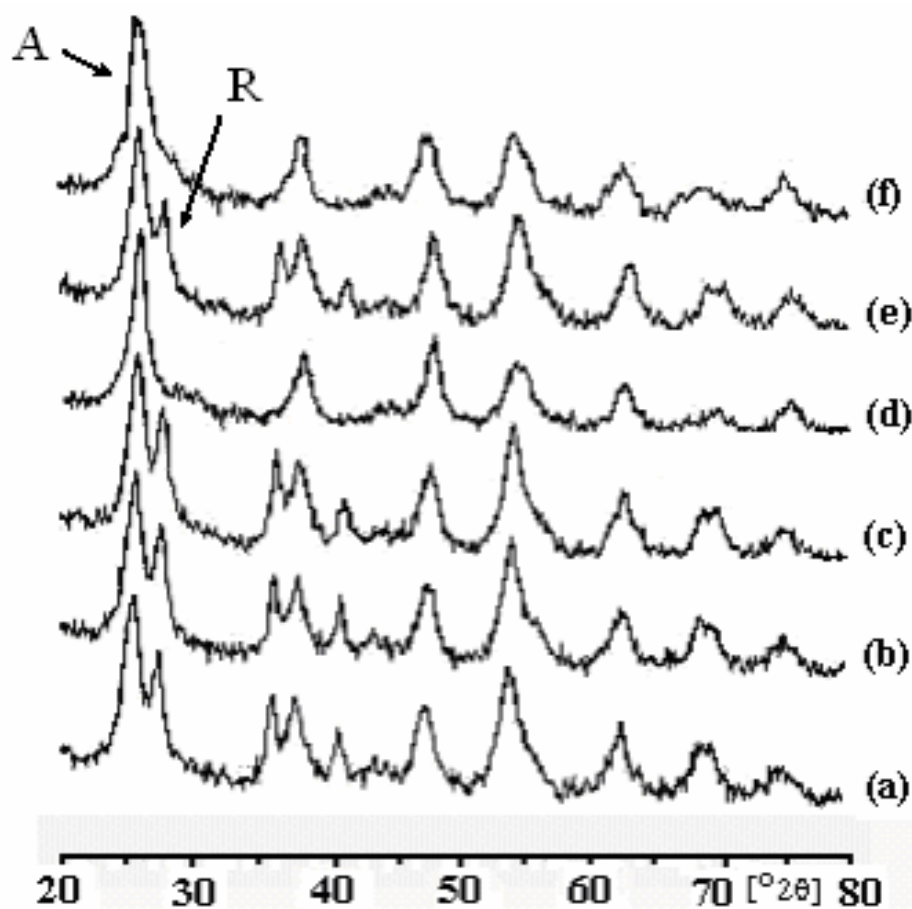


**Figure 12.** XRD patterns of the synthesized  $\text{TiO}_2$  powders (a) Ti-no-acid, (b) Ti-HCl, (c) Ti- $\text{HNO}_3$ , (d) Ti- $\text{H}_2\text{SO}_4$ , (e) Ti- $\text{CH}_3\text{COOH}$ , and (f) Ti- $\text{H}_3\text{PO}_4$ . A denotes anatase and R denotes rutile.

The degrees of crystallinity (the 3<sup>rd</sup> column in Table 3) of the samples were determined from the XRD intensities by using the standard addition method. The commercial titanium dioxide (anatase (Carlo Erba) and rutile (R706)) were mixed with the original synthesized titanium dioxide samples in different percent weight; 0, 10, 20, 40, and 60% and then measured the peak intensities. A calibration curve was made by plotting the total XRD-peak-intensity against the percentage of the added standard. The original percentage of anatase (or rutile) was obtained by the interception point on the percent weight axis. The curve of sample was shown in Figures 13-14.

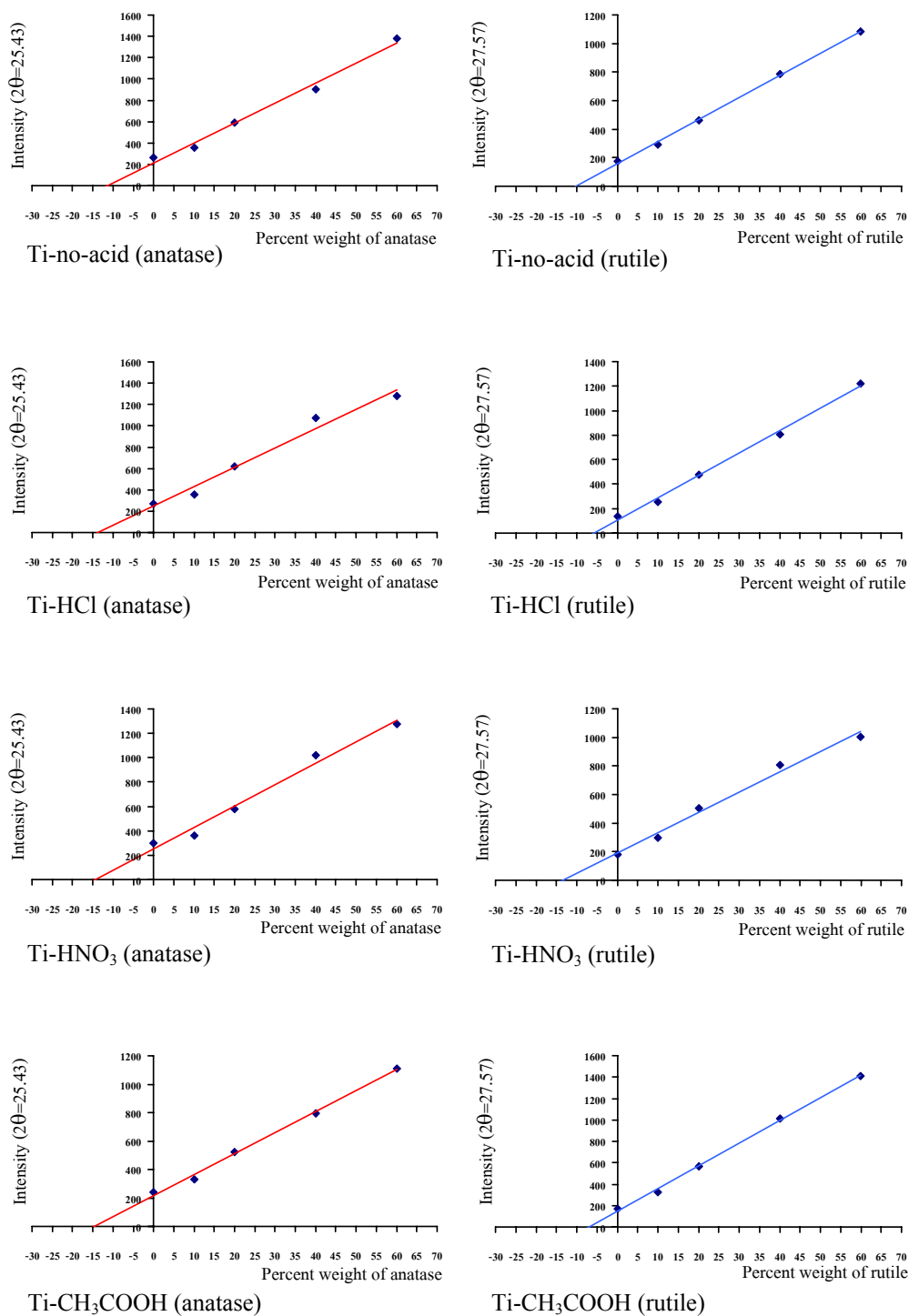


**Figure 13.** The standard addition calibration graphs of Ti-no-acid, Ti-HCl, Ti-HNO<sub>3</sub>, and Ti-CH<sub>3</sub>COOH.

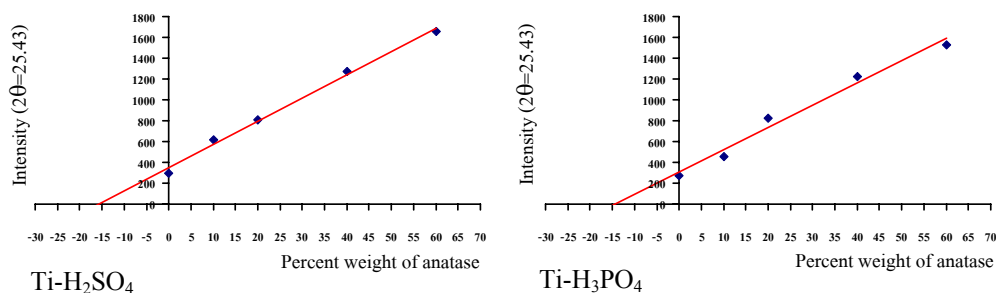


**Figure 14.** The standard addition calibration graphs of Ti-H<sub>2</sub>SO<sub>4</sub> and Ti-H<sub>3</sub>PO<sub>4</sub>.

The crystallite sizes of the samples were calculated using the peak at  $2\theta = 25.4^\circ$  and  $27.5^\circ$  for anatase and rutile phase, respectively, and are also shown in Table 3. The crystallite sizes of all the samples can be classified as nanocrystalline TiO<sub>2</sub> powders and are smaller than those of the commercial ones. When both anatase and rutile are present the anatase crystallite sizes are invariably smaller than rutile. This result is similar to the work reported by Gopal, *et al.*, (1997) where they found that anatase crystallite sizes were smaller than rutile in the mixed sample. That the Ti-H<sub>2</sub>SO<sub>4</sub> and Ti-H<sub>3</sub>PO<sub>4</sub> samples have the crystallite size smaller than the other products (Ti-no-acid, Ti-HCl, Ti-HNO<sub>3</sub>, and Ti-CH<sub>3</sub>COOH) could be the effect from the presence of sulphate and phosphate ions in the TiO<sub>2</sub> network as observed by Samantaray, *et al.*, (2003), and suggested that the sulphate ions could possibly interact with TiO<sub>2</sub> network and thus hinder the growth of the particles.

The infrared spectra of all the synthesized titanium dioxide powders in the range 4000-400 cm<sup>-1</sup> are shown in Figure 15. Table 4 lists the assigned modes of the functional groups that are responsible for the vibration bands in Figure 15.

The large broad band at 3600-3100 cm<sup>-1</sup> can be assigned to mixed  $\nu_{OH}$  and  $\nu_{NH}$  modes (stretching modes). These bands are in the hydroxyl stretching region and correspond to O-H vibration of the Ti-OH groups and H<sub>2</sub>O molecules. The band around 3500 cm<sup>-1</sup> can be assigned to O-H vibration of the Ti-OH groups (Velasco, *et al.*, 1999). The stretching vibration of O-H in Ti-OH bonding could not be removed easily and must be heated until relatively high temperature (Wang, *et al.*, 2000). Near the band around 3500 cm<sup>-1</sup>, a shoulder was generated by an asymmetric vibration

mode of the residual ammonium ions. The rather narrow bands around 1600 and 1400  $\text{cm}^{-1}$  can be assigned to  $\delta_{\text{OH}}$  and  $\delta_{\text{NH}}$  modes (bending modes) of hydroxyl (OH) and ammonium ( $\text{NH}_4^+$ ) groups, respectively (Khalil and Zaki, 1997; Youn, *et al.*, 1999). All of these bands indicated that  $\text{H}_2\text{O}$  and  $\text{NH}_4^+$  were present in the products. In the low energy region (below 800  $\text{cm}^{-1}$ ), the band due to stretching mode of Ti-O ( $\nu_{\text{Ti-O}}$ ) which was the envelope of the phonon bands of a Ti-O-Ti bond of a titanium oxide network could be assigned (Velasco, *et al.*, 1999). The absence of any bands in this spectral region may then suggest that the precipitate is amorphous.

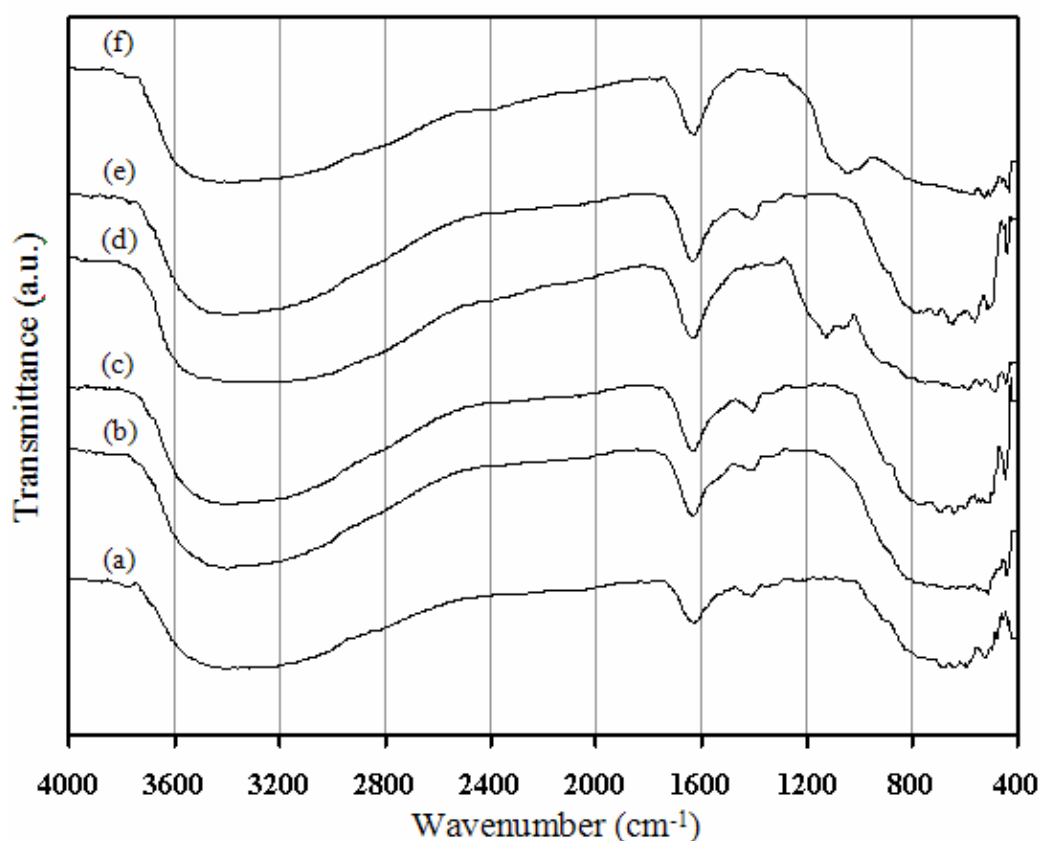


**Figure 15.** FT-IR spectra of the synthesized  $\text{TiO}_2$  powders: (a) Ti-no-acid, (b) Ti-HCl, (c) Ti- $\text{HNO}_3$ , (d) Ti- $\text{H}_2\text{SO}_4$ , (e) Ti- $\text{CH}_3\text{COOH}$ , and (f) Ti- $\text{H}_3\text{PO}_4$ .

Additionally, the spectrum of Ti-H<sub>2</sub>SO<sub>4</sub> in Figure 15d shows broad band at 1250-1100 cm<sup>-1</sup> which is the characteristic frequencies of SO<sub>4</sub><sup>2-</sup> group. The broad band in this region resulted from the lowering of the symmetry in the free SO<sub>4</sub><sup>2-</sup> (Td point group) to either C<sub>2v</sub> (Figure 22B) or C<sub>3v</sub> (Figure 22A and 22C) when SO<sub>4</sub><sup>2-</sup> is bound to the titania surface (Samantaray, *et al.*, 2003; Nakamoto, 1986). The vibrational modes of the PO<sub>4</sub><sup>3-</sup> anion in the sample Ti-H<sub>3</sub>PO<sub>4</sub> are also detected in the IR spectrum (Figure 2f) where the asymmetric ν<sub>P-O</sub> stretching mode appears at 1015 cm<sup>-1</sup> (Bazán, *et al.*, 2003). The results from XRD and FT-IR led to the conclusion that samples were a hydrated amorphous titanium dioxide with minute amount of impurities, such as NH<sub>4</sub><sup>+</sup>, SO<sub>4</sub><sup>2-</sup>, and PO<sub>4</sub><sup>3-</sup>.

**Table 4.** Assignment of the FT-IR bands of titanium dioxide samples (Figure 15).

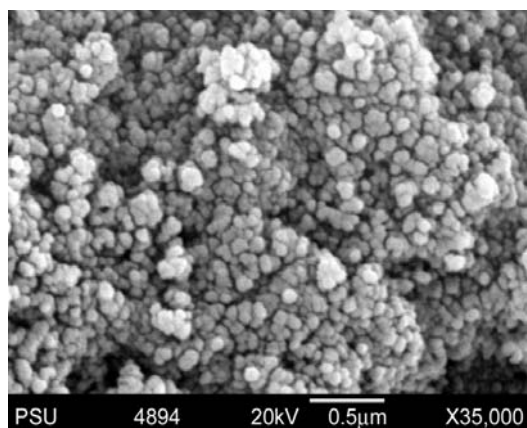
Samples	Wavenumber (cm <sup>-1</sup> )	Assignment	Functional groups /molecule	Literatures
a-f	3600 - 3100	ν <sub>OH</sub> and ν <sub>NH</sub>	H <sub>2</sub> O and NH <sub>4</sub> <sup>+</sup>	Khalil and Zaki, 1997 Youn, <i>et al.</i> , 1999
a-f	~1600	δ <sub>OH</sub>	OH groups	Khalil and Zaki, 1997 Youn, <i>et al.</i> , 1999
a, b, c, and e	~1400	δ <sub>NH</sub>	NH <sub>4</sub> <sup>+</sup> groups	Khalil and Zaki, 1997 Youn, <i>et al.</i> , 1999
a-f	Below 800	ν <sub>Ti-O</sub>	Ti-O bond	Velasco, <i>et al.</i> , 1999
d	1200-1100	ν <sub>S-O</sub>	SO <sub>4</sub> <sup>2-</sup>	Samantaray, <i>et al.</i> , 2003
f	1015	ν <sub>P-O</sub>	PO <sub>4</sub> <sup>3-</sup>	Bazán, <i>et al.</i> , 2003.

(a) Ti-no-acid, (b) Ti-HCl, (c) Ti-HNO<sub>3</sub>, (d) Ti-H<sub>2</sub>SO<sub>4</sub>, (e) Ti-CH<sub>3</sub>COOH, and (f) Ti-H<sub>3</sub>PO<sub>4</sub>

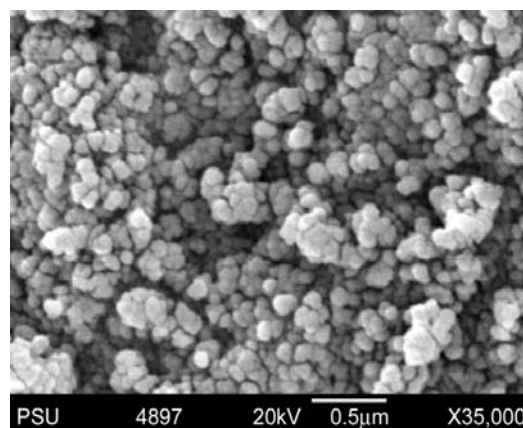
**Table 5.** Specific surface area of TiO<sub>2</sub> powders.

Samples	Specific surface area (m <sup>2</sup> /g)	
	This work	Literatures
Ti-no-acid	194.7	-
Ti-HCl	192.8	-
Ti-HNO <sub>3</sub>	196.6	-
Ti-H <sub>2</sub> SO <sub>4</sub>	220.6	-
Ti-CH <sub>3</sub> COOH	212.1	-
Ti-H <sub>3</sub> PO <sub>4</sub>	308.5	-
Anatase (Carlo Erba)	7.6	5.9 (Sclafani, <i>et al.</i> , 1990)
Rutile:R706 (Dupont)	9.9	-
P25 (Degussa)	51.4	50 (Neppolian, <i>et al.</i> , 2002)

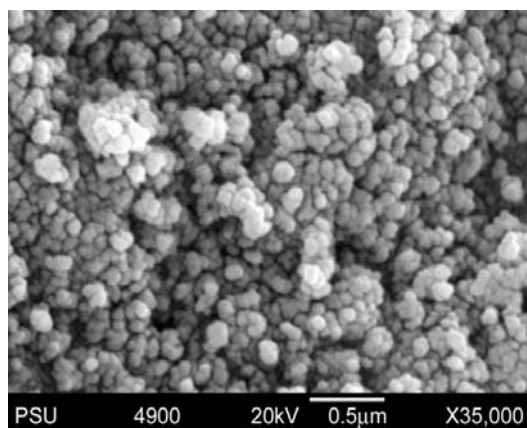
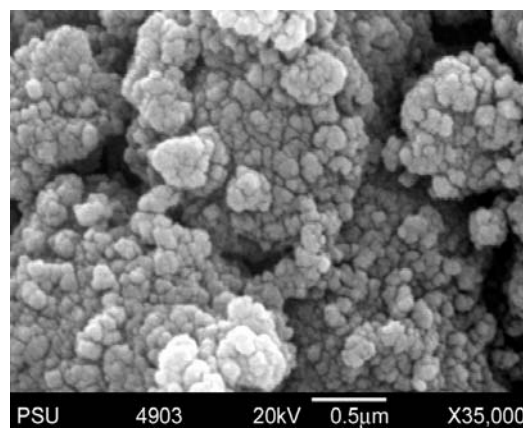
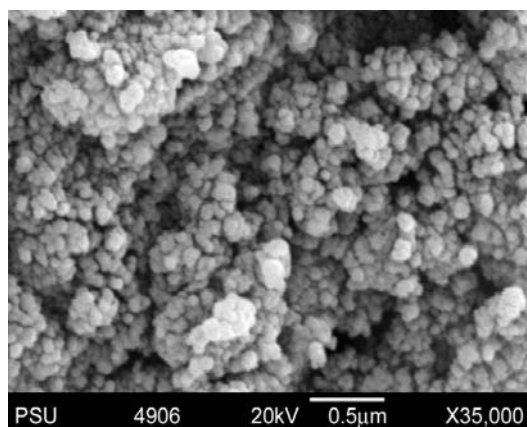
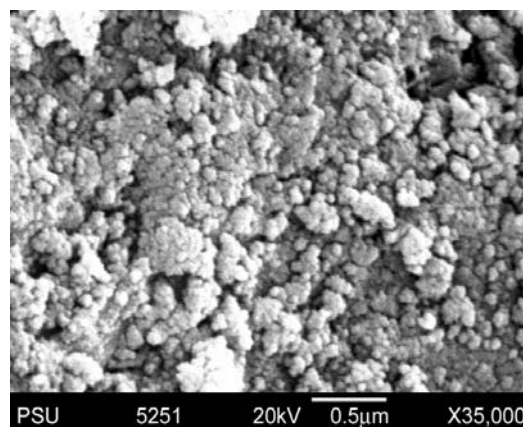
The specific surface areas of samples are also shown in Table 5. The data were compared between the synthesized TiO<sub>2</sub> and the commercial TiO<sub>2</sub>. All the synthesized titanium dioxide samples exhibited higher surface area than the commercial ones due to lower crystallinity of the synthesized samples without calcination in this work. Among the synthesized samples, both Ti-H<sub>2</sub>SO<sub>4</sub> and Ti-H<sub>3</sub>PO<sub>4</sub> exhibited higher surface area than Ti-no-acid, Ti-HCl, Ti-HNO<sub>3</sub>, and Ti-CH<sub>3</sub>COOH. This result agrees with those in the reports that the surface area of sulfated-titania was higher than that of pure TiO<sub>2</sub> (Gómez, *et al.*, 2003) and the nanosized TiO<sub>2</sub> prepared in the presence of sulfate ion had higher BET surface than those prepared in the absence of sulfate ion (Zhang, *et al.*, 2000). The values of surface area of all these commercial TiO<sub>2</sub> came out similar to those given in literatures. Data in 3<sup>rd</sup> column of Table 3 are examples of such literature values.



(a) Ti-no-acid



(b) Ti-HCl

(c) Ti-HNO<sub>3</sub>(d) Ti-H<sub>2</sub>SO<sub>4</sub>(e) Ti-CH<sub>3</sub>COOH(f) Ti-H<sub>3</sub>PO<sub>4</sub>

**Figure 16.** SEM images of the synthesized TiO<sub>2</sub> powders: (a) Ti-no-acid, (b) Ti-HCl, (c) Ti-HNO<sub>3</sub>, (d) Ti-H<sub>2</sub>SO<sub>4</sub>, (e) Ti-CH<sub>3</sub>COOH, and (f) Ti-H<sub>3</sub>PO<sub>4</sub>.

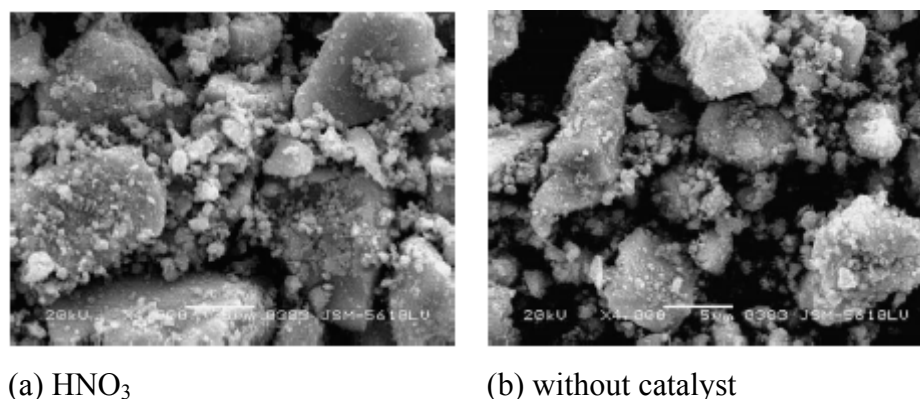
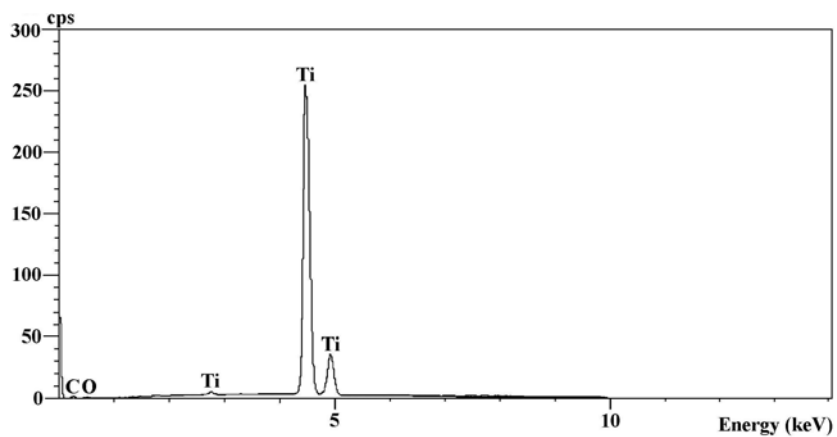


**Figure 17.** SEM images of TiO<sub>2</sub> reported by Yu, *et al.*, (2003).

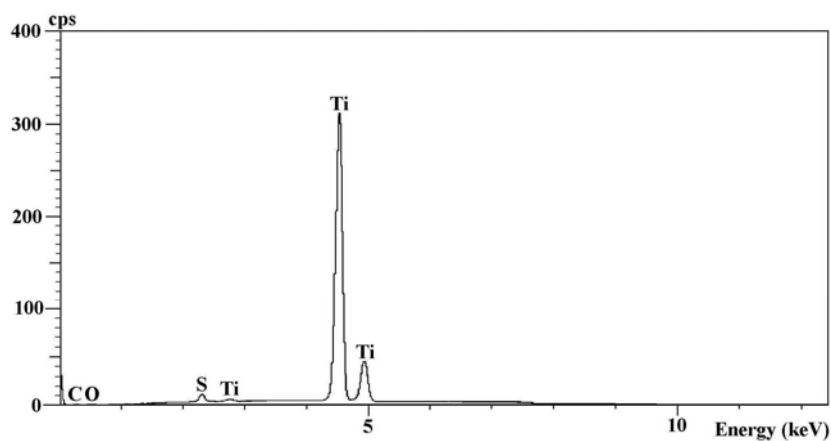
Figure 16 shows SEM images of TiO<sub>2</sub> powders prepared under various acid catalysts. From the SEM images, magnified by 35,000 $\times$ , the images show delicate structures of spherical shape particles. The images of Ti-no-acid, Ti-HCl, Ti-HNO<sub>3</sub>, and Ti-CH<sub>3</sub>COOH samples appear as dense and uniform structures with fewer aggregation of particles. For the Ti-H<sub>2</sub>SO<sub>4</sub> and Ti-H<sub>3</sub>PO<sub>4</sub> samples, the dense and non-uniform structure with higher aggregation (than the Ti-no-acid, Ti-HCl, Ti-HNO<sub>3</sub>, and Ti-CH<sub>3</sub>COOH samples) were observed. From SEM images of this study, it could be seen that the difference in the morphology could be ascribed to different preparation conditions, especially the hydrolysis catalyst which may affect the aggregation of each sample.

The morphology of this work are similar to the results of Yu, *et al.*, (2003) who investigated the effect of acidic and basic hydrolysis catalysts on the photocatalytic activity and microstructure of titanium dioxide prepared by sol-gel process. Their results (Figure 17) showed that the morphology of titanium dioxide prepared by the hydrolysis of titanium tetraisopropoxide at pH 6.8 and without using HNO<sub>3</sub> as catalyst appears as a dense structure and fewer in aggregation.

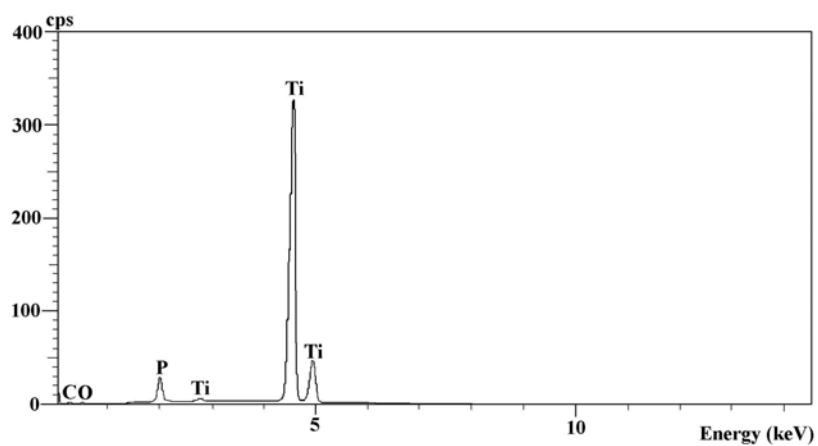




(a) Ti-no-acid, Ti-HCl, Ti-HNO<sub>3</sub>, and Ti-CH<sub>3</sub>COOH



(b) Ti-H<sub>2</sub>SO<sub>4</sub>



(c) Ti-H<sub>3</sub>PO<sub>4</sub>

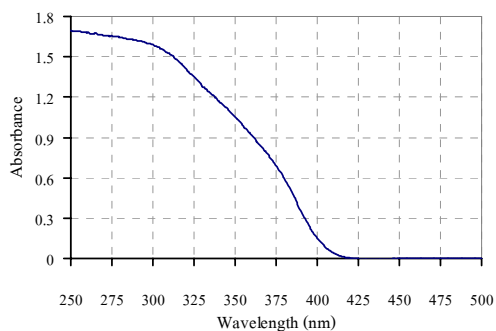
**Figure 18.** EDX spectra of the synthesized TiO<sub>2</sub> powders: (a) Ti-no-acid, Ti-HCl, Ti-HNO<sub>3</sub>, Ti-CH<sub>3</sub>COOH, (b) Ti-H<sub>2</sub>SO<sub>4</sub>, and (c) Ti-H<sub>3</sub>PO<sub>4</sub>.

Figure 18 shows EDX patterns of TiO<sub>2</sub> powders prepared under various acid catalysts. The EDX results revealed that, with the exception of two samples, all powder samples did not contain chloride anion which indicated that it was washed out completely at the washing stage. However, the samples obtained from using sulfuric acid and phosphoric acid showed the presence of S and P indicating the SO<sub>4</sub><sup>2-</sup> and PO<sub>4</sub><sup>3-</sup> ions still adhered to the titanium dioxide surfaces which agreed with the FT-IR results.

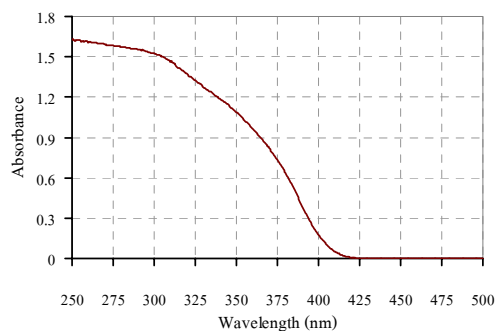
The diffuse reflectance UV-Vis spectra of synthesized and commercial titanium dioxide are shown in Figure 19 and 20, respectively. The absorption edge can be approximated by the intersection of two straight lines: a straight line extrapolated from the baseline, and a line drawn through the ascending slope of the onset of absorption (Chandler, *et al.*, 1993). The band gap energies of the titanium dioxide calculated from Plank's equation are shown in Table 6.

The absorption edges of Ti-no-acid, Ti-HCl, Ti-HNO<sub>3</sub>, and Ti-CH<sub>3</sub>COOH appear at longer wavelength than that of Ti-H<sub>3</sub>PO<sub>4</sub> and Ti-H<sub>2</sub>SO<sub>4</sub>. In the case of commercial TiO<sub>2</sub>, the absorption edge of rutile (R706) appears at longer wavelength than that of anatase (Carlo Erba). The absorption edge wavelengths of commercial titanium dioxide are in order of rutile (R706) > Degussa P25 > anatase (Carlo Erba). The bandgap energies, calculated using Planck's equation, of rutile (R706), Degussa P25, and anatase (Carlo Erba) are 3.00, 3.14, and 3.22 eV, respectively, which are identical to the literature values of 3.00, 3.14, and 3.20 eV (Miao, *et al.*, 2003; Zielińska, *et al.*, 2003).

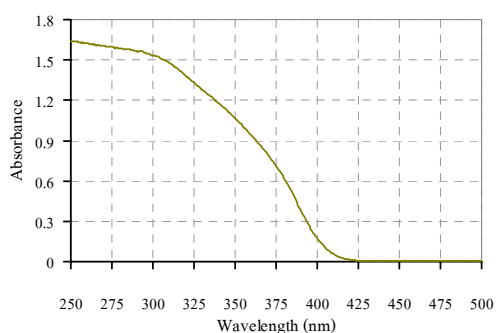
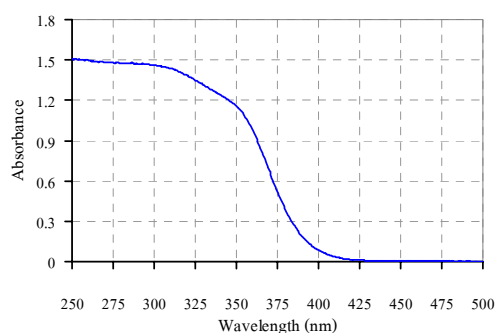
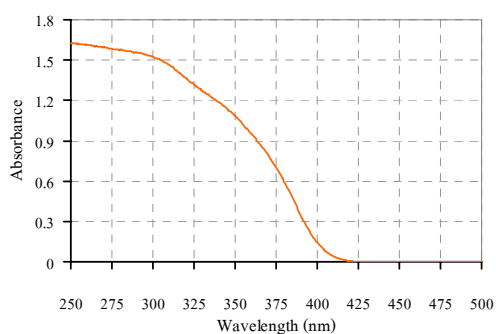
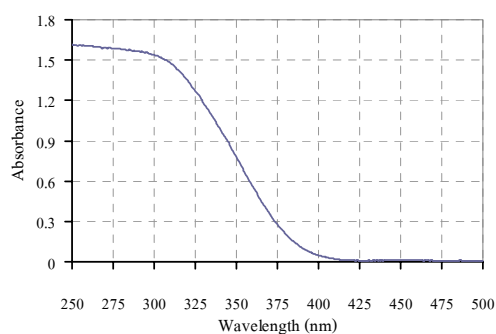
The bandgap energies of Ti-no-acid, Ti-HCl, Ti-HNO<sub>3</sub>, and Ti-CH<sub>3</sub>COOH are slightly larger than rutile (R706). Both Ti-H<sub>3</sub>PO<sub>4</sub> and Ti-H<sub>2</sub>SO<sub>4</sub> have larger bandgap energy and are in the same range of anatase (Carlo Erba).



(a) Ti-no-acid



(b) Ti-HCl

(c) Ti-HNO<sub>3</sub>(d) Ti-H<sub>2</sub>SO<sub>4</sub>(e) Ti-CH<sub>3</sub>COOH(f) Ti-H<sub>3</sub>PO<sub>4</sub>

**Figure 19.** Diffuse reflectance UV-Vis spectra of the synthesized TiO<sub>2</sub> powders: (a) Ti-no-acid, (b) Ti-HCl, (c) Ti-HNO<sub>3</sub>, (d) Ti-H<sub>2</sub>SO<sub>4</sub>, (e) Ti-CH<sub>3</sub>COOH, and (f) Ti-H<sub>3</sub>PO<sub>4</sub>.

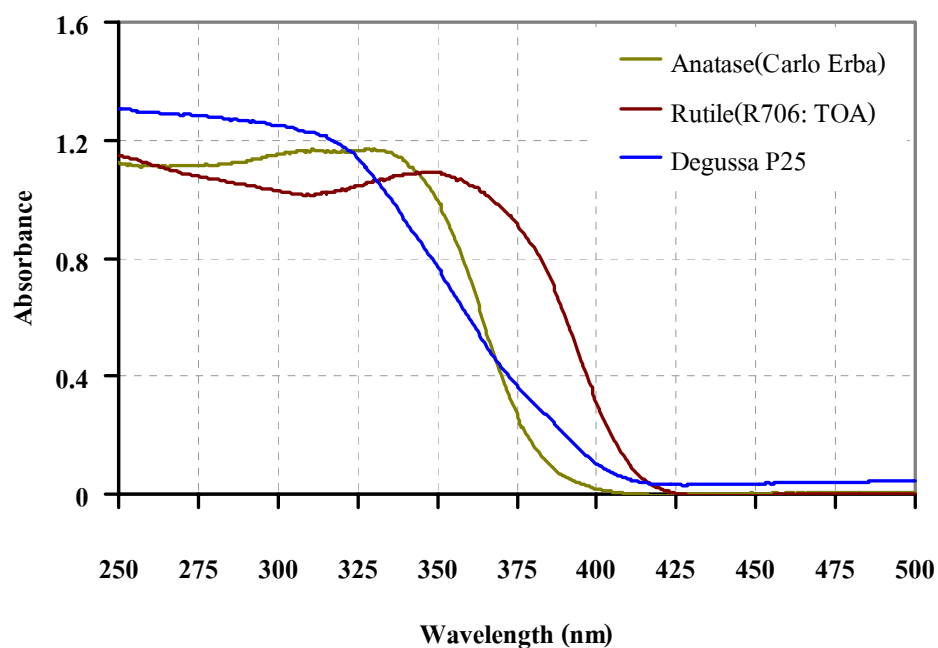


**Figure 20.** Diffuse reflectance UV-Vis spectra of the commercial TiO<sub>2</sub> powders.

**Table 6.** The absorption edges and band gap energies of titanium dioxide powders.

Samples	Absorption edge (nm)	Bandgap energy (eV)	
		This work	Literatures
Ti-no-acid	408	3.04	-
Ti-HCl	405	3.06	-
Ti-HNO <sub>3</sub>	406	3.05	-
Ti-H <sub>2</sub> SO <sub>4</sub>	390	3.18	-
Ti-CH <sub>3</sub> COOH	406	3.05	-
Ti-H <sub>3</sub> PO <sub>4</sub>	386	3.21	-
Anatase (Carlo Erba)	385	3.22	3.20 <sup>a</sup>
Rutile-R706 (TOA)	413	3.00	3.00 <sup>a</sup>
P25 (Degussa)	395	3.14	3.14 <sup>b</sup>

<sup>a</sup> Sclafani, *et al.*, 1990; Miao, *et al.*, 2003

<sup>b</sup> Zielińska, *et al.*, 2003

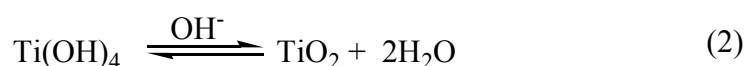
### 3.1.2 The possible mechanism for anatase and rutile TiO<sub>2</sub> formation

The sol-gel method consists of the hydrolysis and condensation reactions which are catalysed in the presence of acid. The hydrolysis reaction leads to the formation of original nuclei or basic units of titanium dioxide while the condensation reaction leads to the growth of network system of the original basic units (Kumar, *et al.*, 1999).

The hydrolysis reaction (eq.1)



The condensation reaction (eq.2)



The product powders obtained in this work were mixtures of amorphous TiO<sub>2</sub>, anatase, and rutile. The amorphous phase was dominant with small amount of anatase or mixed anatase and rutile (see the 3<sup>rd</sup> column in Table 3). The key to the differences in anatase and rutile formation stems from the structure of the two polymorphs. In rutile, two opposite edges of each (TiO<sub>6</sub><sup>2-</sup>) octahedra are shared forming a linear chain along the (001) direction. Chains are then linked to each other by sharing corner oxygen atoms. Anatase has no corner sharing, but has four edges shared per octahedron. The anatase structure can be viewed as zigzag chains of octahedra, linked to each other through shared edges (Gopal, *et al.*, 1997).

There have been reported that excellently discussed the possible mechanism of the anatase and rutile formations (Gopal, *et al.*, 1997; Yanqing, *et al.*, 2001). The basic unit of (TiO<sub>6</sub><sup>2-</sup>) octahedra in solution can join together to form oligomers which are the growth units leading to both anatase and rutile phases. The joining of the basic octahedra unit if takes place at the opposite edges will give a growth unit for the rutile phase, however, if it takes place at the non-opposite edges will give a growth unit for the anatase phase (and possibly the brookite phase, too).

The (TiO<sub>6</sub><sup>2-</sup>) octahedra in this system can be written in full as [TiO(H<sub>2</sub>O)<sub>5</sub>]<sup>2+</sup> or [Ti(OH)<sub>2</sub>(H<sub>2</sub>O)<sub>4</sub>]<sup>2+</sup> ion. In fact, the initial complex species first formed in the hydrolysis should be [Ti(H<sub>2</sub>O)<sub>6</sub>]<sup>4+</sup> which, due to its acidic nature, would

undergo the first deprotonation to  $[\text{Ti}(\text{OH})(\text{H}_2\text{O})_5]^{3+}$  and subsequently through the second deprotonation yielding the dipositive ions as  $[\text{TiO}(\text{H}_2\text{O})_5]^{2+}$  or  $[\text{Ti}(\text{OH})_2(\text{H}_2\text{O})_4]^{2+}$  ion. The latter is probably more preferred based on the evidence reported that both forms co-existed in the solution and in the oligomers growth unit no titanyl (Ti=O) moiety was found so  $[\text{TiO}(\text{H}_2\text{O})_5]^{2+}$  ion was not the basic unit growing into oligomers (Comba and Merbach, 1987). This leaves the  $[\text{Ti}(\text{OH})_2(\text{H}_2\text{O})_4]^{2+}$  as the most likely basic unit. However, the two hydroxyl (OH) groups in this complex basic unit can take two geometrical sites: *cis* and *trans* with respect to one another. In the previously proposed diagram only the *trans* isomer was demonstrated (Yanqing, *et al.*, 2001). In our opinion, the *cis* isomer cannot be left out due to existence of many examples of titanium complexes having two bridging Ti-O moieties in *cis* positions (Cotton and Wilkinson, 1988). The *cis* isomer can grow into larger unit in the same way as the *trans* isomer. The growing of the *cis* isomer can be shown in Figure 21.

At pH~7, the precipitation occurred quite rapidly resulting in low crystallinity, hence, the precipitate mostly appeared in the amorphous form with small amount of anatase and rutile mixed in as shown in Table 3. This behavior had been earlier mentioned in other reports (Gopal, *et al.*, 1997; Bartlett, *et al.*, 1992; Wang, *et al.*, 1992). In this work, the amount of anatase was slightly higher than the rutile in most cases. This may reflect the statistical probability when the basic unit octahedra joined together, sharing other edges leading to anatase has more chances than joining the opposite edge to form rutile.

In the case of adding  $\text{H}_2\text{SO}_4$  and  $\text{H}_3\text{PO}_4$  acids, the products yielded mainly amorphous and only the anatase phase as a minor component. The rutile phase was completely absence in these two cases. The sulfate and phosphate anions both have high negative charge, -2 and -3, respectively. The attraction forces between the  $\text{Ti}^{4+}$  ion and  $\text{SO}_4^{2-}$  or  $\text{PO}_4^{3-}$  are strong so these anions will be bonded to Ti basic unit easily ( the strong attraction is evidenced in the EDX spectra with the characteristic peaks of S and P and FT-IR spectra with the characteristic vibration of the sulphate and phosphate groups on  $\text{TiO}_2$  ). Since both  $\text{SO}_4^{2-}$  and  $\text{PO}_4^{3-}$  have tetrahedral geometry with the negative ends at the oxygen atoms where they can bond to Ti octahedra in three ways as shown in Figure 22. Among the three modes of bonding,

the bidentate and tridentate, Figures 22(B) and 22(C), respectively, are favored due to the well known *chelate effect*. The bonding of  $\text{SO}_4^{2-}$  in these multidentate modes occupy one full face of octahedra and inhibit the growing of chain along the opposite edges as illustrated in Figure 23 and hence inhibit the formation of rutile. The same argument can be applied to  $\text{PO}_4^{3-}$  as well. Therefore, the addition of these two acids yielded only the anatase form, in the mixture with the amorphous form, as shown in Table 3. Our results here are in agreement with other reports that the presence of  $\text{SO}_4^{2-}$  ion helped promote formation of anatase phase (Zhang, *et al.*, 1999; Samantaray, *et al.*, 2003; Xie, *et al.*, 2002).

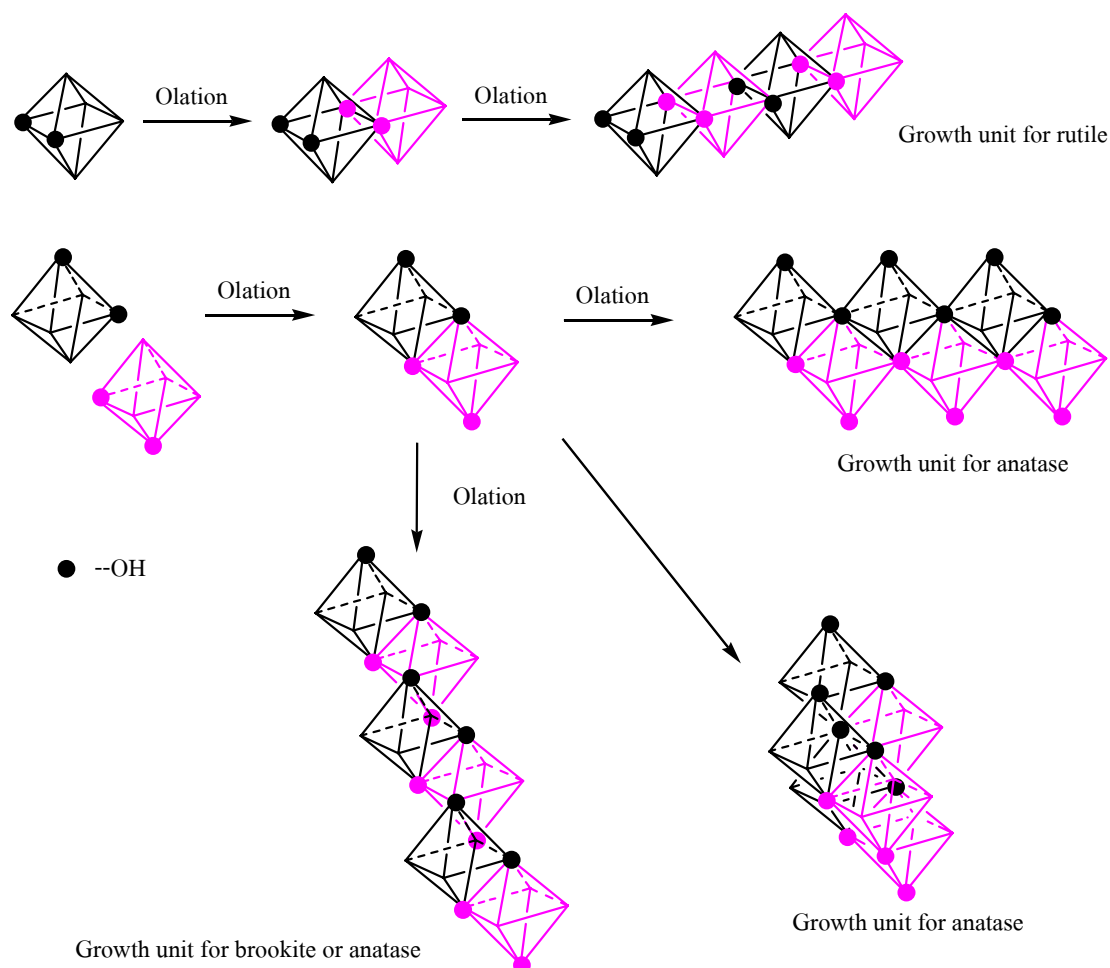


**Figure 21.** Formation of growth units from  $\text{cis-}[\text{Ti}(\text{OH})_2(\text{H}_2\text{O})_4]^{2+}$  ion.

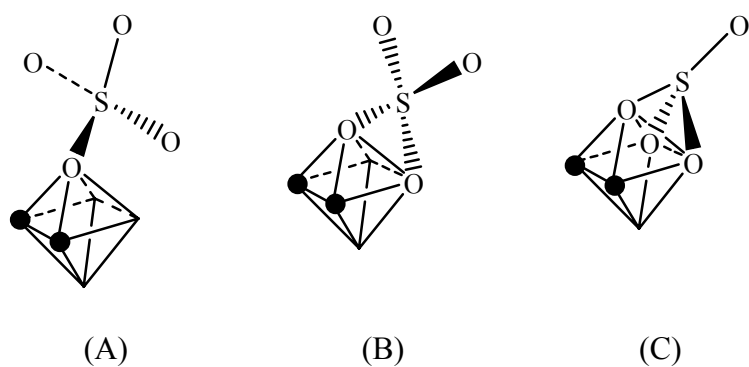


**Figure 22.** Bonding mode of  $\text{SO}_4^{2-}$  anion as, (A) monodentate, (B) bidentate, and (C) tridentate ligand (● indicates OH position).

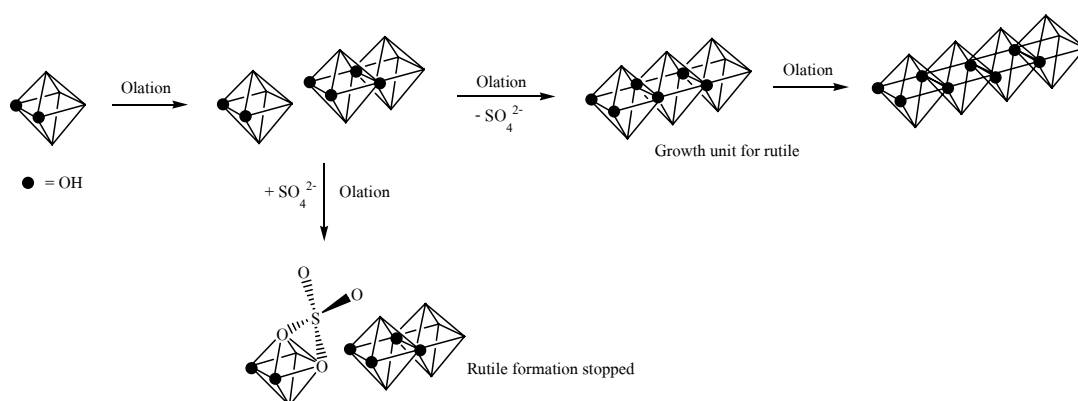


**Figure 23.** Possible pathway to inhibit the formation of rutile by  $\text{SO}_4^{2-}$ .



### 3.1.3 Photocatalytic study

#### 3.1.3.1 Test for photocatalytic activity

Three dyes (methylene blue, congo red, and crystal violet) were separately degraded in the presence of TiO<sub>2</sub> photocatalyst in the form of suspension by irradiation with UV light of black light tube. A blank experiment in the absence of UV light irradiation illustrated the rapid attainment of adsorption equilibrium of the dyes onto titanium dioxide. The adsorption was quite fast and the equilibrium adsorption was reached within 30 min. The contact was carried out up to 330 min, but no significant change in the absorption was observed.

The equilibrium time used in this work was 30 min in accordance with what had been reported by other researchers. For instance, Zielińska, *et al.*, (2003) used 15 min for adsorption dyes (Reactive Red 198, Acid Black 1, Acid Blue 7, and Direct Green 99) onto the TiO<sub>2</sub> surface; Gonçalves, *et al.*, (2005) mixed the dye solution (Reactive Orange 4) and catalyst in the dark for 30 min to equilibrate; and Kumar, *et al.*, (2005) selected 15 min in the dark to allow equilibration of adsorption of two dye (chromotrope 2B and amido black 10B) on TiO<sub>2</sub> before irradiation, and so on.

The percentage of decolorization on irradiation of aqueous solutions of dyes are shown in Figures 26-31. It can be seen from the figures that all the synthesized TiO<sub>2</sub> powders and two commercial TiO<sub>2</sub> samples: Degussa P25 and anatase (Carlo Erba) decolorized the dye solutions upon irradiation with UV-light. The commercial TiO<sub>2</sub> in rutile phase (R706, TOA) had no effect on the dye solutions. (The rutile result agrees what has been reported by other reports. Its lack of photocatalytic activity has been known for some times. It is shown here merely for the completeness of the systematic studies and further discussion is not necessary.) Moreover, either TiO<sub>2</sub> or UV-light had very little effect when each was used separately. These experiments demonstrated that both UV-light and a photocatalyst, such as TiO<sub>2</sub>, were needed for the effective decolorization of dye. This is due to the fact that when TiO<sub>2</sub> is illuminated with the light of energy equal or higher than the band gap energy the electron-hole pairs are produced.

The UV source used in this work was the 20 watts blacklight tube which emits UV light in the range 346-395 nm with maximum at 366 nm (Figure 24). The pathway of dye degradation composed of several chemical steps (Houas, *et al.*, 2001) which can be summarized in a compact diagram (Figure 25) as follows.

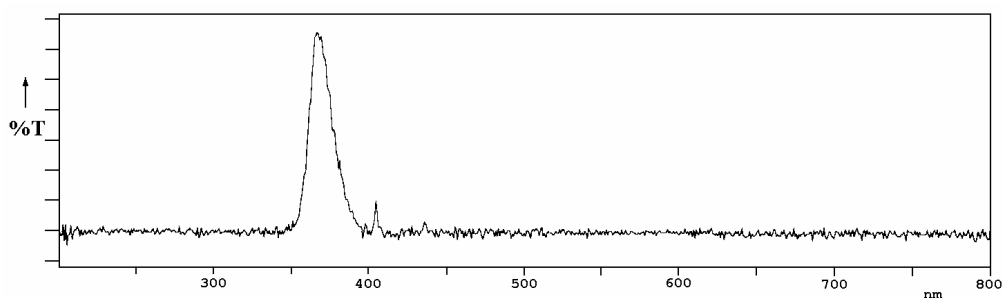


**Figure 24.** Spectrum of UV-light source used in this work (Random, *et al.*, 2004).

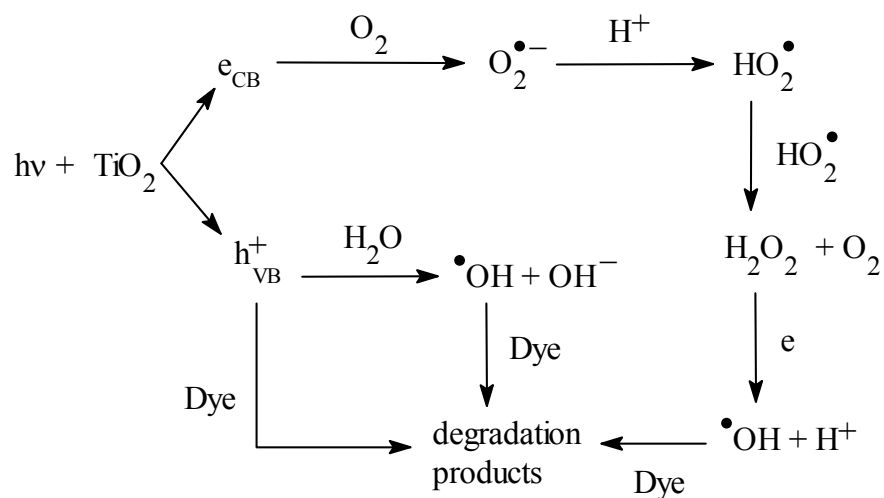
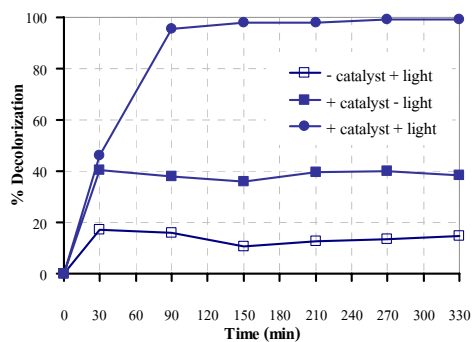
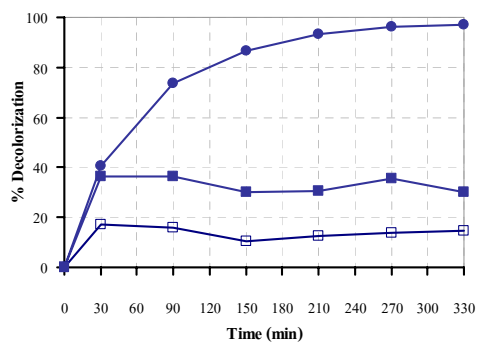


**Figure 25.** Pathway of dye degradation by  $\text{TiO}_2$ .

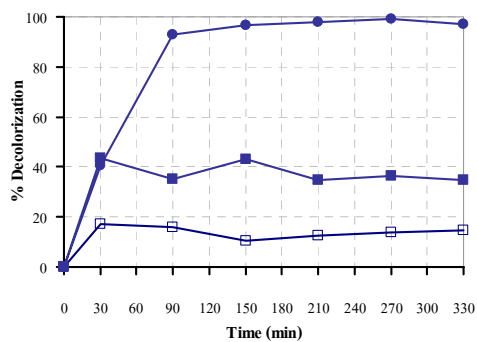
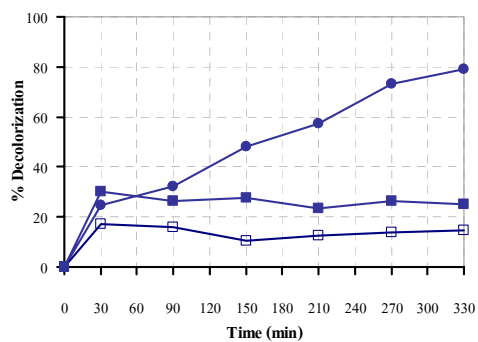
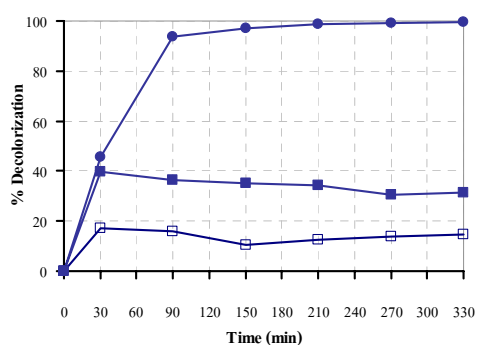
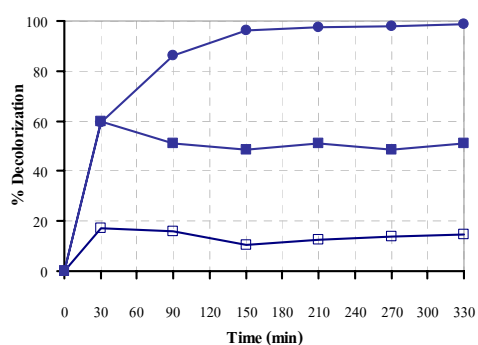
In the most recent report by Hirakawa, *et al.*, (2007) it was shown that pure anatase and a mixture of anatase and a small amount of rutile efficiently generated  $\text{OH}^{\bullet}$  radicals in the photocatalytic process while the amount of  $\text{OH}^{\bullet}$  radicals generated was extremely low with pure rutile.



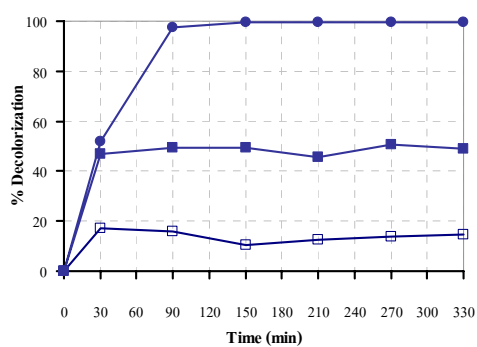
(a) Ti-no-acid



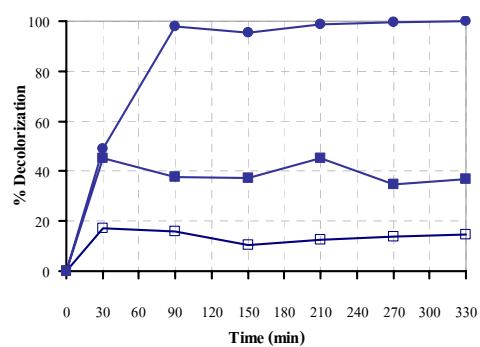
(b) Ti-HCl

(c) Ti-HNO<sub>3</sub>(d) Ti-H<sub>2</sub>SO<sub>4</sub>(e) Ti-CH<sub>3</sub>COOH(f) Ti-H<sub>3</sub>PO<sub>4</sub>

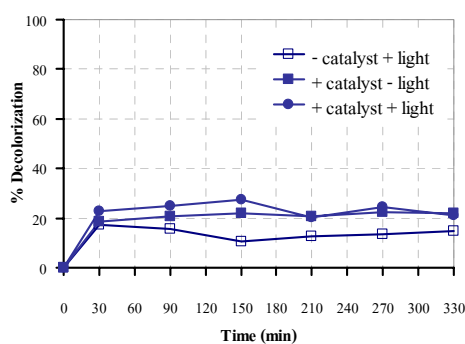
**Figure 26.** Decolorization of MB solution at  $1 \times 10^{-5}$  M as a function of time in the presence of synthesized TiO<sub>2</sub>: (a) Ti-no-acid, (b) Ti-HCl, (c) Ti-HNO<sub>3</sub>, (d) Ti-H<sub>2</sub>SO<sub>4</sub>, (e) Ti-CH<sub>3</sub>COOH, and (f) Ti-H<sub>3</sub>PO<sub>4</sub>.



(a) Degussa P25

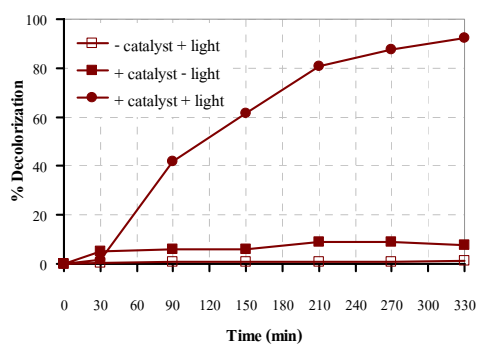


(b) Anatase (Carlo Erba)

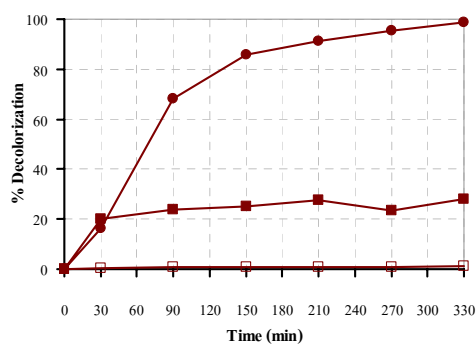


(c) Rutile (R706, TOA)

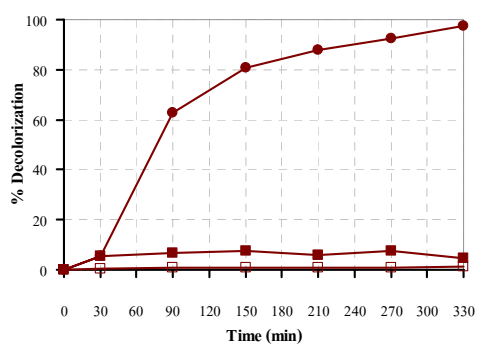
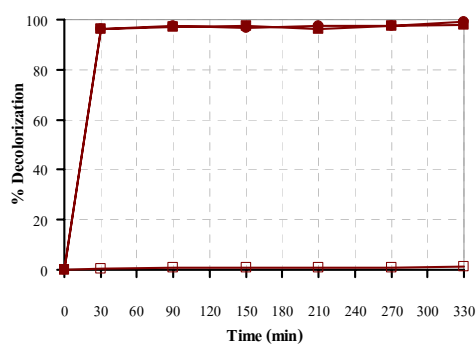
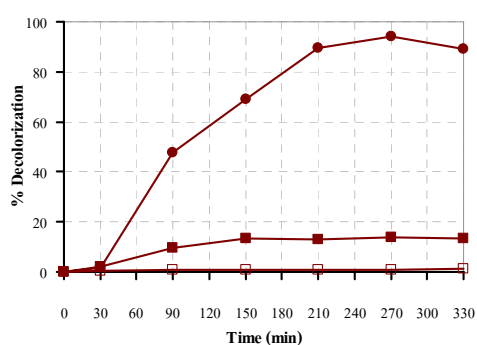
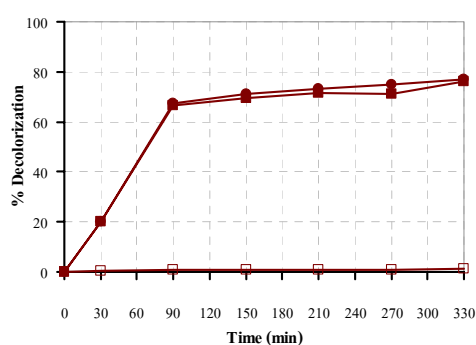
**Figure 27.** Decolorization of MB solution at  $1 \times 10^{-5}$ M as a function of time in the presence of commercial  $\text{TiO}_2$ : (a) Degussa P25, (b) anatase (Carlo Erba), and (c) rutile (R706, TOA).



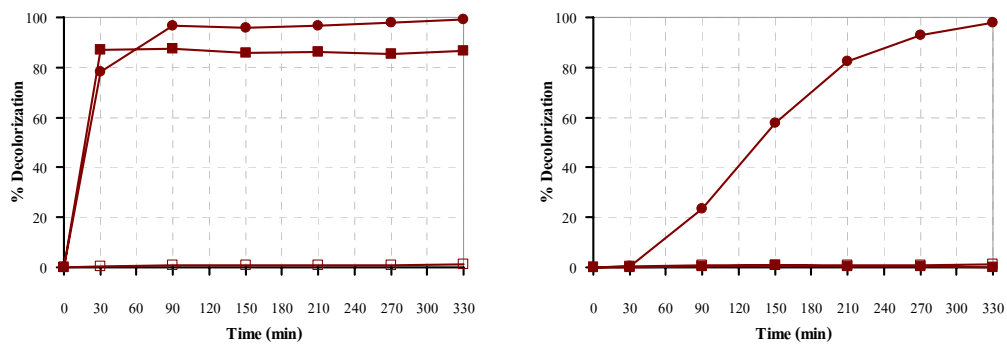
(a) Ti-no-acid



(b) Ti-HCl

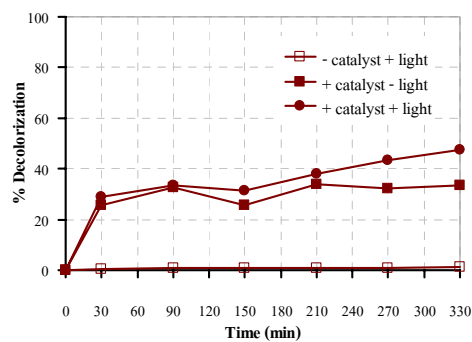
(c) Ti-HNO<sub>3</sub>(d) Ti-H<sub>2</sub>SO<sub>4</sub>(e) Ti-CH<sub>3</sub>COOH(f) Ti-H<sub>3</sub>PO<sub>4</sub>

**Figure 28.** Decolorization of CR solution at  $1 \times 10^{-5}$ M as a function of time in the presence of synthesized TiO<sub>2</sub>: (a) Ti-no-acid, (b) Ti-HCl, (c) Ti-HNO<sub>3</sub>, (d) Ti-H<sub>2</sub>SO<sub>4</sub>, (e) Ti-CH<sub>3</sub>COOH, and (f) Ti-H<sub>3</sub>PO<sub>4</sub>.



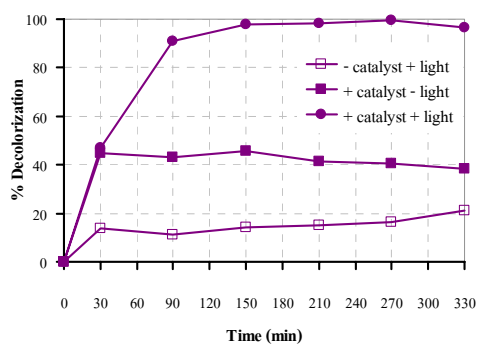
(a) Degussa P25

(b) Anatase (Carlo Erba)

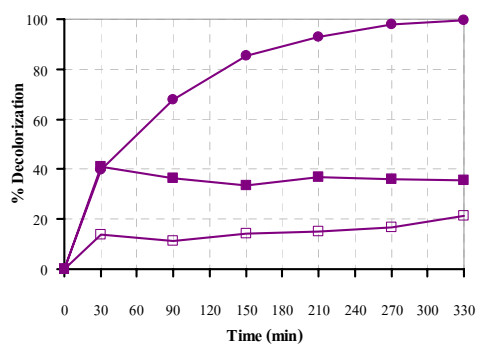


(c) Rutile (R706, TOA)

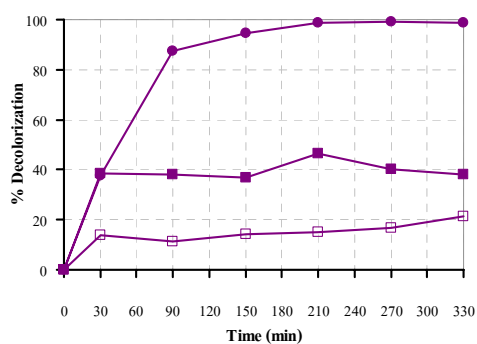
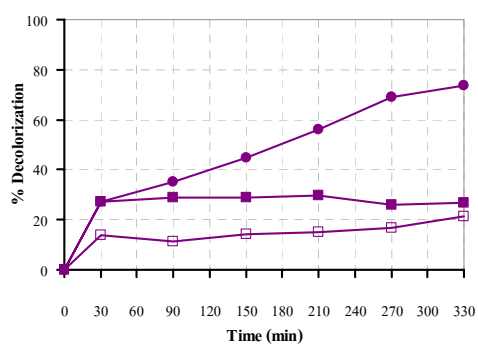
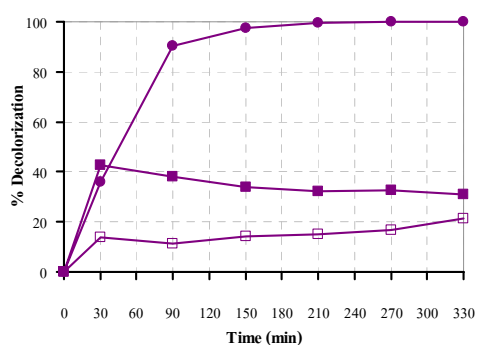
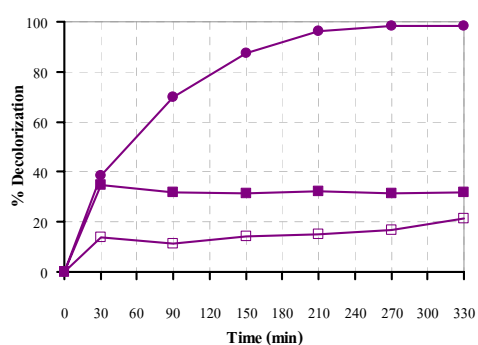
**Figure 29.** Decolorization of CR solution at  $1 \times 10^{-5}$ M as a function of time in the presence of commercial  $\text{TiO}_2$ : (a) Degussa P25, (b) anatase (Carlo Erba), and (c) rutile (R706, TOA).



(a) Ti-no-acid



(b) Ti-HCl

(c) Ti-HNO<sub>3</sub>(d) Ti-H<sub>2</sub>SO<sub>4</sub>(e) Ti-CH<sub>3</sub>COOH(f) Ti-H<sub>3</sub>PO<sub>4</sub>

**Figure 30.** Decolorization of CV solution at  $1 \times 10^{-5}$ M as a function of time in the presence of synthesized TiO<sub>2</sub>: (a) Ti-no-acid, (b) Ti-HCl, (c) Ti-HNO<sub>3</sub>, (d) Ti-H<sub>2</sub>SO<sub>4</sub>, (e) Ti-CH<sub>3</sub>COOH, and (f) Ti-H<sub>3</sub>PO<sub>4</sub>.

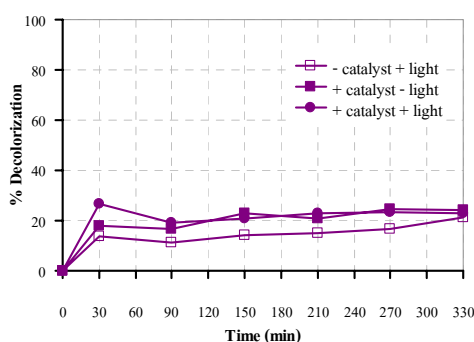
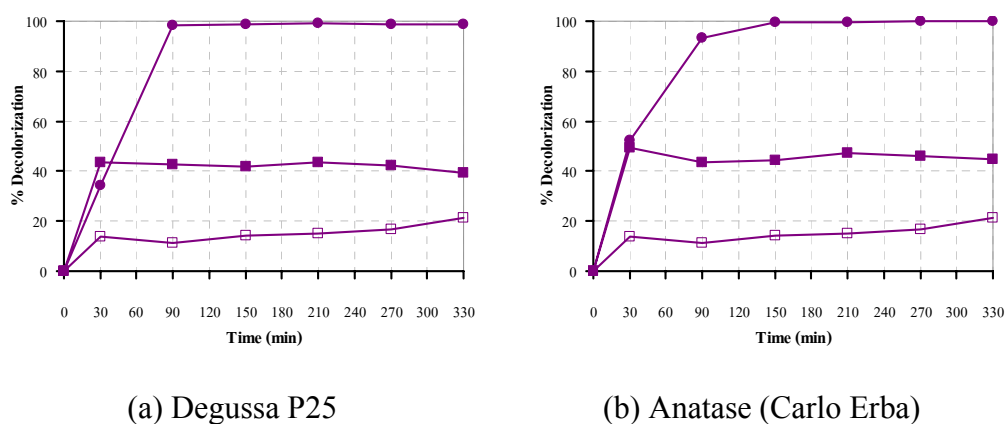


**Figure 31.** Decolorization of CV solution at  $1 \times 10^{-5}$ M as a function of time in the presence of commercial  $\text{TiO}_2$ : (a) Degussa P25, (b) anatase (Carlo Erba), and (c) rutile (R706, TOA).

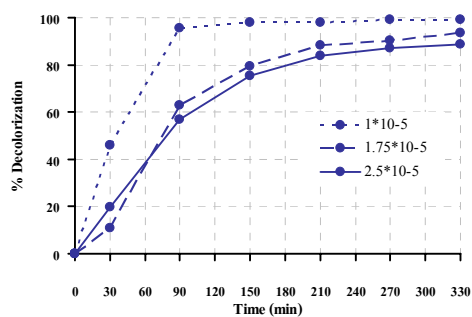
### 3.1.3.2 Effect of initial concentrations of dye

It is important both from mechanistic and from application point of view to study the dependence of initial concentration on the degradation of the pollutant. (Saqib, *et al.*, 2008) Effect of initial concentration on the degradation of three dyes, methylene blue, congo red, and crystal violet, was studied at different concentrations such as  $1 \times 10^{-5}$ ,  $1.75 \times 10^{-5}$ , and  $2.5 \times 10^{-5}$  mol/L with constant catalyst loading (0.5 g/L). The percentages of decolorization of each dye in various

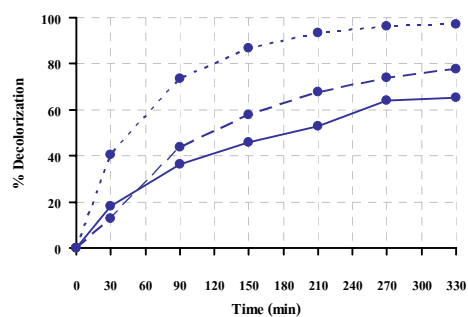


concentrations as a function of time employing  $\text{TiO}_2$  as photocatalyst are shown in Figures 32-37.

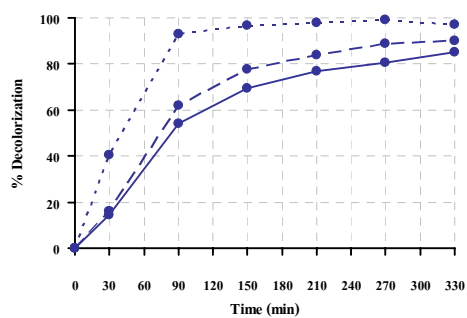
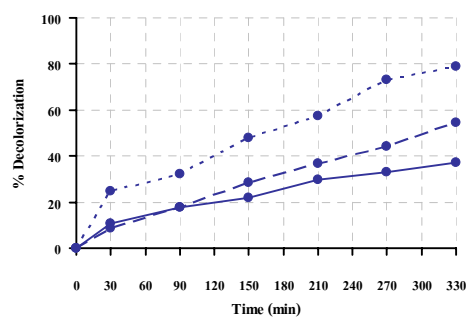
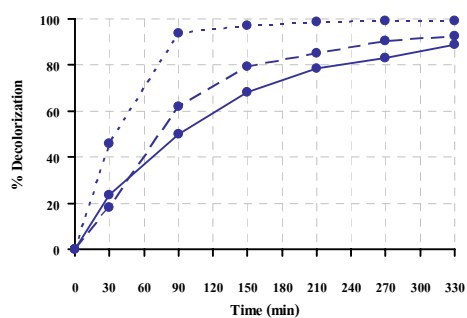
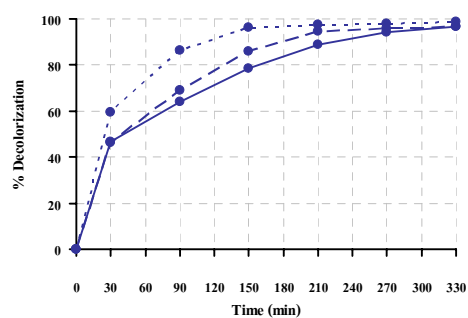
It was observed that the photodegradation of dye decreased with an increase in the initial concentration of dye solution. The decrease of degradation with increase substrate concentration was rationalized as the initial concentrations of dye increased the color of the irradiating mixture became more intense which prevented the penetration of light to the surface of titanium dioxide. Hence, the generation of relative amount of hydroxyl radical ( $\bullet\text{OH}$ ) and superoxide radical ( $\bullet\text{O}_2^-$ ) on the surface of the catalyst did not increase with dye concentration while the intensity of light, irradiation time and catalyst were held constant. The produced  $\bullet\text{OH}$  radical was believed to be the key factor in the photocatalytic degradation of aromatic compounds through the hydroxylation by hydroxyl radicals (Matthews, 1984). In addition, Okamoto *et al.* (1985) pointed out that the rate-determining step of the reaction could be the formation of  $\bullet\text{OH}$  radicals since they reacted very rapidly once they were formed through the reaction of holes with adsorbed  $\text{OH}^-$  and water. If we assume that the positions of adsorbed  $\text{OH}^-$  were replaced by dye ions ( $\text{dye}^-$ ) which had been generated from the dissociation of sodium salt of dye molecules, then the generation of  $\bullet\text{OH}$  radical would be reduced since there were only fewer active sites available for the generation of  $\bullet\text{OH}$  radicals. Another important point for this behavior is that as the initial concentration of dye increased, the path length of photons entering the solution decreased, and in low concentration the reverse effect was observed (Davis, *et al.*, 1994). Consequently, the degradation efficiency of the dye decreased as the dye concentration increased. These results are in agreement with a number of studies reported earlier such as photocatalytic oxidation of azo dye acid red by Daneshvar, *et al.*, (2003), triphenylmethane dye (genial violet) by Saquib and Muneer, (2003), and textile dye reactive blue 4 by Neppolian, *et al.*, (2002).



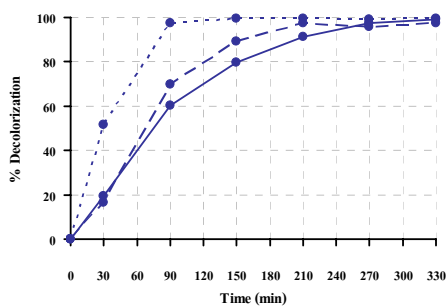
(a) Ti-no-acid



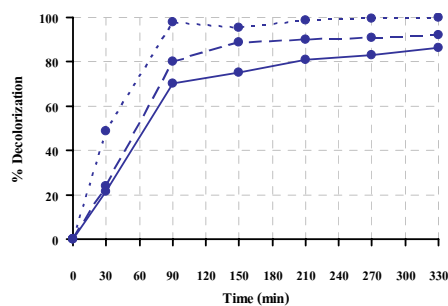
(b) Ti-HCl

(c) Ti-HNO<sub>3</sub>(d) Ti-H<sub>2</sub>SO<sub>4</sub>(e) Ti-CH<sub>3</sub>COOH(f) Ti-H<sub>3</sub>PO<sub>4</sub>

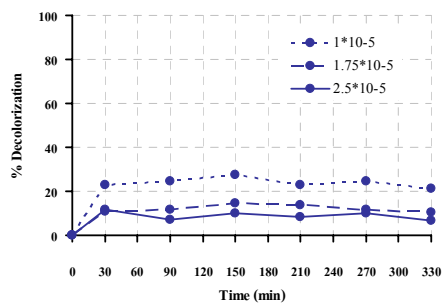
**Figure 32.** Effect of the initial concentration of MB solution as a function of time in the presence of synthesized TiO<sub>2</sub>: (a) Ti-no-acid, (b) Ti-HCl, (c) Ti-HNO<sub>3</sub>, (d) Ti-H<sub>2</sub>SO<sub>4</sub>, (e) Ti-CH<sub>3</sub>COOH, and (f) Ti-H<sub>3</sub>PO<sub>4</sub>.



(a) Degussa P25

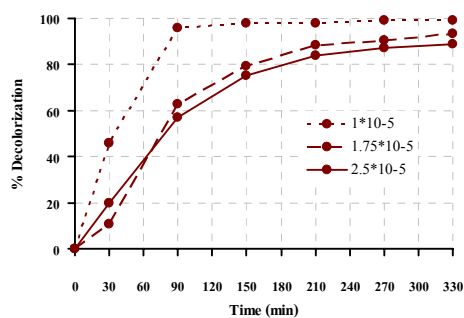


(b) Anatase (Carlo Erba)

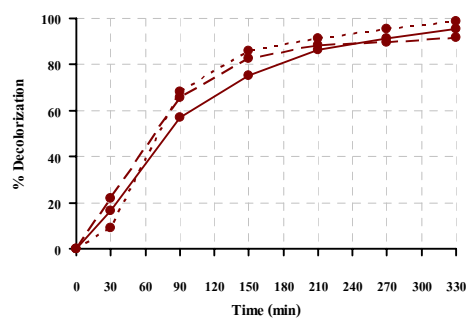


(c) Rutile (R706, TOA)

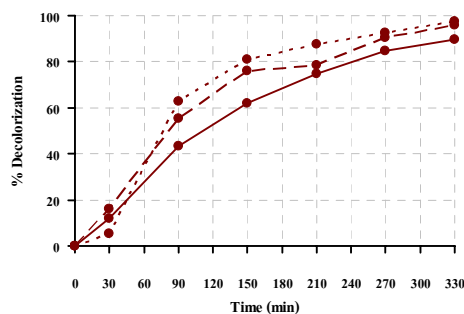
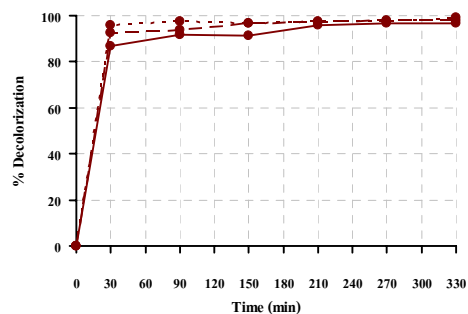
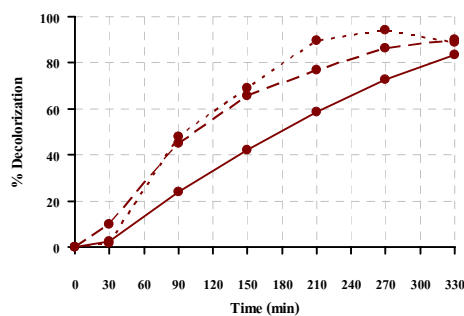
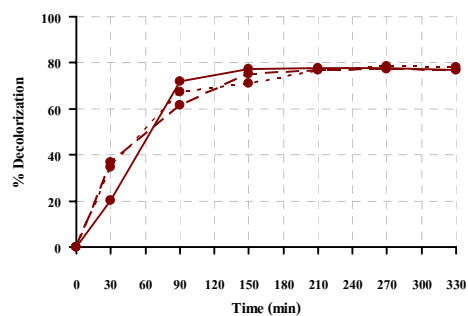
**Figure 33.** Effect of the initial concentration of MB solution as a function of time in the presence of commercial TiO<sub>2</sub>: (a) Degussa P25, (b) anatase (Carlo Erba), and (c) rutile (R706, TOA).



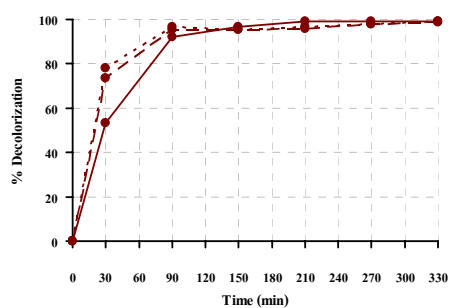
(a) Ti-no-acid



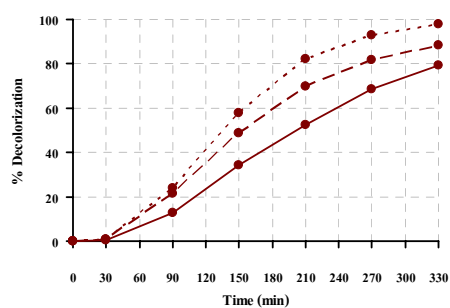
(b) Ti-HCl

(c) Ti-HNO<sub>3</sub>(d) Ti-H<sub>2</sub>SO<sub>4</sub>(e) Ti-CH<sub>3</sub>COOH(f) Ti-H<sub>3</sub>PO<sub>4</sub>

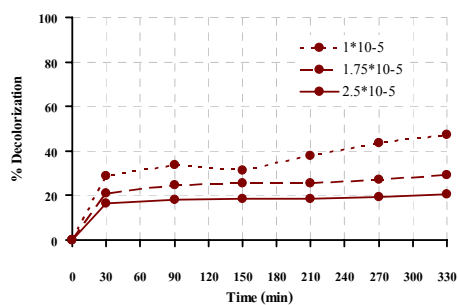
**Figure 34.** Effect of the initial concentration of CR solution as a function of time in the presence of synthesized TiO<sub>2</sub>: (a) Ti-no-acid, (b) Ti-HCl, (c) Ti-HNO<sub>3</sub>, (d) Ti-H<sub>2</sub>SO<sub>4</sub>, (e) Ti-CH<sub>3</sub>COOH, and (f) Ti-H<sub>3</sub>PO<sub>4</sub>.



(a) Degussa P25

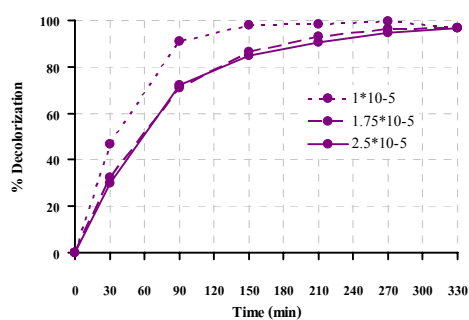


(b) Anatase (Carlo Erba)

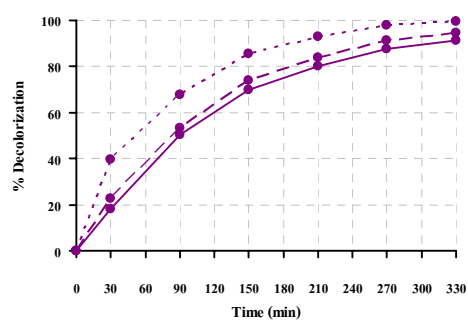


(c) Rutile (R706, TOA)

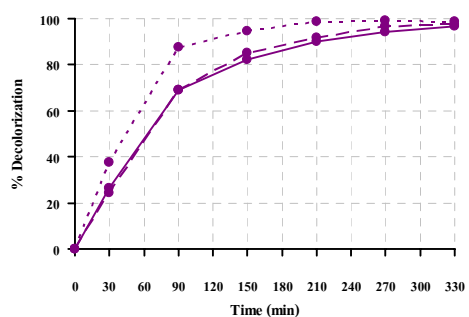
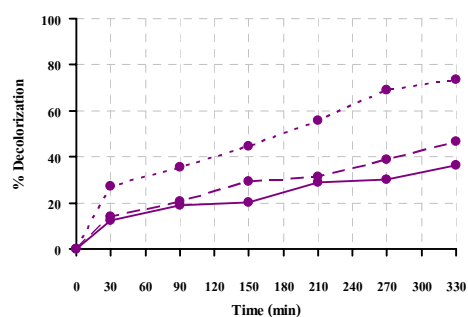
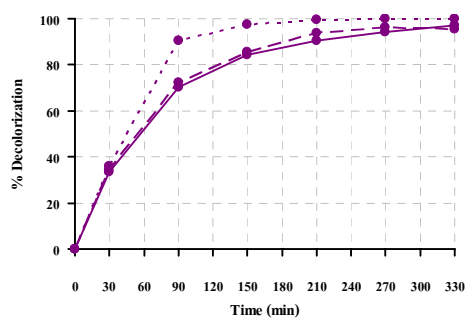
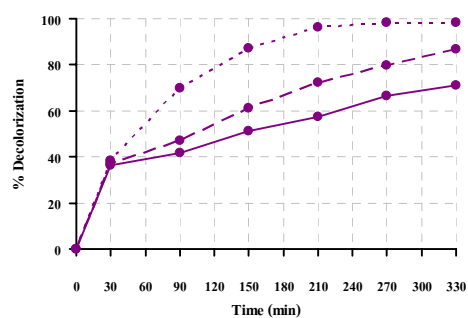
**Figure 35.** Effect of the initial concentration of CR solution as a function of time in the presence of commercial  $\text{TiO}_2$ : (a) Degussa P25, (b) anatase (Carlo Erba), and (c) rutile (R706, TOA).



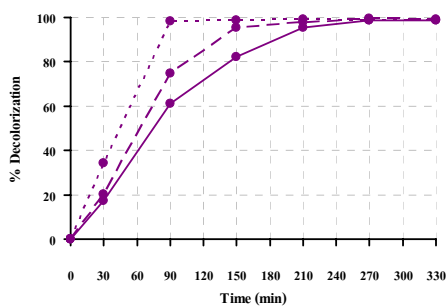
(a) Ti-no-acid



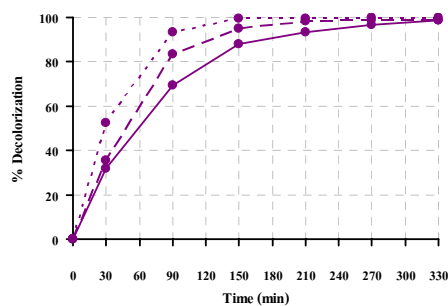
(b) Ti-HCl

(c) Ti-HNO<sub>3</sub>(d) Ti-H<sub>2</sub>SO<sub>4</sub>(e) Ti-CH<sub>3</sub>COOH(f) Ti-H<sub>3</sub>PO<sub>4</sub>

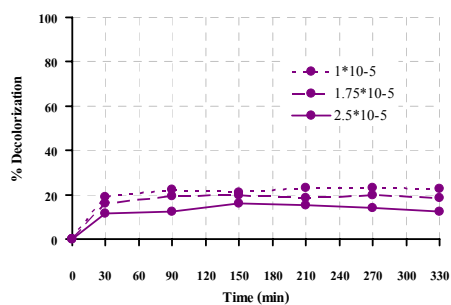
**Figure 36.** Effect of the initial concentration of CV solution as a function of time in the presence of synthesized TiO<sub>2</sub>: (a) Ti-no-acid, (b) Ti-HCl, (c) Ti-HNO<sub>3</sub>, (d) Ti-H<sub>2</sub>SO<sub>4</sub>, (e) Ti-CH<sub>3</sub>COOH, and (f) Ti-H<sub>3</sub>PO<sub>4</sub>.



(a) Degussa P25



(b) Anatase (Carlo Erba)



(c) Rutile (R706, TOA)

**Figure 37.** Effect of the initial concentration of CV solution as a function of time in the presence of commercial TiO<sub>2</sub>: (a) Degussa P25, (b) anatase (Carlo Erba), and (c) rutile (R706, TOA).

### 3.1.3.3 Effect of types of TiO<sub>2</sub>

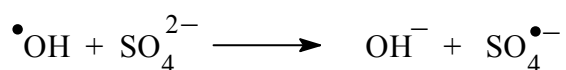
Overview of all the three figures (Figures 38-40) shows that all the six synthesized TiO<sub>2</sub> powders do possess the photocatalytic property as seen by the higher % decolorization of the combined adsorption + photocatalytic activity as compared to the adsorption-only columns in the figures. Degussa P25 was used as a reference with which all the other commercial TiO<sub>2</sub> (anatase and rutile) and the synthesized TiO<sub>2</sub> samples were to be compared. The results in the figures show that P25 has the highest photocatalytic activity for these dyes. Some of the synthesized samples, notably Ti-no-acid and Ti-HNO<sub>3</sub>, constantly showed quite good activity for all the three dyes - only slightly less than P25. The rest of the samples showed some inconsistency performance against these dyes, i.e. good performance with one dye but mediocre with another dye. There seems to be no relation between the band gap energy and photocatalytic property of all the TiO<sub>2</sub> samples under study here.

In many reports P25 and anatase usually show similar activities with P25 is always slightly better. However, with the three dyes under study in this work we can see the different between P25 and anatase in both photocatalytic property and surface adsorption. The commercial anatase showed good photocatalytic activity for MB and CV but only mediocre with CR while P25 showed the best photocatalytic activity for all three dyes. For the surface adsorption, P25 exhibited low adsorption ability for MB and CV but for CR the adsorption dramatically increased. The anatase also showed low adsorption ability, slightly higher than P25, for MB and CV but, unlike P25, the adsorption became extremely low for CR. The adsorption behavior as observed here could be the result from different surface charge between P25 and anatase. Considering the nature of charge on the dye molecules, MB and CV have positive charge while CR has negative charge on the parent molecular fragment. The surface charge on TiO<sub>2</sub> bulk is normally on the negative side. In this case, if we compare P25 with anatase based on the adsorption of the three dyes, we are led to the conclusion that the surface charge of P25 should be less negative than that of anatase. For the six synthesized samples, Ti-no-acid, Ti-HCl, Ti-HNO<sub>3</sub>, Ti-CH<sub>3</sub>COOH, and Ti-H<sub>3</sub>PO<sub>4</sub> showed the same type of adsorption behavior as anatase while Ti-H<sub>2</sub>SO<sub>4</sub> was similar to P25. The surface charge of the former group tends to



be more negative, hence, they adsorbed stronger with MB and CV and vice versa for the latter group. It is noteworthy to mention the rather inert to change for adsorption on the rutile which probably reflects its low surface charge.

The presence of sulphate and phosphate anions in the system was found to retard the photocatalytic activity (Neppolian, *et al.*, 2002; Abdullah, *et al.*, 1990). Taken sulphate as an example, when added, the sulphate anion was immediately adsorbed on the TiO<sub>2</sub> surface and was attacked by the  $\bullet\text{OH}$  radical to become the sulphate radical.



This  $\bullet\text{OH}$  radical scavenging property of the sulphate anion would reduce the number of reactive  $\bullet\text{OH}$  radical, therefore, lower the efficiency of the dye degradation process. The sulphate radical could also attack the dye molecules, too, but it is not as strong as the  $\bullet\text{OH}$  radical. This rationale seems to be applicable to the data of Ti-H<sub>2</sub>SO<sub>4</sub> with MB and CV dyes where Ti-H<sub>2</sub>SO<sub>4</sub> showed low photocatalytic activity. The behavior of Ti-H<sub>2</sub>SO<sub>4</sub> with CR, at first, may seem unfit to this rationale. However, on a closer look at the high % decolorization of Ti-H<sub>2</sub>SO<sub>4</sub> in Figure 29 it is, in fact, the combined adsorption and photocatalytic effects. Therefore, the different between the adsorption-only and the combined adsorption + photocatalytic columns should correspond to the true photocatalytic resulting in a small value for photocatalytic effect as expected.

It is doubtful that the rationale for the sulphate anion could be applicable to the phosphate anion since the photocatalytic activity of Ti-H<sub>3</sub>PO<sub>4</sub> was not that low as in the Ti-H<sub>2</sub>SO<sub>4</sub> case. On the contrary, it was quite high, e.g. almost equal to P25 for MB dye, acceptable for CR dye, and only mediocre for CV dye.

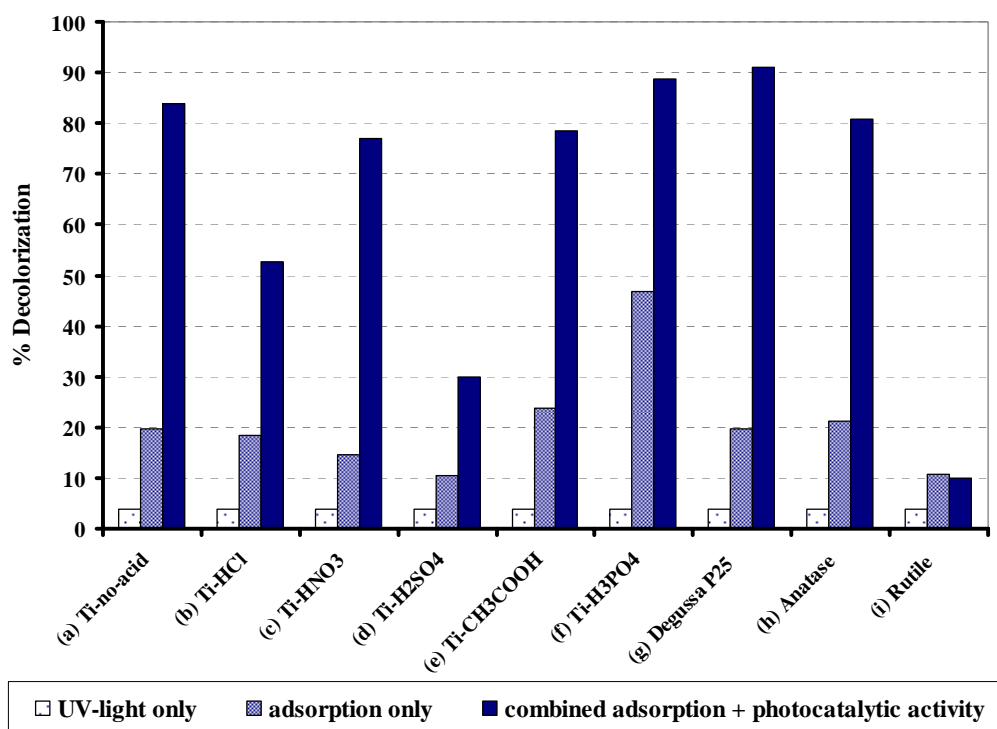


**Figure 38.** Decolorization of MB solution ( $2.5 \times 10^{-5}$ M) with (a) Ti-no acid, (b) Ti-HCl, (c) Ti-HNO<sub>3</sub>, (d) Ti-H<sub>2</sub>SO<sub>4</sub>, (e) Ti-CH<sub>3</sub>COOH, (f) Ti-H<sub>3</sub>PO<sub>4</sub>, (g) Degussa P25, (h) Anatase(Carlo Erba), and (i) Rutile (R706).

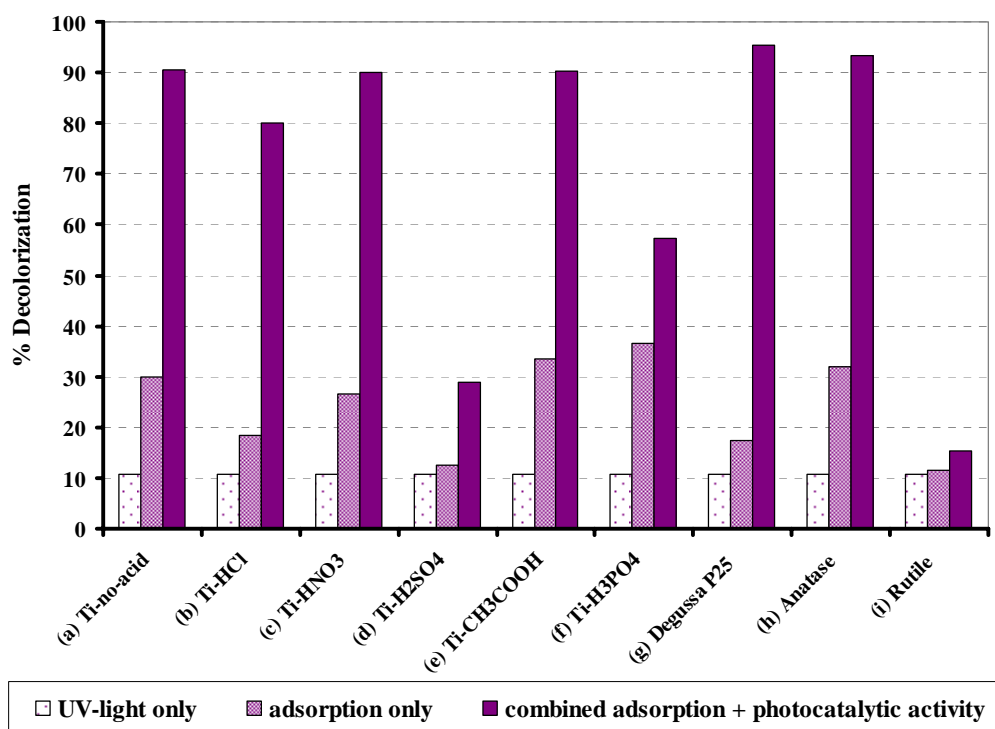


**Figure 39.** Decolorization of CV solution ( $2.5 \times 10^{-5}$ M) with (a) Ti-no acid, (b) Ti-HCl, (c) Ti-HNO<sub>3</sub>, (d) Ti-H<sub>2</sub>SO<sub>4</sub>, (e) Ti-CH<sub>3</sub>COOH, (f) Ti-H<sub>3</sub>PO<sub>4</sub>, (g) Degussa P25, (h) Anatase(Carlo Erba), and (i) Rutile (R706).

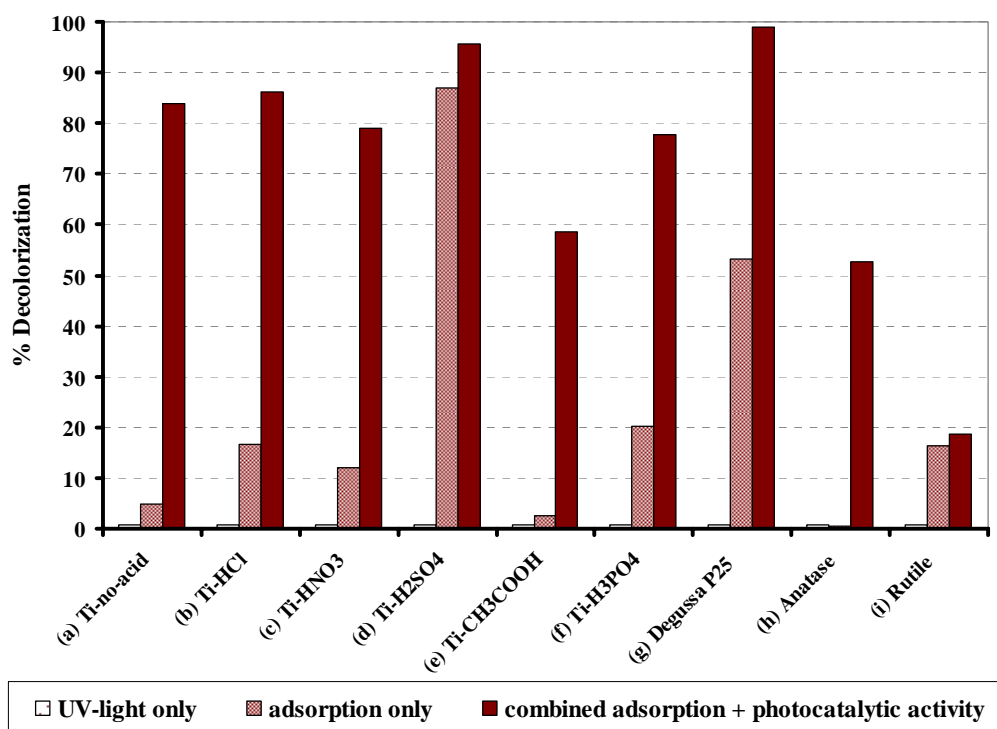
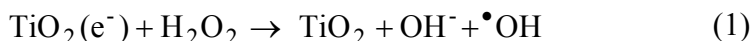


**Figure 40** Decolorization of CR solution ( $2.5 \times 10^{-5}$ M) with (a) Ti-no acid, (b) Ti-HCl, (c) Ti-HNO<sub>3</sub>, (d) Ti-H<sub>2</sub>SO<sub>4</sub>, (e) Ti-CH<sub>3</sub>COOH, (f) Ti-H<sub>3</sub>PO<sub>4</sub>, (g) Degussa P25, (h) Anatase(Carlo Erba), and (i) Rutile (R706).

### 3.1.2.4 Effect of hydrogen peroxide (H<sub>2</sub>O<sub>2</sub>)

The addition of hydrogen peroxide to the heterogeneous system increases the concentration of  $\bullet\text{OH}$ , since it inhibits the electron-hole recombination, according to the following equation:



Hydrogen peroxide is considered to have two functions in the process of photocatalytic degradation. It accepts a photogenerated electron from the conduction band and thus promotes the charge separation, and it also forms  $\bullet\text{OH}$ .

The addition of H<sub>2</sub>O<sub>2</sub> is known to increase the rate of photocatalytic degradation by allowing an enhancement in the quantum yield of formation of hydroxyl radical. Several researchers had studied the effect of the addition of hydrogen peroxide under irradiation with various types of light source such as Nappolian, *et al.*, (2002) studied the effect of the addition of H<sub>2</sub>O<sub>2</sub> to TiO<sub>2</sub> (P25) in the reactive blue 4 degradation at irradiation time equals 8 hours by using solar light. Sun, *et al.*, (2002) studied the role of H<sub>2</sub>O<sub>2</sub> to TiO<sub>2</sub> in degradation of the Cationic Red GTL using two 6 W UV lamps. Sauer, *et al.*, (2002) studied the effect of adding H<sub>2</sub>O<sub>2</sub> to the Degussa P25-containing system for the photooxidation of reactive dyes using medium pressure mercury lamp. Daneshvar, *et al.*, (2003) studied the effect of H<sub>2</sub>O<sub>2</sub> addition on photodegradation efficiency of acid red 14 in UV/TiO<sub>2</sub> process using 30 W mercury lamp (UV-C, Philips). Saquib and Muneer, (2003) studied the effect of H<sub>2</sub>O<sub>2</sub> for photocatalytic degradation of gentian violet in aqueous suspensions of TiO<sub>2</sub>-P25 using 125 W medium pressure Hg lamp as a light source. Senthikumaar, *et al.*, (2004) studied the effect of H<sub>2</sub>O<sub>2</sub> on the photodegradation of methylene blue under nanocrystalline TiO<sub>2</sub> (Ti-US) using 125 W medium pressure Hg arc lamp as a light source. Qamar, *et al.*, (2005) studied the degradation rate for the mineralization and decomposition of chromotrope 2B in the presence of different electron acceptors (H<sub>2</sub>O<sub>2</sub>, (NH<sub>4</sub>)<sub>2</sub>S<sub>2</sub>O<sub>8</sub>, and KBrO<sub>3</sub>) using Degussa P25 with 125 W medium pressure Hg lamp as a light source.

In our earlier work (Random, *et al.*, 2004) we found that the synthesized titania, h-TiO<sub>2</sub>, could decompose methylene blue (MB) when irradiated with UV-light, however, it was slightly inferior to P25. However, in the dark with the adding small volume of H<sub>2</sub>O<sub>2</sub>, h-TiO<sub>2</sub> could bleach MB far better than P25. In this work, we investigated the effect of addition H<sub>2</sub>O<sub>2</sub> in the absence of UV light and compared with the presence of UV light.

### (1) Addition of H<sub>2</sub>O<sub>2</sub> in the absence of light

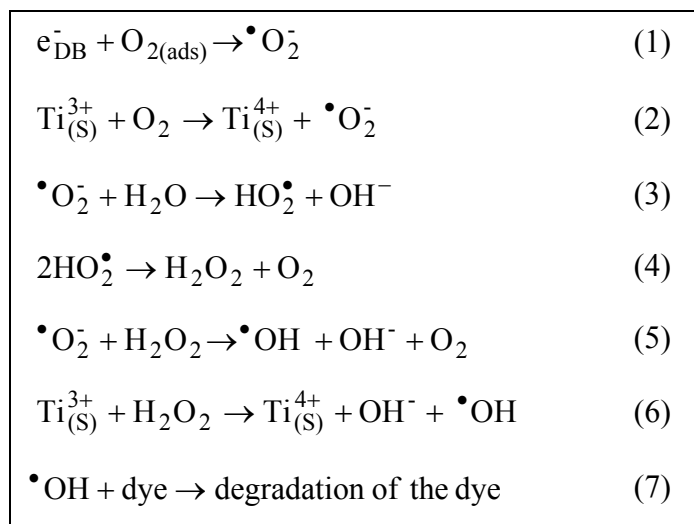
In Figures 41-46, the results obtained by treating each dye sample in the absence of light with TiO<sub>2</sub> alone (▲), H<sub>2</sub>O<sub>2</sub> alone (○), and combination of both TiO<sub>2</sub>/H<sub>2</sub>O<sub>2</sub> (△). From these figures, it is possible to observed that the action of H<sub>2</sub>O<sub>2</sub> alone show a little bit of decolourization. The combination TiO<sub>2</sub> and H<sub>2</sub>O<sub>2</sub> was more effective in the decolourization of dye than both TiO<sub>2</sub> and H<sub>2</sub>O<sub>2</sub> alone. The synthesized TiO<sub>2</sub> powders in this work which have Ti atoms at the surface could have some dangling bonds with an unpaired electron left in some of them. To explain this phenomenon Random, *et al.*, (2004) introduced the concept of the vacant site with a dangling bond at the surface of the transition metal oxide solid. The pathway can be proposed here for the degradation of two dyes by the synthesized TiO<sub>2</sub> with H<sub>2</sub>O<sub>2</sub> in the dark, as shown in Scheme 1.

In Scheme 1, the steps involving the transition metal ion are analogous to the so-called superoxide driven Fenton's reaction with Ti<sup>3+</sup>/Ti<sup>4+</sup> replacing Fe<sup>2+</sup>/Fe<sup>3+</sup> (Buettner, 1997). Step (4) shows that H<sub>2</sub>O<sub>2</sub> was produced and consumed within the process in step (5). Thus, when H<sub>2</sub>O<sub>2</sub> was added directly in trace amounts, the decolorization was enhanced in the dark.

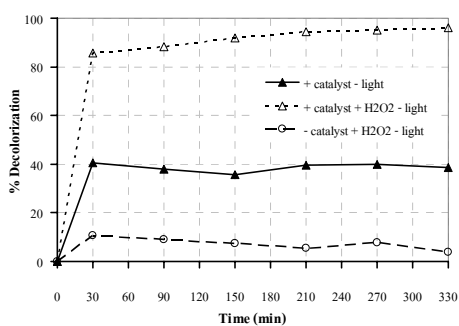
Two types of the nanocrystalline TiO<sub>2</sub> (Ti-H<sub>2</sub>SO<sub>4</sub> and Ti-H<sub>3</sub>PO<sub>4</sub>) and two commercial TiO<sub>2</sub> (P25 and anatase) behave differently from each other because there is another property that we have to bring into the scenario, that is, the functional group adhered to the surface of the catalyst, i.e., OH<sup>-</sup> as identified by FT-IR. The OH<sup>-</sup> groups are present in amorphous TiO<sub>2</sub> more abundantly than in the anatase and rutile form (Tanaka, *et al.*, 1991). The presence of more OH<sup>-</sup> groups means the catalyst is less crystalline, i.e. being more amorphous and hence having

high surface area. The high surface area of the catalyst enables the reactant molecules to be adsorbed more densely on the catalyst surface leading to more rapid reaction. On the other hand, being more amorphous, i.e., low crystallinity, would enhance rate of  $e_{CB}^- - h_{VB}^+$  recombination during irradiation, therefore the amorphous  $TiO_2$  was found to be inferior to anatase as photocatalyst (Ohtani, *et al.*, 1997). The two commercial  $TiO_2$  have high crystallinity and less  $OH^-$  group at the surface hence less surface area as evidenced by its low adsorptivity of MB and CV. While  $Ti-H_2SO_4$  and  $Ti-H_3PO_4$  have less  $OH^-$  group at the surface. As a result, a number of  $H_2O_2$  and dye molecules adsorbed on the surface of the two commercial  $TiO_2$ ,  $Ti-H_2SO_4$ , and  $Ti-H_3PO_4$  are much less than that in the other types of synthesized nanocrystalline  $TiO_2$ .

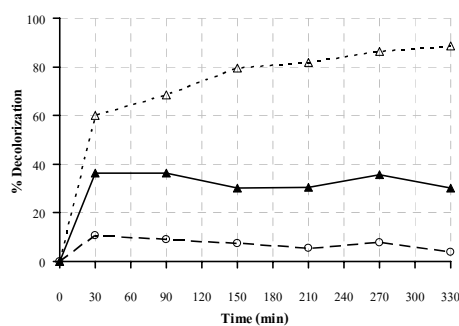
However, congo red exhibit a slight difference from the other dyes. This effect could be due to a competition for adsorption between the dye and the additive (hydrogen peroxide). This is in agreement with a low adsorption of this dye (Hachem, *et al.*, 2001).



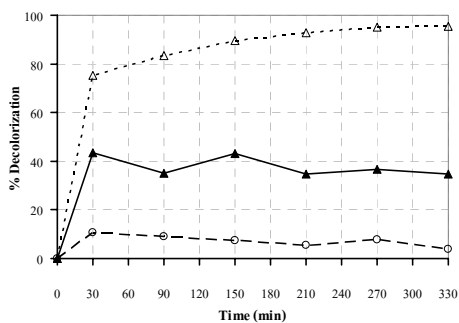
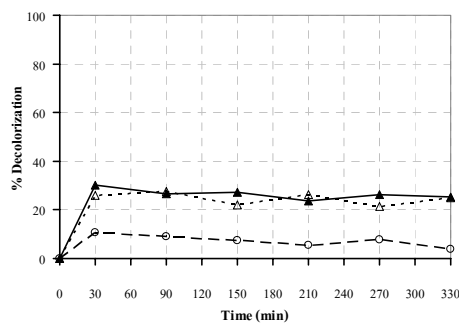
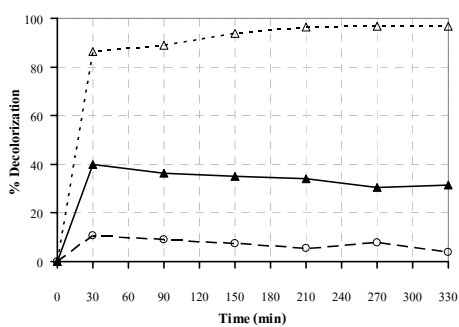
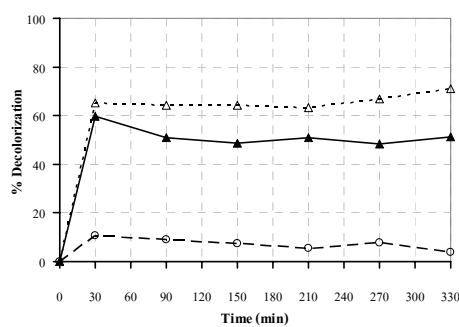
**Scheme 1.** Tentative pathway to degrade dye by the synthesized  $TiO_2$  with  $H_2O_2$  in the dark.  $Ti_{(s)}^{4+}$ ,  $Ti_{(s)}^{3+}$ , and  $e_{DB}^-$  represent metal ions and an electron available from dangling bond, respectively, at the solid surface.



(a) Ti-no-acid

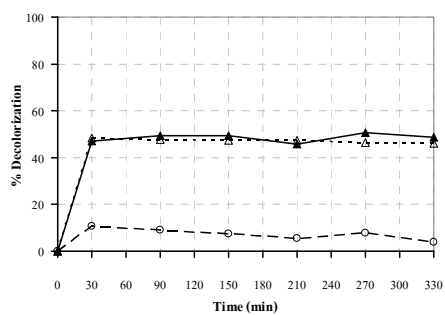


(b) Ti-HCl

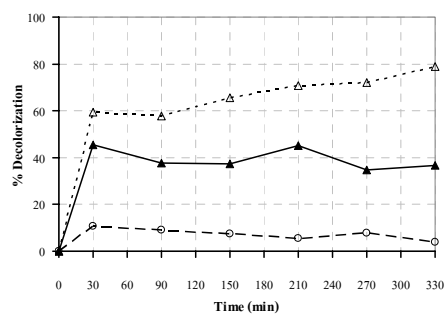
(c) Ti-HNO<sub>3</sub>(d) Ti-H<sub>2</sub>SO<sub>4</sub>(e) Ti-CH<sub>3</sub>COOH(f) Ti-H<sub>3</sub>PO<sub>4</sub>

**Figure 41.** Effect of addition of hydrogen peroxide in absence of light on MB degradation as a function of time in the presence of synthesized TiO<sub>2</sub>: (a) Ti-no-acid, (b) Ti-HCl, (c) Ti-HNO<sub>3</sub>, (d) Ti-H<sub>2</sub>SO<sub>4</sub>, (e) Ti-CH<sub>3</sub>COOH, and (f) Ti-H<sub>3</sub>PO<sub>4</sub>.

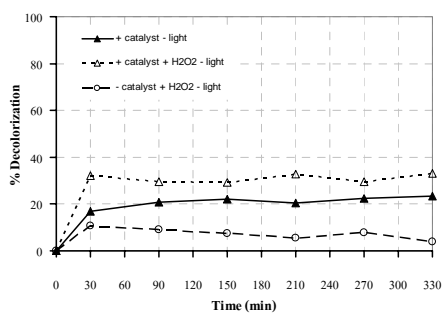




(a) Degussa P25

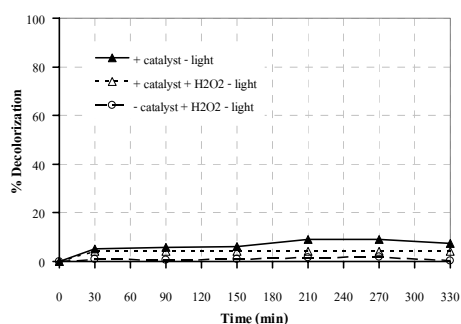


(b) Anatase (Carlo Erba)

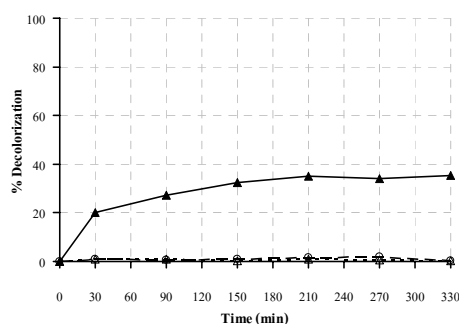


(c) Rutile (R706, TOA)

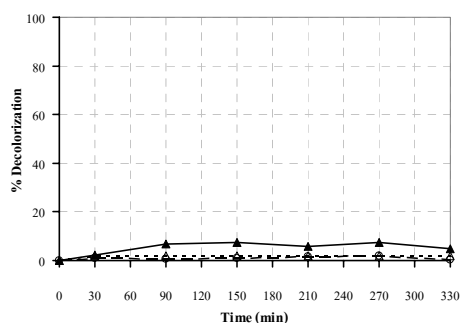
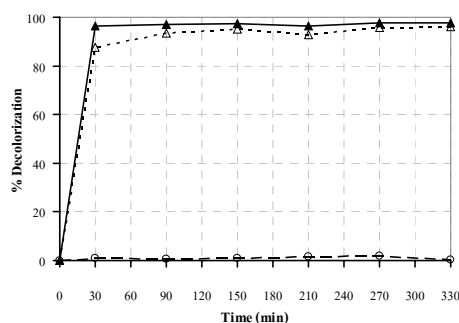
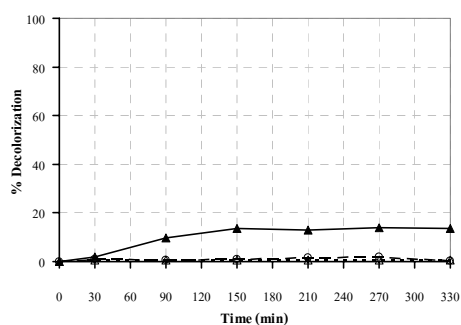
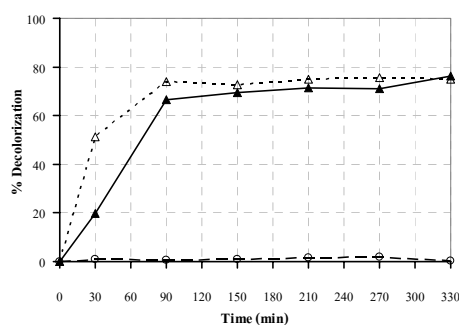
**Figure 42.** Effect of addition of hydrogen peroxide in absence of light on MB degradation as a function of time in the presence of commercial TiO<sub>2</sub>: (a) Degussa P25, (b) Anatase (Carlo Erba), and (c) Rutile (R706, TOA).



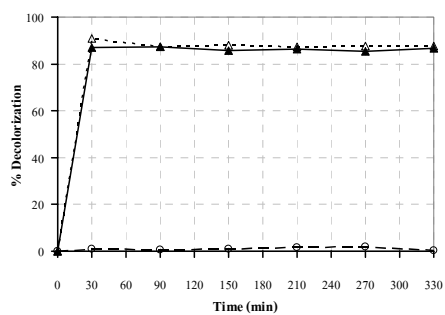
(a) Ti-no-acid



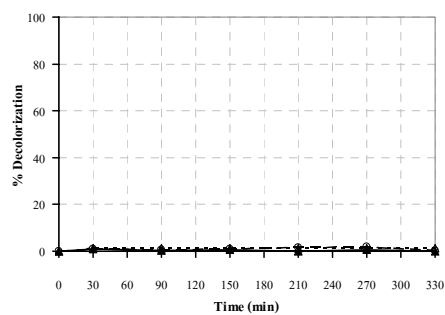
(b) Ti-HCl

(c) Ti-HNO<sub>3</sub>(d) Ti-H<sub>2</sub>SO<sub>4</sub>(e) Ti-CH<sub>3</sub>COOH(f) Ti-H<sub>3</sub>PO<sub>4</sub>

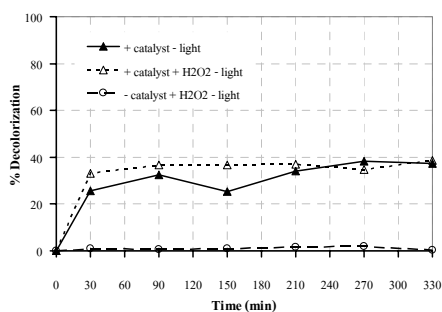
**Figure 43.** Effect of addition of hydrogen peroxide in absence of light on CR degradation as a function of time in the presence of synthesized TiO<sub>2</sub>: (a) Ti-no-acid, (b) Ti-HCl, (c) Ti-HNO<sub>3</sub>, (d) Ti-H<sub>2</sub>SO<sub>4</sub>, (e) Ti-CH<sub>3</sub>COOH, and (f) Ti-H<sub>3</sub>PO<sub>4</sub>.



(a) Degussa P25

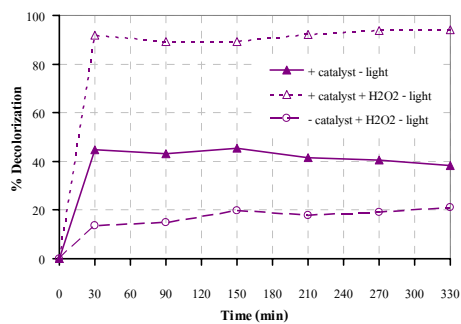


(b) Anatase (Carlo Erba)

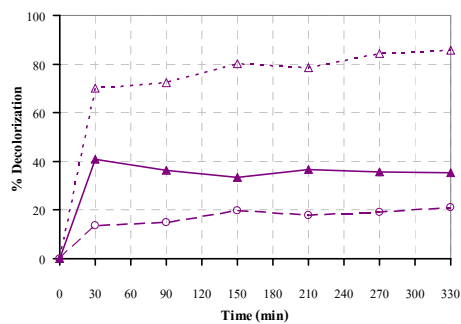


(c) Rutile (R706, TOA)

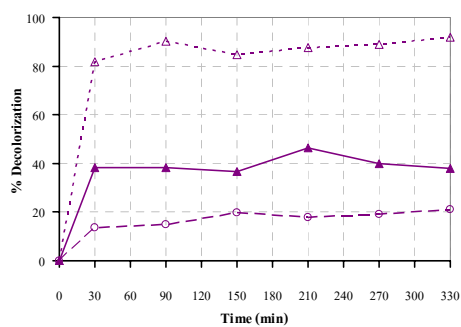
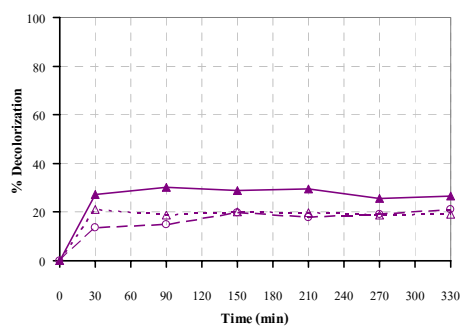
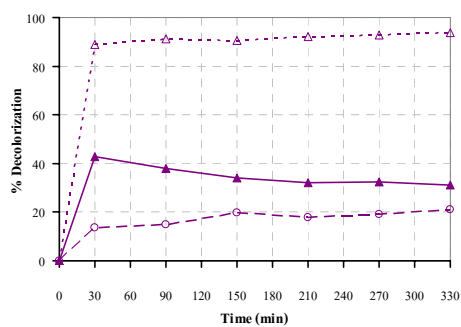
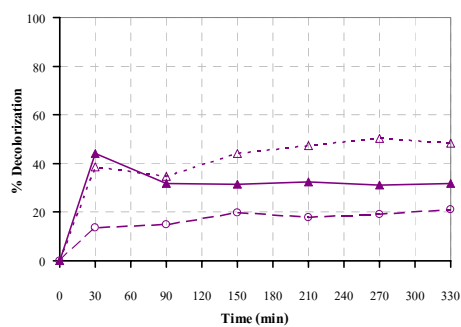
**Figure 44.** Effect of addition of hydrogen peroxide in absence of light on CR degradation as a function of time in the presence of commercial  $\text{TiO}_2$ : (a) Degussa P25, (b) Anatase (Carlo Erba), and (c) Rutile (R706, TOA).



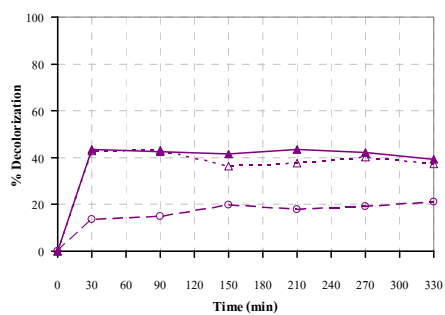
(a) Ti-no-acid



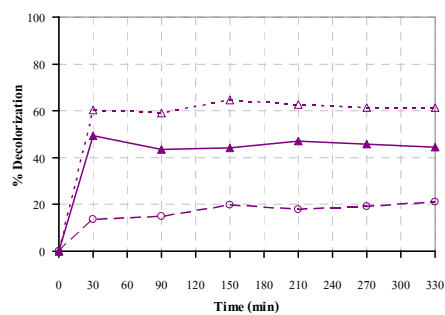
(b) Ti-HCl

(c) Ti-HNO<sub>3</sub>(d) Ti-H<sub>2</sub>SO<sub>4</sub>(e) Ti-CH<sub>3</sub>COOH(f) Ti-H<sub>3</sub>PO<sub>4</sub>

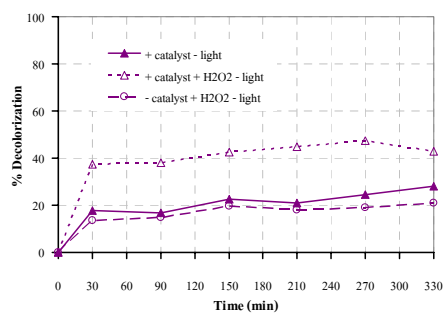
**Figure 45.** Effect of addition of hydrogen peroxide in absence of light on CV degradation as a function of time in the presence of synthesized TiO<sub>2</sub>: (a) Ti-no-acid, (b) Ti-HCl, (c) Ti-HNO<sub>3</sub>, (d) Ti-H<sub>2</sub>SO<sub>4</sub>, (e) Ti-CH<sub>3</sub>COOH, and (f) Ti-H<sub>3</sub>PO<sub>4</sub>.



(a) Degussa P25



(b) Anatase (Carlo Erba)

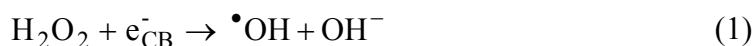


(c) Rutile (R706, TOA)

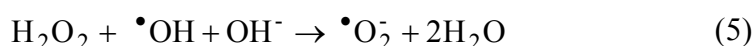
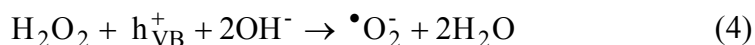
**Figure 46.** Effect of addition of hydrogen peroxide in absence of light on CV degradation as a function of time in the presence of commercial  $\text{TiO}_2$ : (a) Degussa P25, (b) Anatase (Carlo Erba), and (c) Rutile (R706, TOA).

## (2) Addition of H<sub>2</sub>O<sub>2</sub> in the presence of UV light

Hydrogen peroxide (H<sub>2</sub>O<sub>2</sub>) could increase the hydroxyl radical formation through three ways. Firstly, it could act as an alternative electron acceptor to oxygen (reaction (1)), which might restrain the bulk-composite of the photo-excited electrons and holes. This should consequently increase the rate of the photocatalytic process. Secondly, the reduction of H<sub>2</sub>O<sub>2</sub> at the conductance band would also produce hydroxyl radicals. Even if H<sub>2</sub>O<sub>2</sub> was not reduced at the conductance band it could accept an electron from superoxide (O<sub>2</sub><sup>•-</sup>) again producing hydroxyl radical (reaction (2)). Thirdly, the self-decomposition by illumination would also produce hydroxyl radicals (reaction (3)) (Sun, *et al.*, 2002).



Furthermore, H<sub>2</sub>O<sub>2</sub> is oxidized to O<sub>2</sub><sup>•-</sup> by valence band hole, h<sub>VB</sub><sup>+</sup> (reaction (4)) or by •OH (reaction (5)) (Hirakawa, *et al.*, 2007).

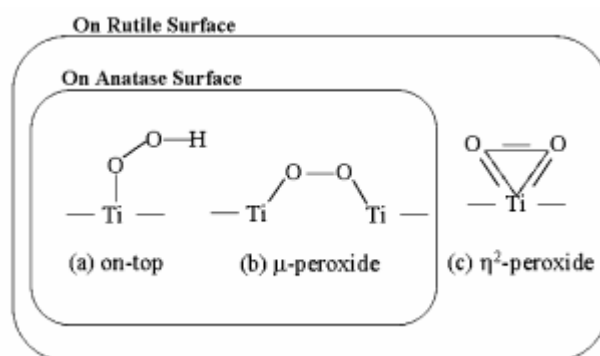


Figures 47-52 show the results of decolourization when added H<sub>2</sub>O<sub>2</sub> in the presence of light (□), in the absence of light (■), and compared with UV light (▲). From these figures, it can be seen that the combination H<sub>2</sub>O<sub>2</sub> and UV light is more effective in the decolourization of dye than either UV light or H<sub>2</sub>O<sub>2</sub> alone. Dye can be attacked by hydroxyl radical which is a powerful oxidant generated from photolysis of H<sub>2</sub>O<sub>2</sub> and UV light, making the degradation of dyes possible.

Hirakawa, *et al.*, (2007) reported that the addition of H<sub>2</sub>O<sub>2</sub> increased the formation of hydroxyl radical for rutile and for anatase mixed with rutile, while anatase showed an opposite tendency. They found a significant effect of crystal structure on the •OH formation from H<sub>2</sub>O<sub>2</sub>. The reaction occurs exclusively at

rutile  $\text{TiO}_2$ , where the  $\bullet\text{OH}$  is not produced in the absence of  $\text{H}_2\text{O}_2$ . Furthermore, this effect was also observed for mixed-phase  $\text{TiO}_2$  with 10-20 % rutile. They suggested that the  $\eta^2$ -peroxide as  $\text{H}_2\text{O}_2$ -adsorption structure on the rutile surface takes peculiarly the reaction. Synergic effect of mixing rutile to anatase on the  $\bullet\text{OH}$  formation was hardly observed.

In the formation of  $\text{O}_2^{\bullet-}$ , the rutile surface is a favorable condition to stabilize  $\text{O}_2^{\bullet-}$ . In the case of the  $\text{O}_2^{\bullet-}$  production from  $\text{H}_2\text{O}_2$ , anatase  $\text{TiO}_2$  surpassed rutile because  $\text{H}_2\text{O}_2$  is not reduced to  $\bullet\text{OH}$  as clarified in their study. The photocatalytic oxidation of  $\text{H}_2\text{O}_2$  to produce  $\text{O}_2^{\bullet-}$  is preferably carried out via the on-top or  $\mu$ -peroxide adsorption structure.



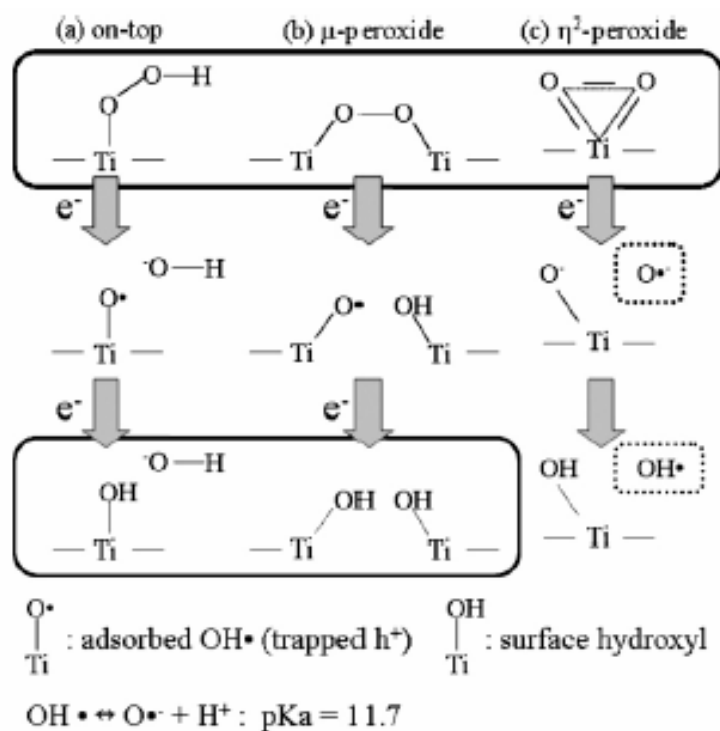
**Scheme 2.** Schematic diagram of  $\text{H}_2\text{O}_2$  adsorption structure on the surface of anatase and rutile  $\text{TiO}_2$  (Hirakawa, *et al.*, 2007).

There are three adsorption structures (Scheme 2) of  $\text{H}_2\text{O}_2$  on the surface of anatase and rutile  $\text{TiO}_2$  reported by Ohno *et al.*, (2001). The  $\text{H}_2\text{O}_2$  adsorbed on the rutile surface of  $\text{TiO}_2$  takes a unique structure of (c)  $\eta^2$ -peroxide. This peroxide is known to form an epoxy molecule under photo-irradiation. The formation rate of  $\bullet\text{OH}$  for rutile is explained by the contribution of the  $\text{H}_2\text{O}_2$  adsorption structure (c). On the anatase  $\text{TiO}_2$ , the adsorption of the  $\text{H}_2\text{O}_2$  are (a) on-top and (b)  $\mu$ -peroxide. Then, a surface-active species called as adsorbed  $\bullet\text{OH}$  may be formed on the anatase surface. The adsorbed  $\bullet\text{OH}$  may not be distinguished from

the trapped  $h^+$ . In the case of anatase the addition of  $H_2O_2$  does not accelerate the formation rate of  $\bullet OH$ . The adsorbed  $\bullet OH$  may be finally reduced to hydroxyl ion or  $H_2O$  as reaction (6)

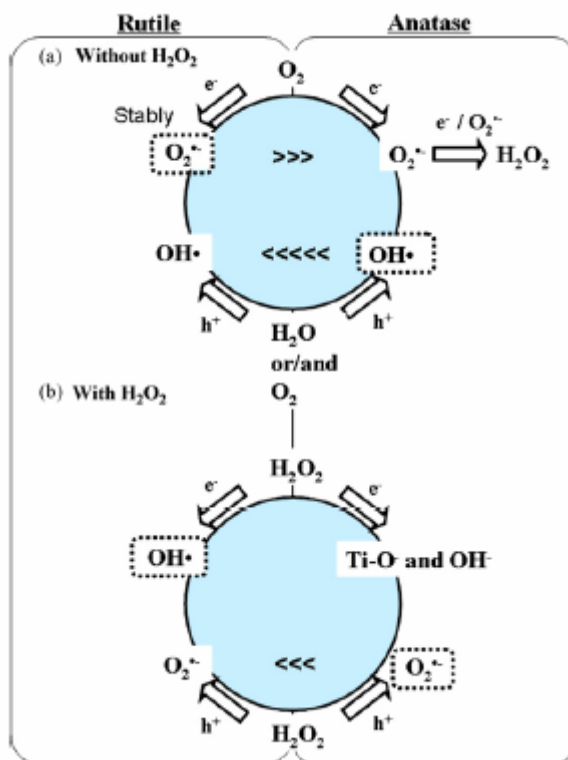


As described above, the preferable reaction is  $\bullet OH$  formation (reaction (1)) for rutile and  $H_2O$  formation (reaction (5)) for anatase. Hirakawa, *et al.*, (2007) showed the difference between rutile and anatase  $TiO_2$  for the photocatalytic reaction mechanism for  $H_2O_2$  decomposition by Scheme 3 and the proposed reaction mechanism in Scheme 4.

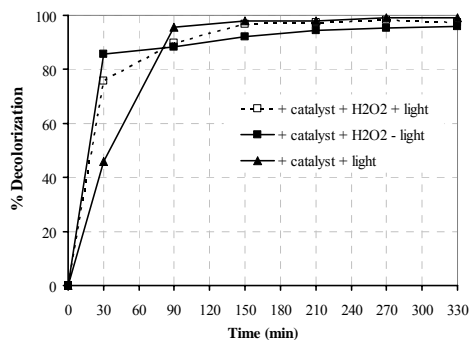


**Scheme 3.** Plausible process in the photocatalytic reduction of  $H_2O_2$  starting from three different adsorption structures (Hirakawa, *et al.*, 2007).

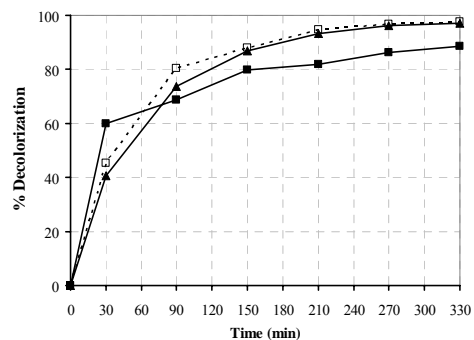




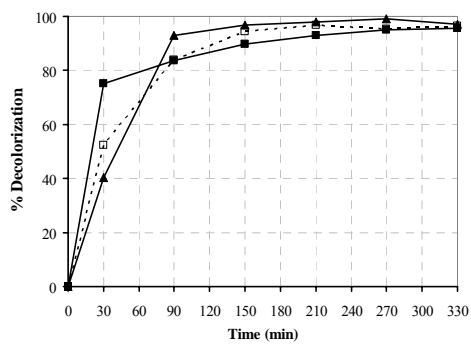
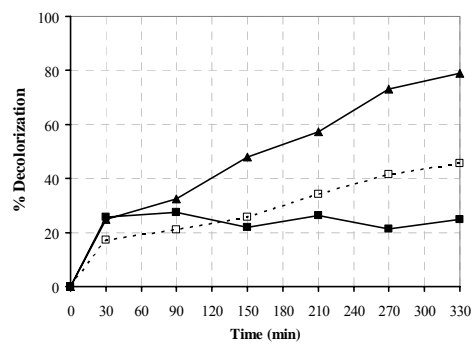
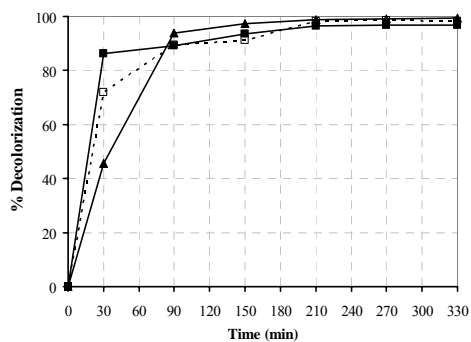
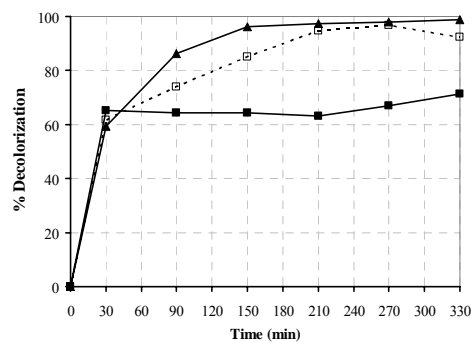
**Scheme 4.** Summary for the proposed formation mechanism of  $\bullet\text{O}_2^-$  and  $\bullet\text{OH}$  on anatase and rutile  $\text{TiO}_2$  crystal. (a) without  $\text{H}_2\text{O}_2$  and (b) with  $\text{H}_2\text{O}_2$  (Hirakawa, *et al.*, 2007).



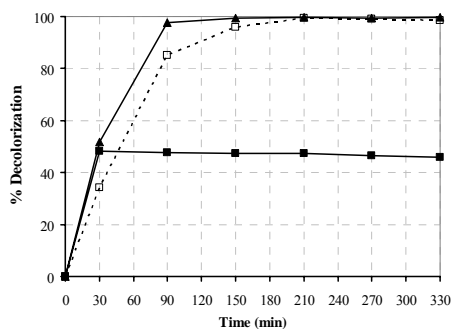
(a) Ti-no-acid



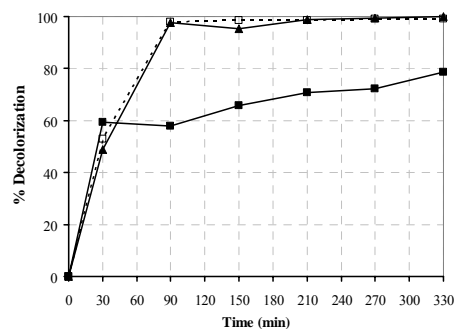
(b) Ti-HCl

(c) Ti-HNO<sub>3</sub>(d) Ti-H<sub>2</sub>SO<sub>4</sub>(e) Ti-CH<sub>3</sub>COOH(f) Ti-H<sub>3</sub>PO<sub>4</sub>

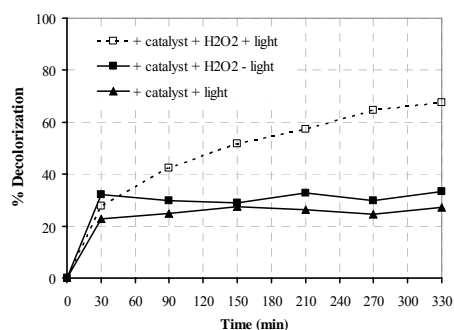
**Figure 47.** Effect of hydrogen peroxide on MB solution ( $1 \times 10^{-5}$ M) as a function on time in the presence of 0.5 g/L synthesized TiO<sub>2</sub>: (a) Ti-no-acid, (b) Ti-HCl, (c) Ti-HNO<sub>3</sub>, (d) Ti-H<sub>2</sub>SO<sub>4</sub>, (e) Ti-CH<sub>3</sub>COOH, and (f) Ti-H<sub>3</sub>PO<sub>4</sub>. (□ denotes + TiO<sub>2</sub> + H<sub>2</sub>O<sub>2</sub> + light, ■ denotes +TiO<sub>2</sub> + H<sub>2</sub>O<sub>2</sub> - light, and ▲ denotes +TiO<sub>2</sub> + light)



(a) Degussa P25

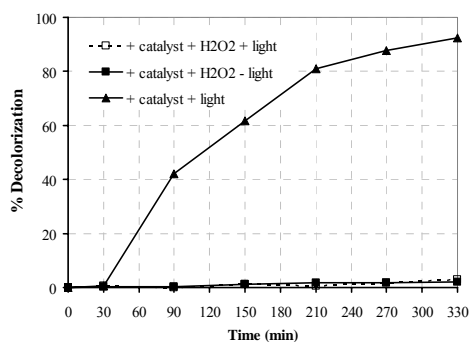


(b) Anatase (Carlo Erba)

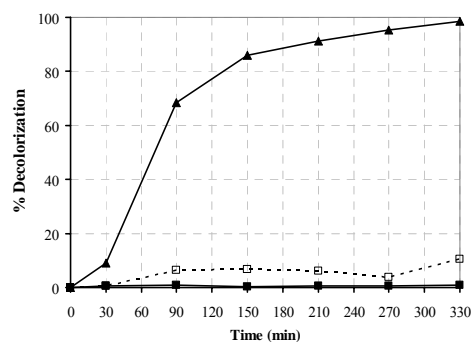


(c) Rutile (R706, TOA)

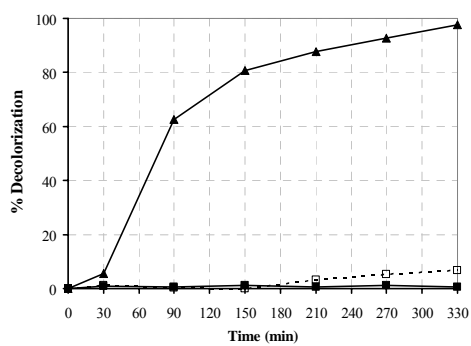
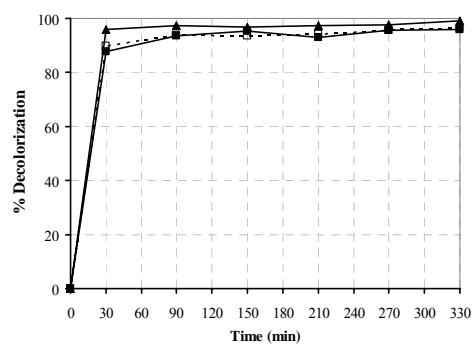
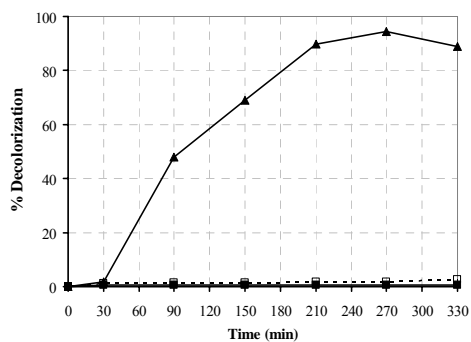
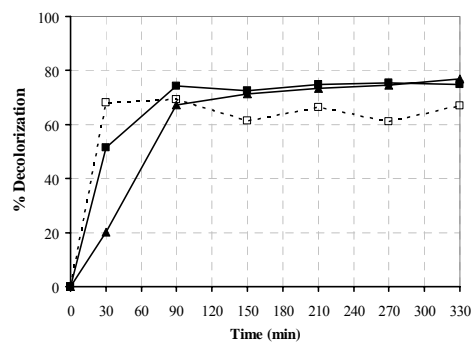
**Figure 48.** Effect of hydrogen peroxide on MB solution ( $1 \times 10^{-5}M$ ) as a function on time in the presence of 0.5 g/L commercial  $TiO_2$ : (a) Degussa P25, (b) Anatase (Carlo Erba), and (c) Rutile (R706, TOA). ( $\square$  denotes +  $TiO_2$  +  $H_2O_2$  + light,  $\blacksquare$  denotes +  $TiO_2$  +  $H_2O_2$  - light, and  $\blacktriangle$  denotes +  $TiO_2$  + light)



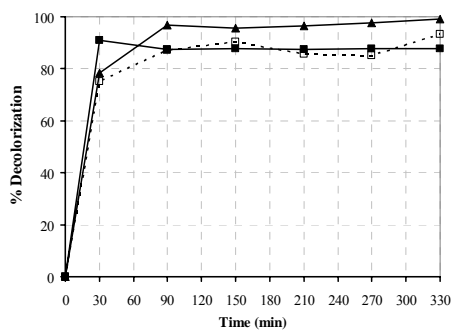
(a) Ti-no-acid



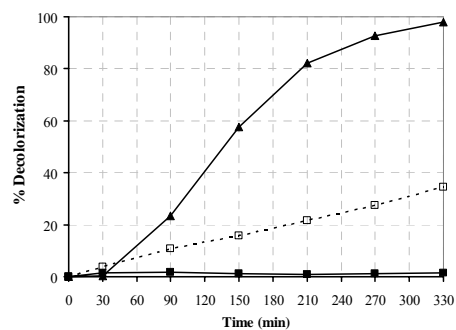
(b) Ti-HCl

(c) Ti-HNO<sub>3</sub>(d) Ti-H<sub>2</sub>SO<sub>4</sub>(e) Ti-CH<sub>3</sub>COOH(f) Ti-H<sub>3</sub>PO<sub>4</sub>

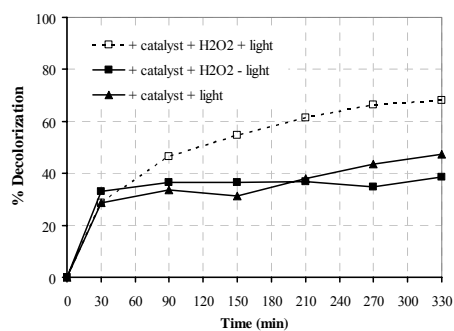
**Figure 49.** Effect of hydrogen peroxide on CR solution ( $1 \times 10^{-5}$ M) as a function on time in the presence of 0.5 g/L synthesized TiO<sub>2</sub>: (a) Ti-no-acid, (b) Ti-HCl, (c) Ti-HNO<sub>3</sub>, (d) Ti-H<sub>2</sub>SO<sub>4</sub>, (e) Ti-CH<sub>3</sub>COOH, and (f) Ti-H<sub>3</sub>PO<sub>4</sub>. (□ denotes + TiO<sub>2</sub> + H<sub>2</sub>O<sub>2</sub> + light, ■ denotes +TiO<sub>2</sub> + H<sub>2</sub>O<sub>2</sub> - light, and ▲ denotes +TiO<sub>2</sub> + light)



(a) Degussa P25

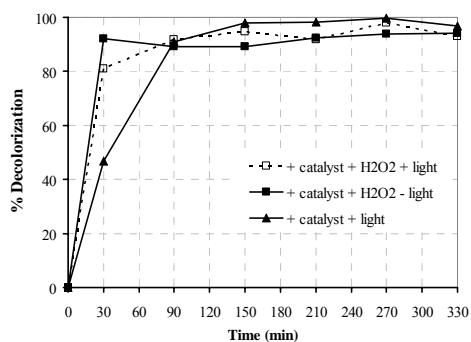


(b) Anatase (Carlo Erba)

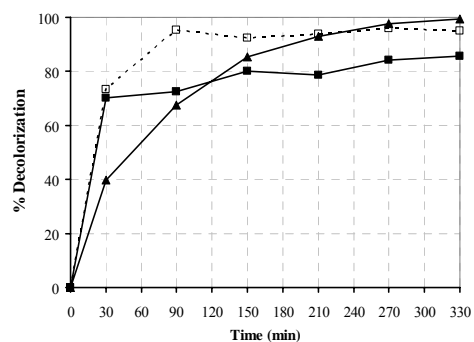


(c) Rutile (R706, TOA)

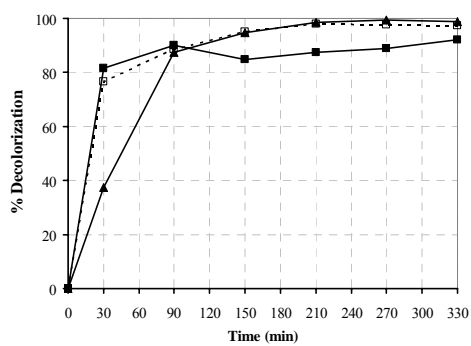
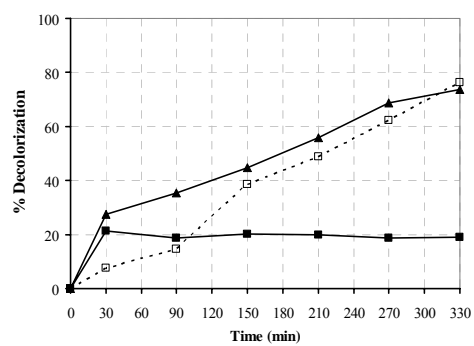
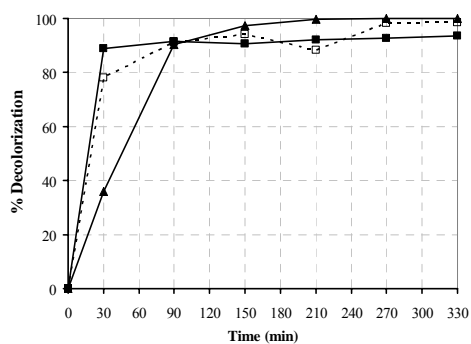
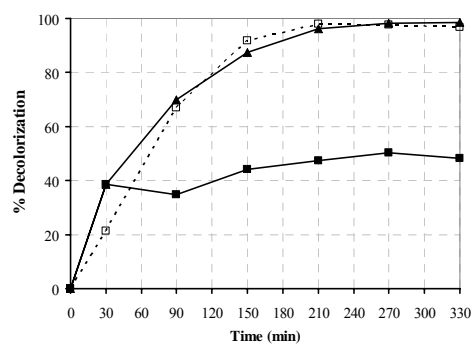
**Figure 50.** Effect of hydrogen peroxide on CR solution ( $1 \times 10^{-5}$ M) as a function on time in the presence of 0.5 g/L commercial TiO<sub>2</sub>: (a) Degussa P25, (b) Anatase (Carlo Erba), and (c) Rutile (R706, TOA). ( $\square$  denotes + TiO<sub>2</sub> + H<sub>2</sub>O<sub>2</sub> + light,  $\blacksquare$  denotes +TiO<sub>2</sub> + H<sub>2</sub>O<sub>2</sub> - light, and  $\blacktriangle$  denotes +TiO<sub>2</sub> + light)



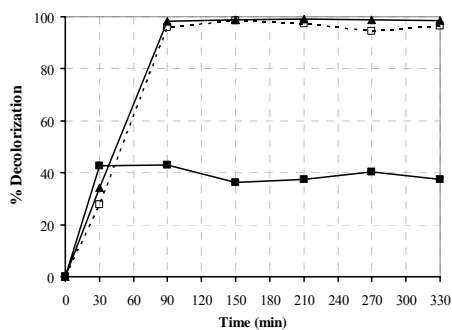
(a) Ti-no-acid



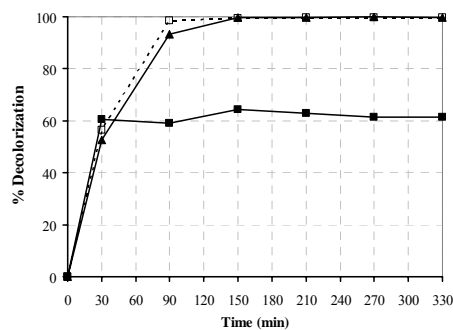
(b) Ti-HCl

(c) Ti-HNO<sub>3</sub>(d) Ti-H<sub>2</sub>SO<sub>4</sub>(e) Ti-CH<sub>3</sub>COOH(f) Ti-H<sub>3</sub>PO<sub>4</sub>

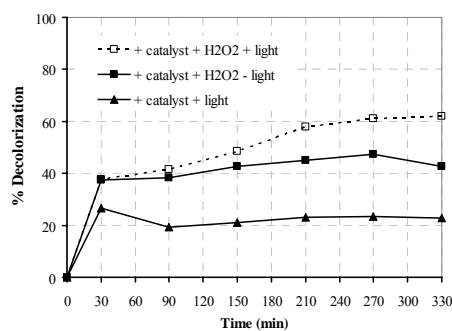
**Figure 51.** Effect of hydrogen peroxide on CV solution ( $1 \times 10^{-5}$ M) as a function on time in the presence of 0.5 g/L synthesized TiO<sub>2</sub>: (a) Ti-no-acid, (b) Ti-HCl, (c) Ti-HNO<sub>3</sub>, (d) Ti-H<sub>2</sub>SO<sub>4</sub>, (e) Ti-CH<sub>3</sub>COOH, and (f) Ti-H<sub>3</sub>PO<sub>4</sub>. (□ denotes + TiO<sub>2</sub> + H<sub>2</sub>O<sub>2</sub> + light, ■ denotes +TiO<sub>2</sub> + H<sub>2</sub>O<sub>2</sub> - light, and ▲ denotes +TiO<sub>2</sub> + light)



(a) Degussa P25



(b) Anatase (Carlo Erba)



(c) Rutile (R706, TOA)

**Figure 52.** Effect of hydrogen peroxide on CV solution ( $1 \times 10^{-5}$ M) as a function on time in the presence of 0.5 g/L commercial TiO<sub>2</sub>: (a) Degussa P25, (b) Anatase (Carlo Erba), and (c) Rutile (R706, TOA). (□ denotes + TiO<sub>2</sub> + H<sub>2</sub>O<sub>2</sub> + light, ■ denotes +TiO<sub>2</sub> + H<sub>2</sub>O<sub>2</sub> - light, and ▲ denotes +TiO<sub>2</sub> + light)

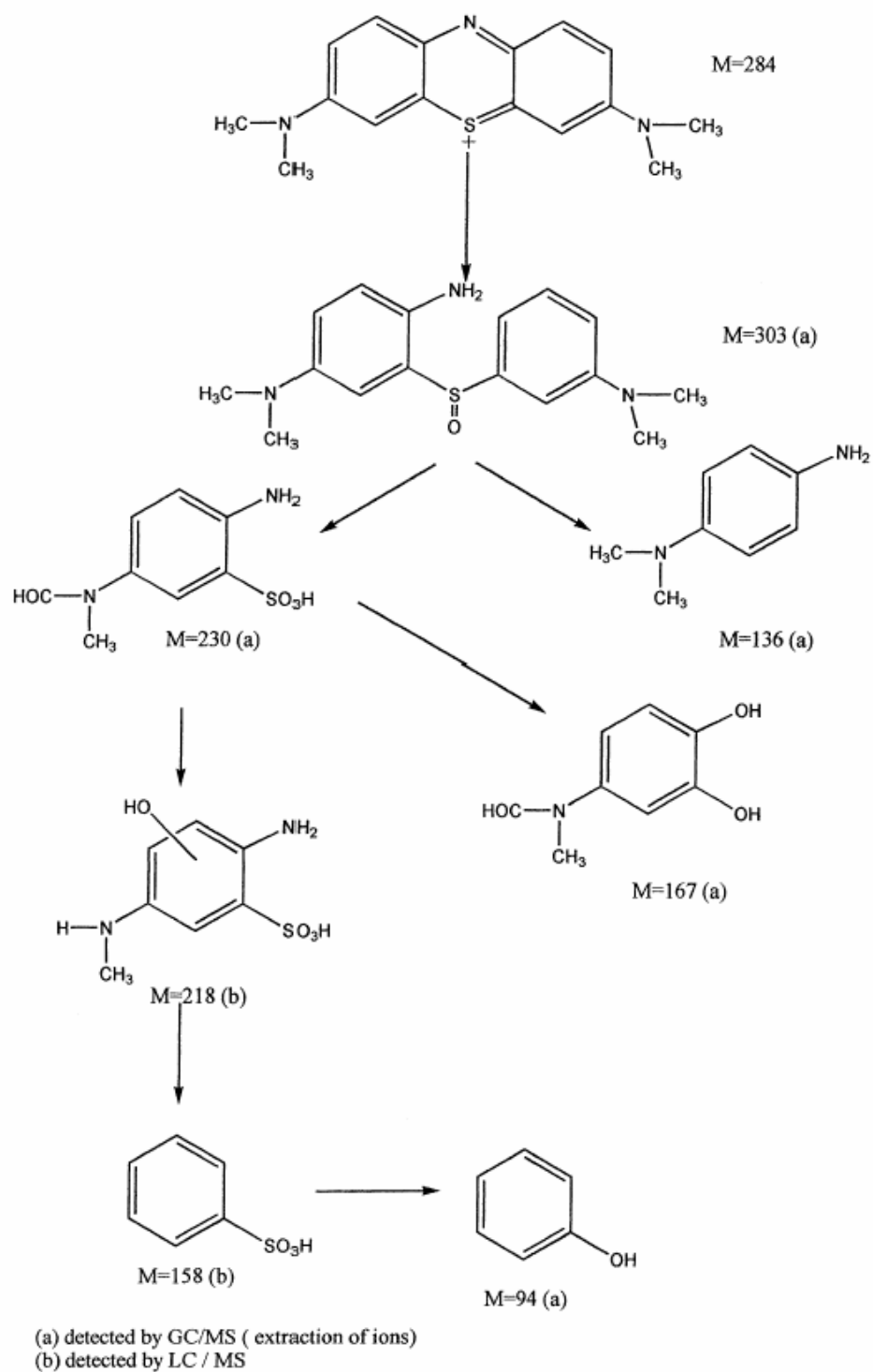
### 3.1.3.5 Photocatalytic degradation pathway of dye from literatures

#### (1) Methylene blue

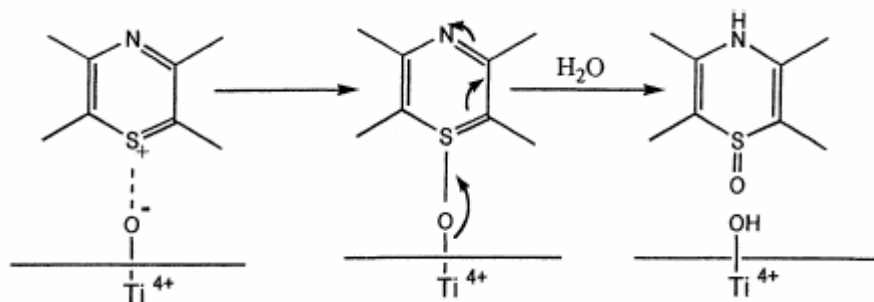
Houas, *et al.*, (2001) studied the TiO<sub>2</sub>/UV photocatalytic degradation of methylene blue in aqueous heterogeneous suspensions. A detailed reaction mechanism was presented from the initial step of adsorption involving the cationic functional group of methylene blue molecule, which was probably adsorbed perpendicularly to the surface down to the final products (CO<sub>2</sub>, SO<sub>4</sub><sup>2-</sup>, NH<sub>4</sub><sup>+</sup>, and NO<sub>3</sub><sup>-</sup>). The degradation intermediates originated from the initial opening of the central aromatic ring and their subsequent metabolites were formed in agreement with general rules already put in evidence in the degradation of other complex molecules in water. It can be concluded that photocatalysis can decontaminate colored used waters. Photocatalysis appears as the only sub-discipline of heterogeneous catalysis, which is able to convert organic pollutants to CO<sub>2</sub> in water without heating nor using high pressure of oxygen nor requiring chemical reactants or additives.

The main aromatic metabolites resulting from methylene blue decomposition are presented in Scheme 5, where they are logically reported according to their decreasing molecular weight. The initial step of methylene blue degradation can be ascribed to the cleavage of the bonds of the C-S<sup>+</sup>=C functional group in methylene blue. The electrophilic attack of •OH concerned the free doublet of heteroatom S, making its oxidation degree pass from -2 to 0. However, the passage from C-S<sup>+</sup>=C to C-S(=O)-C requires the conservation of double bond conjugation, which induces the opening of the central aromatic ring containing both heteroatoms, S and N. The origin of H atoms necessary to C-H and N-H bond formation can be proposed from the proton reduction by photogenerated electrons as already observed in alcohol dehydrogenation and pesticide degradation. An alternative rearrangement of the phenothiazine structure is presented in Scheme 6. The sulfoxide group can undergo a second attack by an •OH radical producing the sulfone (non-detected) and causing the definitive dissociation of the two benzenic rings.





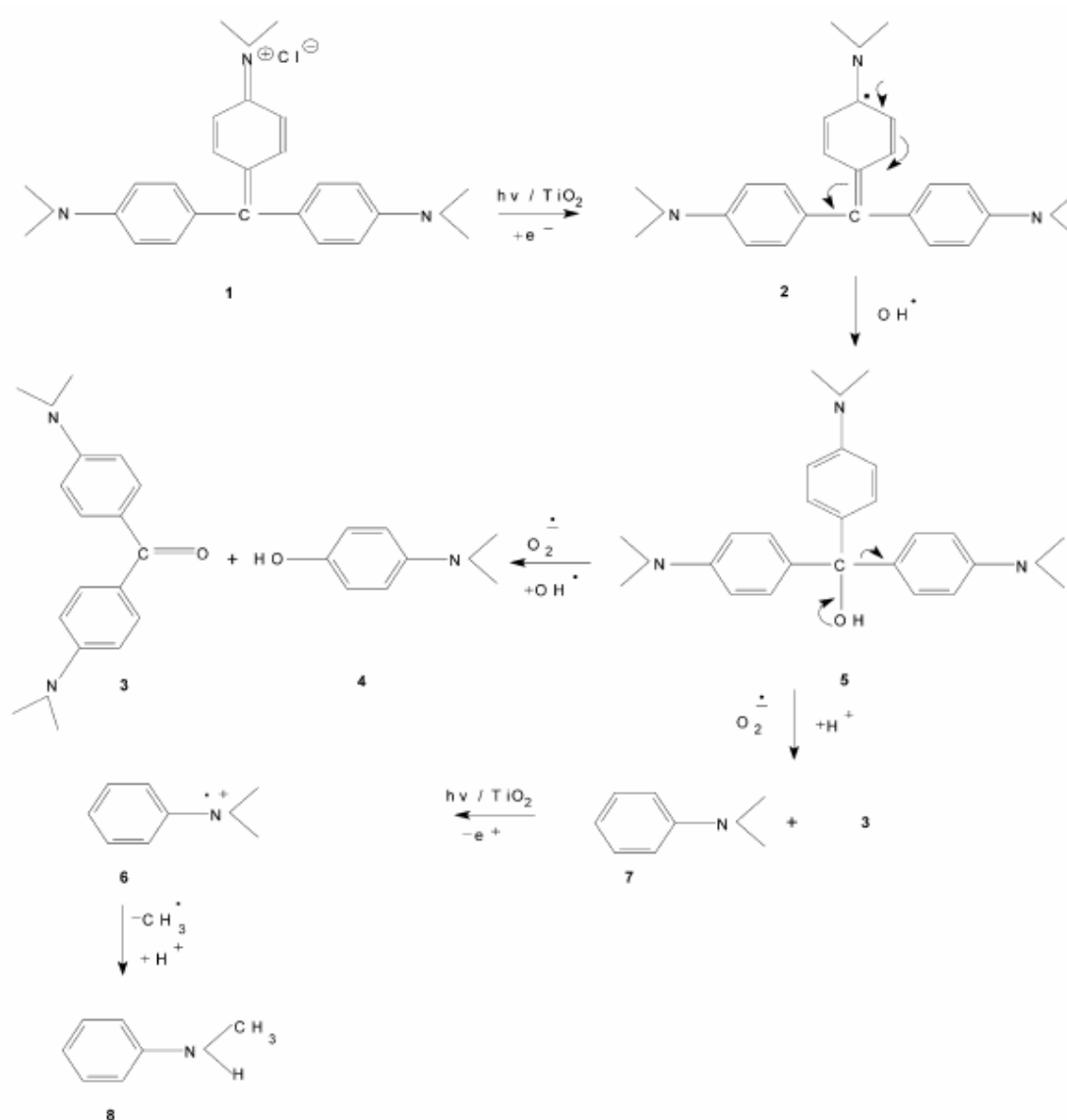
**Scheme 5.** Photocatalytic degradation pathway of methylene blue (Houas, *et al.*, 2001).



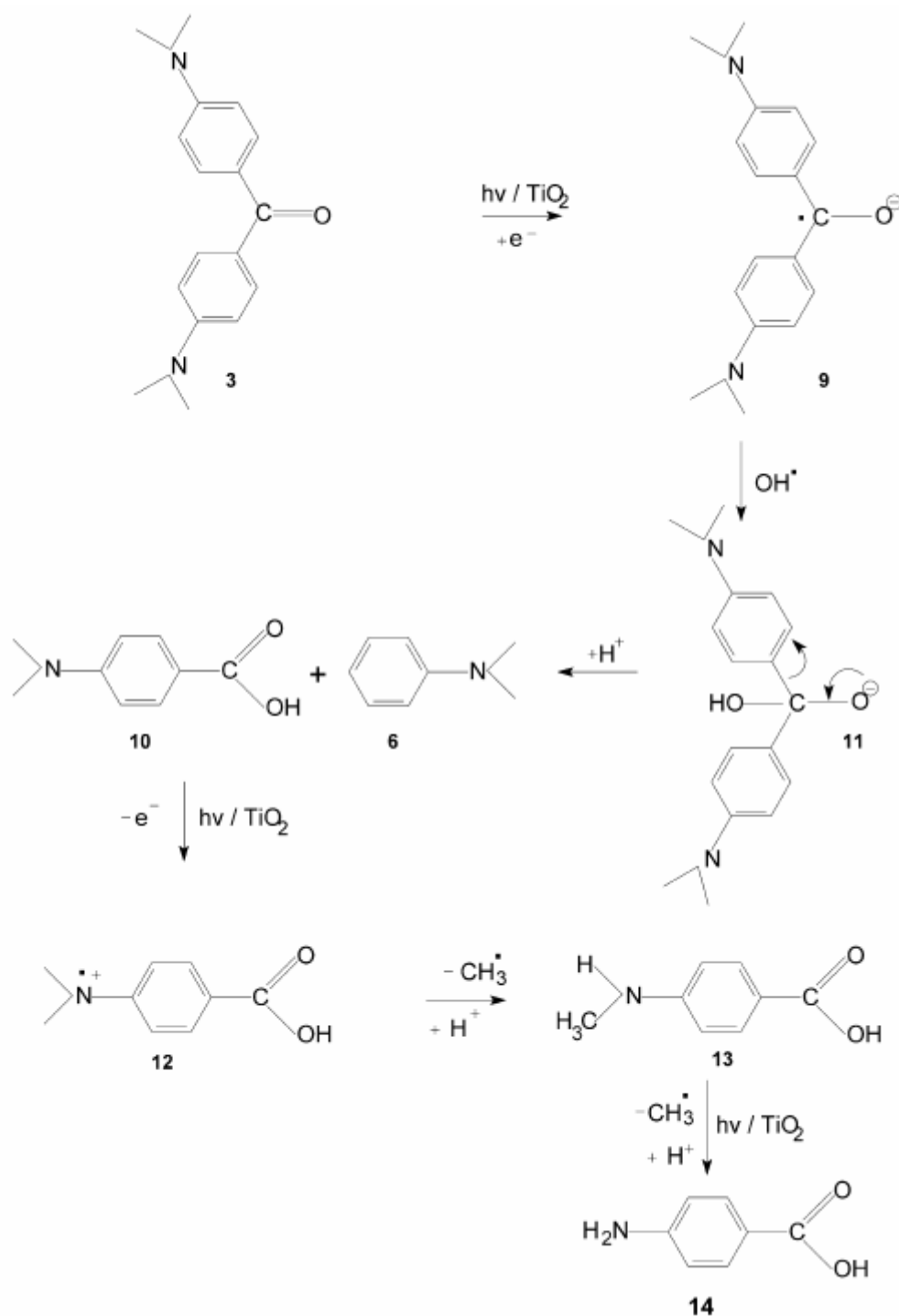
**Scheme 6.** Electronic reorganization during the passage of adsorbed methylene blue to the sulfoxide form (Houas, *et al.*, 2001).

## (2) Crystal violet (Gentian violet)

Saquib and Muneer (2003) proposed a plausible mechanism for the formation of intermediate products involving electron transfer reactions and reaction with hydroxyl radicals formed in the photocatalytic system in Schemes 7 and 8, respectively. The model compound (gentian violet) 1 upon the transfer of an electron can form the radical species 2 which may undergo addition of a hydroxyl radical forming 5 which in turn may undergo cleavage either by abstracting a hydroxyl radical to form 4 or by abstracting a proton to form 7 along with the benzophenone derivative 3. The compound 7 on further transfer of an electron can form the radical cation 6 which may subsequently undergo loss of methyl group to give the observed product 8 as shown in Scheme 7. The formation of *p*-amino-benzoic acid (14) could be understood in terms of the pathways shown in Scheme 8. The benzophenone derivative 3 upon the transfer of an electron can form the radical anion 9 which can undergo addition of a hydroxyl radical forming the anionic species 11 subsequent cleavage of species 11 can lead to the formation of aniline and benzoic acid derivatives 6 and 10, respectively. The compound 10 on further transfer of an electron can give rise to radical cation 12 which may subsequently undergo loss of methyl group to give the observed product 14 as shown in Scheme 8.



**Scheme 7.** A mechanism for the formation of intermediate products involving electron transfer reactions in the photocatalytic system (Saquib and Muneer, 2003).



**Scheme 8.** A mechanism for the formation of intermediate products involving reaction with hydroxyl radicals formed in the photocatalytic system (Saquib and Muneer, 2003).

### (3) Congo red

Ma, *et al.*, (2007) proposed the possible degradation mechanisms of congo red. They suggested mechanism for the reaction of congo red with  $e_{aq}^-$  and  $\bullet OH$  is illustrated in Figure 53a and 53b, respectively.

Figure 53a illustrates the vary fast reaction that  $e_{aq}^-$  attacks the  $-N=N-$  double bond and destroys the conjugated system of congo red molecule. The anion is quickly protonated to form hydrazyl radical as follows:

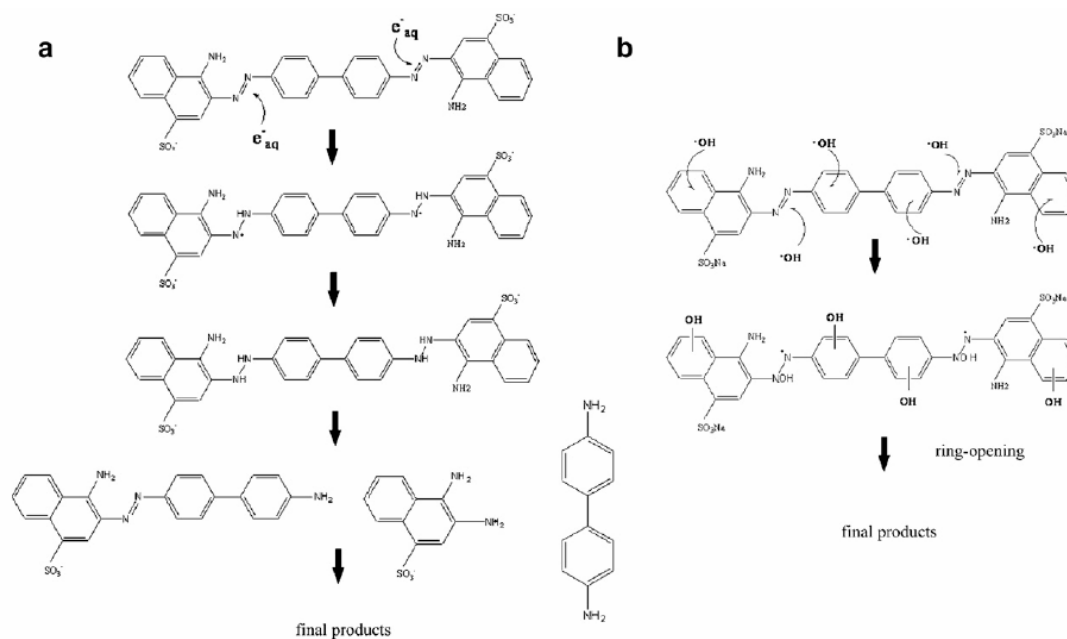
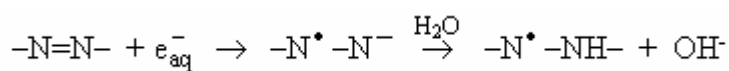


**Figure 53.** The suggested mechanisms for the degradation of congo red initiated by  $e_{aq}^-$  (a) and  $\bullet OH$  (b) (Ma, *et al.*, 2007).

The alternative mechanism for the reaction of  $\bullet\text{OH}$  with congo red is illustrated in Figure 53b. Among the oxidative species,  $\bullet\text{OH}$  is the major oxidative transient, and is known to react with benzene and azo moieties with high rate coefficients. Since one of the  $\bullet\text{OH}$ -adducts (product A) had almost the same visible absorption spectrum as congo red, it did not necessarily cause the destruction of the color centre. Besides, the  $\bullet\text{OH}$  addition to the  $-\text{N}=\text{N}-$  bond produced the hydrazyl radical,  $-\text{N}-\text{N}(\text{OH})\bullet$ , a similar radical to  $-\text{N}-\text{NH}\bullet$ . This reaction probably led to the destruction of the intensive color of the dye.

In the presence of  $\text{O}_2$ , when  $\text{O}_2$  cooperated with  $\bullet\text{OH}$  addition, peroxide was formed when  $\text{O}_2$  added to hydroxycyclohexadienyl radical (Figure 54). Most of the ring cleavage came from these peroxide compounds producing alcohols, aldehydes, and acids. As a result, a more prominent degradation pathway was engendered leading to the final evolution of  $\text{CO}_2$ .

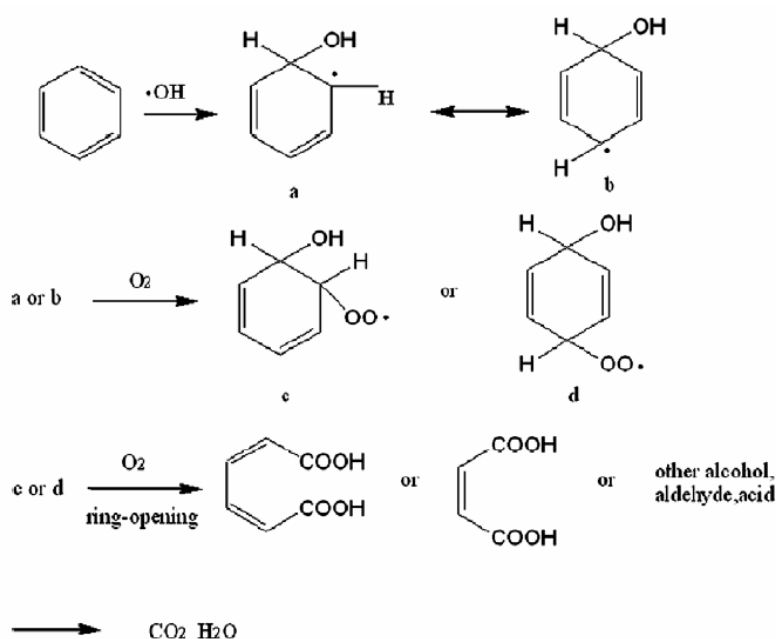
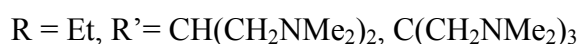
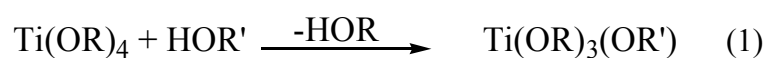


**Figure 54.** Postulated role of  $\text{O}_2$  played in the degradation of aromatic compounds (Ma, *et al.*, 2007).

## 3.2 Synthesis of titanium amino-alkoxides: precursors for the formation of TiO<sub>2</sub> materials

### 3.2.1 Synthesis

New titanium alkoxides [Ti(OR)<sub>3</sub>(OR')] (R = Et, Pr<sup>i</sup>; R' = bdmmap, tdmmap) have been synthesised by heating Ti(OR)<sub>4</sub> and Hbdmap / Htdmap in hexane:



Both ethoxides [Ti(OEt)<sub>3</sub>(bdmmap), Ti(OEt)<sub>3</sub>(tdmmap)] are white solids, though Ti(OEt)<sub>3</sub>(bdmmap) remains sticky after isolation from the recrystallisation solvent (CH<sub>2</sub>Cl<sub>2</sub>) while Ti(OEt)<sub>3</sub>(tdmmap) is very soft; the two iso-propoxide analogues [Ti(O<sup>i</sup>Pr)<sub>3</sub>(bdmmap), Ti(O<sup>i</sup>Pr)<sub>3</sub>(tdmmap)] are liquids. Attempts to purify Ti(O<sup>i</sup>Pr)<sub>3</sub>(bdmmap), Ti(O<sup>i</sup>Pr)<sub>3</sub>(tdmmap) (and other liquid products described in herein) by vacuum distillation resulted in decomposition, the NMR of the distillate containing only signals due to the OPr<sup>i</sup> groups. The formation of a bond between titanium and the aminoalcohol is evidenced by the large downfield <sup>13</sup>C NMR shift of the resonance due to the O-C nucleus with respect to the parent alcohol (bdmmap: *ca.* 64 to 75 ppm; tdmmap: *ca.* 74 to 84 ppm).

The room temperature <sup>1</sup>H and <sup>13</sup>C spectra of Ti(OEt)<sub>3</sub>(bdmmap) are simple and show that the dimeric structure of the compound (Figure 55) is fluxional under these conditions. The <sup>1</sup>H NMR has a broad singlet for the OCH<sub>2</sub> ethoxy protons overlapping with a weaker, also broad, singlet due to CHO of the bdmmap, but only one sharp singlet for the two distinct NMe<sub>2</sub> groups which overlaps a broad singlet from NCH<sub>2</sub> of the aminoalcohol. The OCH<sub>2</sub>CH<sub>3</sub> appear as a sharp triplet, though with some evidence of signal splitting. Similarly, the <sup>13</sup>C NMR shows single, albeit broadened, signals for each type of carbon with no resolution of the distinct ethoxide groups present in the dimer, nor any between chelated and free arms of the bdmmap ligand. On

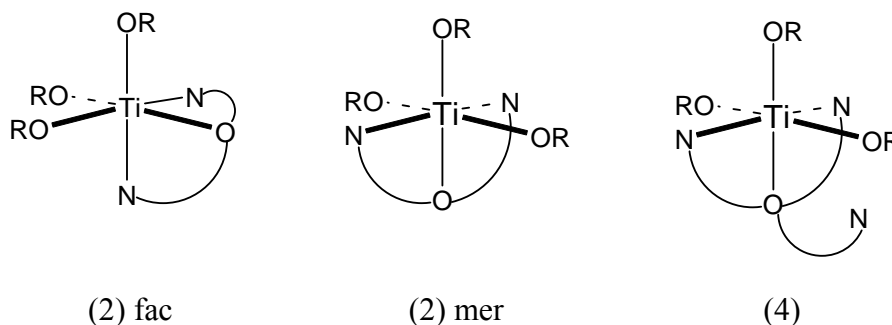
cooling to  $-50^{\circ}\text{C}$  however, the spectra become more complex, with multiple overlapping resonances for both  $\text{OCH}_2\text{CH}_3$  protons, the CH protons of the central part of the bdmmap, along with only minor splitting of the intense  $\text{NMe}_2$  singlet. The low temperature  $^{13}\text{C}$  NMR contains over 20 distinct resonances, which implies that the crystallographic symmetry within the dimer is lost in solution.

Similar, though less definitive, comments can be made about the tdmmap analogue. The  $\text{OCH}_2$  signal of the ethoxy groups is again broad and there is some indication of splitting in the associated  $\text{CH}_3$  triplet, though the remaining  $^1\text{H}$  NMR signals are sharp. The resonance due to the  $\text{NMe}_2$  groups is split into two, and while accurate integration of the separate signals is precluded by their overlapping nature, it is approximately in a 2:1 ratio; there is, however, no apparent splitting of the  $\text{CH}_2\text{N}$  resonance. The corresponding  $^{13}\text{C}$  spectrum has broad signals for both carbons of the ethoxy groups, and two major signals for each of the  $\text{N}(\text{CH}_3)_2$  and  $\text{CH}_2\text{N}$  carbons in *ca.* 2:1 ratio, but the presence of smaller third resonances in each case suggest the presence of a possible second species. It is likely that the structure of  $\text{Ti}(\text{OEt})_3(\text{tdmmap})$  resembles that of  $\text{Ti}(\text{OEt})_3(\text{bdmmap})$ ; the poorly diffracting nature of the crystals of  $\text{Ti}(\text{OEt})_3(\text{tdmmap})$  is consistent with four non-coordinated  $\text{CH}_2\text{NMe}_2$  groups in the dimer, which are probably disordered in the lattice given our experience with similar metal amino alcolates.

In contrast, the room temperature  $^1\text{H}$  NMR of  $\text{Ti}(\text{O}^i\text{Pr})_3(\text{bdmmap})$ , an oil for which no definitive structural data are available, is both sharp and simple. Clear, defined multiplets are visible for both  $\text{OCHMe}_2$  and  $\text{OCH}(\text{CH}_2\text{NMe})_2$  at 4.60 (septet) and 4.38 ppm, respectively. There is a single sharp doublet for the  $\text{OCH}(\text{CH}_3)_2$  protons (1.20 ppm) and a further intense singlet at 2.28 ppm for the  $\text{N}(\text{CH}_3)_2$  group, partially overlapping with one of two multiplets (2.47, 2.33 ppm) due to the  $\text{CH}_2\text{N}$  part of the bdmmap. These multiplets arise when both arms of the bdmmap chelate a metal, making the ligand rigid and the two  $\text{CH}_2$  hydrogens non-equivalent. The  $^{13}\text{C}$  NMR spectrum is equally simple, with only five sharp singlets corresponding to the five unique carbon environments in the molecule. This pattern of data, taken in contrast to that of  $\text{Ti}(\text{OEt})_3(\text{bdmmap})$ , is suggestive of a monomeric, rather than dimeric structure, in which both donor arms of the bdmmap ligand to chelate the metal,



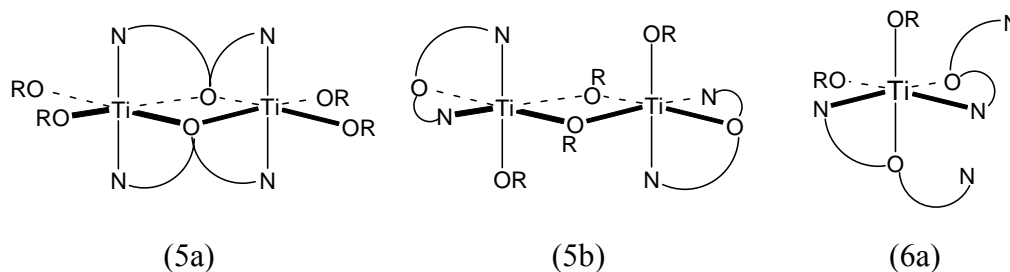
assuming the common octahedral coordination preferred by titanium is maintained. In addition, the data are in keeping with the more symmetrical *mer* isomer, which, for example, allows all the NCH<sub>3</sub> groups to become equivalent.



For [Ti(O<sup>i</sup>Pr)<sub>3</sub>(tdmap)], sharp signals are seen for both nuclei in both the room temperature <sup>1</sup>H and <sup>13</sup>C NMR spectra and indicate only one O<sup>i</sup>Pr, CH<sub>2</sub>N and NMe<sub>2</sub> environment, respectively. Since the coordination number at the metal is unlikely to go beyond six, we suggest that a monomeric structure similar to Ti(O<sup>i</sup>Pr)<sub>3</sub>(bdmap) exists, in which the isopropoxy groups are static but that some rapid fluxionality of the CH<sub>2</sub>NMe<sub>2</sub> groups, with two coordinated and one free, takes place.

Attempts to introduce additional chelating amino-alkoxides groups have only been partially successful. When the reaction described by equation (1) was carried out with increasing amounts of amino alcohol, further substitution of the monodentate alkoxide was evident, though <sup>1</sup>H NMR integrals suggested that the desired substitution was incomplete, a situation which became progressively more evident as the reaction stoichiometry increased in favour of the chelating ligand. Both [Ti(OEt)<sub>2</sub>(bdmap)<sub>2</sub>] and [Ti(O<sup>i</sup>Pr)<sub>2</sub>(bdmap)<sub>2</sub>] are essentially pure by NMR, though both are liquids which could not be obtained analytically purity. The NMR data for these two species seem to follow the same trends as compounds Ti(OEt)<sub>3</sub>(bdmap), Ti(O<sup>i</sup>Pr)<sub>3</sub>(bdmap), Ti(OEt)<sub>3</sub>(tdmap), and Ti(O<sup>i</sup>Pr)<sub>3</sub>(tdmap) : the ethoxy derivative shows broad signals for all protons in the <sup>1</sup>H NMR, and, while the <sup>13</sup>C NMR is generally sharper, the only clear non-equivalence is in the CH<sub>2</sub>N groups, where two signals (*ca.* 3:1 relative intensity) are apparent. The <sup>13</sup>C NMR signals due to the OCH fragments of bdmap overlap with the signals from the solvent (all *ca.* 75 ppm) and

preclude detailed comment on this region of the spectrum, though some evidence for signal splitting occurs here. The structural implications of this data remain conjecture. A monomeric, presumably six-coordinated species, would require two of the four NMe<sub>2</sub> groups to be pendent, inconsistent with both the *ca.* 3:1 CH<sub>2</sub>N moieties and the fluxional nature of the compound suggested by the broad <sup>1</sup>H NMR signals. A rigid, symmetrical, dimeric arrangement such as 5a, while incorporating a common bdmapp bridging mode, is also inconsistent with the NMR data, so a variation incorporating  $\mu$ -OEt groups and exemplified by 5b seems most likely.



For Ti(O<sup>i</sup>Pr)<sub>2</sub>(bdmap)<sub>2</sub>, the NMR signals are uniformly sharp but a difference in the two iso-propoxy environments is evident from overlapping septets due to CHO, while splitting of both the CH<sub>2</sub>N and NMe<sub>2</sub> signals (*ca.* 2:1:1 ratio from the <sup>13</sup>C NMR) is also clear. In comparison with Ti(O<sup>i</sup>Pr)<sub>3</sub>(bdmap), a monomeric complex with two terminal (but marginally different) O<sup>i</sup>Pr groups and two chelating bdmapp ligands (each with one free NMe<sub>2</sub> group) in an isomeric form which renders the two coordinate Me<sub>2</sub>N:→Ti interactions non-equivalent e.g. 6a, would rationalise the NMR data. A small number of crystals of the hydrolysis product [(bdmap)<sub>2</sub>TiO]<sub>2</sub> appeared within the oil that is [Ti(OEt)<sub>2</sub>(bdmap)<sub>2</sub>] on standing over a period of several days.

### 3.2.2 Crystallography

Experimental details relating to the single-crystal X-ray crystallographic studies are summarised in Table 9. For [Ti(OEt)<sub>3</sub>(bdmap)]<sub>2</sub> a symmetry-related (multi-scan) absorption correction was employed. Structure solution followed by full-

matrix least squares refinement was performed using the WinGX-1.70 suite of programmes throughout.

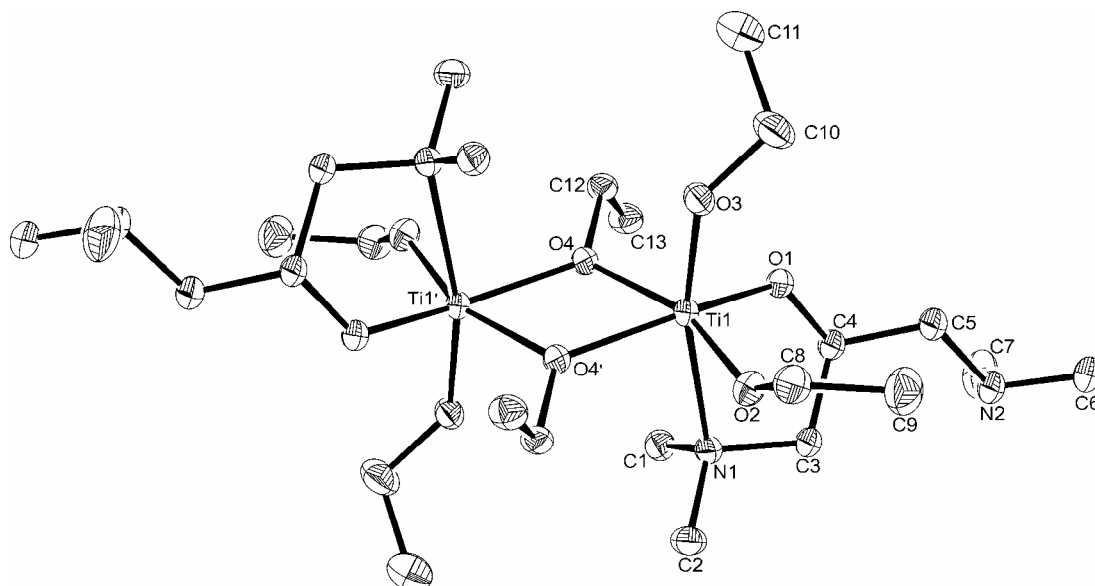


**Figure 55.** The asymmetric unit of  $[\text{Ti}(\text{OEt})_3(\text{bdmap})]_2$  showing the labelling scheme used; thermal ellipsoids are at the 30% probability level. Only one of two essentially identical molecules which make up the asymmetric unit is shown for clarity and discussed in the text.

The structure of  $[\text{Ti}(\text{OEt})_3(\text{bdmap})]_2$  is shown in Figure 55 and is a centrosymmetric dimer containing  $\mu$ -OEt bridges. The selected bond lengths and angles are given in Table 7. Each titanium is six-coordinated with a  $\text{TiO}_5\text{N}$  coordination sphere. The two terminal ethoxy groups are most tightly bound [Ti(1)-O(2) 1.839(2), Ti(1)-O(3) 1.8122(18) Å], followed by the amino-alkoxide [Ti(1)-O(1) 1.866(2) Å] while the bridging interactions are, unsurprisingly, weaker [Ti(1)-O(4) 2.0194(18), Ti(1)-O(4') 2.0793(19) Å]. Coordination is completed by chelation from one terminal amine [Ti(1)-N(1) 2.432(2) Å] while the other amine function based on N(2) remains pendant. The Ti-N bond seems typical of these species (see below) and allows slightly stronger bonding from the ethoxide based on O(3) to which it is *trans*,

in comparison with the other terminal alkoxide [O(2)] despite the latter being *trans* to the bridging  $\mu$ -OEt moiety.

**Table 7.** Selected bond lengths [ $\text{\AA}$ ] and angles [ $^\circ$ ] for  $\text{Ti}(\text{OEt})_3(\text{bdmap})$ .

Atoms	Bond lengths [ $\text{\AA}$ ]	Atoms	Bond angles [ $^\circ$ ]
Ti(1)-O(1)	1.8641(19)	O(1)-Ti(1)-O(2)	102.56(9)
Ti(1)-O(2)	1.839(2)	O(1)-Ti(1)-O(3)	92.42(8)
Ti(1)-O(3)	1.8122(18)	O(1)-Ti(1)-O(4)	157.96(9)
Ti(1)-O(4)	2.0194(18)	O(1)-Ti(1)-O(4')	92.13(8)
Ti(1)-O(4')	2.0793(19)	O(1)-Ti(1)-N(1)	74.38(8)
Ti(1)-N(1)	2.432(2)	O(2)-Ti(1)-O(3)	97.19(9)
		O(2)-Ti(1)-O(4)	91.53(8)
		O(2)-Ti(1)-O(4')	161.68(8)
		O(2)-Ti(1)-N(1)	80.50(8)
		O(3)-Ti(1)-O(4)	102.65(8)
		O(3)-Ti(1)-O(4')	93.01(8)
		O(3)-Ti(1)-N(1)	165.60(8)
		O(4)-Ti(1)-O(4')	71.35(8)
		O(4)-Ti(1)-N(1)	91.64(7)
		N(1)-Ti(1)-O(4')	93.21(7)

Symmetry operation: #1  $-x+2, -y+1, -z$ .

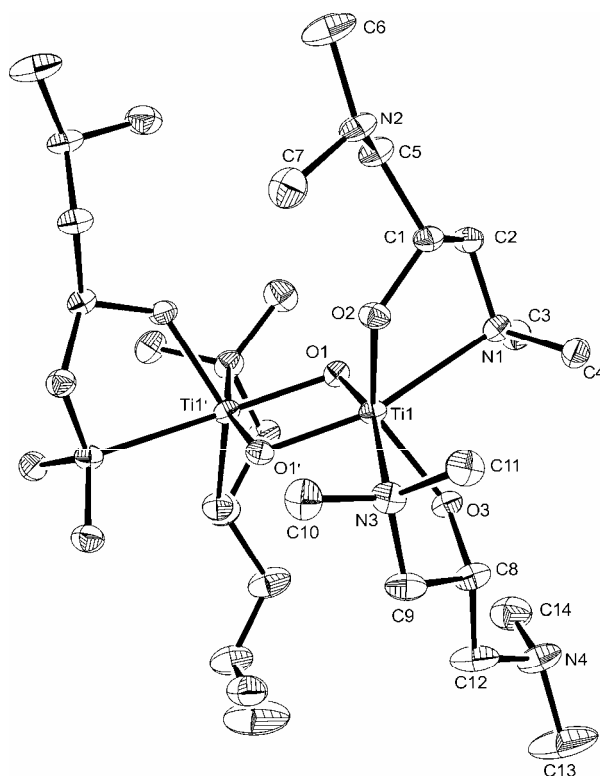


**Figure 56.** The asymmetric unit of  $[(\text{bdmap})\text{TiO}]_2$  showing the labelling scheme used; thermal ellipsoids are at the 30% probability level. The  $\text{NMe}_2$  group based on N(4) is disordered over two sites (65:35); only the major component of the disorder is shown for clarity.

Hydrolysis of  $\text{Ti}(\text{OEt})_3(\text{bdmap})$  affords the  $\mu\text{-O}$  dimer  $[(\text{bdmap})\text{TiO}]_2$  (Figure 56) generated by a crystallographically imposed two-fold axis running through the centre of the  $\text{Ti}_2\text{O}_2$  ring. The selected bond lengths and angles are given in Table 8. Each titanium retains its octahedral coordination, but this is now made up of two chelating amino alcohols in addition to the two bridging groups. The overall coordination is  $\text{TiO}_4\text{N}_2$  in a *cis, cis, trans* arrangement of  $\mu\text{-O}$ , coordinated amines and alkoxides centres, respectively. The  $\text{Ti}_2\text{O}_2$  core is more tightly bound than in  $\text{Ti}(\text{OEt})_3(\text{bdmap})$  [ $\text{Ti}(1)\text{-O}(1)$  1.8445(13),  $\text{Ti}(1)\text{-O}(1')$  1.8474(14) Å], while the two amino-alkoxides show similar bond strengths [ $\text{Ti}(1)\text{-O}(2)$  1.8777(14),  $\text{Ti}(1)\text{-O}(3)$  1.8826(14) Å]. The two coordinated amines [ $\text{Ti}(1)\text{-N}(1)$  2.3962(18),  $\text{Ti}(1)\text{-N}(3)$  2.4529(18) Å], which are *trans* to the two  $\mu\text{-O}$  groups, straddle the observed Ti-N

bond length in  $\text{Ti}(\text{OEt})_3(\text{bdmap})$  [2.432(2) Å], which is *trans* to a terminal OEt unit. As with  $\text{Ti}(\text{OEt})_3(\text{bdmap})$ , two amine groups (one per bdmap ligand) remain uncoordinated to the metal.

**Table 8.** Selected bond lengths [Å] and angles [°] for  $[(\text{bdmap})\text{TiO}]_2$ .

Atoms	Bond lengths [Å]	Atoms	Bond angles [°]
Ti(1)-O(1)	1.8445(13)	O(1)-Ti(1)-O(1')	82.19(6)
Ti(1)-O(1')	1.8474(14)	O(1)-Ti(1)-O(2)	109.35(6)
Ti(1)-O(2)	1.8774(14)	O(1)-Ti(1)-O(3)	104.61(6)
Ti(1)-O(3)	1.8826(14)	O(1)-Ti(1)-N(1)	81.70(6)
Ti(1)-N(1)	2.3962(18)	O(1)-Ti(1)-N(3)	162.97(6)
Ti(1)-N(3)	2.4529(18)	O(1')-Ti(1)-O(2)	103.88(6)
		O(1')-Ti(1)-O(3)	109.15(6)
		O(1')-Ti(1)-N(1)	162.18(6)
		O(1')-Ti(1)-N(3)	82.35(6)
		O(2)-Ti(1)-O(3)	135.08(7)
		O(2)-Ti(1)-N(1)	74.53(6)
		O(2)-Ti(1)-N(3)	81.36(6)
		O(3)-Ti(1)-N(1)	82.36(6)
		O(3)-Ti(1)-N(3)	73.94(6)
		N(1)-Ti(1)-N(3)	114.50(6)

Symmetry operation: #1  $-x+1, y, -z+3/2$

**Table 9.** Crystallographic data for [Ti(OEt)<sub>3</sub>(bdmap)]<sub>2</sub> and [(bdmap)<sub>2</sub>TiO]<sub>2</sub>

	[Ti(OEt) <sub>3</sub> (bdmap)] <sub>2</sub>	[(bdmap) <sub>2</sub> TiO] <sub>2</sub>
Empirical formula	C <sub>26</sub> H <sub>64</sub> N <sub>4</sub> O <sub>8</sub> Ti <sub>2</sub>	C <sub>28</sub> H <sub>68</sub> N <sub>8</sub> O <sub>6</sub> Ti <sub>2</sub>
Formula weight	656.61	708.70
Crystal system	Triclinic	Monoclinic
Space group	P $\bar{1}$	C2/c
<i>a</i> , Å	9.1310(2)	13.0770(3)
<i>b</i> , Å	12.6400(3)	15.9297(4)
<i>c</i> , Å	17.1220(6)	19.8605(6)
$\alpha$ , °	69.905(1)	
$\beta$ , °	76.840(1)	108.460(1)
$\gamma$ , °	81.660(2)	
Volume, Å <sup>3</sup>	1802.30(9)	3924.24(18)
<i>Z</i>	2	4
$\mu$ (Mo-K $\alpha$ ), mm <sup>-1</sup>	0.488	0.452
Crystal size, mm	0.30 x 0.20 x 0.05	0.30 x 0.30 x 0.25
Reflections collected	23405	24881
Independent reflections	7056 [R(int) = 0.0595]	4448 [R(int) = 0.0483]
Reflections observed (>2 $\sigma$ )	5058	3635
Data completeness	0.976	0.986
Max., min. transmission	0.97, 0.87	0.96, 0.90
Data / restraints / parameters	7052 / 0 / 410	4448 / 0 / 237
Goodness-of-fit on F <sup>2c</sup>	1.055	1.092
Final R <sub>1</sub> <sup>a</sup> , wR <sub>2</sub> <sup>b</sup> [I>2 $\sigma$ (I)]	0.0493, 0.1180	0.0441, 0.1059
Final R <sub>1</sub> <sup>a</sup> , wR <sub>2</sub> <sup>b</sup> (all data)	0.0799, 0.1342	0.0582, 0.1146
Largest diff. peak and hole, e Å <sup>-3</sup>	0.948, -0.481	0.430, -0.351

$$^a R_1 = \frac{\sum ||F_o| - |F_c||}{\sum |F_o|}, \quad ^b wR_2 = \left\{ \frac{\sum [w(F_o^2 - F_c^2)^2]}{\sum [w(F_o^2)]} \right\}^{1/2}$$

$$^c \text{GOF} = S = \left\{ \frac{\sum [w(F_o^2 - F_c^2)^2]}{(n-p)} \right\}^{1/2}$$

### 3.2.3 Thermal decomposition of $[\text{Ti}(\text{OEt})_3(\text{bdmap})]_2$

$[\text{Ti}(\text{OEt})_3(\text{bdmap})]_2$  has been thermally decomposed at  $700^\circ\text{C}$  in a sealed steel ampoule, a technique coined RAPET (Reaction under Autogenerated Pressure at Elevated Temperatures) and first described by Gedanken (Pol, *et al.*, 2004). In contrast to CVD where the experimental arrangement allows all the residual carbon to be eliminated thermally, under RAPET conditions this is not the case. In addition, the autogenerated pressure which accrues during decomposition also facilitates the formation of core-shell nanoparticles of different types e.g. carbon coated  $\text{V}_2\text{O}_3$  (Pol, *et al.*, 2004) or  $\text{MoO}_2$  (Pol, *et al.*, 2004), silicon coated carbon spheres (Pol, *et al.*, 2004), or carbon sausages with *in situ*  $\text{WO}_3$  (Pol, *et al.*, 2006).

In the RAPET of  $[\text{Ti}(\text{OEt})_3(\text{bdmap})]_2$  some carbon is lost (presumably as hydrocarbons) as evidenced by a pressure release on opening the apparatus, though considerable amounts of organic matter, but particularly carbon, are still present in the final black residue (C 32.7%, H 0.82%, N 2.32%). This represents approximately two-thirds retention of carbon from  $[\text{Ti}(\text{OEt})_3(\text{bdmap})]_2$  (C 47.5%).

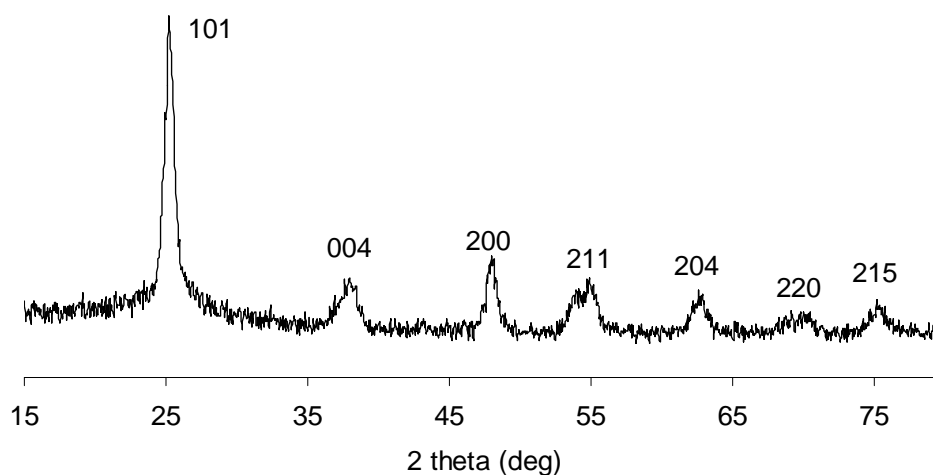


**Figure 57.** XRD of the powder obtained by RAPET of  $[\text{Ti}(\text{OEt})_3(\text{bdmap})]_2$  at  $700^\circ\text{C}$ ; indexing is consistent with anatase  $\text{TiO}_2$  (PDF 84-1286).

Powder XRD of the black residue (Figure 57) shows the only crystalline phase to be present is anatase  $\text{TiO}_2$ . SEM shows this powder, however, reveals it is



made up of two distinct phases: regular elliptical particles of *ca.* 2 x 3  $\mu\text{m}$  and smaller fused spheres *ca.* 300 - 500 nm in diameter (Figure 58), though fusion of particles makes this at best an estimate. EDX of this aggregate shows the presence of both titanium and carbon, but more focused EDX using TEM shows that the ellipses are purely carbon (Figure 59a) while the titanium is in the smaller features which also contain carbon (Figure 59b). TEM of the latter (Figure 60) show them to be core-shell materials with an inner  $\text{TiO}_2$  core of *ca.* 350 nm diameter with an outer carbon shell of width *ca.* 75 nm, consistent with the SEM results, above. The anatase polymorph of  $\text{TiO}_2$  is known to convert to the thermodynamically favoured rutile phase at  $T > 600^\circ\text{C}$  (Inagaki, *et al.*, 2003), so the presence of the carbon coating to these particles acts to suppress this transition.

Gedanken has previously noted the formation of similar structures from RAPET of both  $[\text{Ti}(\text{OPr}^i)_4]$  (Pol, *et al.*, 2004) and  $[\text{Ti}(\text{O})(\text{acac})_2]_2$  (Shammugam, *et al.*, 2006). In the former case, the core shell structure consists of  $\text{TiO}_2$  particles of *ca.* 25 – 50 nm diameter clustered into aggregates of 30 – 40 nm and surrounded by a carbon shell of *ca.* 50 nm thickness (Pol, *et al.*, 2004). Our result seems consistent with this report. On the other hand, with  $[\text{Ti}(\text{O})(\text{acac})_2]_2$  as precursor, the  $\text{TiO}_2@\text{C}$  is 15 – 35 nm in diameter with an outer carbon shell of  $\sim 2$  nm. The formation of these particles depends both on the decomposition mechanism for the precursor and the relative rates of crystallisation of the components of the mixture. If the precursor is atomised into C, Ti, O *etc.* as is widely quoted for RAPET experiments, then one might anticipate little variation in the size of the nanoparticles formed from differing precursors, assuming similar experimental conditions (temperature, cooling rate), as the growth of the  $\text{TiO}_2$  particle would be from atomic Ti and O. Conversely, if the precursor decomposes directly to  $\text{TiO}_2$ , one would expect a link between particle size and precursor structure *i.e.* in terms of both decomposition mechanism and kinetics of the precursor. Gedanken has noted in the case of the RAPET decomposition of  $[\text{Ti}(\text{O})(\text{acac})_2]_2$ ,  $\text{TiO}_2@\text{C}$  particle size decreases with temperature, as the rate of formation of  $\text{TiO}_2$  increases (contrary to the norm, where particle size is expected to increase with increasing temperature) (Shammugam, *et al.*, 2006). With regard to our results, this suggests that the larger  $\text{TiO}_2@\text{C}$  particles formed from  $[\text{Ti}(\text{OPr}^i)_4]$  (Pol, *et*

*al.*, 2004) and  $[\text{Ti}(\text{OEt})_3(\text{bdmap})]_2$  result from slower precursor decomposition than for  $[\text{Ti}(\text{O})(\text{acac})_2]_2$ , which could in turn could be related to the  $\text{Ti}_2\text{O}_2$  already present in the latter.

In neither of these reports are the simultaneous formation of pure carbon spheres / ellipses noted, though this feature has been noted in the RAPET of several species, including mesitylene (Pol, *et al.*, 2004), as smaller (20 – 30 nm) particles along with  $\text{MoO}_2$  nanoparticles when  $[\text{Mo}(\text{O})(\text{OMe})_4]$  is the precursor (Pol, *et al.*, 2004), and as a minor component (along with carbon sausages and sub-stoichiometric  $\text{WO}_3$ ) from  $[\text{W}(\text{OPr}^i)_6]$  in isopropanol (Pol, *et al.*, 2006). The lack of any broad diffraction peak at ca.  $26^\circ$  associated with graphitic carbon suggest that the carbon spheres produced by RAPET of  $[\text{Ti}(\text{OEt})_3(\text{bdmap})]_2$  are amorphous, which contrasts with the formation of analogous, but ordered, carbon particles, either by ball-milling of graphite or by RAPET of mesitylene (Pol, *et al.*, 2006; Pol, *et al.*, 2004). While the importance of interfacial chemistry between the carbon sphere and its surroundings has been stressed by Inagaki (1997), where he also references the formation of glass-like carbon spheres from some organic precursors, it is tempting to also suggest some link with the precursor *i.e.* the lack of any aromatic character to the carbonaceous ligands in  $[\text{Ti}(\text{OEt})_3(\text{bdmap})]_2$ .

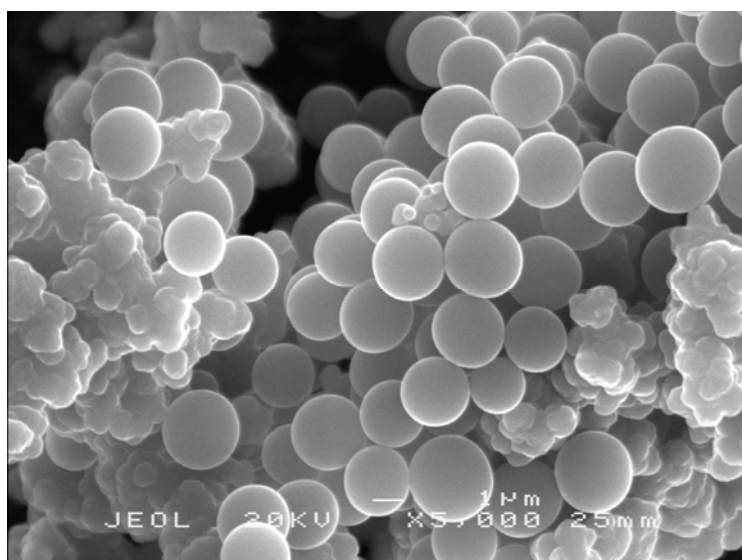
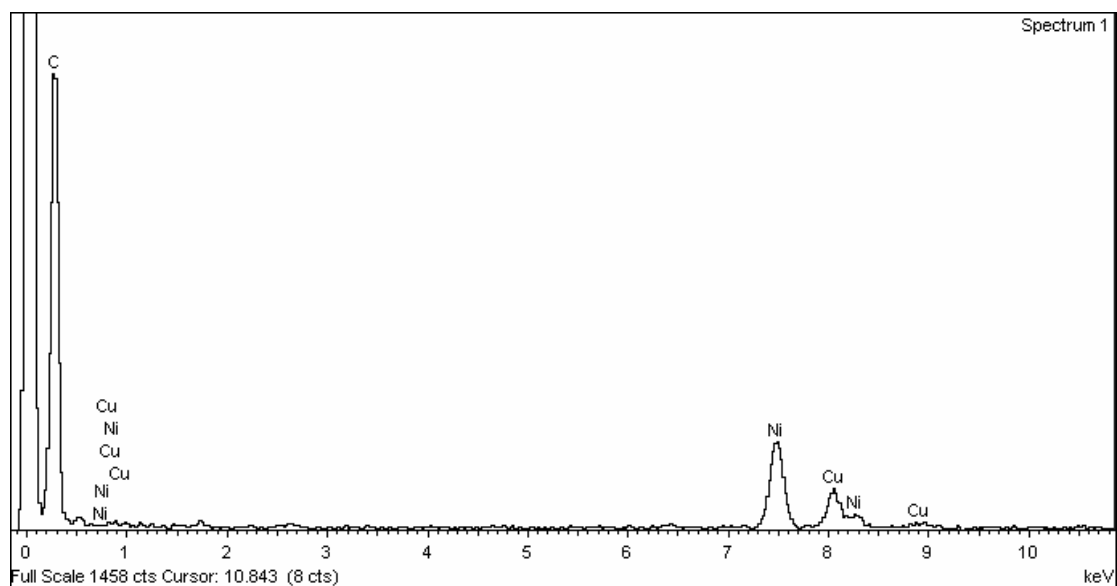


**Figure 58.** SEM of the powder obtained by RAPET of  $[\text{Ti}(\text{OEt})_3(\text{bdmap})]_2$  at  $700^\circ\text{C}$ . Larger spheres are carbon while the smaller spheres are carbon-coated  $\text{TiO}_2$ . Bar = 1  $\mu\text{m}$ .

(a)



(b)

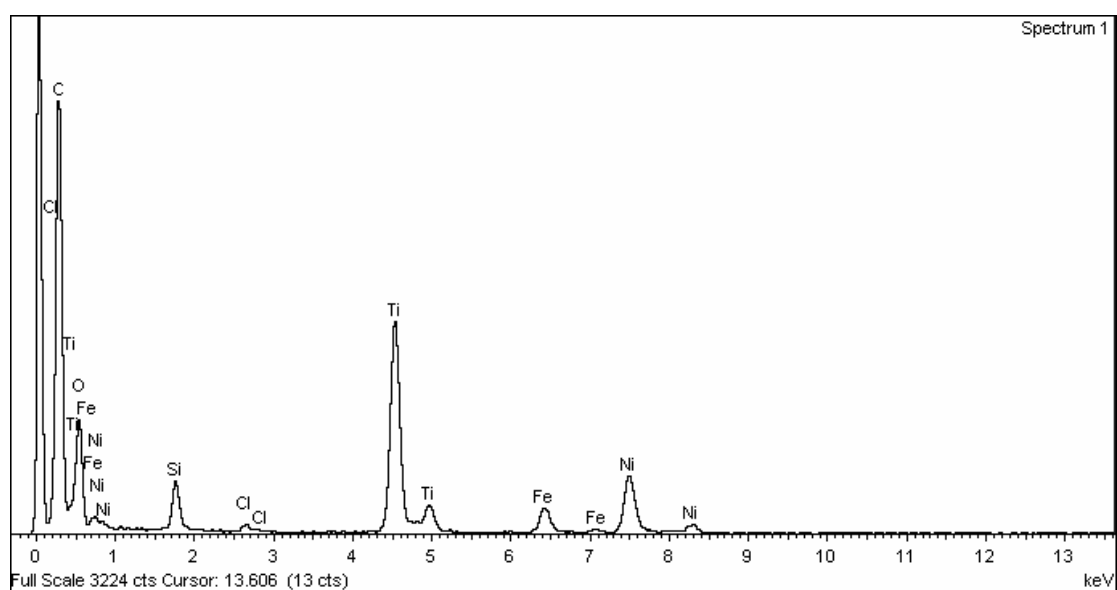


**Figure 59.** EDX of (top) the large elliptical particles (59a) and (bottom) the smaller spherical particle (59b) produced by RAPET of  $[\text{Ti}(\text{OEt})_3(\text{bdmap})]_2$  at  $700^\circ\text{C}$ .

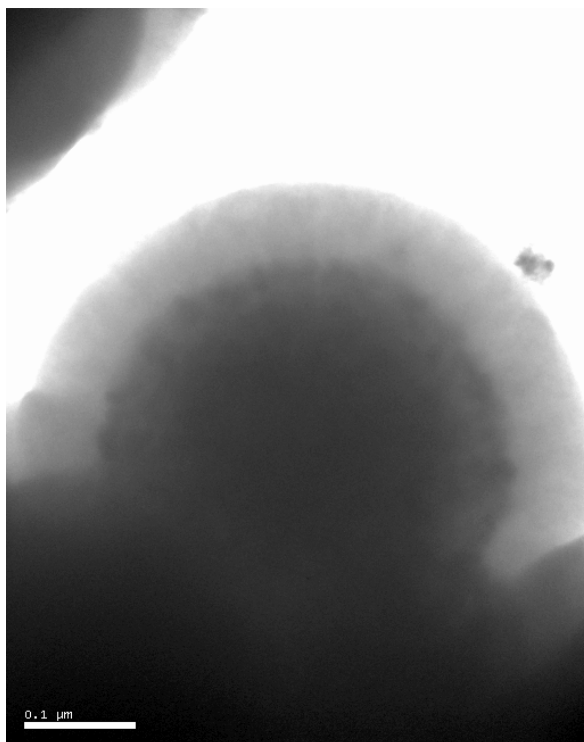


**Figure 60.** TEM of the small particles obtained by RAPET of  $[\text{Ti}(\text{OEt})_3(\text{bdmap})]_2$  at  $700^\circ\text{C}$  showing the dense inner  $\text{TiO}_2$  core and amorphous carbon coating. Bar = 100 nm.

We have also used  $[\text{Ti}(\text{OEt})_3(\text{bdmap})]_2$  to deposit a film of  $\text{TiO}_2$  onto a glass substrate by AACVD at  $440^\circ\text{C}$  (Figure 61). The film is rather featureless and does not yield a diffraction pattern even after annealing in air at  $600^\circ\text{C}$ . EDX (Figure 62) confirms the presence of both titanium and oxygen in the film, though a dominant peak due to Si, originating from the underlying glass substrate, suggests the film is thin (*ca.*  $0.25\ \mu\text{m}$  from Figure 61a). The film texture shows some particulate matter embedded into the film surface (Figure 61b) though these are too small to identify unambiguously. While we cannot exclude these as being an artefact of an island growth mechanism and are also  $\text{TiO}_2$ , it is plausible that these are TiC particles and are the cause of the amorphous nature of the film. The EDX (Figure 62) confirms the presence of carbon contamination in the film, and we have noted earlier (Experimental) that microanalysis of some of these precursors, and notably  $[\text{Ti}(\text{OEt})_3(\text{bdmap})]_2$ , show low carbon analyses, again plausibly due to TiC formation.

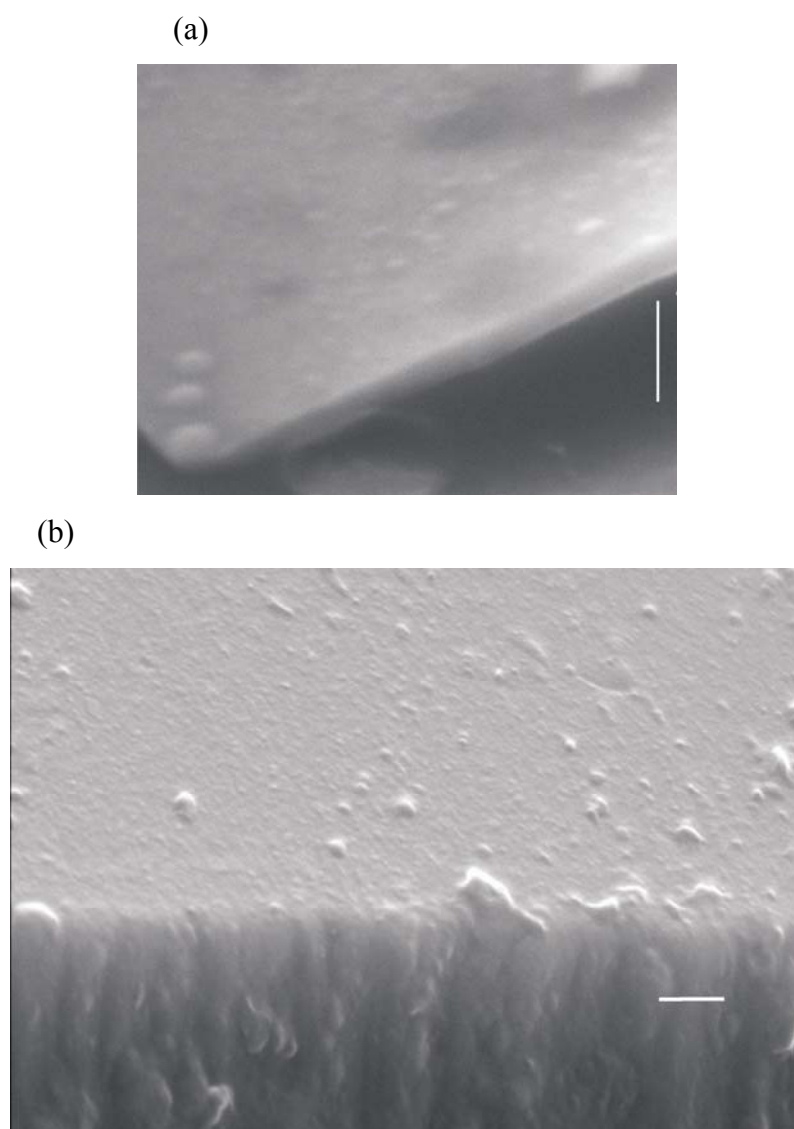


**Figure 61.** Two views of the film deposited from  $[\text{Ti}(\text{OEt})_3(\text{bdmap})]_2$  by AACVD at  $440^\circ\text{C}$  showing (a) film thickness and (b) texture. Bar =  $1\ \mu\text{m}$

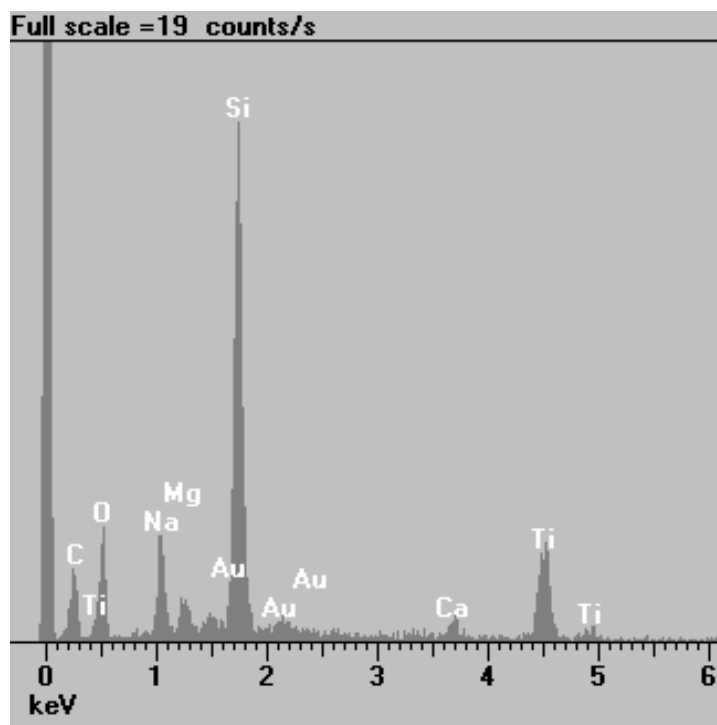


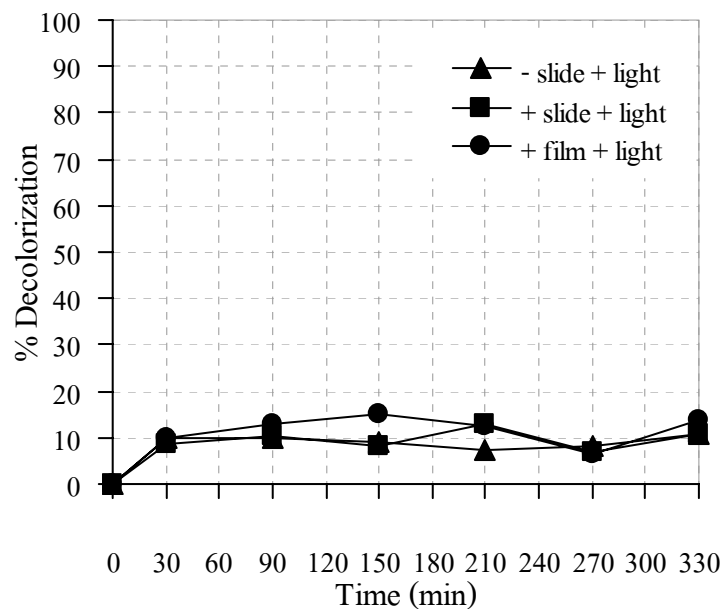
**Figure 62.** EDX of the film deposited from  $[\text{Ti}(\text{OEt})_3(\text{bdmap})]_2$  by AACVD at  $440^\circ\text{C}$ ; gold peaks are due to a sample coating to dissipate charge.

### 3.2.4 Photocatalytic study

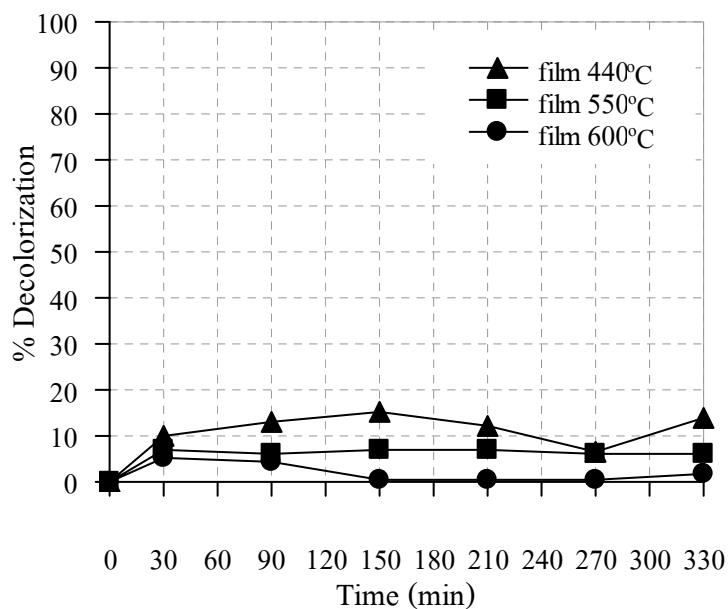
Neither the  $\text{TiO}_2@\text{C}$  particles nor the AACVD deposited film displayed any photocatalytic activity with respect to the decomposition of methylene blue ( $2.5 \times 10^{-5}$  mol/L). Figure 63a (top) shows the decolorization (%) of MB in the presence and absence of  $\text{TiO}_2$  on slide. After annealing at higher temperature (Figure 63b (bottom)), the results show that the calcinations at higher temperature cannot improve the films in the photocatalytic activity. In the case of the film, both its amorphous nature and its lack of thickness are contributing factors

Figure 64 shows the decolorization (%) of MB (a) in the presence and absence of core shell structures of  $\text{TiO}_2$  by the UV light and (b) compare with the commercial  $\text{TiO}_2$ . It can be seen from the figure that core shell structures of  $\text{TiO}_2$  cannot decompose the dye molecules. The  $\text{TiO}_2@\text{C}$  nanoparticles is perhaps more surprising, as photocatalytic activity has been noted for similar materials, albeit much smaller nanoparticles, generated from  $[\text{Ti}(\text{O})(\text{acac})_2]_2$  (Shammugan, *et al.*, 2006).

(a)

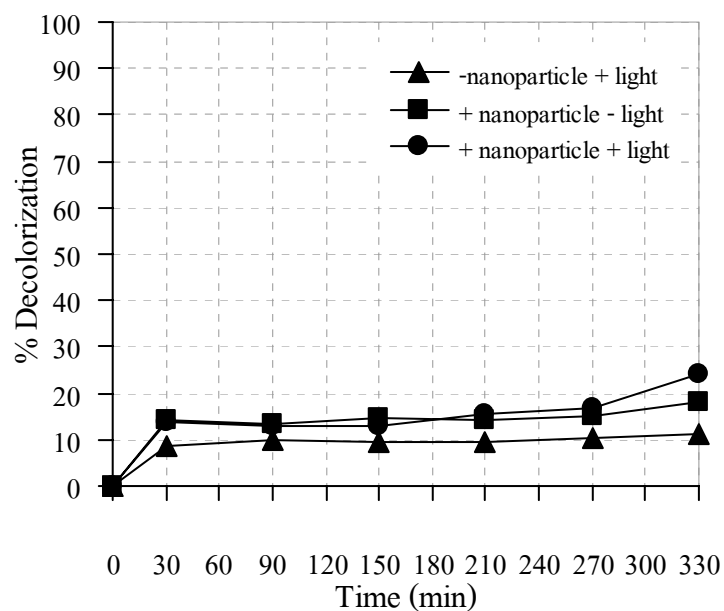


(b)



**Figure 63.** Decolorization (%) as a function of irradiation time of MB solution ( $2.5 \times 10^{-5}$  M) when using (a) film and (b) after annealing film at 440, 550 and 600°C.

(a)



(b)

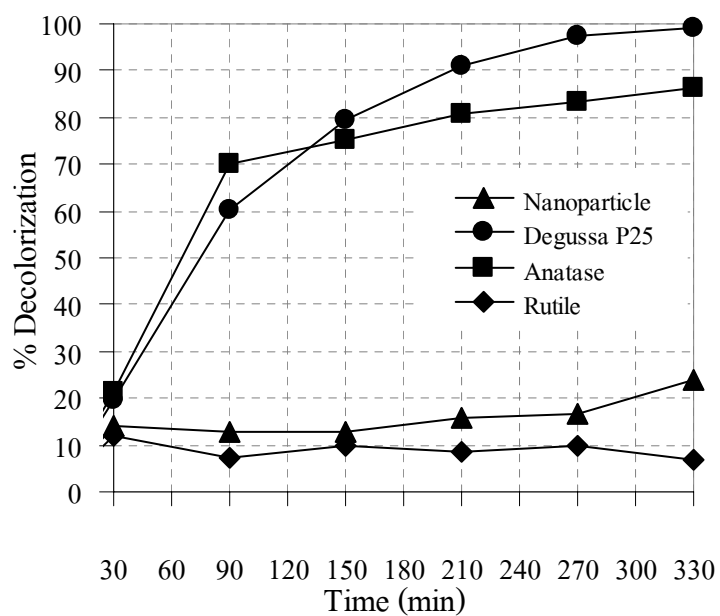


**Figure 64.** Decolorization (%) of MB solution ( $2.5 \times 10^{-5}$  M) with (a) nanoparticle and (b) compare with three commercial TiO<sub>2</sub>.



## CHAPTER 4

### CONCLUSIONS

This research is divided into two parts; part 1: studying TiO<sub>2</sub> in a powder form and part 2: studying TiO<sub>2</sub> in a film form and nanoparticles. In part 1, six samples of TiO<sub>2</sub> of various amorphous-anatase-rutile contents TiO<sub>2</sub> were prepared by the acid-catalyzed sol-gel method without calcination. Powder XRD, SEM, BET, FT-IR, EDX, and UV-Vis techniques were used to characterize these samples. Since the calcination was not employed during the preparation, these products mainly composed of an amorphous phase with small amount of either mixed anatase-rutile phases or solely anatase phase. The products were an amorphous phase with mixtures anatase-rutile phases when prepared by without using acid catalyst and by adding small amount of acid catalyst (hydrochloric acid, nitric acid, and acetic acid). However, when either sulphuric acid or phosphoric acid was used, the products obtained an amorphous phase with anatase phase. The mechanism of crystal growth leading to anatase or rutile phase was proposed. In this work it is proposed that the *cis* isomer of [Ti(OH)<sub>2</sub>(H<sub>2</sub>O)<sub>4</sub>]<sup>2+</sup> can grow into larger unit in the same way as the *trans* isomer. The presence of SO<sub>4</sub><sup>2-</sup> and PO<sub>4</sub><sup>3-</sup> groups were found to inhibit the growth to rutile phase.

The photocatalytic activity of the products was evaluated by decolorizing three dyes, methylene blue, crystal violet, and congo red and comparing them with three commercial TiO<sub>2</sub> powder, P25 (Degussa), anatase (Carlo Erba), and rutile (Dupont). The effects of initial dye concentration, types of TiO<sub>2</sub>, and the addition of hydrogen peroxide on the photocatalytic process have been examined. All samples showed various degrees of photocatalytic activities from almost as good as P25 to mediocre ones. Nevertheless, the effect of addition of H<sub>2</sub>O<sub>2</sub> in absence of light, the prepared TiO<sub>2</sub> sample can bleach dye much better than the commercial sample. For those with good performances, these products can be regarded as an inexpensive alternative to the presently available commercial ones due to simple synthesis without the need for calcination.

In part 2,  $[\text{Ti}(\text{OEt})_3(\text{bdmap})]_2$  was synthesized by the reaction of  $[\text{Ti}(\text{OR})_4]$  ( $\text{R} = \text{Et}, \text{Pr}^i$ ) with the aminoalkoxides  $\text{L} = \text{Hbdmap}$  (I),  $\text{Htdmap}$  (II) generates  $[\text{Ti}(\text{OR})_{4-n}(\text{L})_n]$  and used as a new precursor for  $\text{TiO}_2$  preparation. The structure of  $[\text{Ti}(\text{OEt})_3(\text{bdmap})]_2$ , a  $\mu$ -OEt bridged dimer, has been determined.  $[\text{Ti}(\text{OEt})_3(\text{bdmap})]_2$  can be decomposed in a sealed container at  $700^\circ\text{C}$  to yield  $\text{TiO}_2@\text{C}$  nanoparticles along with spherical carbon particles of diameter *ca.*  $2 \mu\text{m}$ , or can be used in AACVD experiments to yield a film at  $440^\circ\text{C}$  of amorphous  $\text{TiO}_2$  probably contaminated with  $\text{TiC}$ . Neither film nor particles show any photocatalytic activity towards the decomposition of methylene blue.

## REFERENCES

- Aarik, J., Aidla, A., Sammelseg, V., Uustare, T., Titala, M. and Leskala, M. 2000. Characterization of Titanium Dioxide Atomic Layer Growth from Titanium Ethoxide and Water. *Thin Solid Films*. 370: 163-172.
- Abdullah, M., Low, G. W. -C. and Matthews, R. W. 1990. Effects of Common Inorganic Anions on Rates of Photocatalytic Oxidation of Organic Carbon over Illuminated Titanium Dioxide. *J. Phys. Chem.* 94: 6820-6825.
- Akhtar, M. K., Pratsinis, S. E. and Mastrangelo. 1994. Vapour Phase Synthesis of Al-Doped Titania Powders. *J. Mater. Res.* 9: 1241-1249.
- Awati, P. S., Awate, S. V., Shah, P. P. and Ramaswamy, V. 2003. Photocatalytic Decomposition of Methylene Blue Using Nanocrystalline Anatase Titania Prepared by Ultrasonic Technique. *Catal. Commun.* 4: 393-400.
- Baolong, Z., Baishun, C., Keyu, S., Shangjin, H., Xiadong, L., Zongjie, D. and Kelian, Y. 2003. Preparation and Characterization of Nanocrystal Grain TiO<sub>2</sub> Porous Microspheres. *Appl. Catal. B.* 40: 253-258.
- Bartlett, J. R., and Woolfrey, J. L. 1992. *Chemical Processing of Advanced Materials*. John Wiley: New York.

- Baunemann, A., Hellwig, M., Varade, A., Bhakta, R. K., Winter, M., Shivashankar, S. A., Fischer, R. A. and Devi, A. 2006. Precursor Chemistry for TiO<sub>2</sub>: Titanium Complexes with a Mixed Nitrogen/Oxygen Ligand Sphere. Dalton Trans. 3485-3490.
- Bazán, B., Mesa, J. L., Pizarro, J. L., Arriortua, M. I. and Riojo, T. 2003. Hydrothermal Synthesis, Crystal Structure, and Spectroscopic Characterization of a new Organically Templated Mixed-Anion Fluoro-Arsenate-Phosphate Iron (III) Compound, (C<sub>2</sub>H<sub>10</sub>N<sub>2</sub>)[Fe<sub>2</sub>(AsO<sub>4</sub>)<sub>2-x</sub>(PO)<sub>x</sub> F<sub>2</sub>(H<sub>2</sub>O)] (x=0.46). Mater. Res. Bull. 38: 1193-1202.
- Bejarano-Pérez, N. J. and Suárez-Herrera. 2007. Sonophotocatalytic Degradation of Congo Red and Methyl Orange in the presence of TiO<sub>2</sub> as a Catalyst. Ultrason. Sonochem. 14: 589-595.
- Bhakta, R., Thomas. R., Hipler, F., Bettinger, H. F., Müller, J., Ehrhart, P. and Devi, A. 2004. MOCVD of TiO<sub>2</sub> Thin Films and Studies on the nature of Molecular Mechanisms Involved in the Decomposition of [Ti(OPr<sup>i</sup>)<sub>2</sub>(tbaoc)<sub>2</sub>]. J. Mater. Chem. 14: 3231-3238.
- Bonancêa, C. E., Nascimento, G. M., Souza, M. L., Temperini, M. L. A. and Corio, P. 2006. Substrate Development for Surface-Enhanced Raman Study of Photocatalytic Degradation Processes: Congo Red over Silver Modified Titanium Dioxide Films. Appl. Catal. B. 69: 34-42.

- Bumpus, J. A., Tricker, J., Andrzejewski, K., Rhoads, H. and Tatarko, M. 1999. Remediation of Water Contaminated with an Azo Dye: An Undergraduate Laboratory Experiment Utilizing an Inexpensive Photocatalytic Reactor. *J. Chem. Edu.* 76: 1680-1683.
- Buettner, G. R. 1997. Introduction to Free Radical in: Workshop on Detection of Free Radicals, Chulabhorn Research Institute, Bangkok, Thailand.
- Büchner, W., Schliebs, R., Winter, G. and Büchel, K. H. 1989. *Industrial Inorganic Chemistry*. New York: VCH.
- Carp, O., Huisman, C. L. and Reller, A. 2004. Photoinduced Reactivity of Titanium Dioxide. *Progress in Solid State Chemistry*. 32: 33-177.
- Chandler, R. R., Bigham, S. R. and Coffey, J. L. 1993. Spectroscopic Analysis of Semiconductor Colloids. *J. Chem. Edu.* 70: A7-A10.
- Chemat. 1998. Sol-Gel Technology. <http://www.chemat.com/html/solgel.html>  
Chemat Technology, Inc. (accessed 4/08/06)
- Comba, P. and Merbach, A. 1987. The Titanyl Question Revisited. *Inorg. Chem.* 26: 1315-1323.
- Cotton, F. A and Wilkinson, G. 1988. *Advance Inorganic Chemistry*. 5<sup>th</sup> ed. John Wiley&Sons, Inc.: New York.

- Daneshvar, N., Salari, D. and Khataee, A. R. 2003. Photocatalytic Degradation of Azo Dye Acid Red 14 in Water: Investigation of the Effect of Operational Parameters. *J. Photochem. Photobiol. A.* 157: 111-116.
- Ding, X. -Z. and Liu, Z. -H. 1997. Synthesis and Microstructure Control of Nano crystalline Titania Powders via a Sol-Gel Process. *Mater. Sci. Eng. A224:* 210-215.
- Duminica, F. D., Maury, F. and Costines, D. 2006. Growth of Titanium Dioxide Thin Layers by Low Pressure Chemical Vapour Deposition by Chemical Vapour Infiltration for Photocatalysis Applications. *Revista De Chimic.* 57: 52-56.
- Dye from Wikipedia, the free encyclopedia. <http://en.wikipedia.org/wiki/Dye> (accessed 4/04/08)
- Edwards, D. A., Harker, R. M., Mahon, M. F. and Molloy, K. C. 1999. Aerosol-Assisted Chemical Vapour Deposition (AACVD) of Silver Films from Triphenylphosphine Adducts of Silver  $\beta$ -Diketonates and  $\beta$ -Diketoimines, including the Structure of  $[\text{Ag}(\text{hfac})(\text{PPh}_3)]$ . *J. Mater. Chem.* 9: 1771-1780.
- Epling, G. A. and Lin, C. 2002. Photoassisted Bleaching of Dyes Utilizing  $\text{TiO}_2$  and Visible Light. *Chemosphere.* 46: 561-570.
- Evans, P., Pemble, M. E. and Sheel, D. W. 2006. Precursor-Directed Control of Crystalline Type in Atmospheric Pressure CVD Growth of  $\text{TiO}_2$  on Stainless Steel. *Chem. Mater.* 18: 5750-5755.

- Fernández, J., Kiwi, J., Lizama, C., Freer, J., Baeza, J. And Mansilla, H. D. 2002. Factorial Experimental Design of Orange II Photocatalytic Discolouration. *J. Photochem. Photobiol. A.* 151: 213-219.
- Fox, M. A. and Dulay, M. T. 1993. Heterogeneous Photocatalysis. *Chem. Rev.* 93: 341- 357.
- Gopal, M., Chan, W. J. M. and De Jonghe, L. C. 1997. Room Temperature Synthesis of Crystalline Metal Oxides. *J. Mater. Sci.* 32: 6001-6008.
- Gómacz, R., López, T., Ortiz-Islas, E., Navarrete, J., Sánchez, E., Tzompanztzi, F. and Bokhimi, X. 2003. Effect of Sulfation on the Photoactivity of TiO<sub>2</sub> Sol-Gel Derived Catalysts. *J. Mol. Catal. A: Chem.* 193: 217-226.
- Gonçalves, M. S.T., Pinto, E. M. S., Nkeonye, P. And Oliveira-Campos, A. M. F. 2005. Degradation of C.I. Reactive Orange 4 and its Simulated Dyebath Wastewater by Heterogeneous Photocatalysis. *Dyes and Pigments.* 64: 135-139.
- Hachem, C., Bocquillon, F., Zahraa, O. and Bouchy, M. 2001. Decolourization of Textile Industry Wastewater by the Photocatalytic Degradation Process. *Dyes and Pigments.* 49: 117-125.
- Hadjiivanov, K. I. and Klissurski, D. G. 1996. Surface Chemistry of Titania (Anatase) and Titania-Supported Catalysts. *Chem. Soc. Rev.* 61-69.

- Hirakawa, T., Yawata, K. and Nosaka, Y. 2007. Photocatalytic Reactivity for  $O_2^{\bullet-}$  and  $OH^{\bullet}$  Radical Formation in Anatase and Rutile  $TiO_2$  Suspension as the Effect of  $H_2O_2$  Addition. *Appl. Cat. A*. 325: 105-111.
- Hoffman, M. R., Martin, S. T., Choi, W. and Bahnemann, D. W. 1995. Environmental Applications of Semiconductor Photocatalysis. *Chem. Rev.* 95: 69-96.
- Hollingsworth, N., Horley, G. A., Mazhar, M., Mahon, M. F., Molloy, K. C., Myers, C. P. and Critchlow, G. W. 2006. Tin(II) Aminoalkoxides and Heterobimetallic Derivatives: the Structures of  $Sn_6(O)_4(dmae)_4$ ,  $Sn_6(O)_4(OEt)_4$  and  $[Sn(dmae)_2Cd(acac)_2]_2$ . *Appl. Organomet. Chem.* 20: 687-689.
- Houas, A., Lachheb, H., Ksibi, M., Elaloui, E., Guillard, C. and Herrmann, J. -M. 2001. Photocatalytic Degradation Pathway of Methylene Blue in Water. *Appl. Cat. B*. 31: 145-147, and references cited therein.
- Inagaki, M. 1997. Discussion of the Formation of Nanometric Texture in Spherical Carbon Bodies. *Carbon*. 35: 711-713.
- Inagaki, M., Hirose, Y., Matsunaga, T., Tsumura, T. and Toyada, M. 2003. Carbon Coating of Anatase-Type  $TiO_2$  through their Precipitation in PVA Aqueous Solution. *Carbon*. 41: 2619-2624.
- Jones, A. C., Leedham, T. J., Wright, P. J., Crosbie, M. J., Fleeting, K. A., Otway, D. J., O'Brien, P. and Pemble, M. E. 1998. Synthesis and Characterisation of Two Novel Titanium Isopropoxides Stabilised with a Chelating Alkoxide: Their Use in the Liquid Injection MOCVD of Titanium Dioxide Thin Films. *J. Mater. Chem.* 8: 1773-1777.



- Karkmaz, M., Puzenat, E., Guillard, C. and Herrmann, J. M. 2004. Photocatalytic Degradation of the Alimentary Azo Dye Amaranth Mineralization of the Azo group to nitrogen. *Appl. Catal. B.* 51: 183-194.
- Khalil, K. M. S. and Zaki, M. I. 1997. Synthesis of High Surface Area Titania Powders via Basic Hydrolysis of Titanium (IV) Isopropoxide. *Powder Technol.* 92: 233-239.
- Kim, B. H., Lee, J. Y., Choa, Y. H., Higuchi, M. and Mizutani, N. 2004. Preparation of TiO<sub>2</sub> Thin Film by Liquid Sprayed Mist CVD Method. *Mat. Sci. and Eng. B.* 107: 289-294.
- Kiriakidou, F., Kondarides, D. I. And Verykios, X. E. 1999. The Effect of Operational Parameters and TiO<sub>2</sub>-Doping on the Photocatalytic Degradation of Azo-Dyes. *Catalysis Today.* 54: 119-130.
- Kumar, S. R., Suresh, C., Vasudevan, A. K., Suja, N. R. and Mukundan, P. 1999. Phase Transformation in Sol-Gel Titania Containing Silica. *Mater. Lett.* 38: 161-166.
- Lee, J. -H., Kim, J. -Y. and Rhee, S. -W. 1999. Comparison of (Ba, Sr)TiO<sub>3</sub> Thin Films from Chemical Vapor Deposition Metallogenic with it (DMAE)<sub>4</sub> and it (i-OPr)<sub>2</sub>(tmhd)<sub>2</sub> as it Sources. *Electrochem. Solid State Lett.* 2: 507.
- Lee, J. -H., Kim, J. -Y., Shim, J. -Y. and Shee, S. -W. 1999. Metalorganic Chemical Vapor Deposition of Barium Strontium Titanate Thin Films with a more Coordinatively Saturated Ti Precursor, Ti(dmae)<sub>4</sub> (dmae = dimethylaminoethoxide). *J. Vac. Sci. Technol. A.* 17: 3033-3037.

- Litter, M. I. 1999. Heterogeneous Photocatalysis Transition Metal Ions in Photocatalytic Systems. *Appl. Catal. B.* 23: 89-114.
- Ma, H., Wang, M., Yang, R., Wang, W., Zhao, J., Shen, Z. and Yao, S. 2007. Radiation Degradation of Congo Red in Aqueous Solution. *Chemosphere.* 68: 1098-1104.
- Matthews, R. W. and McEvoy, S. R. 1992. A Comparison of 254 and 350 nm Excitation of TiO<sub>2</sub> in Simple Photocatalytic Reactors. *J. Photochem. Photobiol. A.* 66: 355-366.
- Miao, L., Jin, P., Kaneko, K., Terai, A., Nabatova-Gabain, N. and Tanemura, S. 2003. Preparation and Characterization of Polycrystalline Anatase and Rutile TiO<sub>2</sub> Thin Films by rf Magnetron Sputtering. *Appl. Surf. Sci.* 9775: 1-9.
- Mills, A. and Wang, J. 1999. Photobleaching of Methylene Blue Sensitised by TiO<sub>2</sub>: an Ambiguous System? *J. Photochem. Photobiol. A.* 127: 123-134.
- Nakamoto, K. 1986. *Infrared and Raman Spectra of Inorganic and Coordination Compounds*, 4<sup>th</sup> ed., Wiley: New York.
- Nam, H.-D., Lee, B.-H., Kim, S.-J., Jung C.-H., Lee, J.-H. and Park, S. 1998. Preparation of Ultrafine Crystalline TiO<sub>2</sub> Powders from Aqueous TiCl<sub>4</sub> Solution by Precipitation. *Jpn. J. Appl. Phys.* 37: 4603-4608.

- Neppolian, B., Choi, H. C., Sakthivel, S., Arabindoo, B. and Murugesan, V. 2002. Solar Light Induced and TiO<sub>2</sub> Assisted Degradation of Textile Dye Reactive Blue 4. *Chemosphere*. 46: 1173-1181.
- Ohno, T., Sarukawa, K., Tokieda, K. and Matsumura, M. 2001. Morphology of a TiO<sub>2</sub> Photocatalyst (Degussa, P-25) Consisting of Anatase and Rutile Crystalline Phases. *J. Catal.* 203: 82-86.
- Ohtani, B., Ogawa, Y. and Nishimoto, S. -I. 1997. Photocatalytic Activity of Amorphous-Anatase Mixture of Titanium (IV) Oxide Particles Suspended in Aqueous Solutions. *J. Phys. Chem. B*. 101: 3746-3752.
- Pheamhom, R., Sunwoo, C. and Kim, D. H. 2006. Characteristics of Atomic Layer Deposited TiO<sub>2</sub> Films and their Photocatalytic Activity. *J. Vac. Sc. & Technol. A*. 24: 1535-1539.
- Piszczek, P., Richert, M., Grodzicki, A., Talik, E. and Heimann. 2005. CVD of Thin Titanium Dioxide Films Using Hexanuclear Titanium Oxo Carboxylate Isopropoxides. *Chem. Vapor Depos.* 11: 399-403.
- Pol, S. V., Pol, V. G. and Gedenken, A. 2004. Reactions under Autogenic Pressure at Elevated Temperature (RAPET) of Various Alkoxide: Formation of Metals/Metal Oxides-Carbon Core-Shell Structures. *Chem. Eur. J.* 10: 4467-4473.

- Pol, S. V., Pol, V. G., Kessler, V. G., Seisenbaeva, G. A., Sung, M., Asai, S. and Gedanken, A. 2004. The Effect of a Magnetic Field on a RAPET (Reaction under Autogenic Pressure at Elevated Temperature) of  $\text{MoO}(\text{OMe})_4$ : Fabrication of  $\text{MoO}_2$  Nanoparticles Coated with Carbon or Separated  $\text{MoO}_2$  and Carbon Particles. *J. Phys. Chem. B.* 108: 6322-6327.
- Pol, S. V., Pol, V. G., Kessler, V. G. and Gedanken, A. 2006. Growth of Carbon Sausages Filled with in situ Formed Tungsten oxide Nanorods: Thermal Dissociation of Tungsten(VI) Isopropoxide in Isopropanol. *New J. Chem.* 30: 370-376.
- Pol, V. G., Pol, S. V., Markovsky, B., Calderon-Moreno, J. M. and Gedanken, A. 2006. Implementation of an Electric Field (AC and DC) for the Growth of Carbon Filaments via Reaction under Autogenic Pressure at Elevated Temperatures of Mesitylene without Catalyst or Solvent. *Chem. Mater.* 18: 1512-1519.
- Pol, V. G., Pol, S. V., Markovsky, B., Calderon-Moreno, J. M. and Yoshimura, M. 2004. Carbon Spherules, Synthesis, Properties and Mechanistic Elucidation *Carbon.* 42: 111-116.
- Pore, V., Rahtu, A., Leskelä, M., Ritala, M., Sajavaara, T. And Keinonen, J. 2004. Atomic Layer Deposition of Photocatalytic  $\text{TiO}_2$  Thin Films from Titanium Tetramethoxide and Water. *Chem. Vap. Deposition.* 10: 143-148.
- Qumar, M., Saquib, M. and Muneer, M. 2005. Photocatalytic Degradation of Two Selected Dye Derivatives, Chromotrope 2B and Amido Black 10B, in aqueous Suspensions of Titanium Dioxide. *Dyes and Pigments.* 65: 1-9.

- Randorn, C., Wongnawa, S. and Boonsin, P. 2004. Bleaching of Methylene Blue by Hydrated Titanium Dioxide. *ScienceAsia*. 30: 149-156.
- Reddy, K. M., Manorama, S. V. and Reddy, A. R. 2002. Bandgap Studies on Anatase Titanium Dioxide Nanoparticles. *Mater. Chem. Phys.* 78: 239-245.
- Reddy, K. M., Reddy, C. V. G. and Manorama, S. V. 2001. Preparation, Characterization, and Spectral Studies on Nanocrystalline Anatase TiO<sub>2</sub>. *J. Solid State Chem.* 158: 180-186.
- Rodriquez-Castro, J., Mahon, M. F. and Molloy, K. C. 2006. Aerosol-Assisted CVD of Antimony Sulfide from Antimony Dithiocarbamates. *Chem. Vap. Deposition*. 12: 601-607.
- Sahoo, C., Gupta, A. K. and Pal, A. 2005. Photocatalytic Degradation of Crystal Violet (C.I. Basic Violet 3) on Silver Ion doped TiO<sub>2</sub>. *Dyes and Pigments*. 66: 189-196.
- Samantaray, S. K., Mohapatra, P. and Parida, K. 2003. Physico-Chemical Characterization and Photocatalytic Activity of Nanosized SO<sub>4</sub><sup>2-</sup>/TiO<sub>2</sub> towards Degradation of 4-Nitrophenol. *J. Mol. Catal. A: Chem.* 198: 277-287.
- Sanchez, E., Lopez, T., Gomez, R., Morales, A. And Novaro, O. 1996. Synthesis and Characterization of Sol-Gel Pt/TiO<sub>2</sub> catalyst. *J. Solid State Chem.* 122: 309-314.

- Saquib, M. and Muneer, M. 2003. TiO<sub>2</sub>-Mediated Photocatalytic Degradation of a Triphenylmethane Dye (Gential Violet), in Aqueous Suspensions. *Dyes and Pigments*. 56: 37-49.
- Saquib, M., Tariq, M. A., Haque, M. M. and Muneer, M. 2008. Photocatalytic Degradation of Disperse Blue 1 Using UV/TiO<sub>2</sub>/H<sub>2</sub>O<sub>2</sub> Process. *Journal of Environmental Management*. 88: 300-306.
- Sauer, T., Neto, C., José, H. J. and Moreira, R. F. P. M. 2002. Kinetics of Photocatalytic Degradation of Reactive Dyes in a TiO<sub>2</sub> Slurry Reactor *J. Photochem. Photobiol. A*. 149: 147-154.
- Sclafani, A., Palmisano, L. and Schiavello, M. 1990. Influence of the Preparation Methods of TiO<sub>2</sub> on the Photocatalytic Degradation of Phenol in Aqueous Dispersion. *J. Phys. Chem.* 94: 829-832.
- Senthilumaar, S., Porkodi, K. and Vidyalakshmi, R. 2004. Photodegradation of a Textile Dye Catalyzed by Sol-Gel derived Nanocrystalline TiO<sub>2</sub> via Ultrasonic Irradiation. *J. Photochem. Photobiol. A*. 170: 225-232.
- Shammugam, S., Gabashvili, A., Jacob, D.S., Yu, J.C. and Gedanken, A. 2006. Synthesis and Characterization of TiO<sub>2</sub>@C Core-Shell Composite Nanoparticles and Evaluation of their photocatalytic Activities. *Chem. Mater.* 18: 2275-2282.
- Simcock, M. N. 2006. Thin Film Growth of TiO<sub>2</sub> and Ti<sub>2</sub>O<sub>3</sub> by the new method of liquid Injection CVD Investigated Using Optical Interferometry, XRD and AFM. *Surf. Interface Anal.* 38: 1122-1129.

- Sivalingam, G., Nagavei, K., Hegde, M. S. and Madras, G. 2003. Photocatalytic Degradation of Various Dyes by Combustion Synthesized Nano Antase TiO<sub>2</sub> Appl. Catal. B. 45: 23-28.
- Sonnenfeld, A., Hauert, R. and von Rohr, P. R. 2006. UV Absorptance of Titanium Dioxide Thin Films by Plasma Enhanced Deposition from Mixtures of Oxygen and Titanium-Tetrakis-Isopropoxide. Plasma Chem. Plasma Process. 26: 319-334.
- Stylidi, M., Kondarides, D. I. and Verykios, S. E. 2004. Visible Light-Induced Photocatalytic Degradation of Acid Orange 7 in Aqueous TiO<sub>2</sub> Suspensions Appl. Catal. B. 47: 189-201.
- Sun, Z., Chen, Y., Ke, Q., Yang, Y. and Yuan, J. 2002. Photocatalytic Degradation of Cationic Azo Dye by TiO<sub>2</sub>/Bentonite Nanocomposite J. Photochem. Photobiol. A. 149: 169-174.
- Suresh, C., Biju, V., Mukundan, P. and Warriar, K. G. K. 1998. Anatase to Rutile Transformation in Sol-Gel Titania by Modification of Precursor. Polyhedron. 17: 3131-3135.
- Tanaka, K., Campule, M. F. V. and Hisanaga, T. 1991. Effect of Crystallinity of TiO<sub>2</sub> on its photocatalytic Action. Chem. Phys. Lett. 187: 73-76.
- Tanaka, K., Padermpole, K. and Hisanaga, T. 2000. Photocatalytic Degradation of Commercial Azo Dyes. Wat. Res. 34: 327-333.

- Velasco, M. J., Rubio, F., Rubio, J. and Oteo, J. L. 1999. DSC and FT-IR Analysis of the Drying Process of Titanium Alkoxide Derived Precipitates. *Thermochim. Acta.* 326: 91-97.
- Wahi, R. K., Yu, W. W., Liu, Y., Mejia, M. L., Falkner, J. C., Nolte, W. and Colvin, V. L. 2005. Photodegradation of Congo Red Catalyzed by Nanosized TiO<sub>2</sub>” *J. Mol. Cat. A.* 242: 48-56.
- Wang, C., Dang, Z.-X. and Li, Yadong. 2001. The Synthesis of Nanocrystalline Anatase and Rutile Titania in Mixed Organic Media. *Inorg. Chem.* 40: 5210-5214.
- Wang, O. J., Moss, S. C., Shalz, M. L., Glaeser, A. M., Zandbergen, H. W. and Zschack, P. 1992. In *Physics and Chemistry of Finite Systems: from Clusters to Crystals*, vol. II, edited by Jena, P.; Khanna, S. N. and Rao, B. K. Kluwer Academic Publishers, Boston, pp. 1287.
- Wang, Z. C., Chen, J. F. and Hu, X. F. 2000. Preparation of Nanocrystalline TiO<sub>2</sub> Powder at near Room Temperature from Peroxo-Polytitanic Acid Gel. *Mater. Lett.* 43: 87-90.
- Xie, H., Zhang, Q., Xi, T., Wang, J. and Liu, Y. 2002. Thermal Analysis on Nanosized TiO<sub>2</sub> prepared by Hydrolysis. *Thermochim. Acta.* 381: 45- 48.
- Xie, Y. and Yuan, C. 2003. Photocatalytic Activity and Recycle Application of Titanium Dioxide Sol for X-3B Photodegradation *J. Photochem. Photobiol. A.* 206: 419-428.



- Xu, N., Shi, Z., Fan, Y., Dong, J., Shi, J. and Hu, M. Z.-C. 1999. Effects of Particle Size of TiO<sub>2</sub> on Photocatalytic Degradation of Methylene Blue in Aqueous Suspensions. *Ind. Eng. Chem. Res.* 38: 373-379.
- Yamazaki, S., Fujinaga, N. and Araki, K. 2001. Effect of Sulfate Ions for Sol-Gel Synthesis of Titania Photocatalyst. *Appl. Catal. A.* 210: 97-102.
- Yanqing, Z., Erwei, S., Zhizhan, C., Wenjun, L. and Xingfang, H. 2001. Influence of Solution Concentration on the Hydrothermal Preparation of Titania Crystallites. *J. Mater. Chem.* 11: 1547-1551.
- Youn, H. -J., Ha, P. S., Jung, H. S., Hong, K. S., Park, Y. H. and Ko, K. H. 1999. Alcohol Rinsing and Crystallisation Behavior of Precipitated Titanium Oxide. *J. Coll. Inter. Sci.* 211: 321-325.
- Yu, J., Yu, J. C., Leung, M. K. -P., Ho, W., Cheng, B., Zhao, X. and Zhao, J. 2003. Effect of Acidic and Basic Hydrolysis Catalysts on the Photocatalytic Activity and Microstructures of Bimodal Mesoporous Titania. *J. Catal.* 217: 69-78.
- Zaban, A., Aruna, S. T., Tirosh, S., Gregg, B. A. and Mastai, Y. 2000. The Effect of the Preparation Condition of TiO<sub>2</sub>. *J. Phys. Chem. B.* 104: 4130-4133.
- Zielińska, B., Grzechulska, J., Grzmil, B. and Morawski, A. W. 2001. Photocatalytic Degradation of Reactive Black 5 A Comparison between TiO<sub>2</sub>-Tytanpol A11 and TiO<sub>2</sub>-Degussa P25 Photocatalysts. *Appl. Catal. B.* 35: L1-L7.

- Zielińska, B., Grzechulska, J., Grzmil, B. and Morawski, A. W. 2003. The pH Influence on Photocatalytic Decomposition of Organic Dyes over A11 and P25 Titanium Dioxide. *Appl. Catal. B.* 45: 293-300.
- Zielińska, B., Grzechulska, J. and Morawski, A. W. 2003. Photocatalytic Decomposition of Textile Dyes on TiO<sub>2</sub>-Tytanpol A11 and TiO<sub>2</sub>-Degussa P25. *J. Photochem. Photobiol. A.* 157: 65-70.
- Zhang, F., Zhao, J., Shen, T., Hidaka, H., Pelizzetti, E. and Serpone, N. 1998. TiO<sub>2</sub>-Assisted Photodegradation of Dye Pollutants II. Adsorption and Degradation Kinetics of Eosin in TiO<sub>2</sub> Dispersions under Visible Light Irradiation. *Appl. Catal. B.* 45: 147-156.
- Zhang, H., Penn, R. L., Hamers, R. J. and Banfield, J. F. 1999. Enhanced Adsorption of Molecules on Surfaces of Nanocrystalline Particles. *J. Phys. Chem. B.* 103: 4656-4662.
- Zhang, R. and Gao, L. 2001. Effect of Peptization on Phase Transformation of TiO<sub>2</sub> Nanoparticles. *Mater. Res. Bull.* 36: 1957-1965.
- Zhang, Q. -H., Gao, L. and Guo, J. -K. 1999. Preparation and Characterization of Nanosized TiO<sub>2</sub> Powders from Aqueous TiCl<sub>4</sub> Solution. *NanoStruct. Mater.* 11: 1293-1300.
- Zhang, Q., Gao, L. and Guo, J. 2000. Effects of Calcination on the Photocatalytic Properties of Nanosized TiO<sub>2</sub> Powders Prepared by TiCl<sub>4</sub> Hydrolysis. *Appl. Catal. B.* 26: 207-215.

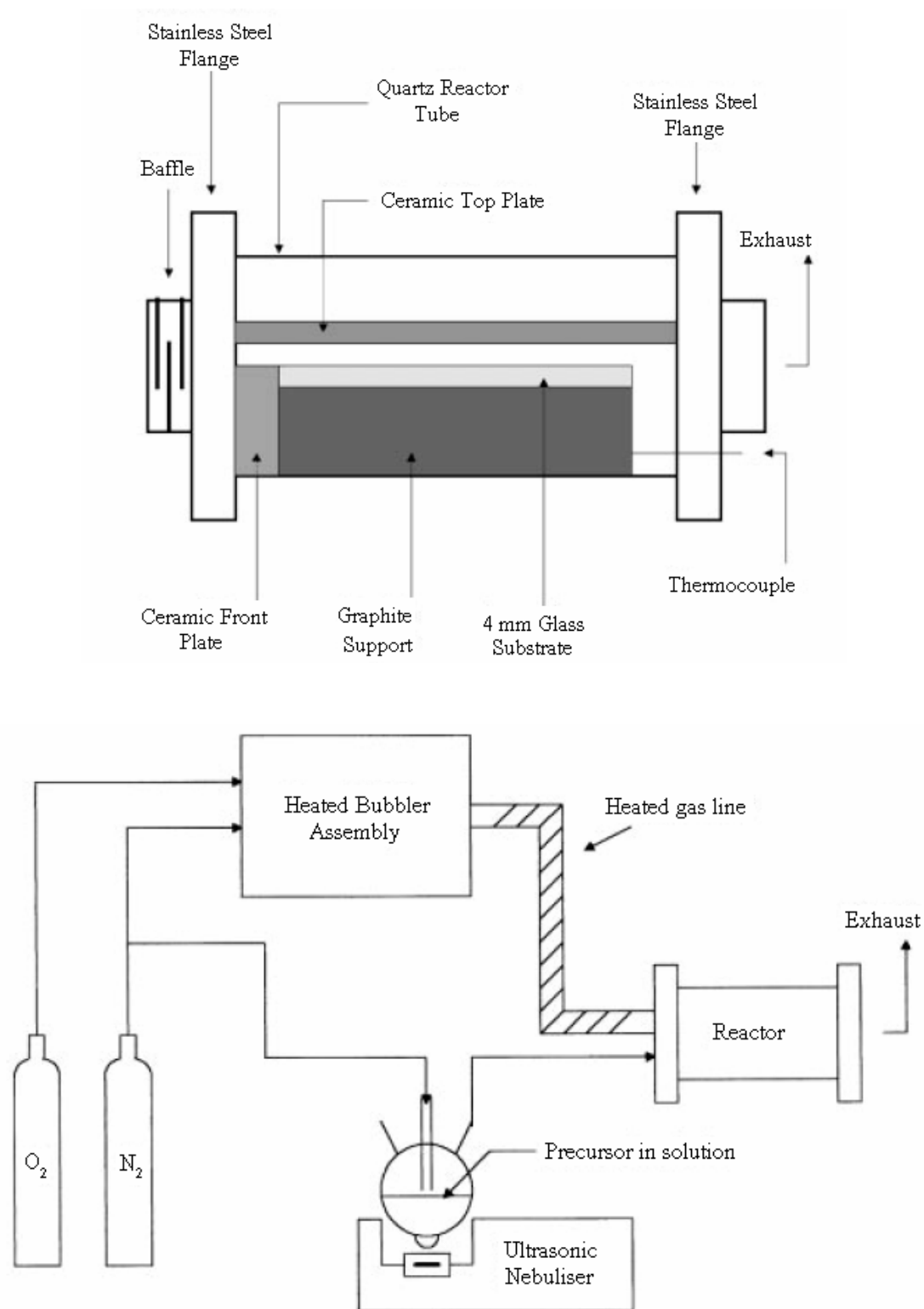
- Zhang, Q., Gao, L. and Guo, J. 2000. Effect of Hydrolysis Conditions on Morphology and Crystallization of Nanosized TiO<sub>2</sub> Powder. *J. Eur. Ceram. Soc.* 20: 2153-2158.
- Zhang, Y., Wang, C.-C., Zakaria, R. and Ying, J. Y. 1998. Role of Particle Size in Nanocrystalline TiO<sub>2</sub>-Based Photocatalysts. *J. Phys. Chem. B.* 102: 10871-10878.
- Zhang, Y., Weidenkaff, A. And Reller, A. 2002. Mesoporous Structure and Phase Transition of Nanocrystalline TiO<sub>2</sub>. *Mater. Lett.* 54: 375-381.
- Zhang, Z. and Maggard, P. A. 2007. Investigation of Photocatalytically-Active Hydrated Forms of Amorphous Titania, TiO<sub>2</sub>•nH<sub>2</sub>O. *J. Photochem. Photobiol. A.* 186: 8-13.
- Zhu, C., Wang, L., Kong, L., Yang, X., Wang, L., Zheng, S., Chen, F., MaiZhi, F. and Zong, H. 2000. Photocatalytic Degradation of AZO Dyes by Supported TiO<sub>2</sub> + UV in Aqueous Solution. *Chemosphere.* 41: 303-309.

## APPENDIX A

### AACVD apparatus

Details of the reactor assembly are shown in Fig. A (top). The CVD apparatus consists of a horizontal, cold-wall reactor with associated gas lines and electrical heater controls. The reactor contains two separate systems, a heated bubbler assembly and an ultrasonic nebulizer line. The nebulizer used was an ultrasonic humidifier from Pifco Health (model No 1077). The piezoelectric transducer, situated in the reservoir containing water, transmits ultrasound through the water and the glass of the flask into the solution to be nebulized. The distance between the piezoelectric transducer and the flask was approximately 3–4 cm. The water in the reservoir was replaced every 30 min in order to cool the transducer.

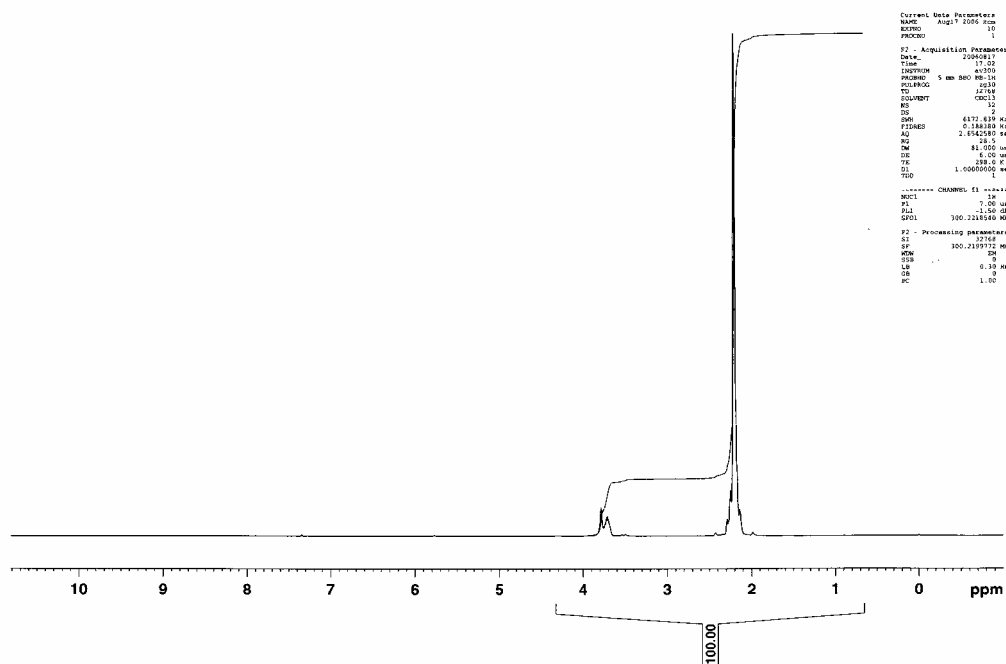
Prior to starting a deposition, the system was purged with nitrogen gas and the substrate brought to the desired temperature. A solution of the precursor was poured into the three-necked round-bottomed flask and placed on the nebulizer. With the nebulizer power on, the solution in the flask fountains to generate an aerosol of fine droplets (droplet size: ca. 0.2–5.0  $\mu\text{m}$ ). The aerosol was swept out of the flask by a flow of nitrogen gas (1.2 L  $\text{min}^{-1}$ ) and transported to a horizontal cold wall CVD reactor [Fig. A (bottom)]. The mist was first passed through a baffle to promote laminar flow, then directly into the reactor chamber (8 mm high, 40 mm wide, and 300 mm long). The ceiling tiles and walls of the reactor are constructed from silica. The glass substrate was positioned upon a large graphite support, heated by three Watlow firewood cartridge heaters. A Watlow series 9965 controller, which monitors the temperature by means of thermocouples positioned inside the block, maintained the temperature of the graphite block. The graphite support was held inside a large silica tube (330 mm long, 100 mm diameter) suspended between stainless-steel flanges upon which many of the electrical and gas line fittings were fixed. Airtight seals were provided by Viton O-rings (Edwards, *et al.*, 1999; Rodriguez-Castro, *et al.*, 2006).



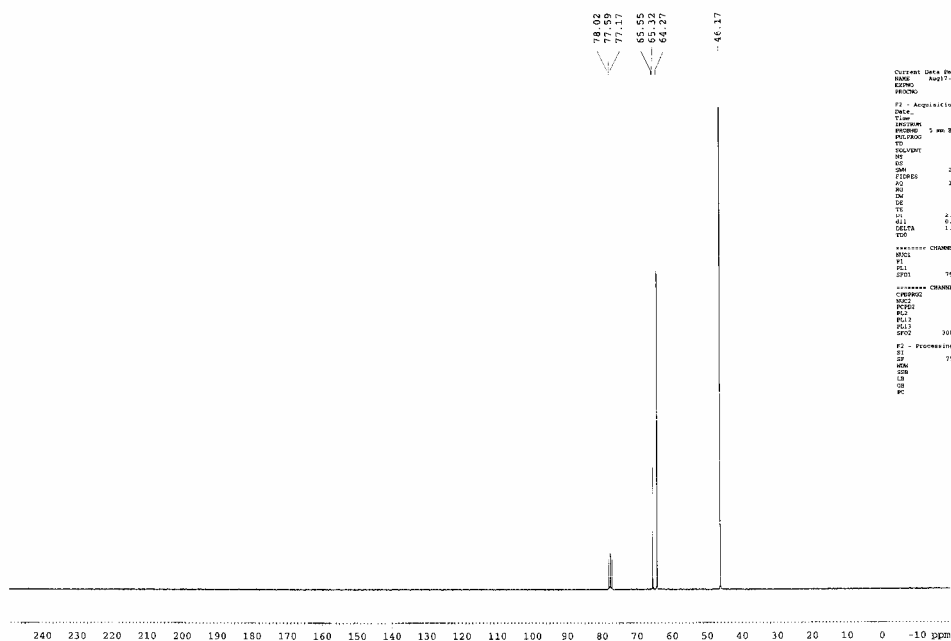
**Figure A.** Schematic diagram of the AACVD apparatus (bottom) and detail of the reaction chamber (top) (Edwards, *et al.*, 1999).

## APPENDIX B

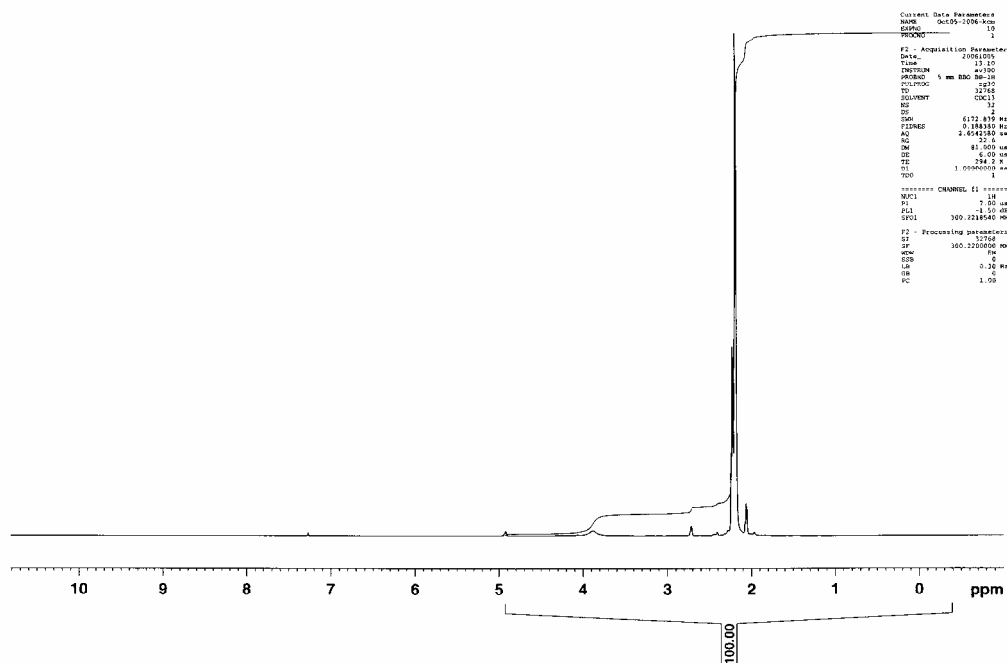
bdmap 16/8/2006



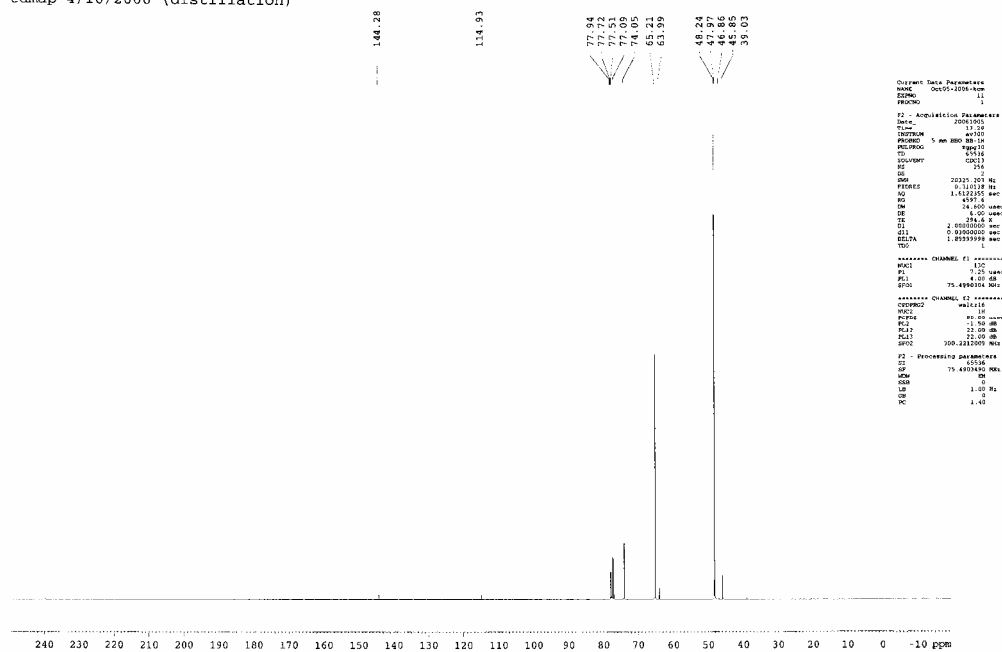
bdmap 16/8/2006

Figure B.  $^1\text{H}$  NMR (top) and  $^{13}\text{C}$  NMR (bottom) spectrum of bdmap.

tdmap 4/10/2006 (distillation)



tdmap 4/10/2006 (distillation)

Figure B1.  $^1\text{H}$  NMR (top) and  $^{13}\text{C}$  NMR (bottom) spectrum of tdmmap.

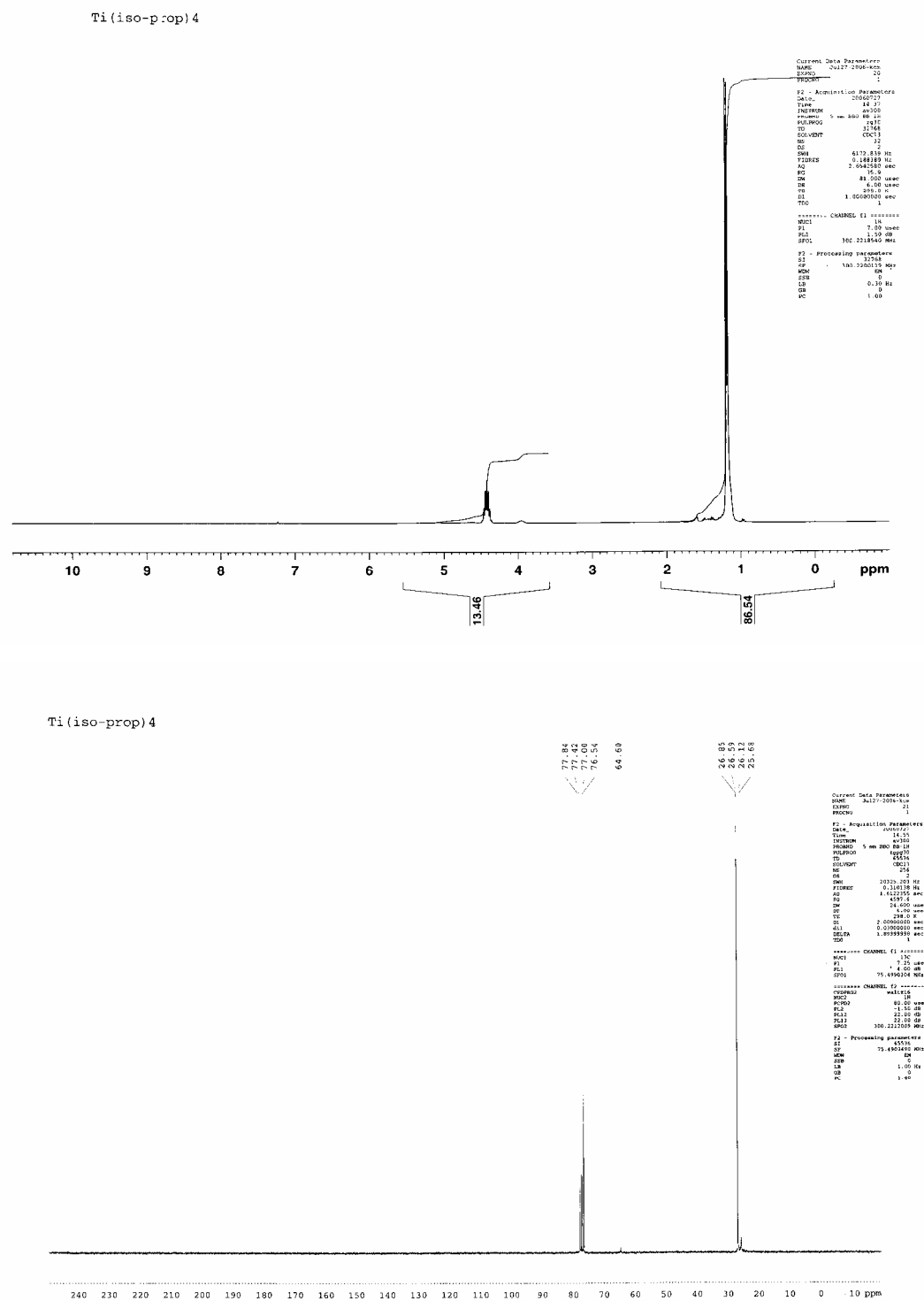


Figure B2.  $^1\text{H}$  NMR (top) and  $^{13}\text{C}$  NMR (bottom) spectrum of  $\text{Ti}(\text{O}^i\text{Pr})_4$ .



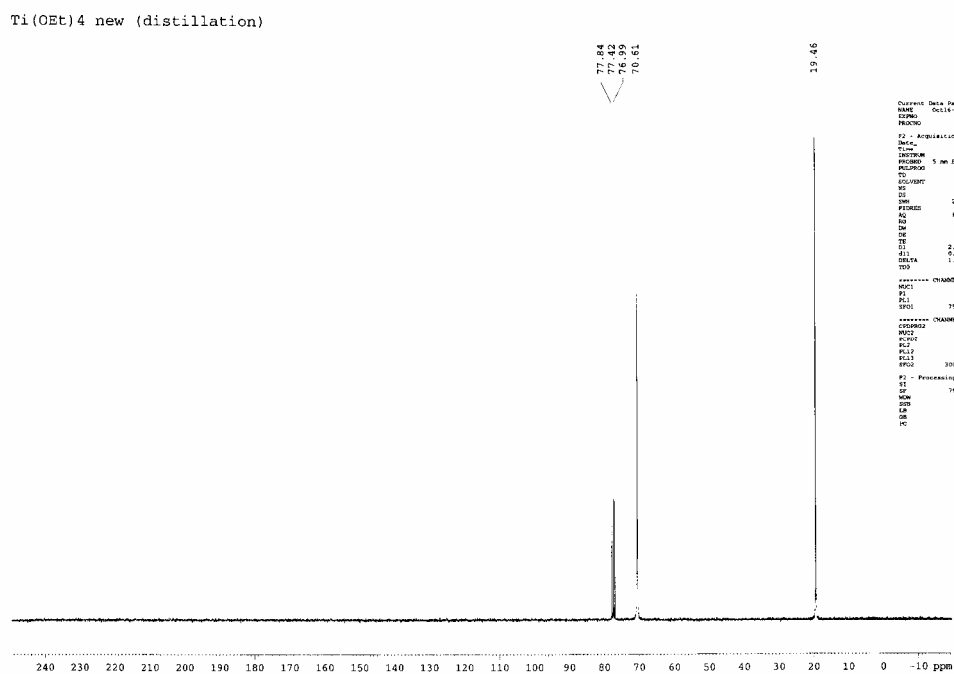
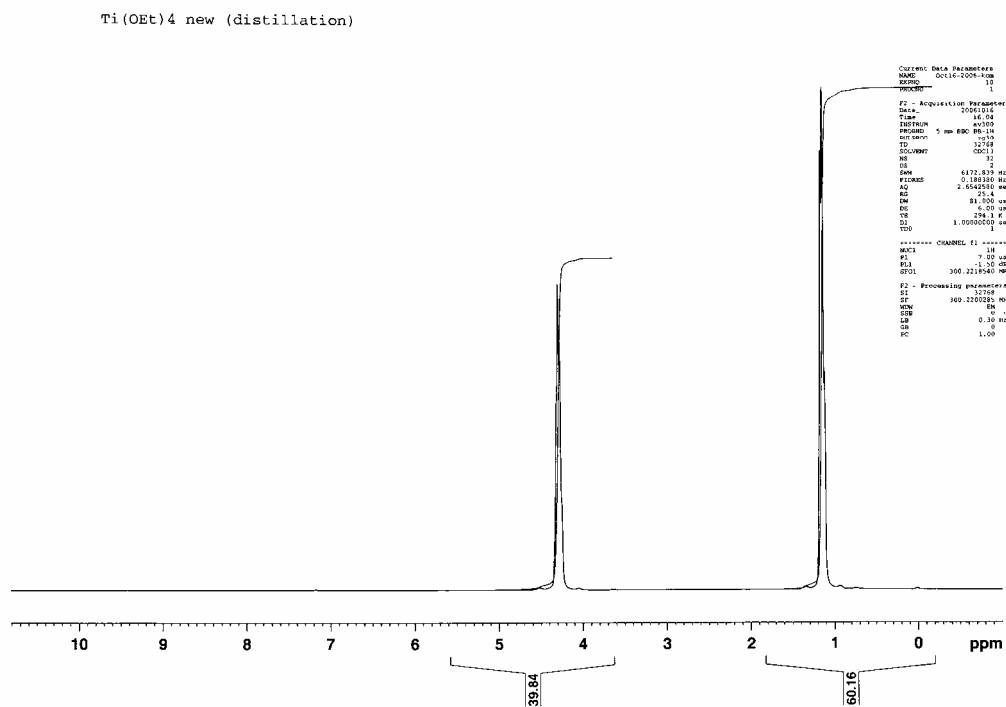
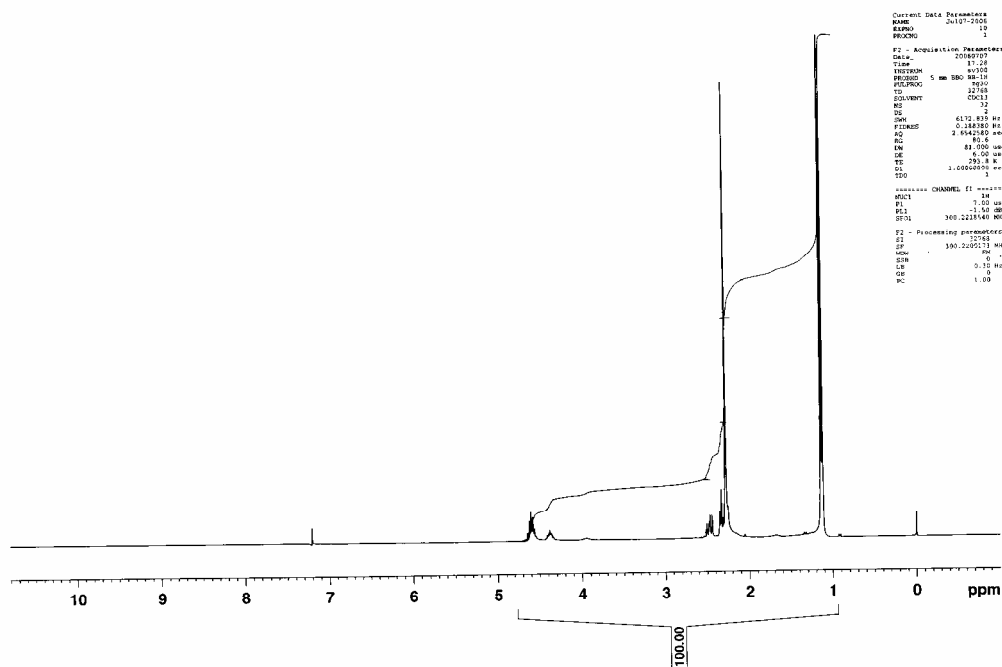
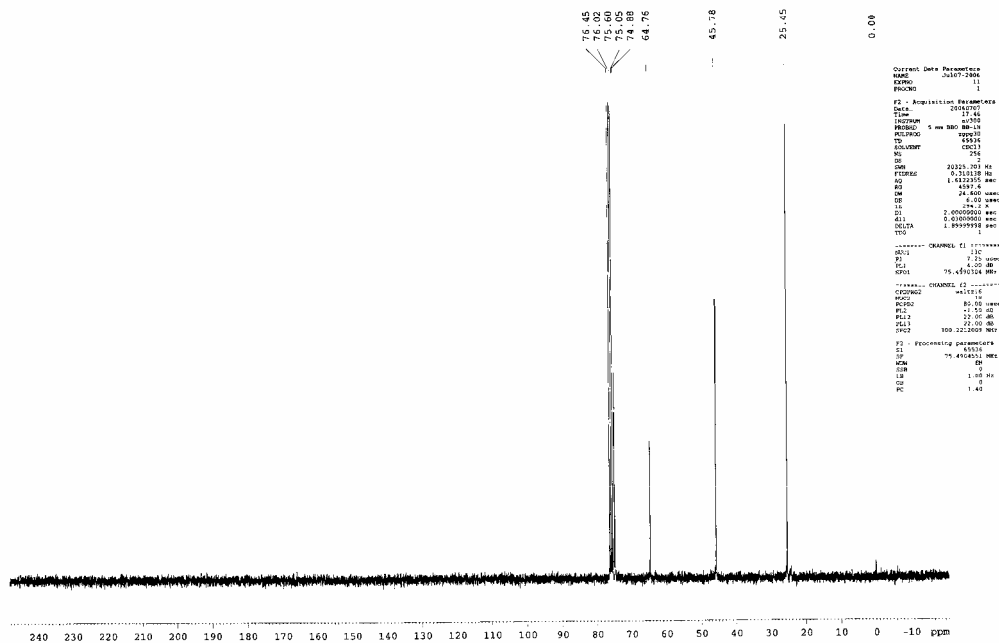


Figure B3. <sup>1</sup>H NMR (top) and <sup>13</sup>C NMR (bottom) spectrum of Ti(OEt)<sub>4</sub>.

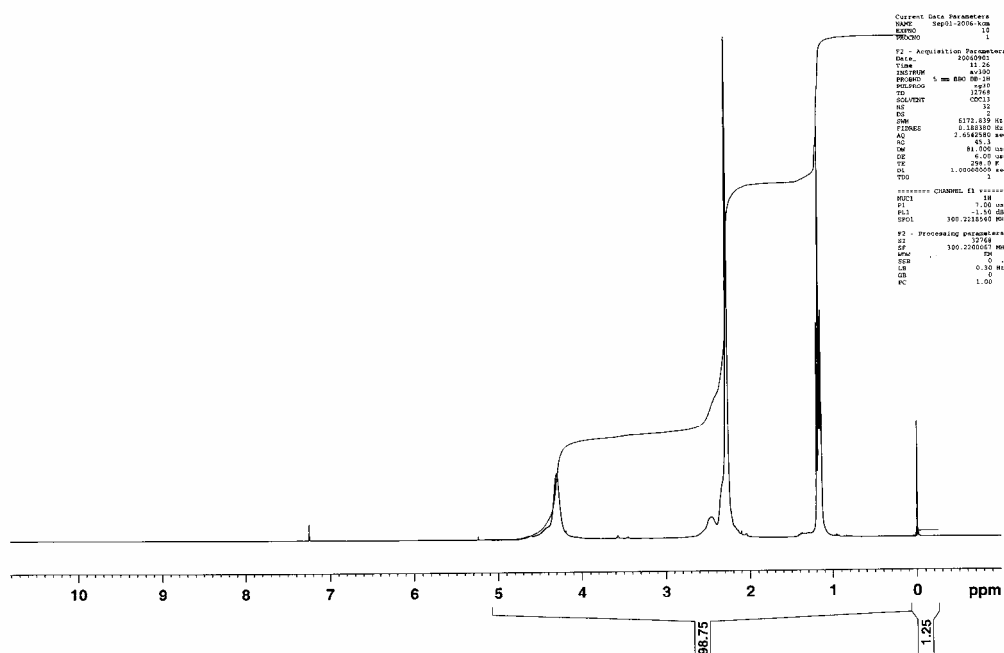
Ti(iso-prop)3(bdmap) A (6/7/2006)



Ti(iso-prop)3(bdmap) A (6/7/2006)

Figure B4.  $^1\text{H}$  NMR (top) and  $^{13}\text{C}$  NMR (bottom) spectrum of  $\text{Ti}(\text{O}^i\text{Pr})_3(\text{bdmap})$ .

Ti (OEt) 3bdmap



Ti (OEt) 3bdmap

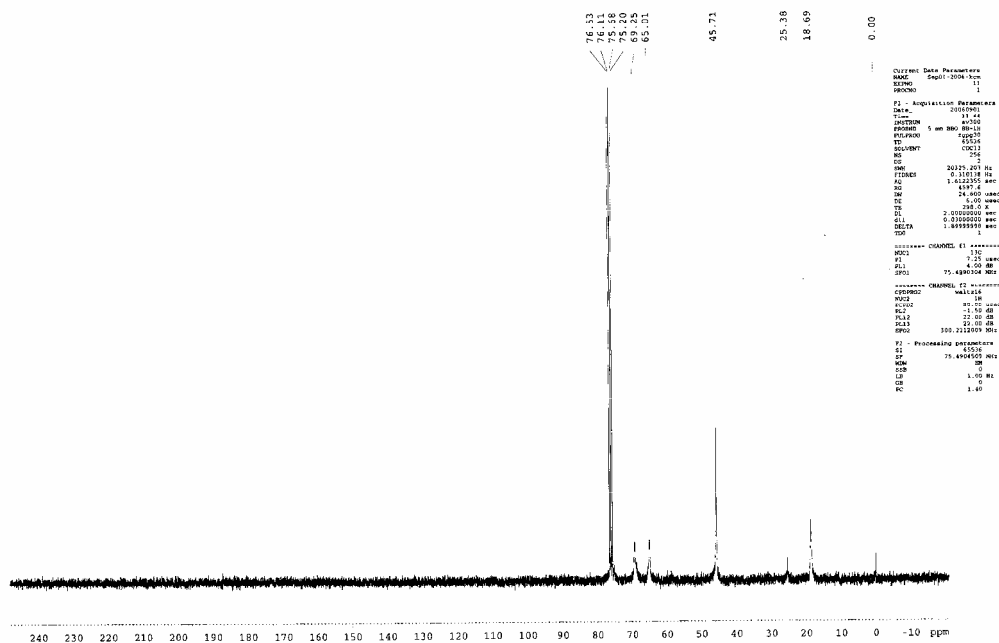
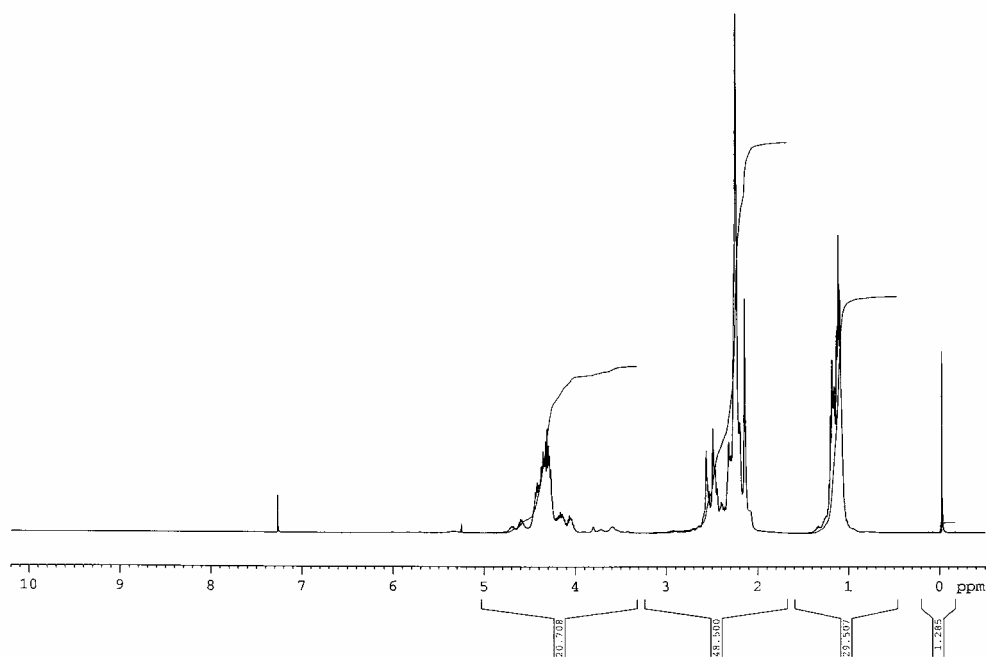
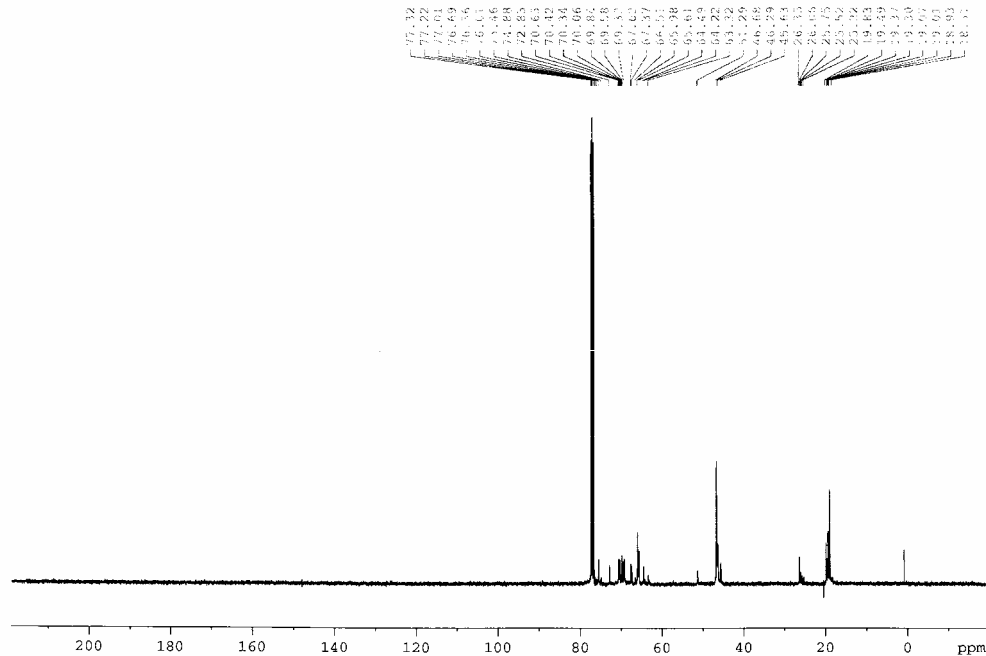


Figure B5.  $^1\text{H}$  NMR (top) and  $^{13}\text{C}$  NMR (bottom) spectrum of  $\text{Ti}(\text{OEt})_3$  (bdmap).

<sup>1</sup>H. 248 K

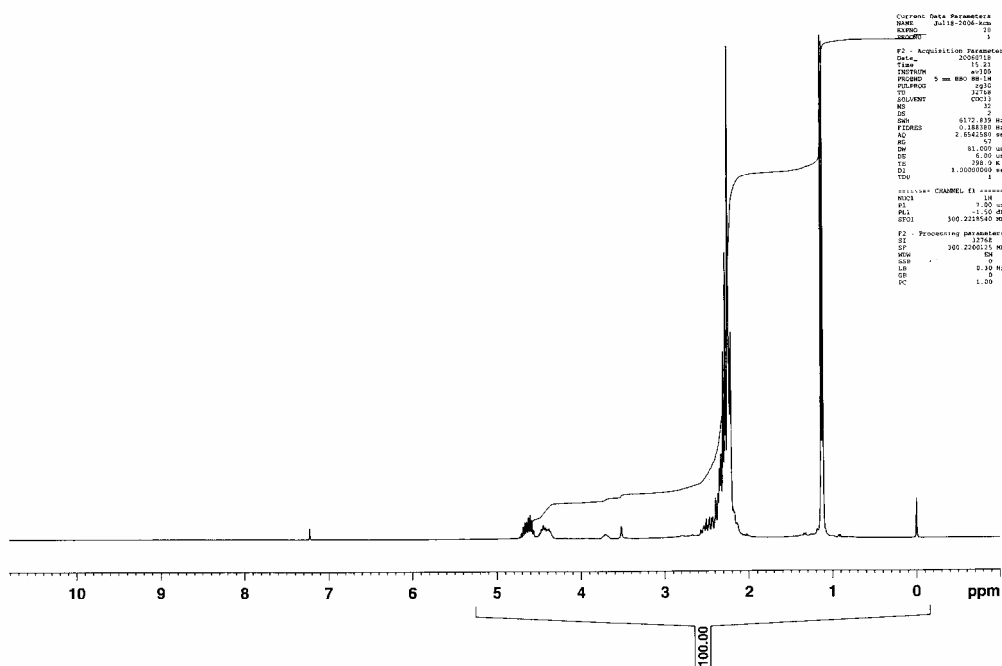


<sup>13</sup>C. 248K



**Figure B6.** <sup>1</sup>H NMR (top) and <sup>13</sup>C NMR (bottom) spectrum of Ti(OEt)<sub>3</sub>(bdmap) at 248 K.

Ti(iso-prop)2(bdmap)2 18/7/2006



Ti(iso-prop)2(bdmap)2 18/7/2006

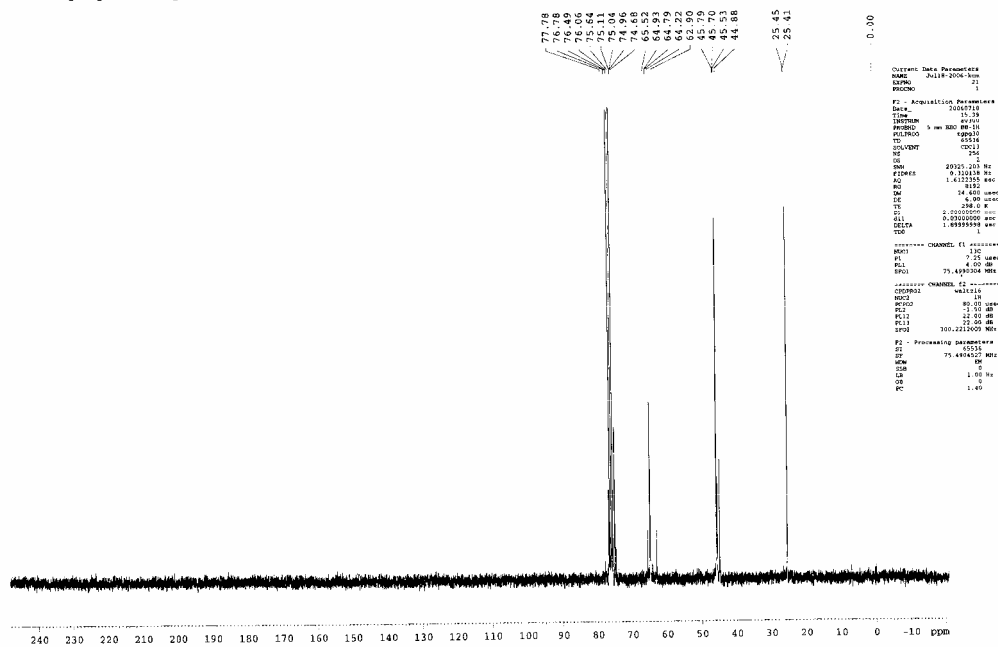


Figure B7.  $^1\text{H}$  NMR (top) and  $^{13}\text{C}$  NMR (bottom) spectrum of  $\text{Ti}(\text{O}^i\text{Pr})_2(\text{bdmap})_2$ .

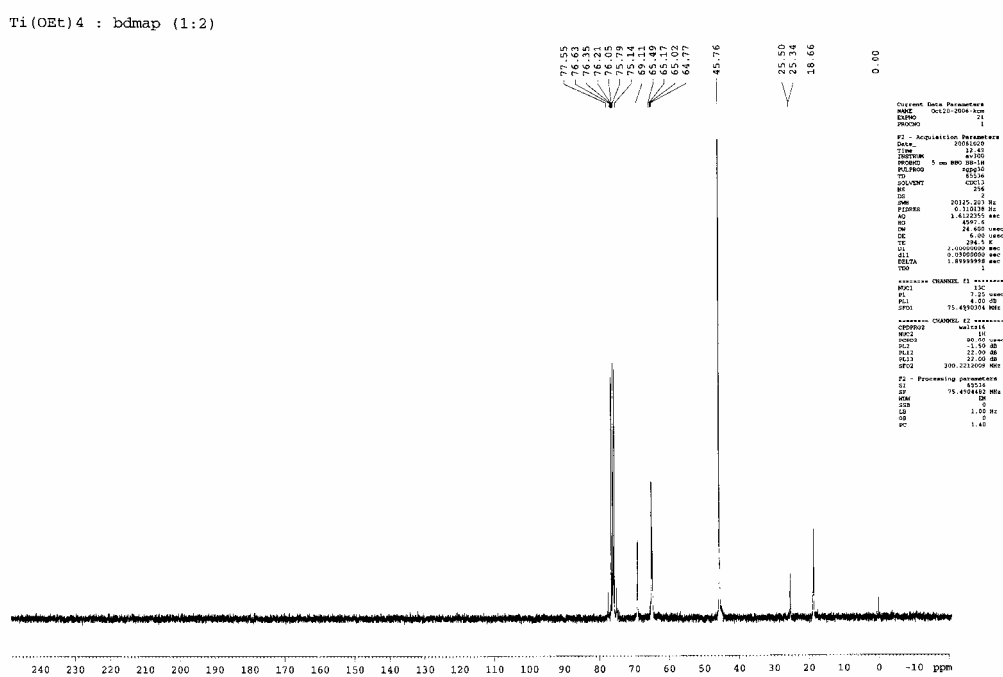
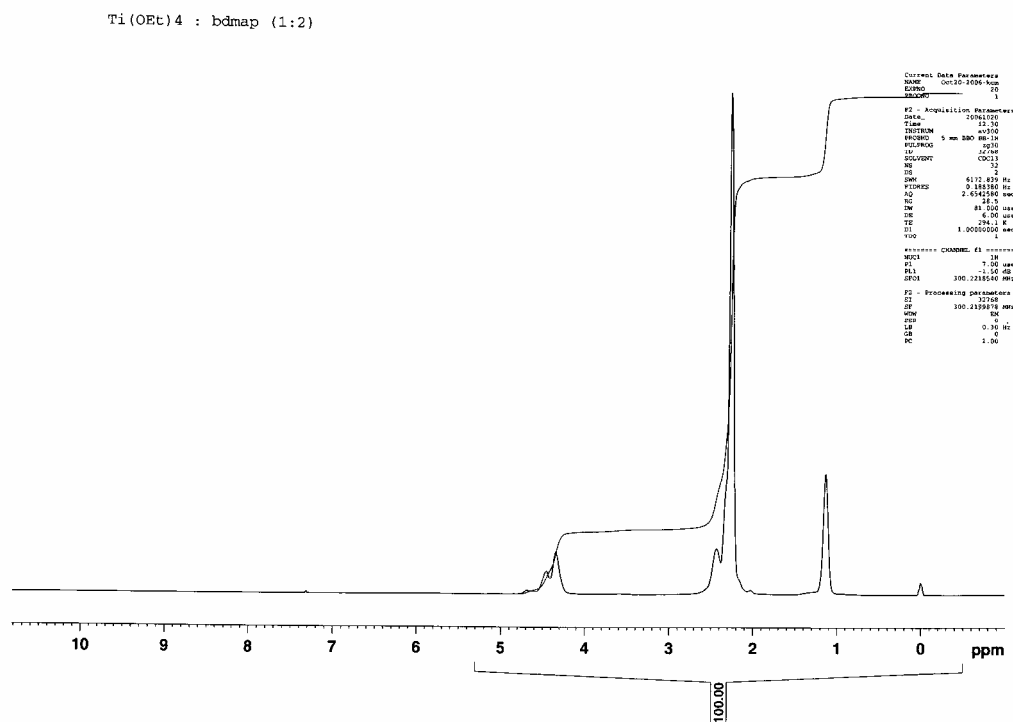


Figure B8. <sup>1</sup>H NMR (top) and <sup>13</sup>C NMR (bottom) spectrum of Ti(OEt)<sub>2</sub>(bdmap)<sub>2</sub>.

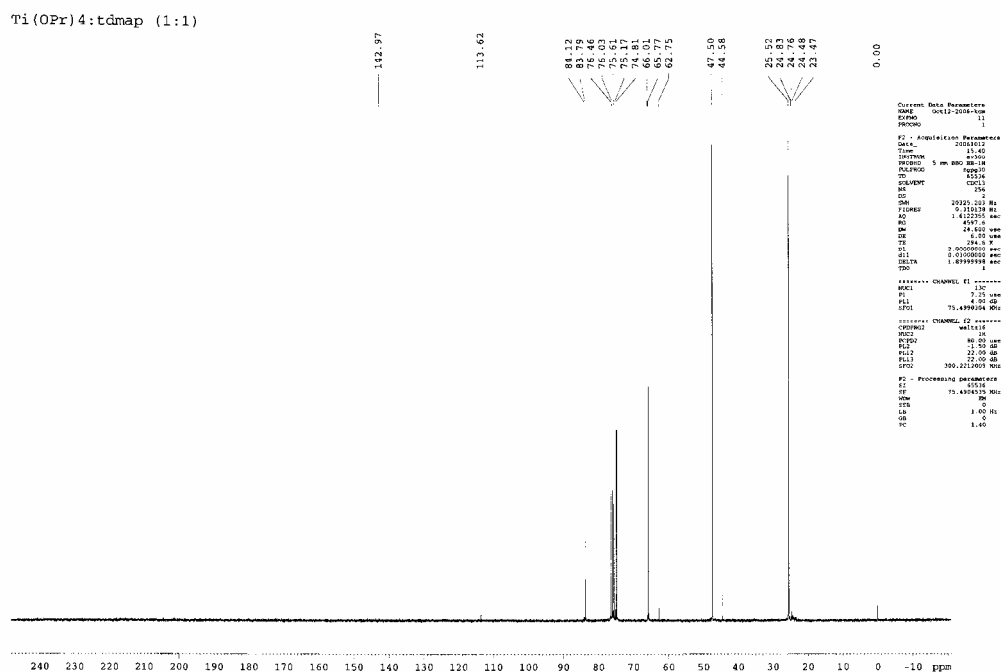
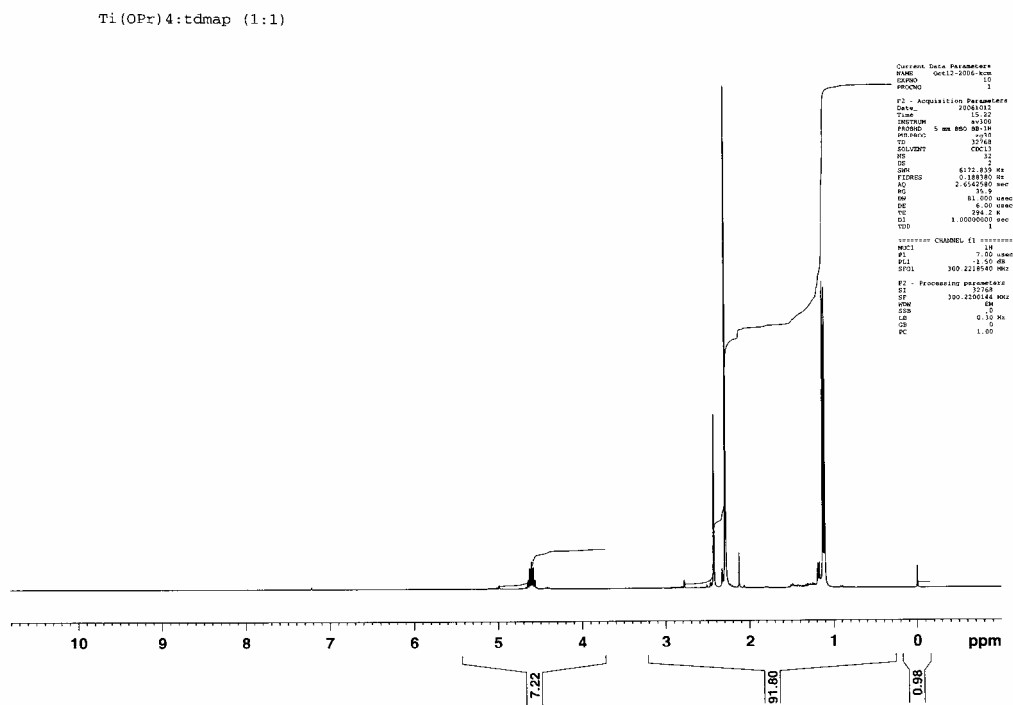
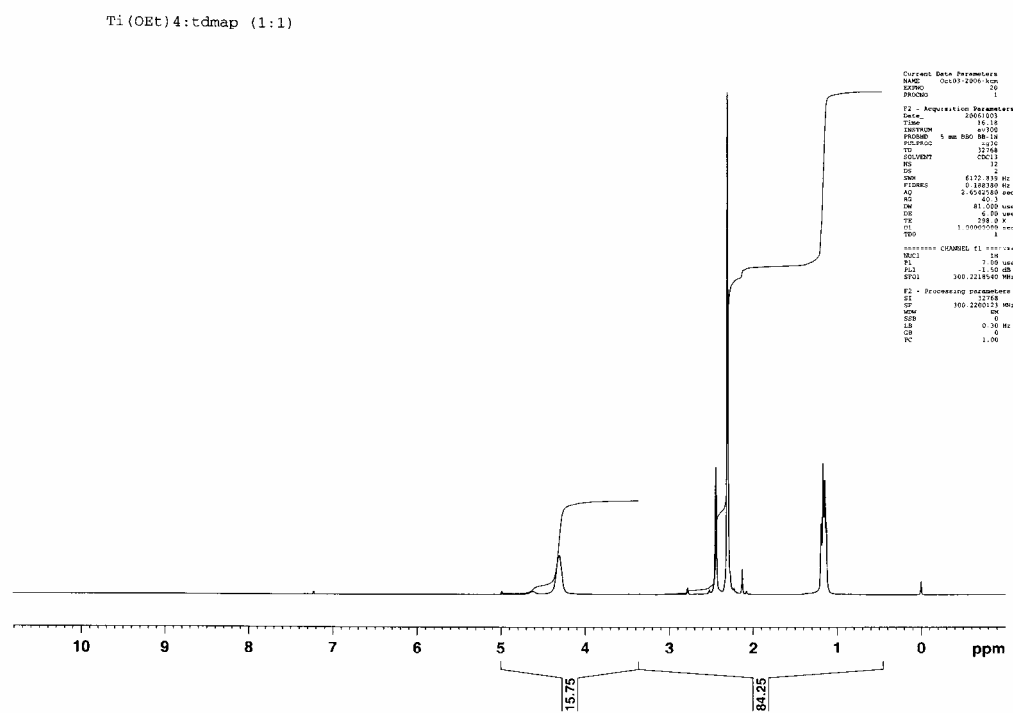


Figure B9. <sup>1</sup>H NMR (top) and <sup>13</sup>C NMR (bottom) spectrum of Ti(O<sup>i</sup>Pr)<sub>3</sub>(tdmap).



Ti(OEt)<sub>3</sub>:tdmap (1:1)

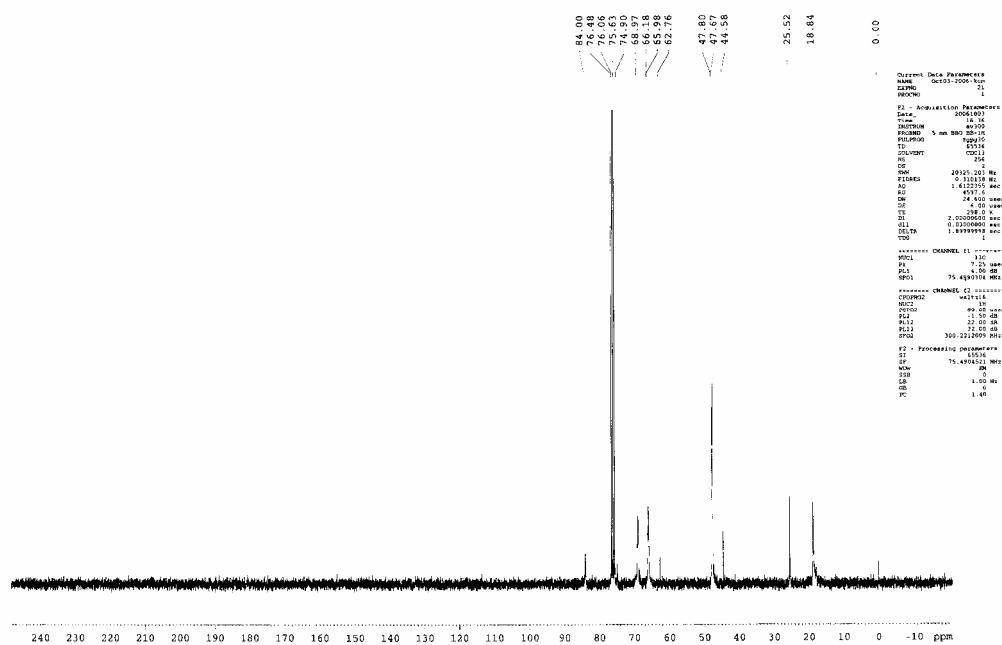


Figure B10. <sup>1</sup>H NMR (top) and <sup>13</sup>C NMR (bottom) spectrum of Ti(OEt)<sub>3</sub>(tdmap).



## APPENDIX C

**Table C1.** Bond lengths [Å] and angles [°] for Ti(OEt)<sub>3</sub>(bdmap).

Ti(1)-O(3)	1.812(2)	Ti(1)-O(2)	1.839(2)
Ti(1)-O(1)	1.866(2)	Ti(1)-O(4)	2.019(2)
Ti(1)-O(4)#1	2.079(2)	Ti(1)-N(1)	2.432(3)
Ti(1)-Ti(1)#1	3.3294(11)	Ti(1A)-O(3A)	1.814(2)
Ti(1A)-O(2A)	1.834(2)	Ti(1A)-O(1A)	1.866(2)
Ti(1A)-O(4A)	2.018(2)	Ti(1A)-O(4A)#2	2.078(2)
Ti(1A)-N(1A)	2.432(3)	Ti(1A)-Ti(1A)#2	3.3300(11)
O(1)-C(4)	1.412(4)	O(2)-C(8)	1.398(4)
O(3)-C(10)	1.415(4)	O(4)-C(12)	1.437(3)
O(4)-Ti(1)#1	2.079(2)	O(1A)-C(4A)	1.403(4)
O(2A)-C(8B)	1.395(10)	O(2A)-C(8A)	1.411(6)
O(3A)-C(10B)	1.403(11)	O(3A)-C(10A)	1.433(6)
O(4A)-C(12A)	1.436(4)	O(4A)-Ti(1A)#2	2.078(2)
N(1)-C(2)	1.474(4)	N(1)-C(3)	1.476(4)
N(1)-C(1)	1.477(4)	N(2)-C(7)	1.448(5)
N(2)-C(6)	1.454(5)	N(2)-C(5)	1.467(4)
N(1A)-C(3A)	1.475(4)	N(1A)-C(1A)	1.475(5)
N(1A)-C(2A)	1.478(4)	N(2A)-C(6A)	1.445(6)
N(2A)-C(5A)	1.456(4)	N(2A)-C(7A)	1.461(5)
C(3)-C(4)	1.523(4)	C(4)-C(5)	1.518(4)
C(8)-C(9)	1.492(5)	C(10)-C(11)	1.474(6)
C(12)-C(13)	1.501(5)	C(3A)-C(4A)	1.522(5)
C(4A)-C(5A)	1.525(5)	C(8A)-C(9A)	1.492(9)
C(10A)-C(11A)	1.469(11)	C(12A)-C(13A)	1.510(5)
C(8B)-C(9B)	1.471(14)	C(10B)-C(11B)	1.437(16)

O(3)-Ti(1)-O(2)	97.10(11)	O(3)-Ti(1)-O(1)	92.49(10)
O(2)-Ti(1)-O(1)	102.58(10)	O(3)-Ti(1)-O(4)	102.61(9)
O(2)-Ti(1)-O(4)	91.53(10)	O(1)-Ti(1)-O(4)	157.95(10)
O(3)-Ti(1)-O(4)#1	93.07(10)	O(2)-Ti(1)-O(4)#1	161.67(9)
O(1)-Ti(1)-O(4)#1	92.12(9)	O(4)-Ti(1)-O(4)#1	71.33(9)
O(3)-Ti(1)-N(1)	165.65(10)	O(2)-Ti(1)-N(1)	80.54(10)
O(1)-Ti(1)-N(1)	74.39(9)	O(4)-Ti(1)-N(1)	91.63(8)
O(4)#1-Ti(1)-N(1)	93.18(9)	O(3)-Ti(1)-Ti(1)#1	99.55(8)
O(2)-Ti(1)-Ti(1)#1	127.51(8)	O(1)-Ti(1)-Ti(1)#1	125.82(8)
O(4)-Ti(1)-Ti(1)#1	36.26(6)	O(4)#1-Ti(1)-Ti(1)#1	35.07(6)
N(1)-Ti(1)-Ti(1)#1	92.97(6)	O(3A)-Ti(1A)-O(2A)	97.05(11)
O(3A)-Ti(1A)-O(1A)	92.80(10)	O(2A)-Ti(1A)-O(1A)	103.11(10)
O(3A)-Ti(1A)-O(4A)	102.80(10)	O(2A)-Ti(1A)-O(4A)	91.39(9)
O(1A)-Ti(1A)-O(4A)	157.28(10)	O(3A)-Ti(1A)-O(4A)#2	93.86(10)
O(2A)-Ti(1A)-O(4A)#2	161.19(10)	O(1A)-Ti(1A)-O(4A)#2	91.58(9)
O(4A)-Ti(1A)-O(4A)#2	71.20(9)	O(3A)-Ti(1A)-N(1A)	165.52(10)
O(2A)-Ti(1A)-N(1A)	80.17(10)	O(1A)-Ti(1A)-N(1A)	74.19(9)
O(4A)-Ti(1A)-N(1A)	91.50(9)	O(4A)#2-Ti(1A)-N(1A)	92.85(9)
O(3A)-Ti(1A)-Ti(1A)#2	100.15(8)	O(2A)-Ti(1A)-Ti(1A)#2	127.25(8)
O(1A)-Ti(1A)-Ti(1A)#2	125.18(8)	O(4A)-Ti(1A)-Ti(1A)#2	36.20(6)
O(4A)#2-Ti(1A)-Ti(1A)#2	35.00(6)	N(1A)-Ti(1A)-Ti(1A)#2	92.69(7)
C(4)-O(1)-Ti(1)	127.47(18)	C(8)-O(2)-Ti(1)	140.2(2)
C(10)-O(3)-Ti(1)	136.4(2)	C(12)-O(4)-Ti(1)	126.11(18)
C(12)-O(4)-Ti(1)#1	122.65(18)	Ti(1)-O(4)-Ti(1)#1	108.67(9)
C(4A)-O(1A)-Ti(1A)	127.36(19)	C(8B)-O(2A)-C(8A)	21.8(5)
C(8B)-O(2A)-Ti(1A)	133.6(5)	C(8A)-O(2A)-Ti(1A)	144.1(3)
C(10B)-O(3A)-C(10A)	26.0(5)	C(10B)-O(3A)-Ti(1A)	129.4(5)
C(10A)-O(3A)-Ti(1A)	138.2(3)	C(12A)-O(4A)-Ti(1A)	126.27(18)
C(12A)-O(4A)-Ti(1A)#2	122.99(19)	Ti(1A)-O(4A)-Ti(1A)#2	108.80(9)
C(2)-N(1)-C(3)	108.8(2)	C(2)-N(1)-C(1)	108.1(3)
C(3)-N(1)-C(1)	110.3(3)	C(2)-N(1)-Ti(1)	116.1(2)
C(3)-N(1)-Ti(1)	98.97(17)	C(1)-N(1)-Ti(1)	114.11(19)
C(7)-N(2)-C(6)	109.6(3)	C(7)-N(2)-C(5)	111.5(3)

C(6)-N(2)-C(5)	109.8(3)	C(3A)-N(1A)-C(1A)	110.6(3)
C(3A)-N(1A)-C(2A)	108.9(3)	C(1A)-N(1A)-C(2A)	107.2(3)
C(3A)-N(1A)-Ti(1A)	99.1(2)	C(1A)-N(1A)-Ti(1A)	114.8(2)
C(2A)-N(1A)-Ti(1A)	116.0(2)	C(6A)-N(2A)-C(5A)	111.1(3)
C(6A)-N(2A)-C(7A)	109.2(3)	C(5A)-N(2A)-C(7A)	109.9(3)
N(1)-C(3)-C(4)	109.6(2)	O(1)-C(4)-C(5)	108.4(3)
O(1)-C(4)-C(3)	108.6(2)	C(5)-C(4)-C(3)	111.4(3)
N(2)-C(5)-C(4)	113.1(3)	O(2)-C(8)-C(9)	111.4(3)
O(3)-C(10)-C(11)	112.0(4)	O(4)-C(12)-C(13)	113.5(2)
N(1A)-C(3A)-C(4A)	109.4(3)	O(1A)-C(4A)-C(3A)	109.2(3)
O(1A)-C(4A)-C(5A)	108.4(3)	C(3A)-C(4A)-C(5A)	112.2(3)
N(2A)-C(5A)-C(4A)	114.1(3)	O(2A)-C(8A)-C(9A)	110.7(5)
O(3A)-C(10A)-C(11A)	109.0(7)	O(4A)-C(12A)-C(13A)	113.0(3)
O(2A)-C(8B)-C(9B)	109.5(10)	O(3A)-C(10B)-C(11B)	111.8(13)

Symmetry transformations used to generate equivalent atoms:

#1 -x+2,-y+1,-z #2 -x+1,-y+1,-z+1

**Table C2.** Bond lengths [Å] and angles [°] for [(bdmap)<sub>2</sub>TiO]<sub>2</sub>.

Ti(1)-O(1)	1.8446(14)	Ti(1)-O(1)#1	1.8476(14)
Ti(1)-O(2)	1.8777(14)	Ti(1)-O(3)	1.8829(15)
Ti(1)-N(1)	2.3965(18)	Ti(1)-N(3)	2.4528(18)
Ti(1)-Ti(1)#1	2.7821(7)	O(1)-Ti(1)#1	1.8476(14)
O(2)-C(1)	1.408(2)	O(3)-C(8)	1.399(2)
N(1)-C(3)	1.465(3)	N(1)-C(2)	1.476(3)
N(1)-C(4)	1.477(3)	N(2)-C(6)	1.455(3)
N(2)-C(7)	1.456(3)	N(2)-C(5)	1.459(3)
N(3)-C(11)	1.457(3)	N(3)-C(10)	1.461(3)
N(3)-C(9)	1.471(3)	N(4)-C(13)	1.452(5)
N(4)-C(14)	1.461(8)	N(4)-C(12)	1.534(6)
N(4A)-C(12)	1.260(12)	N(4A)-C(14A)	1.41(3)
N(4A)-C(13A)	1.511(19)	C(1)-C(5)	1.525(3)
C(1)-C(2)	1.526(3)	C(8)-C(12)	1.514(3)
C(8)-C(9)	1.520(4)		

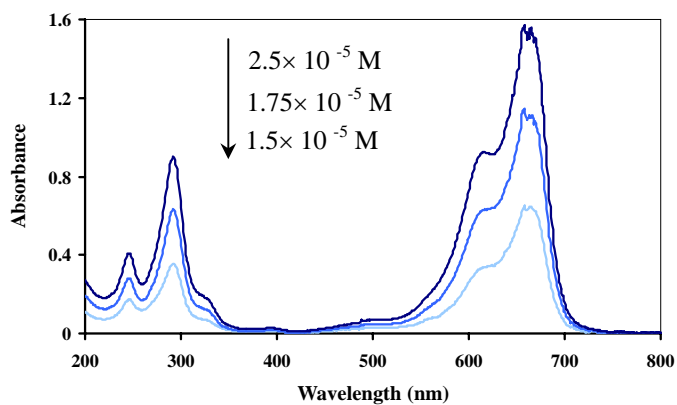
O(1)-Ti(1)-O(1)#1	82.20(6)	O(1)-Ti(1)-O(2)	109.34(6)
O(1)#1-Ti(1)-O(2)	103.87(6)	O(1)-Ti(1)-O(3)	104.62(6)
O(1)#1-Ti(1)-O(3)	109.16(6)	O(2)-Ti(1)-O(3)	135.08(7)
O(1)-Ti(1)-N(1)	81.69(6)	O(1)#1-Ti(1)-N(1)	162.18(6)
O(2)-Ti(1)-N(1)	74.54(6)	O(3)-Ti(1)-N(1)	82.35(6)
O(1)-Ti(1)-N(3)	162.98(6)	O(1)#1-Ti(1)-N(3)	82.34(6)
O(2)-Ti(1)-N(3)	81.35(6)	O(3)-Ti(1)-N(3)	73.96(7)
N(1)-Ti(1)-N(3)	114.50(6)	O(1)-Ti(1)-Ti(1)#1	41.15(4)
O(1)#1-Ti(1)-Ti(1)#1	41.07(4)	O(2)-Ti(1)-Ti(1)#1	111.52(5)
O(3)-Ti(1)-Ti(1)#1	113.40(5)	N(1)-Ti(1)-Ti(1)#1	122.32(5)
N(3)-Ti(1)-Ti(1)#1	123.16(5)	Ti(1)-O(1)-Ti(1)#1	97.79(6)
C(1)-O(2)-Ti(1)	127.74(12)	C(8)-O(3)-Ti(1)	129.09(14)
C(3)-N(1)-C(2)	110.66(17)	C(3)-N(1)-C(4)	109.12(17)

C(2)-N(1)-C(4)	110.85(17)	C(3)-N(1)-Ti(1)	114.38(13)
C(2)-N(1)-Ti(1)	100.81(12)	C(4)-N(1)-Ti(1)	110.82(13)
C(6)-N(2)-C(7)	109.8(2)	C(6)-N(2)-C(5)	111.12(19)
C(7)-N(2)-C(5)	112.10(19)	C(11)-N(3)-C(10)	109.1(2)
C(11)-N(3)-C(9)	111.2(2)	C(10)-N(3)-C(9)	110.6(2)
C(11)-N(3)-Ti(1)	113.48(14)	C(10)-N(3)-Ti(1)	112.19(14)
C(9)-N(3)-Ti(1)	100.14(13)	C(13)-N(4)-C(14)	108.8(4)
C(13)-N(4)-C(12)	109.4(4)	C(14)-N(4)-C(12)	107.2(4)
C(12)-N(4A)-C(14A)	117.5(15)	C(12)-N(4A)-C(13A)	114.6(10)
C(14A)-N(4A)-C(13A)	103.9(17)	O(2)-C(1)-C(5)	112.92(18)
O(2)-C(1)-C(2)	107.80(16)	C(5)-C(1)-C(2)	109.85(17)
N(1)-C(2)-C(1)	108.47(16)	N(2)-C(5)-C(1)	113.57(17)
O(3)-C(8)-C(12)	113.1(2)	O(3)-C(8)-C(9)	107.55(19)
C(12)-C(8)-C(9)	110.8(2)	N(3)-C(9)-C(8)	110.04(19)
N(4A)-C(12)-C(8)	124.7(6)	N(4A)-C(12)-N(4)	14.2(6)
C(8)-C(12)-N(4)	112.4(3)		

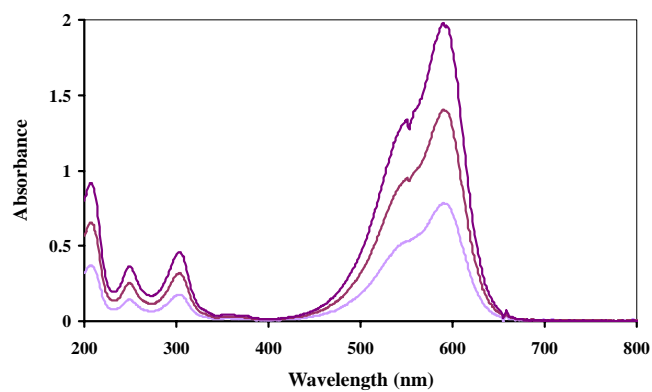
Symmetry transformations used to generate equivalent atoms:

#1 -x+1,y,-z+3/2

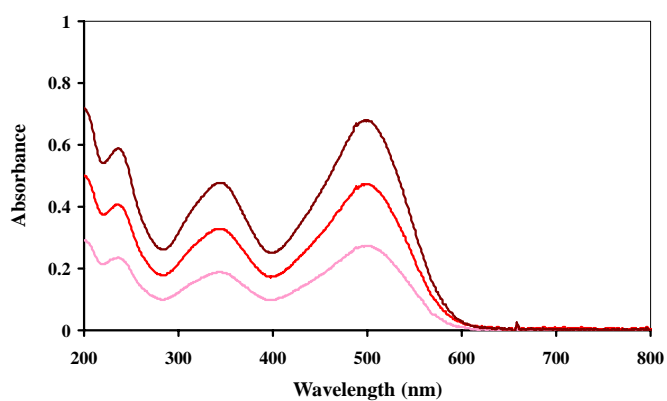
## APPENDIX D



(a) Methylene blue (MB)

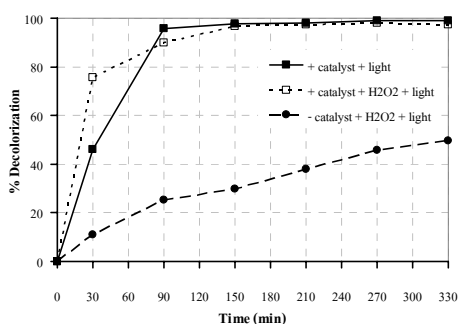


(b) Crystal violet (CV)

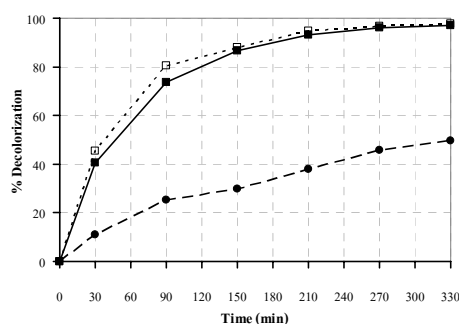


(c) Congo red (CR)

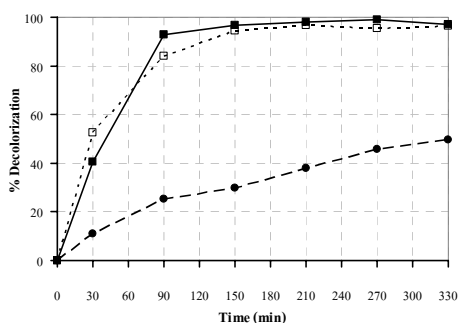
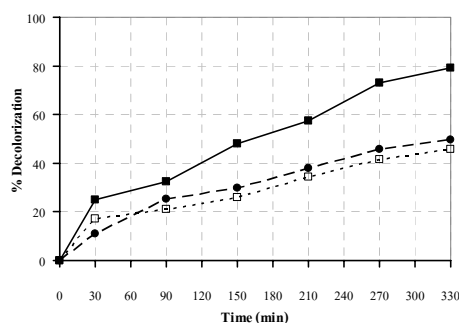
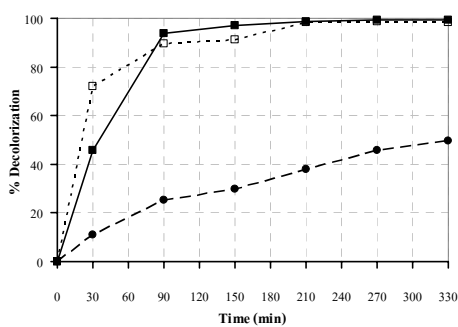
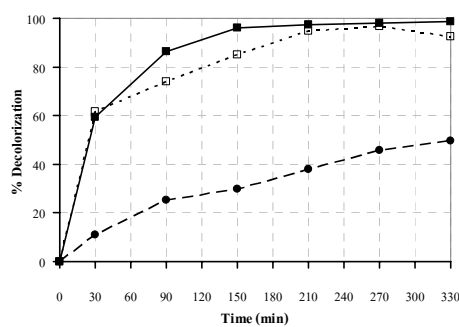
**Figure D1.** The absorption spectrum of (a) Methylene Blue: MB, (b) Crystal Violet: CV, and (c) Congo Red: CR solution.



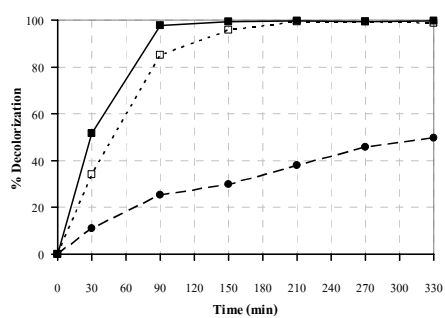
(a) Ti-no-acid



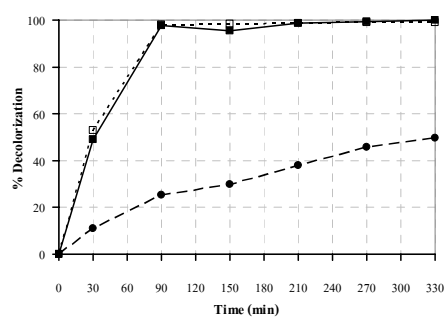
(b) Ti-HCl

(c) Ti-HNO<sub>3</sub>(d) Ti-H<sub>2</sub>SO<sub>4</sub>(e) Ti-CH<sub>3</sub>COOH(f) Ti-H<sub>3</sub>PO<sub>4</sub>

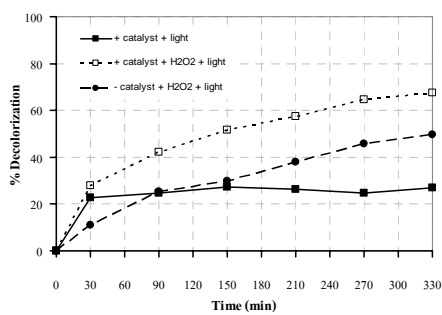
**Figure D2.** Effect of hydrogen peroxide in presence of light on MB degradation as a function of time in the presence of synthesized TiO<sub>2</sub>: (a) Ti-no-acid, (b) Ti-HCl, (c) Ti-HNO<sub>3</sub>, (d) Ti-H<sub>2</sub>SO<sub>4</sub>, (e) Ti-CH<sub>3</sub>COOH, and (f) Ti-H<sub>3</sub>PO<sub>4</sub>.



(a) Degussa P25



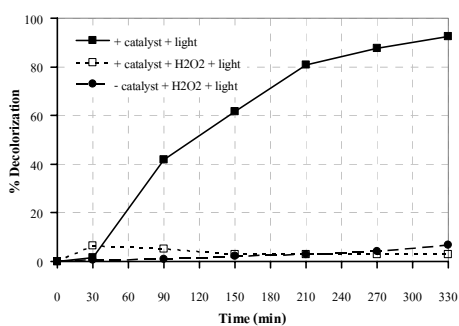
(b) Anatase (Carlo Erba)



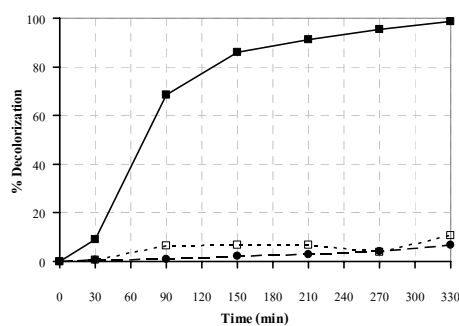
(c) Rutile (R706, TOA)

**Figure D3.** Effect of hydrogen peroxide in presence of light on MB degradation as a function of time in the presence of commercial  $\text{TiO}_2$ : (a) Degussa P25, (b) Anatase (Carlo Erba), and (c) Rutile (R706, TOA).

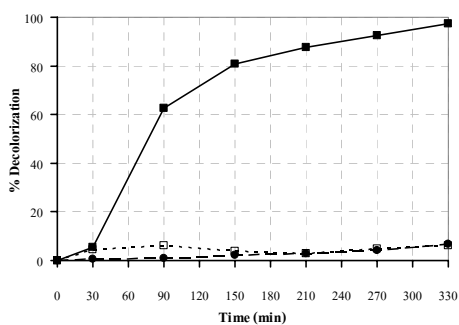
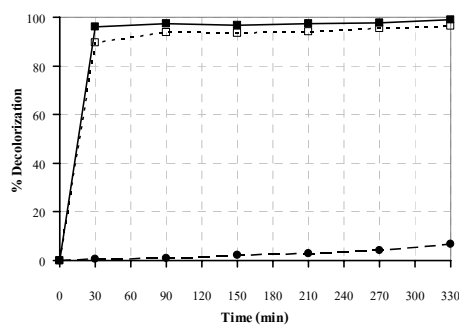
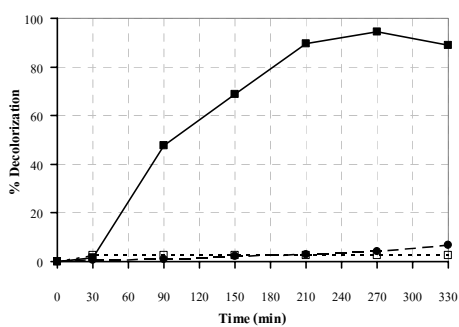
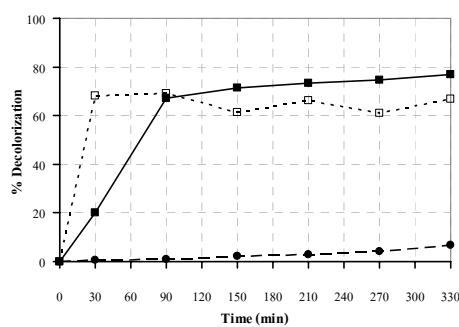




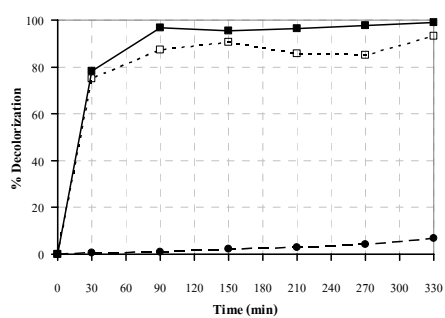
(a) Ti-no-acid



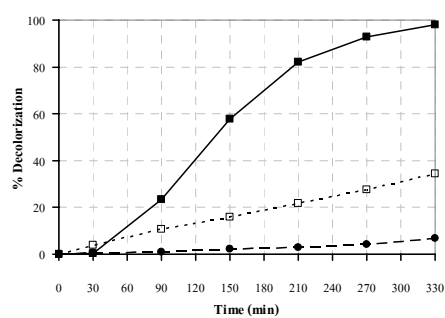
(b) Ti-HCl

(c) Ti-HNO<sub>3</sub>(d) Ti-H<sub>2</sub>SO<sub>4</sub>(e) Ti-CH<sub>3</sub>COOH(f) Ti-H<sub>3</sub>PO<sub>4</sub>

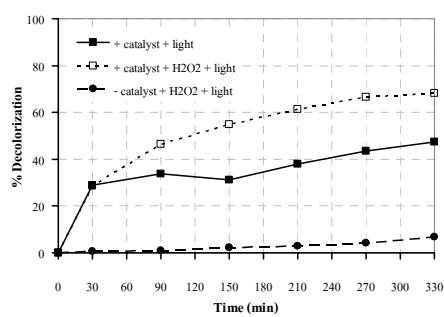
**Figure D4.** Effect of hydrogen peroxide in presence of light on CR degradation as a function of time in the presence of synthesized TiO<sub>2</sub>: (a) Ti-no-acid, (b) Ti-HCl, (c) Ti-HNO<sub>3</sub>, (d) Ti-H<sub>2</sub>SO<sub>4</sub>, (e) Ti-CH<sub>3</sub>COOH, and (f) Ti-H<sub>3</sub>PO<sub>4</sub>.



(a) Degussa P25

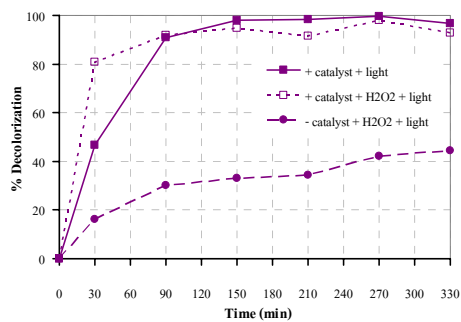


(b) Anatase (Carlo Erba)

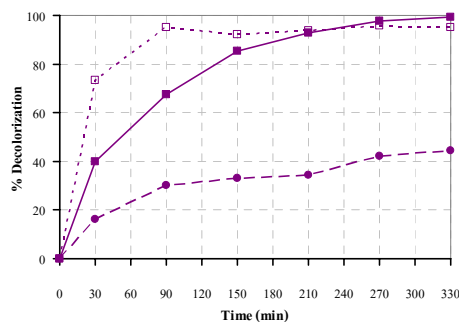


(c) Rutile (R706, TOA)

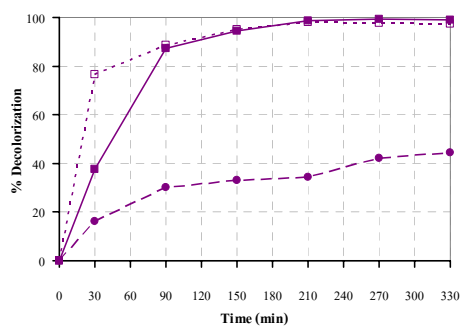
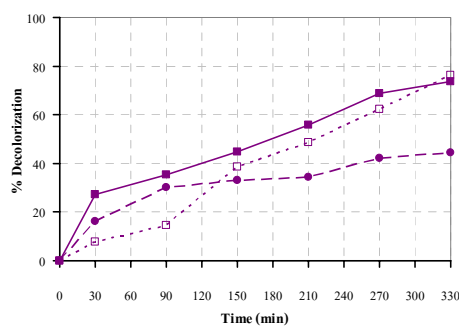
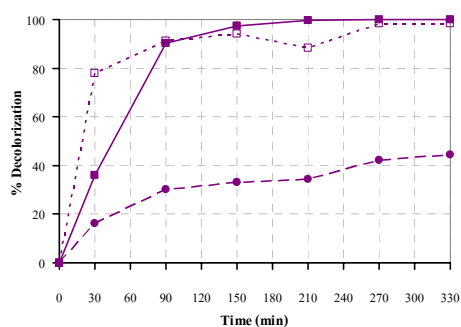
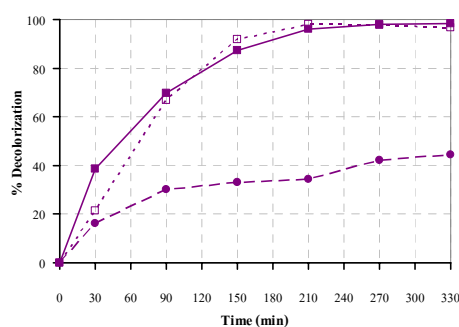
**Figure D5.** Effect of hydrogen peroxide in presence of light on CR degradation as a function of time in the presence of commercial TiO<sub>2</sub>: (a) Degussa P25, (b) Anatase (Carlo Erba), and (c) Rutile (R706, TOA).



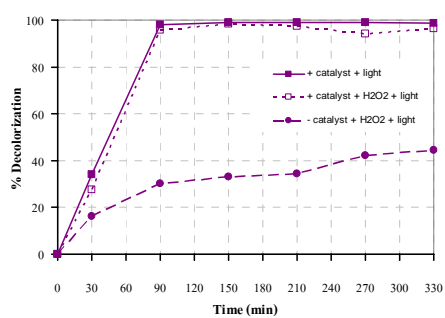
(a) Ti-no-acid



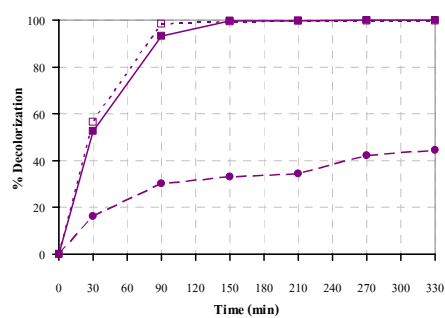
(b) Ti-HCl

(c) Ti-HNO<sub>3</sub>(d) Ti-H<sub>2</sub>SO<sub>4</sub>(e) Ti-CH<sub>3</sub>COOH(f) Ti-H<sub>3</sub>PO<sub>4</sub>

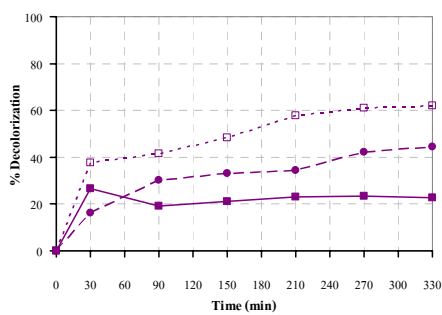
**Figure D6.** Effect of hydrogen peroxide in presence of light on CV degradation as a function of time in the presence of synthesized TiO<sub>2</sub>: (a) Ti-no-acid, (b) Ti-HCl, (c) Ti-HNO<sub>3</sub>, (d) Ti-H<sub>2</sub>SO<sub>4</sub>, (e) Ti-CH<sub>3</sub>COOH, and (f) Ti-H<sub>3</sub>PO<sub>4</sub>.



(a) Degussa P25



(b) Anatase (Carlo Erba)



(c) Rutile (R706, TOA)

**Figure D7.** Effect of hydrogen peroxide in presence of light on CV degradation as a function of time in the presence of commercial TiO<sub>2</sub>: (a) Degussa P25, (b) Anatase (Carlo Erba), and (c) Rutile (R706, TOA).

**APPENDIX E**

**PUBLICATIONS FROM THIS WORK**

## Synthesis and characterisation of new titanium amino-alkoxides: precursors for the formation of TiO<sub>2</sub> materials†

Nathan Hollingsworth,<sup>a</sup> Miki Kanna,<sup>‡,b</sup> Gabriele Kociok-Köhn,<sup>a</sup> Kieran C. Molloy<sup>\*a</sup> and Sumpun Wongnawa<sup>b</sup>

Received 13th August 2007, Accepted 25th October 2007

First published as an Advance Article on the web 13th November 2007

DOI: 10.1039/b712375b

Reaction of the amino-alkoxides HOCH(CH<sub>2</sub>NMe<sub>2</sub>)<sub>2</sub> (Hbdmap) and HOC(CH<sub>2</sub>NMe<sub>2</sub>)<sub>3</sub> (Htdmap) with [Ti(OR)<sub>4</sub>] yields a series of heteroleptic titanium alkoxides [Ti(OR)<sub>4-n</sub>(L)<sub>n</sub>] (L = bdmap, tdmap). Substitution of the monodentate alkoxide with the chelating alkoxides becomes progressively more difficult, with homogeneous products being obtained only for *n* = 1, 2. The structure of [Ti(OEt)<sub>3</sub>(bdmap)]<sub>2</sub>, a μ-OEt bridged dimer, has been determined. Hydrolysis of [Ti(OR)<sub>2</sub>(L)<sub>2</sub>], by adventitious moisture affords the dimeric oxo-alkoxides [Ti(O)(L)<sub>2</sub>]<sub>2</sub>, both of which have been characterised crystallographically. These two compounds have also been prepared by reaction of [Ti(NMe<sub>2</sub>)<sub>2</sub>(L)<sub>2</sub>] with the hydrated metal salts [Zn(acac)<sub>2</sub>·2H<sub>2</sub>O] and [Zn(OAc)<sub>2</sub>·2H<sub>2</sub>O] using the intrinsic water molecules in these salts to react with the labile amido groups, though the former also produces Me(Me<sub>2</sub>N)C=C(H)C(O)Me from reaction of liberated HNMe<sub>2</sub> with the coordinated acac ligand, while the latter also affords the ligand exchange product [Zn(OAc)(bdmap)]. In neither case does the free dimethylamino group of [Ti(O)(L)<sub>2</sub>]<sub>2</sub> coordinate a second metal. The dimeric structure of [Zn(OAc)(bdmap)]<sub>2</sub> has been established, and the structure of the tetrameric oxo-alkoxide [Ti(O)(OPr<sup>i</sup>)(OCH<sub>2</sub>CH<sub>2</sub>NMe<sub>2</sub>)<sub>4</sub>] is reported for comparison with others in this study. [Ti(OEt)<sub>3</sub>(bdmap)]<sub>2</sub> has been used as a precursor in AACVD (Aerosol-Assisted Chemical Vapour Deposition) to generate amorphous TiO<sub>2</sub> films on glass at 440 °C, and TiO<sub>2</sub>@C nanoparticles of approximate diameter 350 nm with a carbon coating of width *ca.* 75 nm on heating in a sealed container at 700 °C.

### Introduction

TiO<sub>2</sub> remains one of the most important of the ceramic metal oxides, with diverse applications ranging from catalysis to materials chemistry. It has a high refractive index, is transparent in the visible and near-IR regions of the spectrum and has thus been used as an anti-reflective coating.<sup>1</sup> TiO<sub>2</sub> also has a high dielectric constant (*k* ~ 80 for ultra-thin films, ~ 170 for single crystals of rutile) and is an alternative to SiO<sub>2</sub> as a gate dielectric.<sup>2,3</sup> TiO<sub>2</sub> doped with a small amount of cobalt has been used in spin-based electronic devices,<sup>4</sup> while more complex oxide materials based on TiO<sub>2</sub> and with a perovskite structure *e.g.* SrTiO<sub>3</sub>, (Ba, Sr)TiO<sub>3</sub> and Pb(Zr, Ti)O<sub>3</sub> have applications in DRAM and FERAM computer memories.<sup>5</sup> TiO<sub>2</sub> has widespread use in catalysis, from both conventional chemistry (ester, poly-olefine production, Sharpless asymmetric epoxidation)<sup>6</sup> to catalytic surfaces and photocatalysis.<sup>7,8</sup> The latter has been the subject of intense activity in recent years, and has resulted in the commercial production of, for example, self-cleaning windows (Pilkington Activ™).

TiO<sub>2</sub> is chemically very stable and exists naturally in three distinct crystallographic modifications, namely rutile, anatase and

brookite,<sup>9</sup> while a high pressure modification (cotunnite) can also be synthesised. Anatase is perceived as generally the easiest modification to achieve synthetically, while rutile is the thermodynamically favoured form and dominates when the synthesis is carried out at high temperatures; a recent report has detailed protocols for the preparation and isolation of all three modifications.<sup>10</sup> Of these, rutile is the most important from the perspective of optical applications while anatase is the more photoactive; brookite and cotunnite are not as utilised, though the latter is one of the hardest known oxide materials.<sup>11</sup> Photocatalytic activity for brookite, as well as anatase, has recently been reported.<sup>10</sup>

Thin films of titania can be produced by metal-organic chemical vapour deposition (MOCVD) and atomic layer deposition (ALD) techniques, which offer the advantage over other techniques of being able to coat large areas and with good aspect ratios over complex geometries. Central to the MOCVD/ALD methodology is the availability and choice of precursor, which can play a significant role in controlling ease of handling, volatility, deposition temperature, film composition and morphology *etc.* Conventional precursors for TiO<sub>2</sub> have employed TiCl<sub>4</sub><sup>12</sup> or a homoleptic alkoxide [Ti(OR)<sub>4</sub>] (R = Me,<sup>13</sup> Et,<sup>14</sup> or, most commonly, OPr<sup>i</sup><sup>15-18</sup>) along with a source of oxygen (H<sub>2</sub>O, ROH are common), but TiCl<sub>4</sub> suffers from the introduction of chlorine contaminant into the film<sup>19</sup> while the alkoxides are relatively air- and moisture-sensitive making them unattractive both from a handling perspective and due to their susceptibility to pre-reaction in a dual-source MOCVD reaction. Other precursors which have been reported include the use of simple volatile Ti(NMe<sub>2</sub>)<sub>4</sub> (used with H<sub>2</sub>O)<sup>20</sup> and more complex precursors such as [Ti<sub>6</sub>(O)<sub>6</sub>(O<sub>2</sub>CR)<sub>6</sub>]

<sup>a</sup>Department of Chemistry, University of Bath, Claverton Down, Bath, UK BA2 7AY

<sup>b</sup>Department of Chemistry, Faculty of Science, Prince of Songkla University, Hat Yai, Songkhla 90112, Thailand

† CCDC reference numbers 657058–657062. For crystallographic data in CIF or other electronic format see DOI: 10.1039/b712375b

‡ 2003 Royal Golden Jubilee PhD scholar, on study leave at the University of Bath.

(R = Bu, Bz);<sup>21</sup> however, most variations attempt to mitigate the sensitivity of titanium alkoxides by the use of chelating ligands which saturate the coordination sphere of the metal. Pre-eminent among these ligands are the  $\beta$ -diketonates, which have been used extensively in conjunction with alkoxides, e.g. [Ti(OPr<sup>i</sup>)<sub>2</sub>(thd)<sub>2</sub>] (thd = 2,2,6,6-tetramethylheptane-3,5-dionate);<sup>22,23</sup> more recently, related  $\beta$ -ketoesters e.g. [Ti(OPr<sup>i</sup>)<sub>2</sub>(tbaoc)<sub>2</sub>] (Htbaoc = t-butylacetoacetate)<sup>24</sup> and related malonates have been reported. The latter, when coupled with amido ligands i.e. [Ti(NMe<sub>2</sub>)<sub>2</sub>(dpml)<sub>2</sub>] (Hdpm = diisopropylmalonate)<sup>25</sup> have generated precursors with a mixed O,N ligand sphere for ALD applications.

Our interest,<sup>26</sup> and the subject of this paper, is the use of chelating amino-alkoxides R<sub>2</sub>N(CH<sub>2</sub>)<sub>n</sub>OH in CVD precursor chemistry. Titanium derivatives of amino ethanol [n = 2; R = Me (Hdmae), Et (Hdeae)] and propanols [n = 3, R = Me (Hdmap)] have been known for some time,<sup>27–29</sup> and several e.g. [Ti(OPr<sup>i</sup>)<sub>2</sub>(dmap)]<sup>30,31</sup> [Ti(OPr<sup>i</sup>)<sub>2</sub>(dmae)<sub>2</sub>]<sup>30,32</sup> [Ti(OPr<sup>i</sup>)(dmae)<sub>3</sub>]<sup>33</sup> [Ti(dmae)<sub>4</sub>]<sup>33,34</sup> have been used in the CVD of TiO<sub>2</sub> and/or related binary oxide films. Indeed, the use of Ti(dmae)<sub>n</sub> precursors has been claimed to lead to more uniform growth of TiO<sub>2</sub> films.<sup>34</sup> To our knowledge, however, use of the more functionalised ligands 1,3-bis-(dimethylamino)propanol (**I**: Hbdmap) and 1,3-bis-(dimethylamino)-2-(dimethylaminomethyl)propanol (**II**: Htdmap) have not been considered. Their use is of interest, firstly because of their enhanced ability to coordinate the metal centre from which the precursors may gain greater stability and, secondly, because unused donor sites have the potential to be further utilised for secondary metal binding. In this paper we report on the synthesis and characterisation of a series of compounds [Ti(OR)<sub>4</sub>-(L)<sub>4–2</sub>] (R = Et, Pr<sup>i</sup>; L = bdmap, tdmmap) and [Ti(OR)<sub>2</sub>-(L)<sub>2</sub> bdmap, tdmmap] and their use for the formation of both TiO<sub>2</sub> films and nanoparticles.



## Experimental

### General procedures

Elemental analyses were performed using an Exeter Analytical CE 440 analyser. The low carbon analyses observed in this study probably arise from the formation of involatile TiC, and has been a feature of the microanalysis of related species.<sup>35</sup> <sup>1</sup>H and <sup>13</sup>C NMR spectra were recorded on a Bruker Advance 300 MHz FT-NMR spectrometer as saturated solutions at room temperature; chemical shifts are in ppm with respect to Me<sub>4</sub>Si; coupling constants are in Hz. SEM was carried out on a JEOL JSM-6310 microscope equipped with Oxford Instruments ISIS EDXS attachment, while TEM used a JEOL 1200EX machine. XRD was performed using a Bruker D8 diffractometer on which coupled  $\theta$ - $2\theta$  scans were carried out.

### Syntheses

Hbdmap<sup>36</sup> and Htdmap<sup>37,38</sup> were prepared by literature methods.

**Synthesis of [Ti(OEt)<sub>2</sub>(bdmap)] (1).** [Ti(OEt)<sub>4</sub>] (1.59 g, 6.9 mmol) was dissolved in dry hexane (10 mL) and Hbdmap (1.02 g, 6.9 mmol) was added. After stirring overnight, the mixture was heated at 50 °C with stirring for 2 h. All volatiles were removed under vacuum, giving 2.17 g (96%) of a white solid. This was subsequently dissolved in dry dichloromethane (5 mL) and placed in the freezer at –12 °C where colourless crystals appeared. Analysis: Found (calc. for TiO<sub>4</sub>N<sub>2</sub>C<sub>13</sub>H<sub>32</sub>): C 45.9 (47.6); H 9.7 (9.8); N 8.3 (8.5)%. <sup>1</sup>H-NMR (CDCl<sub>3</sub>): 4.40 (1H, br sh, OCH), 4.30 (6H, br s, OCH<sub>2</sub>), 2.45 (4H, br s, NCH<sub>2</sub>), 2.25 (12H, s, NCH<sub>3</sub>), 1.20 (9H, t, CCH<sub>3</sub>). <sup>13</sup>C-NMR (CDCl<sub>3</sub>): 75.2 (br, OCH), 69.3 (br, OCH<sub>2</sub>), 65.0 (br, NCH<sub>2</sub>), 45.7 (NCH<sub>3</sub>), 18.7 (br, CCH<sub>3</sub>).

**Synthesis of [Ti(O<sup>i</sup>Pr)<sub>2</sub>(bdmap)] (2).** [Ti(O<sup>i</sup>Pr)<sub>4</sub>] (1.83 g, 6.3 mmol) was dissolved in dry hexane (10 mL) and Hbdmap (0.92 g, 6.3 mmol) was added. After stirring overnight, the mixture was heated at 50 °C with stirring for 2 h. All volatiles were removed under vacuum, giving 2.02 g (87%) of a colourless clear oil. Analysis: Found (calc. for TiO<sub>4</sub>N<sub>2</sub>C<sub>16</sub>H<sub>38</sub>): C 49.9 (51.9); H 10.0 (10.3); N 7.7 (7.6)%. <sup>1</sup>H-NMR (CDCl<sub>3</sub>): 4.60 (3H, septet, CHO), 4.38 (1H, m, CHCH<sub>2</sub>), 2.47 (2H, m, NCH<sub>2</sub>), 2.33 (2H, m, NCH<sub>2</sub>), 2.28 (12H, s, NCH<sub>3</sub>), 1.20 (18H, d, CCH<sub>3</sub>). <sup>13</sup>C-NMR (CDCl<sub>3</sub>): 75.1 (OC of Pr<sup>i</sup>), 74.9 (OCH of bdmap), 64.8 (CH<sub>2</sub>N), 45.8 (NCH<sub>3</sub>), 25.5 (CCH<sub>3</sub>).

**Synthesis of [Ti(OEt)<sub>2</sub>(tdmap)] (3).** [Ti(OEt)<sub>4</sub>] (1.18 g, 5.2 mmol) was dissolved in dry hexane (10 mL) and Htdmap (1.05 g, 5.2 mmol) was added. After stirring overnight, the mixture was heated at 50 °C with stirring for 2 h. All volatiles were removed under vacuum, giving 1.95 g (98%) of a creamy solid. This was subsequently dissolved in dry hexane (5 mL) and placed in the freezer at –12 °C where white crystals appeared; these were found to be soft, diffracting poorly. Analysis: Found (calc. for TiO<sub>4</sub>N<sub>3</sub>C<sub>16</sub>H<sub>39</sub>): C 48.6 (49.9); H 10.0 (10.2); N 10.7 (10.9)%. <sup>1</sup>H-NMR (CDCl<sub>3</sub>): 4.30 (6H, br s, OCH<sub>2</sub>), 2.45 (6H, s, CH<sub>2</sub>N), 2.30 (12H, s, NCH<sub>3</sub>), 2.25 (6H, s, NCH<sub>3</sub>), 1.15 (9H, t, CCH<sub>3</sub>). <sup>13</sup>C-NMR (CDCl<sub>3</sub>): 84.0 (OC), 69.0 (OCH<sub>2</sub>), 66.2, 63.9 (2 : 1, NCH<sub>2</sub>), 47.9, 47.0 (2 : 1, NCH<sub>3</sub>), 18.9 (CCH<sub>3</sub>); minor signals also observed at 62.7, 44.6 ppm.

**Synthesis of [Ti(O<sup>i</sup>Pr)<sub>2</sub>(tdmap)] (4).** [Ti(O<sup>i</sup>Pr)<sub>4</sub>] (1.35 g, 4.6 mmol) was dissolved in dry hexane (10 mL) and Htdmap (0.94 g, 4.6 mmol) was added. After stirring overnight, the mixture was heated at 50 °C with stirring for 2 h. All volatiles were removed under vacuum, giving 1.87 g (95%) of a colourless clear oil. Analysis: Found (calc. for TiO<sub>4</sub>N<sub>3</sub>C<sub>19</sub>H<sub>45</sub>): C 49.4 (53.4); H 10.1 (10.6)%; N 8.9 (9.8)%. <sup>1</sup>H-NMR (CDCl<sub>3</sub>): 4.60 (3H, septet, OCH), 2.45 (6H, s, CH<sub>2</sub>N), 2.30 (18H, s, NCH<sub>3</sub>), 1.15 (18H, d, CCH<sub>3</sub>). <sup>13</sup>C-NMR (CDCl<sub>3</sub>): 83.9 (OC), 74.8 (OCH), 66.0 (CH<sub>2</sub>N), 47.5 (NCH<sub>3</sub>), 24.8 (CCH<sub>3</sub>).

**Synthesis of [Ti(OEt)<sub>2</sub>(bdmap)<sub>2</sub>] (5).** [Ti(OEt)<sub>4</sub>] (0.78 g, 3.4 mmol) was dissolved in dry hexane (10 mL) and Hbdmap (0.99 g, 6.8 mmol) was added. After stirring overnight, the mixture was heated at 50 °C with stirring for 2 h. All volatiles were removed under vacuum, giving 1.36 g (47%) of a colourless oil (**5**). Crystals of the hydrolysis product [(bdmap)<sub>2</sub>TiO<sub>2</sub>] (**7**) appeared on standing over a few days. (**5**): <sup>1</sup>H-NMR (CDCl<sub>3</sub>): 4.50 (2H, br s, OCH), 4.32 (4H, br s, OCH<sub>2</sub>), 2.45 (8H, br s, CH<sub>2</sub>N), 2.25 (24H, br s, NCH<sub>3</sub>), 1.15 (6H, br s, CCH<sub>3</sub>). <sup>13</sup>C-NMR (CDCl<sub>3</sub>): 77.5 (OCH), 69.1 (OCH<sub>2</sub>), 65.1, 64.8 (3:1, NCH<sub>2</sub>), 45.8 (NCH<sub>3</sub>), 18.7 (CCH<sub>3</sub>).

**Synthesis of [Ti(O<sup>i</sup>Pr)<sub>2</sub>(bdmap)<sub>2</sub>] (6).** [Ti(O<sup>i</sup>Pr)<sub>4</sub>] (1.07 g, 3.6 mmol) was dissolved in dry hexane (10 mL) and Hbdmap (1.03 g, 7.1 mmol) was added. After stirring overnight, the mixture was heated at 50 °C with stirring for 2 h. All volatiles were removed under vacuum, giving 1.52 g (94%) of a colourless clear oil. Analysis: Found (calc. for TiO<sub>4</sub>N<sub>4</sub>C<sub>20</sub>H<sub>48</sub>): C 49.1(52.7); H 10.0 (10.6%); N 12.0 (12.3%); <sup>1</sup>H-NMR (CDCl<sub>3</sub>): 4.60 (2H, m, CHO), 4.40 (2H, m, CHCH<sub>2</sub>), 2.25 (32H, overlapping m, NCH<sub>3</sub> and CH<sub>2</sub>N), 1.15 (12H, d, CCH<sub>3</sub>). <sup>13</sup>C-NMR (CDCl<sub>3</sub>): 77.8, 75.0 (CHO of OPr<sup>i</sup> and bdmap), 65.2, 64.9, 62.9 (*ca.* 1 : 2 : 1, CH<sub>2</sub>N), 45.8, 45.5, 44.9 (*ca.* 2 : 1 : 1, NCH<sub>3</sub>), 25.5 (CCH<sub>3</sub>).

**Reaction between [Ti(NMe<sub>2</sub>)<sub>2</sub>(bdmap)<sub>2</sub>] and [Zn(acac)<sub>2</sub>·2H<sub>2</sub>O].** [Ti(NMe<sub>2</sub>)<sub>4</sub>] (0.74 g, 3.3 mmol) was dissolved in dry hexane (10 mL) and Hbdmap (0.97 g, 6.6 mmol) was added. After stirring overnight, the mixture was heated at 50 °C with stirring for 2 h. All volatiles were removed under vacuum, giving 1.25 g (2.9 mmol) of a clear red oil. This was subsequently dissolved in dry hexane (10 mL) and [Zn(acac)<sub>2</sub>·2H<sub>2</sub>O] (0.43 g, 1.4 mmol) was added, giving a pale yellow solution. This was then placed in a freezer at -12 °C where colourless crystals containing a mixture of [(bdmap)<sub>2</sub>TiO<sub>2</sub>] (7) and Me<sub>2</sub>N(Me)C=C(H)C(O)Me (8) appeared.

**Reaction between [Ti(NMe<sub>2</sub>)<sub>2</sub>(tdmap)<sub>2</sub>] and [Zn(OAc)<sub>2</sub>·2H<sub>2</sub>O].** [Ti(NMe<sub>2</sub>)<sub>4</sub>] (0.67 g, 2.9 mmol) was dissolved in dry hexane (10 mL) and Htdmap (1.22 g, 6.0 mmol) was added. After that, the mixture was heated at 50 °C with stirring for 2 h. All volatiles were removed under vacuum, giving 1.49 g (2.75 mmol) of a clear red oil. This was subsequently dissolved in dry hexane (10 mL), [Zn(OAc)<sub>2</sub>·2H<sub>2</sub>O] (0.30 g, 1.36 mmol) added and the solution warmed at 50 °C until [Zn(OAc)<sub>2</sub>·2H<sub>2</sub>O] disappeared, leaving a colourless solution. This was then placed in the freezer at -12 °C where colourless crystals appeared, containing a mixture of [(tdmap)<sub>2</sub>TiO<sub>2</sub>] (9) and [Zn(OAc)<sub>2</sub>(tdmap)<sub>2</sub>] (10).

**Reaction of [Ti(OPr<sup>i</sup>)<sub>4</sub>] and [Sn(dmae)<sub>2</sub>].** [Ti(OPr<sup>i</sup>)<sub>4</sub>] (0.76 mL, 2.59 mmol) was added to a Schlenk containing [Sn(dmae)<sub>2</sub>] (1.00 g, 2.59 mmol); prepared directly from the addition of two equivalents of Hdmae to Sn[N(SiMe<sub>3</sub>)<sub>2</sub>]<sub>2</sub> yielding a white precipitate, which was allowed to stir overnight. The precipitate was washed with hexane and a yellow solution of hexane-soluble material separated from an insoluble white residue by cannula. The yellow solution was placed in the freezer at -12 °C, yielding crystals after one month which were determined to be [Ti<sub>4</sub>O<sub>4</sub>(OPr<sup>i</sup>)<sub>4</sub>(dmae)<sub>4</sub>] by X-ray crystallography. Recrystallisation of the hexane-insoluble white powder from dry tetrahydrofuran at -12 °C afforded crystals of the known compound [Sn<sub>6</sub>O<sub>4</sub>(OPr<sup>i</sup>)<sub>4</sub>], characterised by comparison of crystallographic cell parameters with those available in the literature.<sup>39</sup>

### Crystal structures†

Experimental details relating to the single-crystal X-ray crystallographic studies are summarised in Table 1. For all structures, data were collected on a Nonius Kappa CCD diffractometer at 150(2) K using Mo-Kα radiation (λ = 0.71073 Å). For 1 and 7 a symmetry-related (multi-scan) absorption correction was employed. Structure solution followed by full-matrix least squares refinement was performed using the WinGX-1.70 suite of programs throughout.<sup>40</sup>

Table 1 Crystallographic data for 1, 7, 9, 10 and 11

	(1)	(7)	(9)	(10)	(11)
Empirical formula	C <sub>52</sub> H <sub>64</sub> N <sub>4</sub> O <sub>8</sub> Ti <sub>4</sub>	C <sub>52</sub> H <sub>64</sub> N <sub>4</sub> O <sub>8</sub> Ti <sub>4</sub>	C <sub>50</sub> H <sub>60</sub> N <sub>4</sub> O <sub>8</sub> Ti <sub>4</sub>	C <sub>52</sub> H <sub>64</sub> N <sub>4</sub> O <sub>8</sub> Zn <sub>2</sub>	C <sub>52</sub> H <sub>64</sub> N <sub>4</sub> O <sub>8</sub> Ti <sub>4</sub>
Formula weight	656.61	708.70	980.17	653.47	844.46
Crystal system	Triclinic	Monoclinic	Tetragonal	Monoclinic	Monoclinic
Space group	<i>P</i> 1	<i>C</i> 2/c	<i>I</i> 4 <sub>1</sub> /a	<i>P</i> 2 <sub>1</sub> /c	<i>P</i> 2 <sub>1</sub> /c
<i>a</i> /Å	9.131(02)	13.077(03)	42.871(06)	9.6443(3)	9.8514(3)
<i>b</i> /Å	12.640(03)	15.9297(4)	42.871(06)	16.8905(6)	22.0293(8)
<i>c</i> /Å	17.122(06)	19.8665(6)	12.3339(2)	10.4920(4)	10.8310(3)
<i>a</i> /°	69.903(1)	108.460(1)	90	90	90
<i>b</i> /°	76.840(1)	81.600(2)	90	111.741(2)	117.830(2)
<i>c</i> /°	81.600(2)	3924.24(18)	2.2668(96)	90	2078.67(11)
Volume/Å <sup>3</sup>	1802.3(09)	4	16	2	2
<i>ρ</i> (M <sub>o</sub> -K $\alpha$ )/mm <sup>-1</sup>	0.488	0.452	0.332	1.555	0.796
Crystal size/mm	0.30 × 0.20 × 0.05	0.30 × 0.30 × 0.25	0.30 × 0.18 × 0.15	0.20 × 0.30 × 0.30	0.20 × 0.20 × 0.08
Reflections collected	23 405	24 881	72 564	12 765	22 055
Independent reflections	7056 [R(int) = 0.0595]	4448 [R(int) = 0.0483]	12 742 [R(int) = 0.0839]	3482 [R(int) = 0.0461]	3593 [R(int) = 0.1501]
Reflections observed (> 2 $\sigma$ )	5058	3635	8011	2600	2710
Data completeness	0.976	0.986	0.985	0.956	0.982
Max., min. transmission	0.97, 0.87	0.96, 0.90	0.9518, 0.9069	0.6527, 0.6527	1.504, -0.637
Data/restraints/parameters	7052/0/410	4448/0/237	12 742/5/619	3482/0/179	3593/1/240
Goodness-of-fit on <i>F</i> <sup>2</sup>	1.055	1.092	1.021	1.035	1.097
Final <i>R</i> <sub>1</sub> <sup>a</sup> , <i>wR</i> <sub>2</sub> <sup>b</sup> [ <i>I</i> > 2 $\sigma$ ( <i>I</i> )]	0.0493, 0.1180	0.0441, 0.1059	0.0535, 0.1152	0.0332, 0.0691	0.0844, 0.2169
Final <i>R</i> <sub>1</sub> <sup>a</sup> , <i>wR</i> <sub>2</sub> <sup>b</sup> (all data)	0.0799, 0.1342	0.0582, 0.1146	0.1065, 0.1400	0.0587, 0.0755	0.1111, 0.2420
Extinction coefficient <sup>c</sup>	—	—	—	—	0.019(5)
Largest diff. peak and hole/e Å <sup>-3</sup>	0.948, -0.481	0.430, -0.351	0.273, -0.370	0.379, -0.354	1.746, -0.794

$$^a R_1 = \sum ||F_o| - |F_c|| / \sum |F_o|, ^b wR_2 = \{ \sum [w(F_o^2 - F_c^2)]^2 / \sum [w(F_o^2) + 2p] \}^{1/2}, ^c dF_c^* = kF_c^* = hF_c^* + 0.001 F_c^* \lambda^2 / \sin(2\theta)]^{1/4}$$



Compound **1** forms two crystallographically independent dimers with one molecule [based on Ti(1A)] showing some disorder (65 : 35) in two of the ethoxy groups [based on O(2A) and O(3A)]. Due to similar metrical data for the two independent dimers, only data for the ordered unit is discussed. In **7**, one pendant NMe<sub>2</sub> group [N(4), C(13) and C(14)] is disordered over two sites in 65 : 35 ratio. Compound **9** co-crystallises with a molecule of hexane, which was found to be disordered about a crystallographic  $\bar{4}$  axis with 50% site occupancy. Data collection on compound **11** resulted in a weak data set. One of the isopropyl groups binding to Ti(1) and based on C(21) was found to be disordered in the ratio 50 : 50, and the bond between C21 and C23 within this group had to be restrained.

#### Thermal decomposition of [Ti(OEt)<sub>3</sub>(bdmap)]

The experiment follows the procedure outlined by Gedanken.<sup>41</sup> A 0.5 g sample of [Ti(OEt)<sub>3</sub>(bdmap)] (**1**) was introduced into the Swagelok cell at room temperature in a nitrogen-filled glove box. The filled cell was closed tightly with the two plugs and placed inside an iron pipe in the middle of a tube furnace. The temperature was raised at a rate of 10 °C per minute to 700 °C and held at that temperature for 1 h. The Swagelok fitting was gradually cooled (1.5 °C per minute) to room temperature (25 °C). 0.12 g of a dark black powder was collected.

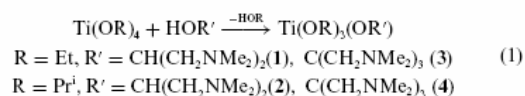
#### CVD study

Films were deposited on a 76 × 26 × 1.0 mm microscope slide using a cold wall AACVD reactor which has been described elsewhere.<sup>42</sup> [Ti(OEt)<sub>3</sub>(bdmap)] (**1**) (ca. 0.2 g) was dissolved in dry toluene (20 mL) and an aerosol generated using a domestic household humidifier. The aerosol was transported to the reactor using argon carrier gas (1.2 L min<sup>-1</sup>). The glass substrate temperature was held at 440 °C. The run time was 60 min.

## Results and discussion

### Synthesis

New titanium alkoxides [Ti(OR)<sub>3</sub>(OR')] (R = Et, Pr<sup>i</sup>; R' = bdmap, tdmmap) have been synthesised by heating Ti(OR)<sub>4</sub> and Hbdmap/Htdmap in hexane:



Both ethoxides (**1,3**) are white solids, though **1** remains sticky after isolation from the recrystallisation from the solvent (CH<sub>2</sub>Cl<sub>2</sub>) while **3** is very soft; the two isopropoxide analogues (**2,4**) are liquids. Attempts to purify **2,4** (and other liquid products described in this paper) by vacuum distillation resulted in decomposition, the NMR of the distillate containing only signals due to the OPr<sup>i</sup> groups. The formation of a bond between titanium and the amino alcohol is evidenced by the large downfield <sup>13</sup>C NMR shift of the resonance due to the O–C nucleus with respect to the parent alcohol (bdmap: ca. 64 to 75 ppm; tdmmap: ca. 74 to 84 ppm).

The room temperature <sup>1</sup>H and <sup>13</sup>C spectra of **1** are simple and show that the dimeric structure of the compound (Fig. 1)

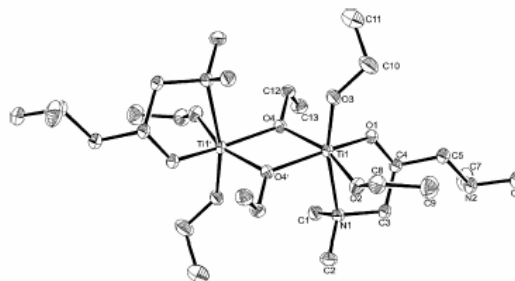
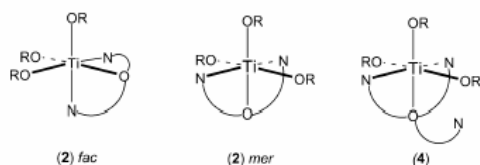


Fig. 1 The asymmetric unit of **1** showing the labelling scheme used; thermal ellipsoids are at the 30% probability level. Only one of two essentially identical molecules which make up the asymmetric unit is shown for clarity and discussed in the text. Selected metrical data: Ti(1)–O(1) 1.8641(19), Ti(1)–O(2) 1.839(2), Ti(1)–O(3) 1.8122(18), Ti(1)–O(4) 2.0194(18), Ti(1)–O(4') 2.0793(19), Ti(1)–N(1) 2.432(2) Å; O(1)–Ti(1)–O(2) 102.56(9), O(1)–Ti(1)–O(3) 92.42(8), O(1)–Ti(1)–O(4) 157.96(9), O(1)–Ti(1)–O(4') 92.13(8), O(1)–Ti(1)–N(1) 74.38(8), O(2)–Ti(1)–O(3) 97.19(9), O(2)–Ti(1)–O(4) 91.53(8), O(2)–Ti(1)–O(4') 161.68(8), O(2)–Ti(1)–N(1) 80.50(8), O(3)–Ti(1)–O(4) 102.65(8), O(3)–Ti(1)–O(4') 93.01(8), O(3)–Ti(1)–N(1) 165.60(8), O(4)–Ti(1)–O(4') 71.35(8), O(4)–Ti(1)–N(1) 91.64(7), N(1)–Ti(1)–O(4') 93.21(7)°. Symmetry operation: 2 – x, 1 – y, –z.

is fluxional under these conditions. The <sup>1</sup>H NMR has a broad singlet for the OCH<sub>2</sub> ethoxy protons overlapping with a weaker, also broad, singlet due to CHO of the bdmap, but only one sharp singlet for the two distinct NMe<sub>2</sub> groups which overlaps a broad singlet from NCH<sub>2</sub> of the amino alcohol. The OCH<sub>2</sub>CH<sub>3</sub> appear as a sharp triplet, though with some evidence of signal splitting. Similarly, the <sup>13</sup>C NMR shows single, albeit broadened, signals for each type of carbon with no resolution of the distinct ethoxide groups present in the dimer, nor any between chelated and free arms of the bdmap ligand. On cooling to –50 °C, however, the spectra become more complex, with multiple overlapping resonances for both OCH<sub>2</sub>CH<sub>3</sub> protons, the CH protons of the central part of the bdmap, along with only minor splitting of the intense NMe<sub>2</sub> singlet. The low temperature <sup>13</sup>C NMR contains over 20 distinct resonances, which implies that the crystallographic symmetry within the dimer is lost in solution.

Similar, though less definitive, comments can be made about the tdmmap analogue (**3**). The OCH<sub>2</sub> signal of the ethoxy groups is again broad and there is some indication of splitting in the associated CH<sub>3</sub> triplet, though the remaining <sup>1</sup>H NMR signals are sharp. The resonance due to the NMe<sub>2</sub> groups is split into two, and while accurate integration of the separate signals is precluded by their overlapping nature, it is approximately in a 2 : 1 ratio; there is, however, no apparent splitting of the CH<sub>2</sub>N resonance. The corresponding <sup>13</sup>C spectrum has broad signals for both carbons of the ethoxy groups, and two major signals for each of the N(CH<sub>3</sub>)<sub>2</sub> and CH<sub>2</sub>N carbons in a ca. 2 : 1 ratio, but the presence of smaller third resonances in each case suggest the presence of a possible second species. It is likely that the structure of **3** resembles that of **1**; the poorly diffracting nature of the crystals of **3** is consistent with four non-coordinated CH<sub>2</sub>NMe<sub>2</sub> groups in the dimer, which are probably disordered in the lattice given our experience with similar metal amino alcohols.

In contrast, the room temperature  $^1\text{H}$  NMR of **2**, an oil for which no definitive structural data are available, is both sharp and simple. Clear, defined multiplets are visible for both  $\text{OCHMe}_2$  and  $\text{OCH}(\text{CH}_2\text{NMe}_2)$  at 4.60 (septet) and 4.38 ppm, respectively. There is a single sharp doublet for the  $\text{OCH}(\text{CH}_3)_2$  protons (1.20 ppm) and a further intense singlet at 2.28 ppm for the  $\text{N}(\text{CH}_3)_2$  group, partially overlapping with one of two multiplets (2.47, 2.33 ppm) due to the  $\text{CH}_2\text{N}$  part of the bdmapp. These multiplets arise when both arms of the bdmapp chelate a metal, making the ligand rigid and the two  $\text{CH}_2$  hydrogens non-equivalent. The  $^{13}\text{C}$  NMR spectrum is equally simple, with only five sharp singlets corresponding to the five unique carbon environments in the molecule. This pattern of data, taken in contrast to that of **1**, is suggestive of a monomeric, rather than dimeric structure, in which both donor arms of the bdmapp ligand chelate to the metal, assuming the common octahedral coordination preferred by titanium is maintained. In addition, the data are in keeping with the more symmetrical *mer* isomer, which, for example, allows all the  $\text{NCH}_3$  groups to become equivalent.



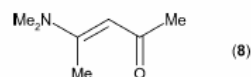
For  $[\text{Ti}(\text{OPr}^i)_2(\text{tdmap})]$  (**4**), sharp signals are seen for both nuclei in both the room temperature  $^1\text{H}$  and  $^{13}\text{C}$  NMR spectra and indicate only one  $\text{OPr}^i$ ,  $\text{CH}_2\text{N}$  and  $\text{NMe}_2$  environment, respectively. Since the coordination number at the metal is unlikely to go beyond six, we suggest that a monomeric structure similar to **2** exists, in which the isopropoxy groups are static but that some rapid fluxionality of the  $\text{CH}_2\text{NMe}_2$  groups, with two coordinated and one free, takes place.

Attempts to introduce additional chelating amino-alkoxide groups have only been partially successful. When the reaction described by eqn (1) was carried out with increasing amounts of amino alcohol, further substitution of the monodentate alkoxide was evident, though  $^1\text{H}$  NMR integrals suggested that the desired substitution was incomplete, a situation which became progressively more evident as the reaction stoichiometry increased in favour of the chelating ligand. Both  $[\text{Ti}(\text{OEt})_2(\text{bdmap})_2]$  (**5**) and  $[\text{Ti}(\text{OPr}^i)_2(\text{bdmap})_2]$  (**6**) are essentially pure by NMR, though both are liquids which could not be obtained with analytical purity. The NMR data for these two species seem to follow the same trends as compounds **1–4**: the ethoxy derivative shows broad signals for all protons in the  $^1\text{H}$  NMR, and, while the  $^{13}\text{C}$  NMR is generally sharper, the only clear non-equivalence is in the  $\text{CH}_2\text{N}$  groups, where two signals (*ca.* 3 : 1 relative intensity) are apparent. The  $^{13}\text{C}$  NMR signals due to the  $\text{OCH}$  fragments of bdmapp overlap with the signals from the solvent (all *ca.* 75 ppm) and preclude detailed

comment on this region of the spectrum, though some evidence for signal splitting also occurs here. The structural implications of this data remain conjecture. A monomeric, presumably six-coordinated species (*e.g.* **6a**), would require two of the four  $\text{NMe}_2$  groups to be pendent, inconsistent with both the *ca.* 3 : 1  $\text{CH}_2\text{N}$  moieties and the fluxional nature of the compound suggested by the broad  $^1\text{H}$  NMR signals. Both dimeric arrangements **5a** and **5b**, however, incorporate a 3 : 1 ratio of pendant to chelating  $\text{NMe}_2$  groups, however, based on the known structure of **1** and the apparent fluxional nature of the OEt groups, **5a** would appear the most likely.

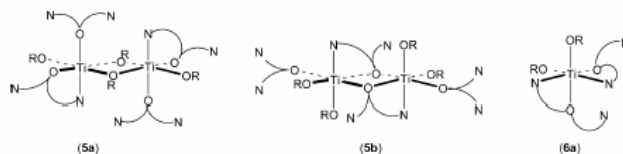
For **6**, the NMR signals are uniformly sharp but a difference in the two isopropoxy environments is evident from overlapping septets due to  $\text{CHO}$ , while splitting of both the  $\text{CH}_2\text{N}$  and  $\text{NMe}_2$  signals (*ca.* 2 : 1 : 1 ratio from the  $^{13}\text{C}$  NMR) is also clear. In comparison with **2**, a monomeric complex with two terminal (but marginally different)  $\text{OPr}^i$  groups and two chelating bdmapp ligands (each with one free  $\text{NMe}_2$  group) in an isomeric form which renders the two coordinated  $\text{Me}_2\text{N} \rightarrow \text{Ti}$  interactions non-equivalent *e.g.* **6a**, would rationalise the NMR data.

A small number of crystals of the hydrolysis product  $[(\text{bdmap})_2\text{TiO}]_2$  (**7**) appeared within the oil **5** on standing over a period of several days. We have targeted a more rational synthesis of **7** by reacting  $[\text{Ti}(\text{NMe}_2)_2(\text{bdmap})_2]$  (generated *in situ* from reaction of  $[\text{Ti}(\text{NMe}_2)_4]$  and two equivalents of Hbdmap) with half an equivalent of  $[\text{Zn}(\text{acac})_2 \cdot 2\text{H}_2\text{O}]$ , in the hope that hydrolysis of the  $\text{Ti}(\text{NMe}_2)_2$  unit would accrue from reaction with the water of crystallisation and, additionally, the coordinatively unsaturated anhydrous  $[\text{Zn}(\text{acac})_2]$  would coordinate to the amine groups of the bdmapp which are not complexed to titanium. In practice, only the first of these goals, the hydrolysis, was achieved. However, the reaction is complicated by a secondary reaction between the liberated amine ( $\text{HNMe}_2$ ) and the coordinated acac ligand, generating the condensation product (**8**), which was characterised crystallographically. $\S$



When a similar approach was attempted by reacting  $[\text{Ti}(\text{NMe}_2)_2(\text{tdmap})_2]$  with  $[\text{Zn}(\text{OAc})_2 \cdot 2\text{H}_2\text{O}]$  using the same reaction sequence and stoichiometries as above, crystals of both the desired hydrolysis product  $[(\text{tdmap})_2\text{TiO}]_2$  (**9**) and those of a secondary product resulting from ligand exchange,  $[\text{Zn}(\text{OAc})(\text{tdmap})_2]$  (**10**) were found in the product mixture. We have been unable to separate this mixture into analytically pure components, though their nature has been unambiguously determined by X-ray crystallography. Furthermore, we have also

$\S$  Crystal data:  $\text{C}_7\text{H}_{13}\text{NO}$ ,  $M_r$  127.18, monoclinic,  $P2_1/n$ ,  $a = 6.3720(2)$ ,  $b = 13.8350(6)$ ,  $c = 8.4500(4)$  Å,  $\beta = 100.111(1)^\circ$ ,  $V = 733.35(5)$  Å $^3$ ,  $Z = 4$ , final  $R_1$ ,  $wR_2$  indices [ $I > 2\sigma(I)$ ] 0.0675, 0.1751, [all data] 0.1082, 0.1985.



failed to isolate [(tdmap)(OAc)TiO]<sub>2</sub> which we assume is the second product resulting as a consequence of ligand exchange. Interestingly, when Hbdmap is allowed to react with anhydrous [Zn(OAc)<sub>2</sub>] directly, tetrameric [Zn<sub>4</sub>(bdmap)<sub>2</sub>(OAc)<sub>6</sub>] results.<sup>43</sup>

### Crystallography

The structure of **1** is shown in Fig. 1 and is a centrosymmetric dimer containing  $\mu$ -OEt bridges. Each titanium is six-coordinated with a TiO<sub>5</sub>N coordination sphere. The two terminal ethoxy groups are most tightly bound [Ti(1)–O(2) 1.839(2), Ti(1)–O(3) 1.8122(18) Å], followed by the amino-alkoxide [Ti(1)–O(1) 1.866(2) Å] while the bridging interactions are, unsurprisingly, weaker [Ti(1)–O(4) 2.0194(18), Ti(1)–O(4') 2.0793(19) Å]. Coordination is completed by chelation from one terminal amine [Ti(1)–N(1) 2.432(2) Å] while the other amine function based on N(2) remains pendant. The Ti–N bond seems typical of these species (see below) and allows slightly stronger bonding from the ethoxide based on O(3) to which it is *trans*, in comparison with the other terminal alkoxide [O(2)] despite the latter being *trans* to the bridging  $\mu$ -OEt moiety.

Hydrolysis of **1** affords the  $\mu$ -O dimer [(bdmap)TiO]<sub>2</sub> (**7**) (Fig. 2) generated by a crystallographically imposed two-fold axis running through the centre of the Ti<sub>2</sub>O<sub>2</sub> ring. Each titanium retains its octahedral coordination, but this is now made up of two chelating amino alcohols in addition to the two bridging groups. The overall coordination is TiO<sub>4</sub>N<sub>4</sub>, in a *cis, cis, trans* arrangement of  $\mu$ -O,

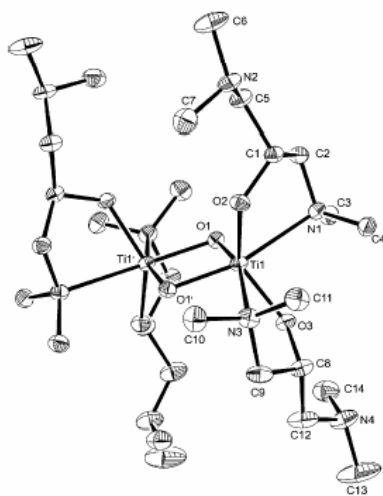


**Fig. 2** The asymmetric unit of **7** showing the labelling scheme used; thermal ellipsoids are at the 30% probability level. The NMe<sub>2</sub> group based on N(4) is disordered over two sites (65 : 35); only the major component of the disorder is shown for clarity. Selected metrical data: Ti(1)–O(1) 1.8445(13), Ti(1)–O(1') 1.8474(14), Ti(1)–O(2) 1.8774(14), Ti(1)–O(3) 1.8826(14), Ti(1)–N(1) 2.3962(18), Ti(1)–N(3) 2.4529(18) Å; O(1)–Ti(1)–O(1') 82.19(6), O(1)–Ti(1)–O(2) 109.35(6), O(1)–Ti(1)–O(3) 104.61(6), O(1)–Ti(1)–N(1) 81.70(6), O(1)–Ti(1)–N(3) 162.97(6), O(1')–Ti(1)–O(2) 103.88(6), O(1')–Ti(1)–O(3) 109.15(6), O(1')–Ti(1)–N(1) 162.18(6), O(1')–Ti(1)–N(3) 82.35(6), O(2)–Ti(1)–O(3) 135.08(7), O(2)–Ti(1)–N(1) 74.53(6), O(2)–Ti(1)–N(3) 81.36(6), O(3)–Ti(1)–N(1) 82.36(6), O(3)–Ti(1)–N(3) 73.94(6), N(1)–Ti(1)–N(3) 114.50(6)°. Symmetry operation: 1 – x, y, 3/2 – z.

coordinated amines and alkoxides centres, respectively. The Ti<sub>2</sub>O<sub>2</sub> core is more tightly bound than in **1** [Ti(1)–O(1) 1.8445(13), Ti(1)–O(1') 1.8474(14) Å], while the two amino-alkoxides show similar bond strengths [Ti(1)–O(2) 1.8777(14), Ti(1)–O(3) 1.8826(14) Å]. The two coordinated amines [Ti(1)–N(1) 2.3962(18), Ti(1)–N(3) 2.4529(18) Å], which are *trans* to the two  $\mu$ -O groups, straddle the observed Ti–N bond length in **1** [2.432(2) Å], which is *trans* to a terminal OEt unit. As with **1**, two amine groups (one per bdmap ligand) remain uncoordinated to the metal.

[(tdmap)<sub>2</sub>TiO]<sub>2</sub> (**9**) (Fig. 3) has a similar dimeric structure to **7** though it lacks the crystallographic symmetry of the latter. In all other respects—the TiO<sub>4</sub>N<sub>2</sub> coordination sphere and the relative disposition of ligating atoms around the metal centre—**9** is isostructural with **7**. The Ti<sub>2</sub>O<sub>2</sub> core is marginally less robust than in **7** [Ti–O: 1.8507(17)–1.8601(17) Å], and, like **7**, the Ti–O bonds to the amino alcohol ligands are weaker than those in the core [1.8856(17)–1.8936(17) Å]. In contrast, the coordinated amines bind more tightly [2.374(2)–2.410(2) Å], while two such groups per tdmap ligand remain free.

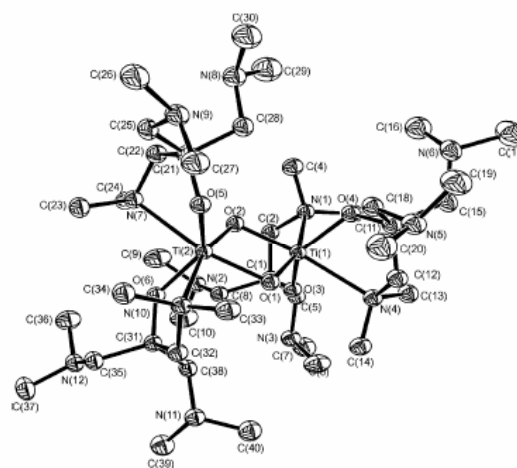


**Fig. 3** The asymmetric unit of **9** showing the labelling scheme used; thermal ellipsoids are at the 30% probability level. The molecule of hexane which co-crystallises has been omitted for clarity. Selected metrical data: Ti(1)–O(1) 1.8601(17), Ti(1)–O(2) 1.8553(17), Ti(1)–O(3) 1.8898(17), Ti(1)–O(4) 1.8936(17), Ti(1)–N(1) 2.390(2), Ti(1)–N(4) 2.374(2), Ti(2)–O(1) 1.8586(17), Ti(2)–O(2) 1.8507(17), Ti(2)–O(5) 1.8912(17), Ti(2)–O(6) 1.8856(17), Ti(2)–N(7) 2.410(2), Ti(2)–N(10) 2.386(2) Å; O(1)–Ti(1)–O(2) 82.08(7), O(1)–Ti(1)–O(3) 108.73(7), O(1)–Ti(1)–O(4) 104.53(8), O(1)–Ti(1)–N(1) 163.11(7), O(1)–Ti(1)–N(4) 83.08(7), O(2)–Ti(1)–O(3) 105.15(8), O(2)–Ti(1)–O(4) 107.91(8), O(2)–Ti(1)–N(1) 81.25(7), O(2)–Ti(1)–N(4) 164.96(8), O(3)–Ti(1)–O(4) 135.56(8), O(3)–Ti(1)–N(1) 73.31(7), O(3)–Ti(1)–N(4) 81.94(7), O(4)–Ti(1)–N(1) 83.22(7), O(4)–Ti(1)–N(4) 73.63(7), N(1)–Ti(1)–N(4) 113.68(7), O(1)–Ti(2)–O(2) 82.24(7), O(1)–Ti(2)–O(5) 109.48(7), O(1)–Ti(2)–O(6) 104.55(7), O(1)–Ti(2)–N(7) 162.62(8), O(1)–Ti(2)–N(10) 82.67(7), O(2)–Ti(2)–O(5) 105.50(7), O(2)–Ti(2)–O(6) 108.42(8), O(2)–Ti(2)–N(7) 80.54(7), O(2)–Ti(2)–N(10) 164.76(7), O(5)–Ti(2)–O(6) 134.39(8), O(5)–Ti(2)–N(7) 73.25(7), O(5)–Ti(2)–N(10) 81.63(7), O(6)–Ti(2)–N(7) 83.17(7), O(6)–Ti(2)–N(10) 73.47(7), N(7)–Ti(2)–N(10) 114.62(7)°.

The heteroleptic [Zn(OAc)(tdmap)] (**10**) is also dimeric (*via* an inversion centre) based around a central M<sub>2</sub>O<sub>2</sub> unit, though the

Zn–O bonds are significantly weaker [Zn–O(1) 2.0496(14), Zn–O(1') 2.0294(14) Å] (Fig. 4). Each zinc is octahedral with a  $\text{ZnO}_4\text{N}_2$  coordination sphere, in which the tdmmap ligand is tridentate and acts in concert with a chelating, bidentate carboxylate. Specifically, the tdmmap bridges both metals through  $\mu$ -O centres while two of the available donors each bind one of the two metals [Zn–N(1) 2.1898(17), Zn–N(2') 2.2593(18) Å]. In this respect, the tdmmap acts essentially as a bdmmap ligand by leaving one amine [N(3)] uncoordinated, and mimics the type of bridging behaviour that is often seen in bdmmap complexes, for example the related  $[\text{Zn}_4(\text{bdmap})_2(\text{OAc})_6]$  for which two isomers have been isolated.<sup>43</sup> The acetate group in **10** chelates the zinc in an anisobidentate manner [Zn–O(2) 2.0409(15), Zn–O(3) 2.6119(17) Å].

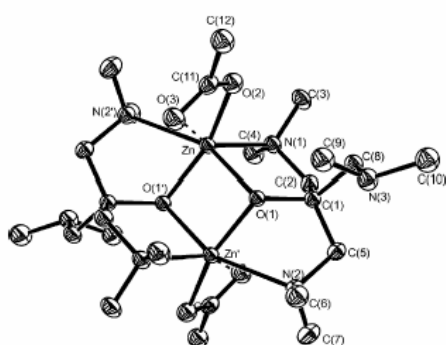


**Fig. 4** The asymmetric unit of **10** showing the labelling scheme used; thermal ellipsoids are at the 30% probability level. Selected metrical data: Zn–O(1) 2.0496(14), Zn–O(1') 2.0294(14), Zn–O(2) 2.0409(15), Zn–O(3) 2.6119(17), Zn–N(1) 2.1898(17), Zn–N(2') 2.2593(18) Å; O(1)–Zn–O(1') 83.00(6), O(1)–Zn–O(2) 102.23(6), O(1)–Zn–O(3) 87.34(5), O(1)–Zn–N(1) 83.10(6), O(1)–Zn–N(2') 153.34(6), O(1')–Zn–O(2) 162.12(6), O(1')–Zn–O(3) 108.63(5), O(1')–Zn–N(1) 102.25(6), O(1')–Zn–N(2') 75.79(6), O(2)–Zn–N(1) 95.39(6), O(2)–Zn–N(2') 93.70(6), O(3)–Zn–N(1) 146.24(6), O(3)–Zn–N(2') 84.37(6), N(1)–Zn–N(2') 116.84(7)°. Symmetry operation:  $-x, -y, -z$ .

We also include in this ranging discussion of Ti-aminoalcoholates the structure of  $[\text{Ti}_4(\text{O})_4(\text{OPr}^i)_4(\text{dmae})_4]$  (**11**), obtained along with  $[\text{Sn}_6(\text{O})_4(\text{OPr}^i)_4]$  from an aged sample of a  $[\text{Ti}(\text{OPr}^i)_4]/[\text{Sn}(\text{dmae})_2]$  mixture. Presumably, the first step in this reaction is also ligand exchange to generate  $[\text{Ti}(\text{OPr}^i)_3(\text{dmae})]$  and  $[\text{Sn}(\text{dmae})(\text{OPr}^i)]$ , followed by hydrolysis to generate the two oxoclusters;  $[\text{Sn}_6(\text{O})_4(\text{OPr}^i)_4]$  was identified by comparison of its crystal data with that reported previously.<sup>39</sup> Compound **11** is also of interest for comparison with  $[\text{Ti}_4(\text{O})_4(\text{dmae})_8]$  previously prepared and structurally characterised by Johnson.<sup>35</sup> It is interesting to contrast the different outcomes in terms of molecular nuclearity of the hydrolysis products from  $[(\text{bdmap})_2\text{TiX}_2]$  and  $[(\text{tdmap})_2\text{TiX}_2]$  ( $X = \text{NMe}_2, \text{OEt}$ ), namely dimeric **7** and **9**, with the tetrameric **11** obtained by hydrolysis of  $[\text{Ti}(\text{OPr}^i)_3(\text{dmae})]$  containing the purely bidentate dmae ligand.

Compound **11**, which, like **10** is based about a crystallographic inversion centre, is isostructural with  $[\text{Ti}_4(\text{O})_4(\text{dmae})_8]$  but in which four monodentate dmae ligands have been replaced by analogous  $\text{OPr}^i$  groups (Fig. 5). There are two distinct metal sites within the cluster, and although both have  $\text{TiO}_5\text{N}$  coordination spheres these are arrived at in different ways. Ti(1) bonds to two  $\mu_2$ -O, a

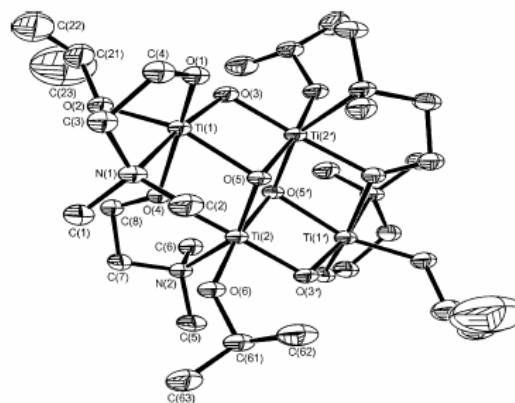


**Fig. 5** The asymmetric unit of **11** showing the labelling scheme used; thermal ellipsoids are at the 40% probability level. The isopropyl group based on C(21) is disordered over two sites with only one component of the disorder depicted for clarity. Symmetry operation:  $1 - x, -y, -z$ .

terminal  $\text{OPr}^i$ , and both a  $\mu_2$ -O and an O,N-chelating dmae ligand. In contrast, Ti(2) at the core of the cluster bonds to two  $\mu_3$ -O and one  $\mu_2$ -O, a terminal  $\text{OPr}^i$ , and a  $\mu_2$ -O of a dmae ligand. Overall, the structure can be considered as two facially-fused cubes each with a diametrically opposed vertex missing.

Only broad comments can be made about the spread of the Ti–O bonds in **11** (Table 2), given the quality of the data. The bridging Ti–O bonds to the  $\mu_3$ -O and  $\mu_2$ -O each span distinct bond lengths: the  $\mu_3$ -O has one short [Ti(2)–O(5) 1.863(4) Å] and two long [Ti(1)–O(5) 2.076(4), Ti(2')–O(5) 2.066(4) Å] interactions, while the  $\mu_2$ -O has one of each [Ti(1)–O(3) 1.799(4); Ti(2')–O(3) 1.883(4) Å]. As a result, each  $\text{Ti}_2\text{O}_2$  involving only  $\mu$ -O bridges at the core of the structure has two short and two long interactions. The terminal Ti– $\text{OPr}^i$  bonds are all consistent and of similar strength to the stronger Ti–O( $\mu$ ) (*ca.* 1.85 Å), while the  $\mu_2$ -O involving the bridging dmae ligands are weaker than Ti–O( $\mu_2$ ) but similar to

**Table 2** Ti–O and Ti–N bond lengths (Å) for **11**

Ti– $\mu_3$ -O		Ti– $\mu_2$ -O	
Ti(1)–O(5)	2.076(4)	Ti(1)–O(3)	1.799(4)
Ti(2)–O(5)	1.863(4)	Ti(2')–O(3)	1.883(4)
Ti(2')–O(5)	2.066(4)		
Ti– $\mu_2$ -O (dmae)		Ti–O (chelating dmae)	
Ti(1)–O(4)	2.039(4)	Ti(1)–O(1)	1.877(5)
Ti(2)–O(4)	2.019(4)		
Ti– $\text{OPr}^i$			
Ti(1)–O(2)	1.855(4)		
Ti(2)–O(6)	1.834(4)		
Ti–N ( $\mu$ -dmae)		Ti–N (chelating-dmae)	
Ti(2)–N(2)	2.292(6)	Ti(1)–N(1)	2.372(5)

the weaker Ti–O( $\mu_3$ ) (ca. 2.00 Å). Ti–O bonds to the chelating dmae groups are stronger than their bridging counterparts, while the Ti–N interactions are all ca. 2.3 Å, irrespective of whether the dmae ligand is bridging or chelating in nature. The two dmae ligands differ, both in terms of bridging vs. chelating, but also in as much as the chelating ligand has a strong Ti–O and a weaker Ti–N interaction [Ti(1)–O(1) 1.877(5); Ti(1)–N(1) 2.372(5) Å] while the bridging dmae bonds to titanium more symmetrically [Ti(2)–O(4) 2.019(4), Ti(2)–N(2) 2.292(6) Å].

#### Thermal decomposition of [Ti(OEt)<sub>2</sub>(bdmap)]<sub>2</sub>

Compound **1** has been thermally decomposed at 700 °C in a sealed steel ampoule, a technique coined RAPET (Reaction under Autogenerated Pressure at Elevated Temperatures) and first described by Gedanken.<sup>41</sup> In contrast to CVD where the experimental arrangement allows all the residual carbon to be eliminated thermally, under RAPET conditions this is not the case. In addition, the autogenerated pressure which accrues during decomposition also facilitates the formation of core-shell nanoparticles of different types e.g. carbon coated V<sub>2</sub>O<sub>5</sub><sup>41,44</sup> or MoO<sub>3</sub>,<sup>45</sup> silicon coated carbon spheres,<sup>41</sup> or carbon sausages with *in situ* WO<sub>3</sub>.<sup>46</sup>

In the RAPET of **1** some carbon is lost (presumably as hydrocarbons) as evidenced by a pressure release on opening the apparatus, though considerable amounts of organic matter, but particularly carbon, are still present in the final black residue (C 32.7%, H 0.82%, N 2.32%). This represents approximately two-thirds retention of carbon from **1** (C 47.5%).

Powder XRD of the black residue (Fig. 6) shows the only crystalline phase to be present is anatase TiO<sub>2</sub>. SEM shows that this powder, however, reveals it is made up of two distinct phases: regular elliptical particles of ca. 2 × 3 μm and smaller fused spheres ca. 300–500 nm in diameter (Fig. 7), though fusion of particles makes this at best an estimate. EDX of this aggregate shows the presence of both titanium and carbon, but more focused EDX using TEM shows that the ellipses are purely carbon (Fig. 8a) while the titanium is in the smaller features which also contain carbon (Fig. 8b). TEM of the latter (Fig. 9) show them to be core-shell materials with an inner TiO<sub>2</sub> core of ca. 350 nm diameter with an outer carbon shell of width ca. 75 nm, consistent with the SEM results, above. The anatase polymorph of TiO<sub>2</sub> is known to convert to the thermodynamically favoured rutile phase at *T* > 600 °C,<sup>47</sup> so the presence of the carbon coating to these particles acts to suppress this transition.

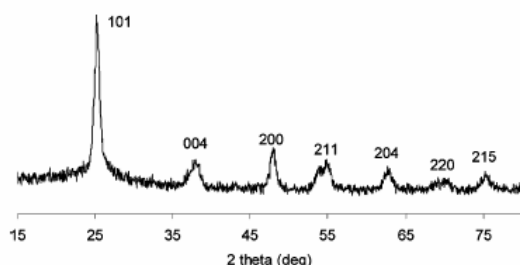


Fig. 6 XRD of the powder obtained by RAPET of **1** at 700 °C; indexing is consistent with anatase TiO<sub>2</sub> (powder diffraction file 84-1286).

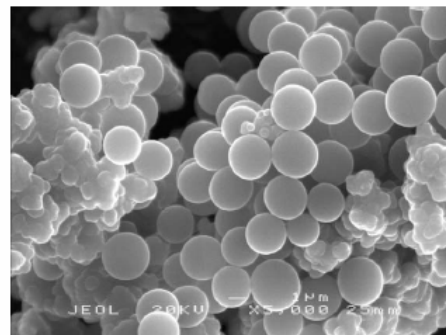


Fig. 7 SEM of the powder obtained by RAPET of **1** at 700 °C. Larger spheres are carbon while the smaller spheres are carbon-coated TiO<sub>2</sub>. Bar = 1 μm.

Gedanken has previously noted the formation of similar structures from RAPET of both [Ti(OPr<sup>i</sup>)<sub>4</sub>]<sup>41</sup> and [Ti(O)(acac)<sub>2</sub>]<sub>2</sub>.<sup>48</sup> In the former case, the core shell structure consists of TiO<sub>2</sub> particles of ca. 25–50 nm diameter clustered into aggregates of 30–40 and surrounded by a carbon shell of ca. 50 nm thickness.<sup>41</sup> Our result seems consistent with this report. On the other hand, with [Ti(O)(acac)<sub>2</sub>]<sub>2</sub> as the precursor, the TiO<sub>2</sub>@C is 15–35 nm in diameter with an outer carbon shell of ~2 nm. The formation of these particles depends both on the decomposition mechanism for the precursor and the relative rates of crystallisation of the components of the mixture. If the precursor is atomised into C, Ti, O *etc.* as is widely quoted for RAPET experiments, then one might anticipate little variation in the size of the nanoparticles formed from differing precursors, assuming similar experimental conditions (temperature, cooling rate), as the growth of the TiO<sub>2</sub> particle would be from atomic Ti and O. Conversely, if the precursor decomposes directly to TiO<sub>2</sub>, one would expect a link between particle size and precursor structure *i.e.* in terms of both decomposition mechanism and kinetics of the precursor. Gedanken has noted in the case of the RAPET decomposition of [Ti(O)(acac)<sub>2</sub>]<sub>2</sub>, TiO<sub>2</sub>@C particle size decreases with temperature, as the rate of formation of TiO<sub>2</sub> increases (contrary to the norm, where particle size is expected to increase with increasing temperature).<sup>48</sup> With regard to our results, this suggests that the larger TiO<sub>2</sub>@C particles formed from [Ti(OPr<sup>i</sup>)<sub>4</sub>]<sup>41</sup> and **1** result from slower precursor decomposition than for [Ti(O)(acac)<sub>2</sub>]<sub>2</sub>, which could in turn could be related to the strong Ti<sub>2</sub>O<sub>3</sub> already present in the latter.

In neither of these reports is the simultaneous formation of pure carbon spheres/ellipses noted, though this feature has been noted in the RAPET of several species, including mesitylene,<sup>49,50</sup> as smaller (20–30 nm) particles along with MoO<sub>3</sub> nanoparticles when [Mo(O)(OMe)<sub>4</sub>] is the precursor,<sup>45</sup> and as a minor component (along with carbon sausages and sub-stoichiometric WO<sub>3</sub>) from [W(OPr<sup>i</sup>)<sub>6</sub>] in isopropanol.<sup>46</sup> The lack of any broad diffraction peak at ca. 26° associated with graphitic carbon suggest that the carbon spheres produced by RAPET of **1** are amorphous, which contrasts with the formation of analogous, but ordered, carbon particles, either by ball-milling of graphite<sup>51</sup> or by RAPET of mesitylene.<sup>49,50</sup> While the importance of interfacial chemistry

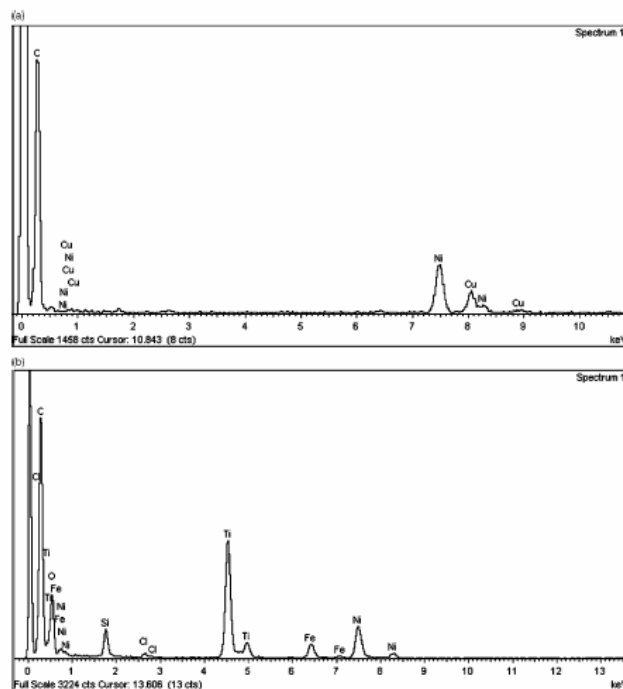


Fig. 8 EDX of (top) the large elliptical particles (8a) and (bottom) the smaller spherical particles (8b) produced by RAPET of **1** at 700 °C.

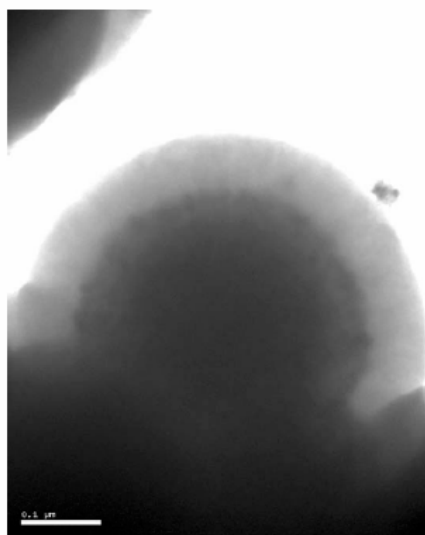


Fig. 9 TEM of the small particles obtained by RAPET of **1** at 700 °C showing the dense inner TiO<sub>2</sub> core and amorphous carbon coating. Bar = 100 nm.

between the carbon sphere and its surroundings has been stressed by Inagaki,<sup>52</sup> where he also references the formation of glass-like

carbon spheres from some organic precursors, it is tempting to also suggest some link with the precursor *i.e.* the lack of any aromatic character to the carbonaceous ligands in **1**.

We have also used **1** to deposit a film of TiO<sub>2</sub> onto a glass substrate by AACVD at 440 °C (Fig. 10). The film is rather featureless and does not yield a diffraction pattern even after annealing in air at 600 °C. EDX (Fig. 11) confirms the presence of both titanium and oxygen in the film, though a dominant peak due to Si, originating from the underlying glass substrate, suggests the film is thin (*ca.* 0.25 μm from Fig. 10a). The film texture shows some particulate matter embedded into the film surface (Fig. 10b) though these are too small to identify unambiguously. While we cannot exclude these as being an artefact of an island growth mechanism and are also TiO<sub>2</sub>, it is plausible that these are TiC particles and are the cause of the amorphous nature of the film. The EDX (Fig. 11) confirms the presence of carbon contamination in the film, and we have noted earlier (Experimental) that microanalysis of some of these precursors, and notably **1**, show low carbon analyses, again plausibly due to TiC formation.

Neither the TiO<sub>2</sub>@C particles nor the AACVD deposited film displayed any photocatalytic activity with respect to the decomposition of methylene blue ( $2.5 \times 10^{-5}$  mol L<sup>-1</sup>). In the case of the film, both its amorphous nature and its lack of thickness are contributing factors, though the case of the TiO<sub>2</sub>@C nanoparticles is perhaps more surprising, as photocatalytic activity has been noted for similar materials, albeit much smaller nanoparticles (see above), generated from [Ti(O)(acac)<sub>2</sub>]<sup>48</sup>

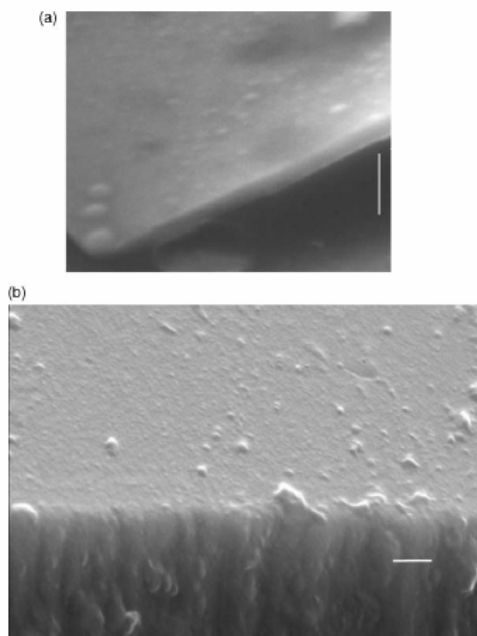


Fig. 10 Two views of the film deposited from 1 by AACVD at 440 °C showing (a) film thickness and (b) texture. Bar = 1 µm.

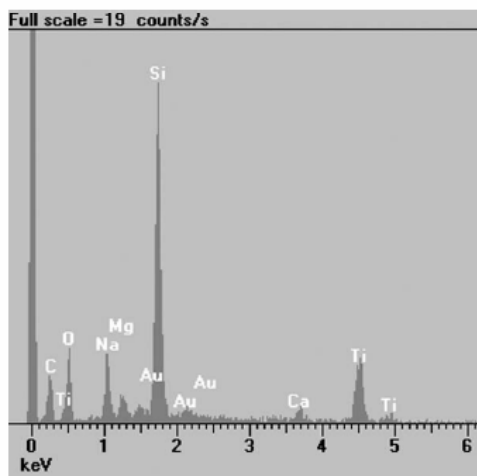


Fig. 11 EDX of the film deposited from 1 by AACVD at 440 °C; gold peaks are due to a sample coating to dissipate charge.

## Conclusions

Reaction of  $[\text{Ti}(\text{OR})_4]$  ( $\text{R} = \text{Et}, \text{Pr}^i$ ) with the amino-alkoxides  $\text{L} = \text{Hbdmap}$  (**I**),  $\text{Htdmap}$  (**II**) generates  $[\text{Ti}(\text{OR})_{4-n}(\text{L})_n]$  with increasing difficulty of *trans*-alcoholysis, particularly when  $n > 2$ . Hydrolysis of these mixed alkoxides leads to the dimeric oxides  $[(\text{L})_2\text{TiO}]_2$  with cleavage of the more labile monodentate alcohols. In reactions with hydrated zinc salts,  $[\text{Ti}(\text{L})_2(\text{NMe}_2)_2]$  also generate

the dimeric oxides, but these fail to coordinate the anhydrous metal with the pendant  $\text{NMe}_2$  functionalities.

$[\text{Ti}(\text{OEt})_2(\text{bdmap})]$  can be decomposed in a sealed container at 700 °C to yield  $\text{TiO}_2@C$  nanoparticles along with spherical carbon particles of diameter *ca.* 2 µm, or can be used in AACVD experiments to yield a film of amorphous  $\text{TiO}_2$  probably contaminated with TiC. Neither film nor particles show any photocatalytic activity towards the decomposition of methylene blue.

## Acknowledgements

We thank the EPSRC for financial support and the EPSRC/JREI for purchase of the diffractometer. Financial supports from the Thailand Research Fund through the Royal Golden Jubilee PhD Program (Grant No. PHD/0126/2546), the Center for Innovation in Chemistry: Postgraduate Education and Research Program in Chemistry (PERCH-CIC), Commission on Higher Education, Ministry of Education, and the Graduate School of Prince of Songkla University to Miki Kanna are also gratefully acknowledged.

## References

- 1 H. Selhofer, *Vacuum Thin Films*, 1999, 15.
- 2 R. C. Smith, T. Z. Ma, N. Hoilien, L. Y. Tsung, M. J. Bevan, L. Colombo, J. Roberts, S. A. Campbell and W. L. Gladfelter, *Adv. Mater. Opt. Electron.*, 2000, 10, 105.
- 3 G. D. Wilk, R. M. Wallace and J. M. Anthony, *Appl. Phys. Rev.*, 1991, 89, 5243.
- 4 Y. Matsumoto, T. Shono, T. Fukumura, M. Kawasaki, P. Ahmet, T. Chikyow, S. Koshihara and H. Koinuma, *Science*, 2001, 291, 854.
- 5 M. Shimizu and T. Shiosaki, *Mater. Res. Soc. Symp. Proc.*, 1995, 361, 295.
- 6 R. O. Duthaler and A. Haffner, *Chem. Rev.*, 1992, 92, 807.
- 7 A. M. Linsebigler, G. Lu and J. T. Yates, *Chem. Rev.*, 1995, 95, 735.
- 8 S. A. O'Neill, I. P. Parkin, R. J. H. Clark, A. Mills and N. Elliot, *J. Mater. Chem.*, 2003, 13, 56.
- 9 M. P. Moret, R. Zallen, D. P. Vijay and S. B. Desu, *Thin Solid Films*, 2000, 366, 8.
- 10 M. Addamo, M. Bellardita, A. Di Paola and L. Palmisano, *Chem. Commun.*, 2006, 4943.
- 11 L. S. Dubrovinsky, N. A. Dubrovinskaia, V. Swamy, J. Muscat, N. M. Harrison, R. Ahuja, B. Holm and B. Johansson, *Nature*, 2001, 410, 653.
- 12 M. K. Aktar, S. E. Pratsinis and S. V. R. Mastrangelo, *J. Mater. Res.*, 1994, 9, 1241.
- 13 V. Pore, A. Rahtu, M. Leskela, M. Ritala, D. Sajavaara and J. Keinonen, *Chem. Vap. Deposition*, 2004, 10, 143.
- 14 B. H. Kim, J. Y. Lee, Y. H. Choa, M. Higuchi and N. Mizutani, *Mater. Sci. Eng., B*, 2004, 107, 289.
- 15 P. Evans, M. E. Pemble and D. W. Sheel, *Chem. Mater.*, 2006, 18, 5750.
- 16 M. N. Simcock, *Surf. Interface Anal.*, 2006, 38, 1122.
- 17 A. Sonnenfeld, R. Hauert and P. R. von Rohr, *Plasma Chem. Plasma Process.*, 2006, 26, 319.
- 18 F. D. Duminica, F. Maury and D. Costinel, *Rev. Chim.*, 2006, 57, 52.
- 19 J. Aarik, A. Aidla, V. Sammelselg, T. Uustare, M. Ritala and M. Leskela, *Thin Solid Films*, 2000, 370, 163.
- 20 R. Pheamhom, C. Sunwoo and D. H. Kim, *J. Vac. Sci. Technol., A*, 2006, 24, 1535.
- 21 P. Piszczek, M. Richert, A. Grodzicki, E. Talik and J. Heimann, *Chem. Vap. Deposition*, 2005, 11, 399.
- 22 J. F. Roeder, B. A. Vaartstra, P. C. Van Buskirk and H. R. Beratan, *Mater. Res. Soc. Symp. Proc.*, 1996, 415, 123.
- 23 D. B. Beach and C. E. Vallet, *Mater. Res. Soc. Symp. Proc.*, 1996, 415, 225.
- 24 R. Bhakta, R. Thomas, F. Hipler, H. F. Bettinger, J. Müller, P. Ehrhart and A. Devi, *J. Mater. Chem.*, 2004, 14, 3231.

- 25 A. Baunemann, M. Hellwig, A. Varade, R. K. Bhakta, M. Winter, S. A. Shivashankar, R. A. Fischer and A. Devi, *Dalton Trans.*, 2006, 3485.
- 26 N. Hollingsworth, G. A. Horley, M. Mazhar, M. F. Mahon, K. C. Molloy, C. P. Myers and G. W. Critchlow, *Appl. Organomet. Chem.*, 2006, 20, 687.
- 27 P. C. Bharara, V. D. Gupta and R. C. Mehrotra, *J. Indian Chem. Soc.*, 1974, 51, 859.
- 28 P. C. Bharara, V. D. Gupta and R. C. Mehrotra, *Z. Anorg. Allg. Chem.*, 1974, 403, 337.
- 29 E. C. Alyea and P. H. Merrell, *Inorg. Nucl. Chem. Lett.*, 1973, 9, 69.
- 30 A. C. Jones, T. J. Leedham, P. J. Wright, M. J. Crosbie, K. A. Fleeting, D. J. Otway, P. O'Brien and M. E. Pemble, *J. Mater. Chem.*, 1998, 8, 1773.
- 31 C. L. Clarke, N. M. Boag and M. E. Pemble, *Proc. Electrochem. Soc.*, 2003, 2003-8, 1514.
- 32 J. P. Lee, M. H. Park, T.-M. Chung, Y. Kim and M. M. Sung, *Bull. Korean Chem. Soc.*, 2004, 25, 475.
- 33 J.-H. Lee, J.-Y. Kim and S.-W. Rhee, *Electrochem. Solid-State Lett.*, 1999, 2, 507.
- 34 J.-H. Lee, J.-Y. Kim, J.-Y. Shim and S.-W. Rhee, *J. Vac. Sci. Technol., A*, 1999, 17, 3033.
- 35 B. F. G. Johnson, M. C. Klunduk, T. J. O'Connell, C. McIntosh and J. Ridland, *J. Chem. Soc., Dalton Trans.*, 2001, 1553.
- 36 K. N. Campbell, R. A. LaForge and B. K. Campbell, *J. Org. Chem.*, 1949, 14, 346.
- 37 G. Müller and T. Schätzle, *Z. Naturforsch., B: Chem. Sci.*, 2004, 59, 1400.
- 38 J. Gasteiger and C. Herzig, *J. Chem. Res. (S)*, 1981, 113.
- 39 Y. Sasaki and N. Miyazawa, *Kinki Daigaku Rikogakubu Kenkyu Hokoku*, 1992, 28, 237.
- 40 L. J. Farrugia, *J. Appl. Crystallogr.*, 1999, 32, 837.
- 41 S. V. Pol, V. G. Pol and L. Gedanken, *Chem.-Eur. J.*, 2004, 10, 4467.
- 42 J. Rodriguez Castro, M. F. Mahon and K. C. Molloy, *Chem. Vap. Deposition*, 2006, 12, 601.
- 43 A. Demšar, J. Kosmirj and S. Petricek, *J. Am. Chem. Soc.*, 2002, 124, 3951.
- 44 A. Odani, V. G. Pol, S. V. Pol, M. Kolytyn, A. Gedanken and D. Aurbach, *Adv. Mater.*, 2006, 18, 1431.
- 45 S. V. Pol, V. G. Pol, V. G. Kessler, G. A. Seisenbaeva, M. Sung, S. Asai and A. Gedanken, *J. Phys. Chem. B*, 2004, 108, 6322.
- 46 S. V. Pol, V. G. Pol, V. G. Kessler and A. Gedanken, *New J. Chem.*, 2006, 30, 370.
- 47 M. Inagaki, Y. Hirose, T. Matsunaga, T. Tsumura and M. Toyada, *Carbon*, 2003, 41, 2619.
- 48 S. Shammugam, A. Gabashvili, D. S. Jacob, J. C. Yu and A. Gedanken, *Chem. Mater.*, 2006, 18, 2275.
- 49 V. G. Pol, S. V. Pol, B. Markovsky, J. M. Calderon-Moreno and A. Gedanken, *Chem. Mater.*, 2006, 18, 1512.
- 50 V. G. Pol, M. Motiei, A. Gedanken, J. Calderon-Moreno and M. Yoshimura, *Carbon*, 2004, 42, 111.
- 51 J. L. Li, L. J. Wang and W. Jiang, *Appl. Phys. A: Mater. Sci. Process.*, 2006, 83, 385.
- 52 M. Inagaki, *Carbon*, 1997, 35, 711.



Available online at [www.sciencedirect.com](http://www.sciencedirect.com)

Materials Chemistry and Physics 110 (2008) 166–175

**MATERIALS  
CHEMISTRY AND  
PHYSICS**
[www.elsevier.com/locate/matchemphys](http://www.elsevier.com/locate/matchemphys)

## Mixed amorphous and nanocrystalline TiO<sub>2</sub> powders prepared by sol–gel method: Characterization and photocatalytic study

Miki Kanna, Sumpun Wongnawa\*

*Department of Chemistry, Faculty of Science, Prince of Songkla University, 15 Kanjanavanich Road, Hat Yai, Songkhla 90112, Thailand*

Received 6 September 2007; received in revised form 6 January 2008; accepted 21 January 2008

### Abstract

Mixed titanium dioxide (TiO<sub>2</sub>) powders of various amorphous–anatase–rutile contents were prepared by acid-catalyzed sol–gel method at 80 °C without calcination. The physico-chemical properties of the powders were investigated by powder XRD, SEM, Brunauer–Emmett–Teller (BET), Fourier-transformed infrared (FT-IR), X-ray energy-dispersive (EDX), and UV–vis techniques. The results showed that the products were mixtures of mainly amorphous TiO<sub>2</sub> with small amount of anatase and rutile phases when prepared by without using acid catalyst and by adding small amount of acid catalyst (hydrochloric acid, nitric acid, and acetic acid). However, when either sulfuric acid or phosphoric acid was used the products obtained were mainly amorphous TiO<sub>2</sub> with small amount of anatase. Mechanism of growth from basic units to nanocrystalline was also proposed. Positive photocatalytic activities of these products were found and some could be compared favorably with Degussa P25. Three dyes, methylene blue, crystal violet, and congo red were used in the photocatalytic studies.

© 2008 Elsevier B.V. All rights reserved.

**Keywords:** Amorphous titanium dioxide; Sol–gel method; Nanocrystalline titanium dioxide; Titanium dioxide photocatalysts; Dye degradation; Methylene blue; Crystal violet; Congo red

### 1. Introduction

Soon after the report of Fujishima and Honda in 1972 [1] which showed that titanium dioxide (TiO<sub>2</sub>) could be useful in other ways besides using as the white pigment, TiO<sub>2</sub> has attracted much attention because of its photocatalytic property. Titanium dioxide or titania since then has been widely studied for applications in a variety of problems of environmental interest in addition to water and air purifications. It has been shown to be useful for the destruction of micro-organisms such as bacteria and viruses, the inactivation of cancer cells, the control of odors, the photosplitting of water to produce hydrogen gas, the fixation of nitrogen and the clean up of oil spills. Titanium dioxide has considerable advantages over other similar photocatalysts due to its good characteristic in terms of chemical stability, endurance, thin film transparency, and lower production costs [2,3]. Among the three crystalline phases of TiO<sub>2</sub> (anatase, rutile, and brookite) it is generally accepted that anatase shows higher photocatalytic activity than rutile, whereas rutile is a more suitable material for

white pigments and coatings because of its great refractivity and notable chemical inertness. In many cases, an anatase/rutile mixture exhibits better photocatalytic activity than does the single phase [4,5]. There have been some works reported the syntheses of the two phases of TiO<sub>2</sub>, for example, nanocrystalline TiO<sub>2</sub> powders either rutile or anatase form was prepared from titanium isopropoxide at temperature below 100 °C [6], a mixture of anatase and rutile-type TiO<sub>2</sub> was prepared from polyperoxotitanic acid gel obtained by the addition of Ti(OBu<sup>n</sup>)<sub>4</sub> to H<sub>2</sub>O<sub>2</sub> solution and the gel was heat-treated in air at temperatures ranging from 150 °C to 750 °C [7], and the preparation of nanocrystalline TiO<sub>2</sub> in anatase or mixed phase from controlling the hydrolysis of TiCl<sub>4</sub> [8]. The latter also showed that the addition of small amount of (NH<sub>4</sub>)<sub>2</sub>SO<sub>4</sub> promoted occurrence of anatase phase, however, these were not studied for photocatalytic activity.

Good catalytic property is governed by two major opposing physical properties: crystallinity and surface area of the photocatalysts. The high crystallinity helps to prolong the recombination rate of the photoexcited electron and positive hole, hence, strong reducing and oxidizing power of the photocatalyst. The high surface area helps to facilitate adsorption of the target molecules onto the surface of the catalyst; as higher

\* Corresponding author. Tel.: +66 7428 8443; fax: +66 7421 2918.  
E-mail address: [sumpun.w@psu.ac.th](mailto:sumpun.w@psu.ac.th) (S. Wongnawa).

number of molecules are adsorbed the faster the rate of reaction [9]. Among the two properties, crystallinity and surface area, one has to decide and choose one over the other since both cannot be obtained simultaneously from the syntheses. Most of the literature works usually used the precalcined titanium dioxide at around 300–400 °C to induce crystallization of the anatase form. It has been reported that the different methods for the syntheses of titanium dioxide result in products with different structures (anatase or rutile), crystallinity, and contaminants. As a consequence, the surface properties of TiO<sub>2</sub> strongly depend on the preparation techniques [8,10].

In our earlier work [11] we found that the mixture of amorphous form with small amount of crystalline anatase form also showed photocatalytic properties. This predominated amorphous form sample could be synthesized by a simple precipitation method to produce TiO<sub>2</sub>, however, the subsequent calcination was excluded. Since no calcination was employed, the product powder was mostly present in an amorphous form with some hydrated water molecules. Its surface area was also significantly higher than that of commercially available anatase/rutile or P25 due to its amorphous morphology. Simple synthesis with elimination of the calcination step would mean lower cost due to less energy consumption and a shorter lapse time between the synthesis and the application stages.

There are two main methods for obtaining titania for industrial purposes. The first is the so-called “sulphate method”. The other widespread technique for manufacturing titania is the vapour-phase oxidation of TiCl<sub>4</sub> [12]. These two methods have their drawbacks either in purity or in controlling of the particle shape, size, and distribution [7,13]. On a laboratory scale, titania is usually prepared from a solution of titanium salts or titanium alkoxides. The preparation methods such as hydrolysis, flame synthesis, precipitation, hydrothermal, and the alkoxide sol–gel methods have been reported by several researchers to synthesize nanocrystalline titanium dioxide [14,15]. In preparing oxide materials, the sol–gel technique can exhibit a number of advantages over conventional methods. The homogeneous property of the products prepared by this method is very satisfactory [5,16]. In these processes, titania is usually prepared by the hydrolysis and polycondensation reactions of titanium alkoxides. It is well known that titanium alkoxide hydrolyzes vigorously in water, and many catalysts typically various simple acids, e.g., nitric acid, hydrochloric acid, acetic acid, and sulfuric acid have been applied to lower the reaction rates [5,17–20]. The use of phosphoric acid, however, has not been reported.

In this work, samples of TiO<sub>2</sub> powder were synthesized by the sol–gel method using TiCl<sub>4</sub> as a starting material. The TiO<sub>2</sub> samples were prepared in various amorphous-anatase–rutile contents by using different acids as hydrolysis catalysts such as hydrochloric acid, nitric acid, sulphuric acid, acetic acid, and phosphoric acid. The physico-chemical properties of the products were characterized by several techniques (XRD, SEM, Brunauer–Emmett–Teller (BET), Fourier-transformed infrared (FT-IR), X-ray energy-dispersive (EDX), and UV–vis) and their photoactivities to decolorize dyes (methylene blue, crystal violet, and congo red) were studied and compared to the commercially available samples (P25, anatase, and rutile).

## 2. Experimental

### 2.1. Materials

Titanium tetrachloride, AR grade (Merck), P25 titanium dioxide (Degussa AG, Germany), anatase (Carlo Erba, Italy, code no. 488257), rutile (R706 Dupont, USA), methylene blue (UNILAB, Australia), crystal violet, and Congo red (BDH, England) were used as received. All other reagents, AR grade, were obtained from various well-known suppliers.

### 2.2. Synthesis of TiO<sub>2</sub> powders

Titanium tetrachloride (TiCl<sub>4</sub>), 20 mL, was added slowly to 200 mL of cold distilled water which had been cooled in an ice-water bath at least 10 min prior to the addition. The solution was then mixed with each corresponding acid<sup>1</sup> (acts as hydrolysis catalyst) and refluxed at 80 °C for 1 h under vigorous stirring. The solution was then treated with ammonia solution until the pH value was 7 and maintained at the same temperature for 24 h. The white precipitate formed was filtered and then washed with distilled water until free of chloride ion (AgNO<sub>3</sub> test). The product was dried overnight and ground to fine powder. The product codes were assigned as Ti–HCl, Ti–HNO<sub>3</sub>, Ti–H<sub>2</sub>SO<sub>4</sub>, Ti–CH<sub>3</sub>COOH, and Ti–H<sub>3</sub>PO<sub>4</sub> corresponding to the preparation method of each by adding HCl, HNO<sub>3</sub>, H<sub>2</sub>SO<sub>4</sub>, CH<sub>3</sub>COOH, and H<sub>3</sub>PO<sub>4</sub> acids, respectively, plus another sample designated as Ti–no-acid since it was prepared in the absence of acid catalyst.

### 2.3. Products characterization

The XRD patterns were obtained via the Philips PW 3710 powder diffractometer using Cu Kα radiation and equipped with a Ni filter. Diffraction patterns of both anatase and rutile phase were compared with reference to JCPDS powder diffraction files (21-1272, 21-1276). From the line broadening of the corresponding X-ray diffraction peaks and using the Scherrer's formula, the crystallite size has been estimated by

$$L = \frac{K\lambda}{\beta \cos \theta} \quad (1)$$

where  $L$  is the average crystallite size in nm,  $\lambda$  is the wavelength of the X-ray radiation (0.154056 nm for copper lamp),  $K$  is a constant usually taken as 0.9,  $\beta$  is the line width at half-maximum height in radians, and  $\theta$  is the diffracting angles [21,22].

The infrared spectra were recorded using Fourier-transformed infrared spectrophotometer (EQUINOX55, Bruker, Germany) in diffused reflectance mode at 400–4000 cm<sup>-1</sup> with KBr as blank. The SEM micrographs were performed on gold-coated samples using a Jeol apparatus (JSM-5800 LV) equipped with a Link analyzer (ISIS 300) for X-ray energy-dispersive analyses. The Brunauer–Emmett–Teller surface area of TiO<sub>2</sub> powders were determined by means of Coulter SA 3100 using nitrogen adsorption at –196 °C.

The bandgap energies of titanium dioxide samples were determined using UV–vis spectrophotometer (Shimadzu UV-2401). The spectra were recorded in diffused reflectance mode with BaSO<sub>4</sub> as a reference. The bandgap energies ( $E_g$ ) of the catalyst were calculated by the Planck's equation:

$$E_g = h \frac{c}{\lambda} = \frac{1240}{\lambda} \quad (2)$$

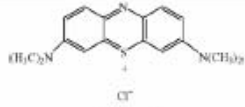
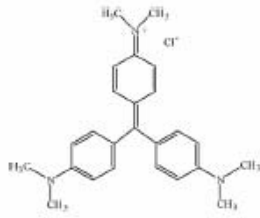
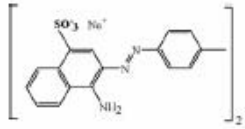
where  $E_g$  is the bandgap energy (eV),  $h$  is the Planck's constant,  $c$  is the light velocity (m/s), and  $\lambda$  is the wavelength (nm).

### 2.4. Photocatalytic study: decolorization of dyes

A predetermined amount of dye solution ( $2.5 \times 10^{-5}$  M) and TiO<sub>2</sub> were placed in a beaker (0.5 g of TiO<sub>2</sub> per liter of dye solution). Prior to the illumination, the suspension was stirred for 30 min to allow for the dye adsorption

<sup>1</sup> Hydrochloric acid, nitric acid, sulfuric acid, acetic acid, and phosphoric acid.

Table 1  
Structures and characteristics of dyes

Dye	$\lambda_{\max}$ (nm)	Chemical structure	Type of dye	Class of dye [Ref.]
Methylene blue (MB) $C_{16}H_{18}N_3ClS \cdot 2H_2O$	665		Thiazine	Cationic [23]
Crystal violet (CV) $C_{25}H_{30}N_3Cl$	590		Triphenyl	Cationic [24]
Congo red (CR) $C_{32}H_{22}N_6Na_2O_6S_2$	500		Diazo	Direct [24]

onto the  $TiO_2$  surface. The UV irradiation was carried out using the fluorescence black light tube (20 W,  $\lambda_{\max}$  366 nm) as previously reported [11] but with newly designed wooden compartment that can accommodate up to five tubes of black light. The entire setup was placed in a tightly closed compartment to avoid interference from ambient light. In all studies, the mixture was magnetically stirred, before and during illumination. At specific time intervals, 5 mL of the sample was sampled and centrifuged to remove  $TiO_2$  particles. The change in absorbance of dye solution was measured using UV-vis spectrophotometer (Specord S100, Germany) at fixed wavelength of 665 nm, 590 nm, and 500 nm for methylene blue (MB), crystal violet (CV), and congo red (CR), respectively. Controlled experiments with either light or  $TiO_2$  were performed to demonstrate that decolorization of dyes was dependent on the presence of both light and  $TiO_2$ . During adsorption in the darkness, the beaker was wrapped with aluminum foil to shield it from the ambient light. Characteristics of the dyes in this study are shown in Table 1.

### 3. Results and discussion

#### 3.1. Physical properties of the synthesized $TiO_2$ powders

The X-ray diffraction patterns in Fig. 1 illustrate the effect of type of acids (hydrolysis catalysts) on the phase formation. The composition of the synthesized Ti-no-acid, Ti-HCl, Ti- $HNO_3$ , and Ti- $CH_3COOH$  were a mixture of mainly amorphous  $TiO_2$  with small amount of anatase and rutile phases. For the Ti- $H_2SO_4$  and Ti- $H_3PO_4$  (Fig. 1d and f), the peaks are broad indicating a weak crystallinity of anatase phase. The possible mechanism for anatase and rutile  $TiO_2$  formation will be discussed in Section 3.2. Summary of results obtained from the X-ray diffraction patterns and BET surface area of all the samples are shown in Table 2. The degrees of crystallinity (the third column) of the samples were determined from the XRD intensities by using the standard addition method. The commercial titanium dioxide (anatase (Carlo Erba) and rutile (R706)) was mixed with the original synthesized titanium dioxide samples in

different percent weights: 0%, 10%, 20%, 40%, and 60% and then measured the peak intensities. A calibration curve was made by plotting the total XRD-peak-intensity against the percentage of the added standard. The original percentage of analyst was obtained by the interception point on the percent weight axis. The crystallite sizes of the samples were calculated using the peak at  $2\theta = 25.4^\circ$  and  $27.5^\circ$  for anatase and rutile phase, respectively, and are also shown in Table 2. The crystallite sizes of all the samples can be classified as nanocrystalline  $TiO_2$  powders and are smaller than those of the commercial ones. When both

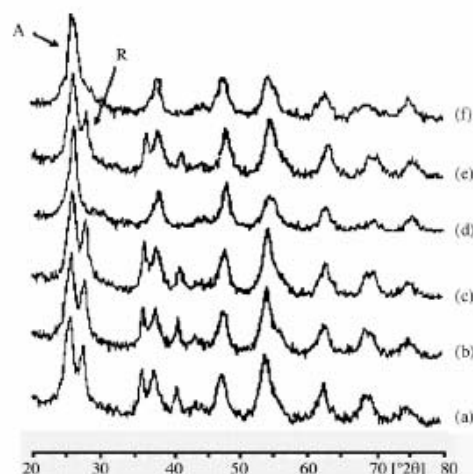


Fig. 1. Powder XRD patterns of the synthesized  $TiO_2$  powders: (a) no acid, (b) HCl, (c)  $HNO_3$ , (d)  $H_2SO_4$ , (e)  $CH_3COOH$ , and (f)  $H_3PO_4$ . A denotes anatase and R denotes rutile.

Table 2  
Comparison of TiO<sub>2</sub> powders prepared under various acid-catalyzed conditions

Samples	Crystallite size <sup>a</sup> (nm)	Crystallinity <sup>b</sup> (%)	Surface area (m <sup>2</sup> g <sup>-1</sup> )	
			This work	Literature
Ti-no-acid	4.1 (A), 12.8 (R)	11(A), 10(R)	194.7	–
Ti-HCl	4.2 (A), 13.8 (R)	13(A), 6(R)	192.8	–
Ti-HNO <sub>3</sub>	4.7 (A), 13.6 (R)	15(A), 13(R)	196.6	–
Ti-H <sub>2</sub> SO <sub>4</sub>	4.1 (A)	15(A)	220.6	–
Ti-CH <sub>3</sub> COOH	4.0 (A), 13.2 (R)	12(A), 8(R)	212.1	–
Ti-H <sub>3</sub> PO <sub>4</sub>	3.8 (A)	14(A)	308.5	–
Anatase	16.3 (A)	100(A)	7.6	5.9 [25]
Rutile	42.7 (R)	100(R)	9.9	–
P25 <sup>c</sup>	10.2 (A), 42.7 (R)	80 (A), 20 (R) [26]	51.4	50 [27]

<sup>a</sup> Calculated from XRD data using Eq. (1). A denotes anatase and R denotes rutile.

<sup>b</sup> Determined by XRD using standard addition method, the rest is an amorphous phase.

<sup>c</sup> Average particle size 30 nm [27].

anatase and rutile are present the anatase crystallite sizes are invariably smaller than the rutile. This result is similar to the work reported by Gopal et al., where they found that anatase crystallite sizes were smaller than rutile in the mixed sample [6]. That Ti-H<sub>2</sub>SO<sub>4</sub> and Ti-H<sub>3</sub>PO<sub>4</sub> have the crystallite size smaller than the other products (Ti-no-acid, Ti-HCl, Ti-HNO<sub>3</sub>, and Ti-CH<sub>3</sub>COOH) could be the effect from the presence of sulphate and phosphate ions in the TiO<sub>2</sub> network as observed by Samantary et al., and suggested that the sulphate ions could possibly interact with TiO<sub>2</sub> network and thus hinder the growth of the particle [18].

The infrared spectra of all the synthesized titanium dioxide powders in the range 4000–400 wavenumber are shown in Fig. 2. The large broad band at 3600–3100 cm<sup>-1</sup> can be assigned to mixed ν<sub>OH</sub> and ν<sub>NH</sub> modes (stretching modes). These bands are in the hydroxyl stretching region and should correspond to O–H vibration of the Ti–OH groups and H<sub>2</sub>O molecules. The band around 3500 cm<sup>-1</sup> can be assigned to O–H vibration of the Ti–OH groups [28]. The stretching vibration of Ti–OH bonding could not be removed easily and must be heated until relatively high temperature [7]. Near the band

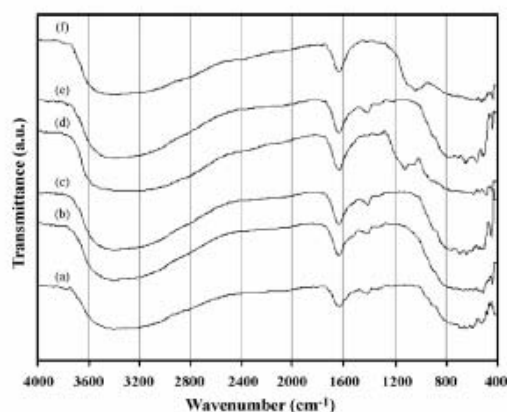


Fig. 2. FT-IR spectra of the synthesized TiO<sub>2</sub> powders: (a) Ti-no-acid, (b) Ti-HCl, (c) Ti-HNO<sub>3</sub>, (d) Ti-H<sub>2</sub>SO<sub>4</sub>, (e) Ti-CH<sub>3</sub>COOH, and (f) Ti-H<sub>3</sub>PO<sub>4</sub>.

around 3500 cm<sup>-1</sup>, a shoulder was generated by an asymmetric vibration mode of the residual ammonium ions. The rather narrow bands around 1600 cm<sup>-1</sup> and 1400 cm<sup>-1</sup> can be assigned to δ<sub>OH</sub> and δ<sub>NH</sub> modes (bending modes) of hydroxyl (OH) and ammonium (NH<sub>4</sub><sup>+</sup>) groups, respectively [29,30]. All of these bands indicated that H<sub>2</sub>O and NH<sub>4</sub><sup>+</sup> were present in the products. In the low energy region (below 800 cm<sup>-1</sup>), the band due to stretching mode of Ti–O (ν<sub>Ti-O</sub>) which was the envelope of the phonon bands of a Ti–O–Ti bond of a titanium oxide network could be assigned [28]. The absence of any band in this spectral region may then suggests that the precipitate is amorphous.

Additionally, the spectrum of Ti-H<sub>2</sub>SO<sub>4</sub> in Fig. 2d shows broad band at 1250–1100 cm<sup>-1</sup> which is the characteristic frequencies of SO<sub>4</sub><sup>2-</sup> group. The broad band in this region resulted from the lowering of the symmetry in the free SO<sub>4</sub><sup>2-</sup> (Td point group) to either C<sub>2v</sub> (Fig. 6B) or C<sub>3v</sub> (Fig. 6A and C) when SO<sub>4</sub><sup>2-</sup> is bound to the titania surface [18,31]. The vibrational modes of the PO<sub>4</sub><sup>3-</sup> anion in the sample Ti-H<sub>3</sub>PO<sub>4</sub> are also detected in the IR spectrum (Fig. 2f) where the asymmetric ν<sub>P-O</sub> stretching mode appears at 1015 cm<sup>-1</sup> [32]. The results from XRD and FT-IR led to the conclusion that samples were a hydrated amorphous titanium dioxide with minute amount of impurities, such as NH<sub>4</sub><sup>+</sup>, SO<sub>4</sub><sup>2-</sup>, and PO<sub>4</sub><sup>3-</sup>.

The specific surface areas of samples are also shown in Table 2. All the synthesized titanium dioxide samples exhibited higher surface area than the commercial ones due to lower crystallinity of the synthesized samples without calcination in this work. Among the synthesized samples, both Ti-H<sub>2</sub>SO<sub>4</sub> and Ti-H<sub>3</sub>PO<sub>4</sub> exhibited higher surface area than Ti-no-acid, Ti-HCl, Ti-HNO<sub>3</sub>, and Ti-CH<sub>3</sub>COOH. This result agrees with those in the reports that the surface area of sulphated-titania was higher than that of pure TiO<sub>2</sub> [33] and the nanosized TiO<sub>2</sub> prepared in the presence of sulphate ion had higher BET surface than those prepared in the absence of sulphate ion [34].

Figs. 3 and 4 show SEM images and EDX patterns of TiO<sub>2</sub> powders prepared under various acid catalysts. From the SEM images (Fig. 3), magnified by 35,000×, the images show delicate structures of spherical shape particles. The images of Ti-no-acid, Ti-HCl, Ti-HNO<sub>3</sub>, and Ti-CH<sub>3</sub>COOH samples appear

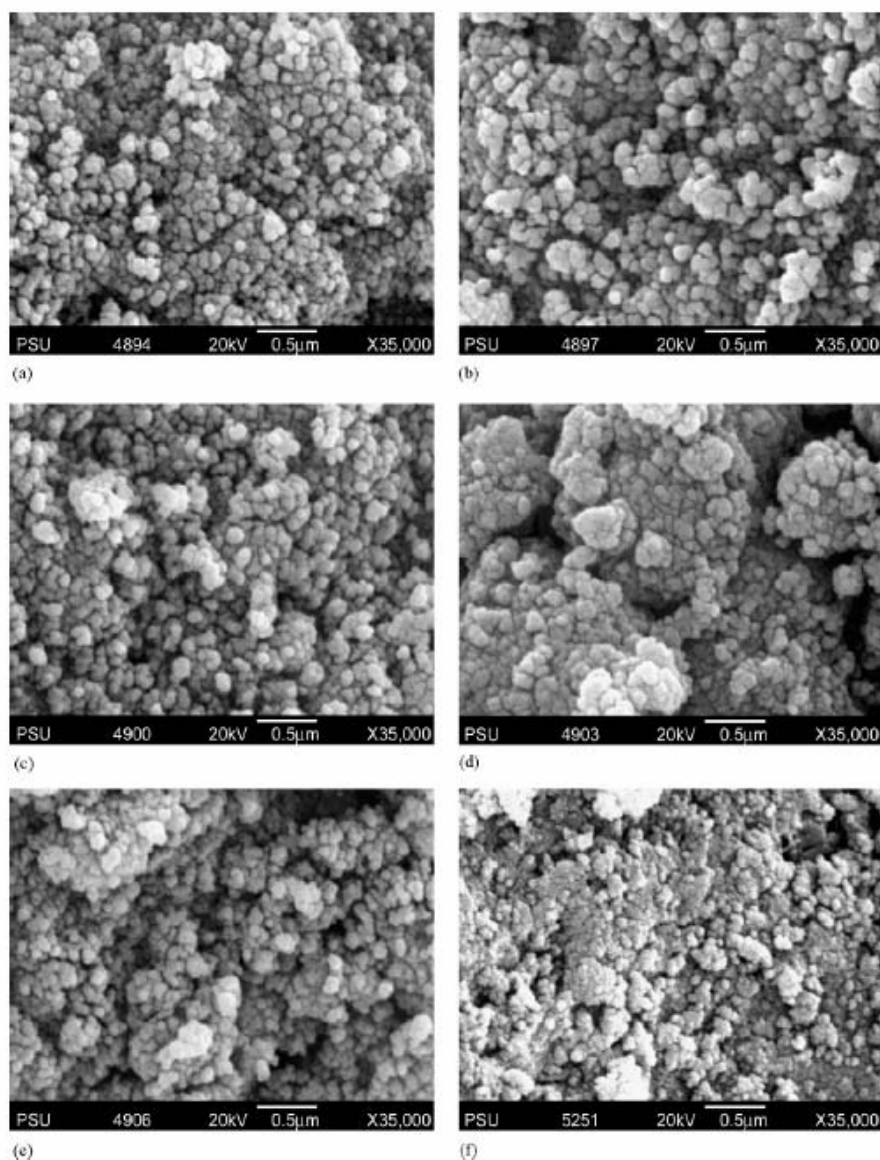


Fig. 3. SEM images of the synthesized  $\text{TiO}_2$  powders: (a) Ti-no-acid, (b) Ti-HCl, (c) Ti-HNO<sub>3</sub>, (d) Ti-H<sub>2</sub>SO<sub>4</sub>, (e) Ti-CH<sub>3</sub>COOH, and (f) Ti-H<sub>3</sub>PO<sub>4</sub>.

as the dense and uniform structures with fewer aggregation of particles. For the Ti-H<sub>2</sub>SO<sub>4</sub> and Ti-H<sub>3</sub>PO<sub>4</sub> samples, the dense and non-uniform structure with higher aggregation (than the Ti-no-acid, Ti-HCl, Ti-HNO<sub>3</sub>, and Ti-CH<sub>3</sub>COOH samples) was observed. From SEM images of this study, it could be seen that the difference in the morphology could be ascribed to different preparation conditions, especially the hydrolysis catalyst which may affect the aggregation of each sample. The morphology of this work is similar to the results of Yu et al., who investigated the effect of acidic and basic hydrolysis catalysts on the photocat-

alytic activity and microstructure of titanium dioxide prepared by sol-gel process. Their results showed that the morphology of titanium dioxide prepared by the hydrolysis of titanium tetraisopropoxide at pH 6.8 and without using HNO<sub>3</sub> as catalyst appears as a dense structure and fewer in aggregation [35].

The EDX results (Fig. 4) revealed that, with the exception of two samples, all powder samples did not contain chloride anion which indicated that it was washed out completely at the washing stage. However, the samples obtained from using sulphuric acid and phosphoric acid showed the presence of S and P indicating

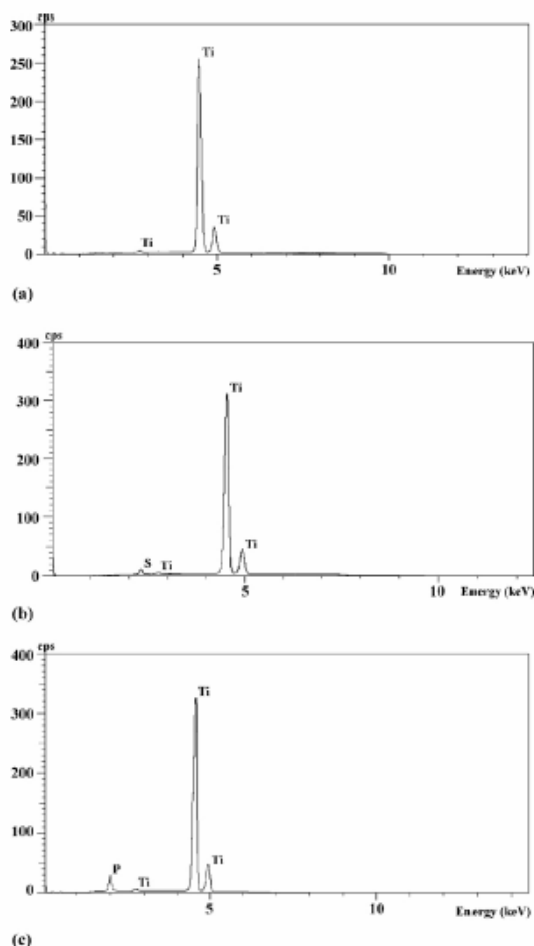


Fig. 4. EDX spectra of the synthesized  $\text{TiO}_2$  powders: (a) Ti-no-acid, Ti-HCl, Ti-HNO<sub>3</sub>, Ti-CH<sub>3</sub>COOH, (b) Ti-H<sub>2</sub>SO<sub>4</sub>, and (c) Ti-H<sub>3</sub>PO<sub>4</sub>.

the  $\text{SO}_4^{2-}$  and  $\text{PO}_4^{3-}$  ions still adhered to the titanium dioxide surfaces which agreed with the FT-IR results.

UV-vis diffused reflectance spectroscopy was used to study the absorption across the energy band gap and the results are shown in Table 3. The absorption edge of Ti-no-acid, Ti-HCl, Ti-HNO<sub>3</sub>, and Ti-CH<sub>3</sub>COOH appears at longer wavelength than that of Ti-H<sub>3</sub>PO<sub>4</sub> and Ti-H<sub>2</sub>SO<sub>4</sub>. In the case of commercial  $\text{TiO}_2$ , the absorption edge of rutile (R706) appears at longer wavelength than that of anatase (Carlo Erba). The absorption edge wavelengths of commercial titanium dioxide are in the order of rutile (R706) > Degussa P25 > anatase (Carlo Erba). The bandgap energies, calculated using Eq. (2), of rutile (R706), Degussa P25, and anatase (Carlo Erba) are 3.00 eV, 3.14 eV, and 3.22 eV, respectively, which are identical to the literature values of 3.00 eV, 3.14 eV, and 3.20 eV [36,37]. The bandgap energy of Ti-no-acid, Ti-HCl, Ti-HNO<sub>3</sub>, and Ti-CH<sub>3</sub>COOH is slightly larger than rutile (R706). Both Ti-H<sub>3</sub>PO<sub>4</sub> and Ti-H<sub>2</sub>SO<sub>4</sub> have

Table 3  
The absorption edge and bandgap energy of the synthesized  $\text{TiO}_2$

Samples	Absorption edge (nm)	Bandgap energy (eV)	
		This work	Literature
Ti-no-acid	408	3.04	–
Ti-HCl	405	3.06	–
Ti-HNO <sub>3</sub>	406	3.05	–
Ti-H <sub>2</sub> SO <sub>4</sub>	390	3.18	–
Ti-CH <sub>3</sub> COOH	406	3.05	–
Ti-H <sub>3</sub> PO <sub>4</sub>	386	3.21	–
Anatase (Carlo Erba)	385	3.22	3.20 [25,36]
Rutile (R706)	413	3.00	3.00 [25,36]
P25 (Degussa)	395	3.14	3.14 [37]

larger bandgap energy and are in the same range of anatase (Carlo Erba).

### 3.2. The possible mechanism for anatase and rutile $\text{TiO}_2$ formation

The sol-gel method consists of the hydrolysis and condensation reactions which are catalyzed in the presence of acid. The hydrolysis reaction leads to the formation of original nuclei or basic units of titanium dioxide while the condensation reaction leads to the growth of network system of the original basic units [38]. The product powders obtained in this work were mixtures of amorphous  $\text{TiO}_2$ , anatase, and rutile. The amorphous phase was dominant with small amount of anatase or mixed anatase and rutile (see the third column in Table 2). The key to the differences in anatase and rutile formation stems from the structure of two polymorphs. In rutile, two opposite edges of each ( $\text{TiO}_6^{2-}$ ) octahedra are shared forming a linear chain along the (001) direction. Chains are then linked to each other by sharing corner oxygen atoms. Anatase has no corner sharing, but has four edges shared per octahedron. The anatase structure can be viewed as zigzag chains of octahedra, linked to each other through shared edges [6].

There have been reports that excellently discussed the possible mechanism of the anatase and rutile formations [6,39]. The basic unit of ( $\text{TiO}_6^{2-}$ ) octahedra in solution can join together to form oligomers which are the growth units leading to both anatase and rutile phases. The joining of the basic octahedra unit if takes place at the opposite edges will give a growth units for the rutile phase, however, if it takes place at the non-opposite edges will give a growth unit for the anatase phase (and possibly the brookite phase, too).

The ( $\text{TiO}_6^{2-}$ ) octahedra in this system can be written in full as  $[\text{Ti}(\text{H}_2\text{O})_5]^{2+}$  or  $[\text{Ti}(\text{OH})_2(\text{H}_2\text{O})_4]^{2+}$  ion. In fact, the initial complex species first formed in the hydrolysis should be  $[\text{Ti}(\text{H}_2\text{O})_6]^{4+}$  which, due to its acidic nature, would undergo the first deprotonation to  $[\text{Ti}(\text{OH})(\text{H}_2\text{O})_5]^{3+}$  and subsequently through the second deprotonation yielding the dipositive ions as  $[\text{Ti}(\text{H}_2\text{O})_5]^{2+}$  or  $[\text{Ti}(\text{OH})_2(\text{H}_2\text{O})_4]^{2+}$  ion. The latter is probably more preferred based on the evidence reported that both forms co-existed in the solution and in the oligomers growth unit no titanyl (Ti=O) moiety was found so  $[\text{Ti}(\text{H}_2\text{O})_5]^{2+}$  ion was not the basic unit growing into oligomers [40]. This leaves

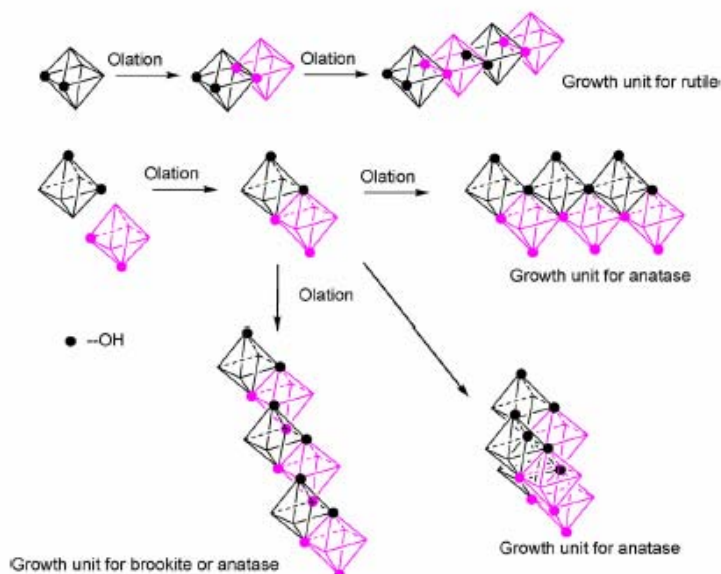


Fig. 5. Formation of growth units from  $cis$ - $[Ti(OH)_2(H_2O)_4]^{2+}$  ion.

the  $[Ti(OH)_2(H_2O)_4]^{2+}$  as the most likely basic unit. However, the two hydroxyl (OH) groups in this complex basic unit can take two geometrical sites: *cis* and *trans* with respect to one another. In the previously proposed diagram only the *trans* isomer was demonstrated [39]. In our opinion, the *cis* isomer cannot be left out due to existence of many examples of titanium complexes having two bridging Ti–O moieties in *cis* positions [41]. The *cis* isomer can grow into larger unit in the same way as the *trans* isomer. The growing of the *cis* isomer can be shown in Fig. 5.

At pH  $\sim 7$ , the precipitation occurred quite rapidly resulting in low crystallinity, hence, the precipitate mostly appeared in the amorphous form with small amount of anatase and rutile mixed in as shown in Table 2. This behavior had been earlier mentioned in other reports [6,42,43]. In this work, the amount of anatase was slightly higher than the rutile in most cases. This may reflect the statistical probability when the basic unit octahedra joined together, sharing other edges leading to anatase has more chances than joining the opposite edge to form rutile.

In the case of adding  $H_2SO_4$  and  $H_3PO_4$  acids, the products yielded amorphous and only the anatase phase. The rutile phase was completely absent in these two cases. The sulphate and phosphate anions both have high negative charge,  $-2$  and  $-3$ , respectively. The attraction forces between the  $Ti^{4+}$  ion and  $SO_4^{2-}$  or  $PO_4^{3-}$  are strong so these anions will be bonded to Ti basic unit easily (the strong attraction is evidenced in the EDX spectra with the characteristic peaks of S and P and FT-IR spectra with the characteristic vibration of the sulphate and phosphate groups on  $TiO_2$ ). Since both  $SO_4^{2-}$  and  $PO_4^{3-}$  have tetrahedral geometry with the negative ends at the oxygen atoms where they can bond to Ti octahedra in three ways as shown in Fig. 6. Among the three modes of bonding, the bidentate and tridentate, Fig. 6B and C, respectively, are favored due to the

well-known *chelate effect*. The bonding of  $SO_4^{2-}$  in these multidentate modes occupy one full face of octahedra and inhibit the growing of chain along the opposite edges as illustrated in Fig. 7 and hence inhibit the formation of rutile. The same argument can be applied to  $PO_4^{3-}$  as well. Therefore, the addition of these two acids yielded only the anatase form, in the mixture with the amorphous form, as shown in Table 2. Our results here are in agreement with other reports that the presence of  $SO_4^{2-}$  ion helped to promote the formation of anatase phase [8,18,44].

### 3.3. Decolorization of dyes by the synthesized $TiO_2$ powders

Decolorizations of MB, CV, and CR were studied in the presence of  $TiO_2$  powders in the form of suspension by irradiation with UV light. The percentages of decolorization on irradiation for 3 h of the aqueous solution of the three dyes are shown in Figs. 8–10, respectively. It can be seen from the figures that all the synthesized  $TiO_2$  powders and two commercial  $TiO_2$ : Degussa P25 and anatase (Carlo Erba) decolorized the dye solutions upon irradiation with UV light. The commercial  $TiO_2$  in

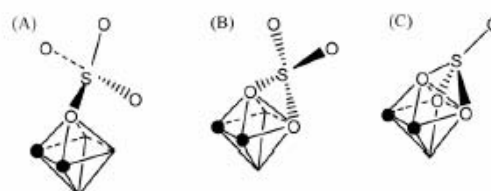


Fig. 6. Bonding mode of  $SO_4^{2-}$  anion as (A) monodentate, (B) bidentate, and (C) tridentate ligand (● indicates OH position).

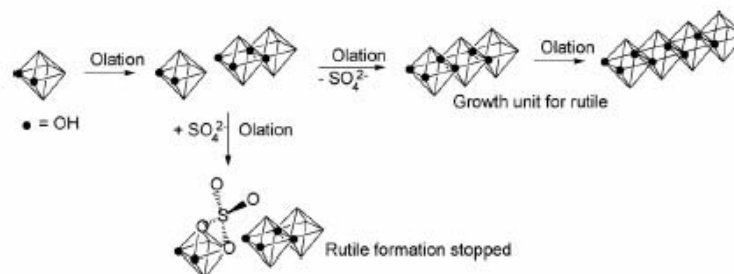


Fig. 7. Possible pathway to inhibit the formation of rutile by  $\text{SO}_4^{2-}$ .

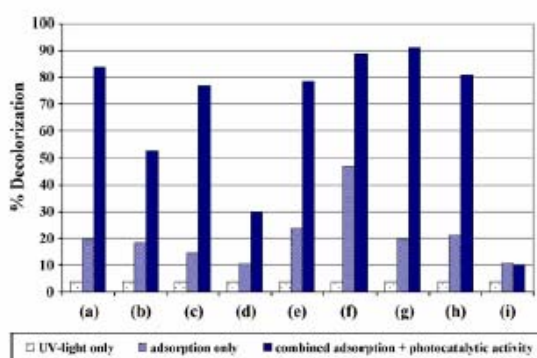


Fig. 8. Decolorization of MB solution ( $2.5 \times 10^{-5}$  M) with (a) Ti-no acid, (b) Ti-HCl, (c) Ti-HNO<sub>3</sub>, (d) Ti-H<sub>2</sub>SO<sub>4</sub>, (e) Ti-CH<sub>3</sub>COOH, (f) Ti-H<sub>3</sub>PO<sub>4</sub>, (g) Degussa P25, (h) anatase (Carlo Erba), and (i) rutile (R706).

rutile phase (R706) had no effect on the dye solutions. (The rutile result is shown merely for the completeness of the systematic studies and need no further discussions.) Moreover, either TiO<sub>2</sub> or UV light had very little effect when each was used separately. These experiments demonstrated that both UV light and the photocatalyst, such as the commercial or the synthesized TiO<sub>2</sub>, were needed for the effective decolorization of dyes. This is, of course, due to the well-known photocatalytic activity that prevails in

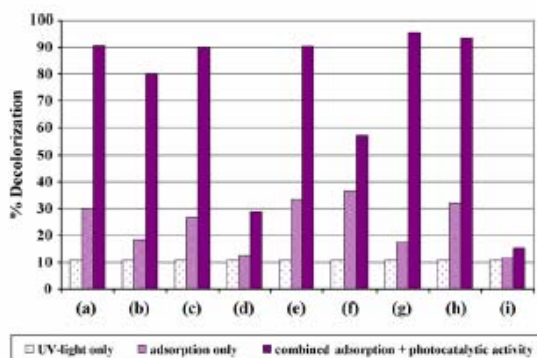


Fig. 9. Decolorization of CV solution ( $2.5 \times 10^{-5}$  M) with (a) Ti-no acid, (b) Ti-HCl, (c) Ti-HNO<sub>3</sub>, (d) Ti-H<sub>2</sub>SO<sub>4</sub>, (e) Ti-CH<sub>3</sub>COOH, (f) Ti-H<sub>3</sub>PO<sub>4</sub>, (g) Degussa P25, (h) anatase (Carlo Erba), and (i) rutile (R706).

many metal oxide semiconductors, especially with TiO<sub>2</sub>. The pathway of dye degradation composed of several chemical steps and has been well documented [45].

Overview of all the three figures (Figs. 8–10) shows that all the six synthesized TiO<sub>2</sub> powders do possess the photocatalytic property as seen by the higher % decolorization of the combined adsorption + photocatalytic activity as compared to the adsorption-only columns in the figures. Degussa P25 was used as a reference with which all the other commercial TiO<sub>2</sub> (anatase and rutile) and the synthesized TiO<sub>2</sub> samples were to be compared. The results in the figures show that P25 has the highest photocatalytic activity for these dyes. Some of the synthesized samples, notably Ti-no-acid and Ti-HNO<sub>3</sub>, constantly showed quite good activity for all the three dyes—only slightly less than P25. The rest of the samples showed some inconsistency performance against these dyes, i.e. good performance with one dye but mediocre with another dye. There seem to be no relation between the bandgap energy and photocatalytic property of all the TiO<sub>2</sub> samples under study here.

In many reports P25 and anatase usually show similar activities with P25 is always slightly better. However, with the three dyes under study in this work we can see the difference between P25 and anatase in both photocatalytic property and surface adsorption. The commercial anatase showed good photocatalytic activity for MB and CV but only mediocre with CR while P25 showed the best photocatalytic activity for all three dyes. For

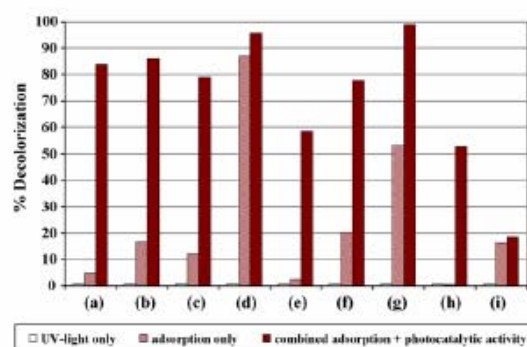
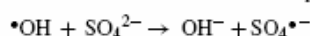


Fig. 10. Decolorization of CR solution ( $2.5 \times 10^{-5}$  M) with (a) Ti-no acid, (b) Ti-HCl, (c) Ti-HNO<sub>3</sub>, (d) Ti-H<sub>2</sub>SO<sub>4</sub>, (e) Ti-CH<sub>3</sub>COOH, (f) Ti-H<sub>3</sub>PO<sub>4</sub>, (g) Degussa P25, (h) anatase (Carlo Erba), and (i) rutile (R706).



the surface adsorption, P25 exhibited low adsorption ability for MB and CV but for CR the adsorption dramatically increased. The anatase also showed low adsorption ability, slightly higher than P25, for MB and CV but, unlike P25, the adsorption became extremely low for CR. The adsorption behavior as observed here could be the result from different surface charges between P25 and anatase. Considering the nature of charge on the dye molecules, MB and CV have positive charge while CR has negative charge on the parent molecular fragment. The surface charge on TiO<sub>2</sub> bulk is normally on the negative side. In this case, if we compare P25 with anatase based on the adsorption of the three dyes, we are led to the conclusion that the surface charge of P25 should be less negative than that of anatase. For the six synthesized samples, Ti-no-acid, Ti-HCl, Ti-HNO<sub>3</sub>, Ti-CH<sub>3</sub>COOH, and Ti-H<sub>3</sub>PO<sub>4</sub> showed the same type of adsorption behavior as anatase while Ti-H<sub>2</sub>SO<sub>4</sub> was similar to P25. The surface charge of the former group tends to be more negative, hence, they adsorbed stronger with MB and CV and vice versa for the latter group. It is noteworthy to mention the rather inert to change for adsorption on the rutile which probably reflects its low surface charge.

The presence of sulphate and phosphate anions in the system was found to retard the photocatalytic activity [27,46]. Taken sulphate as an example, when added, the sulphate anion was immediately adsorbed on the TiO<sub>2</sub> surface and was attacked by the •OH radical to become the sulphate radical.



This •OH radical scavenging property of the sulphate anion would reduce the number of reactive •OH radical, therefore, lower the efficiency of the dye degradation process. The sulphate radical could also attack the dye molecules, too, but it is not as strong as the •OH radical. This rationale seems to be applicable to the data of Ti-H<sub>2</sub>SO<sub>4</sub> with MB and CV dyes where Ti-H<sub>2</sub>SO<sub>4</sub> showed low photocatalytic activity. The behavior of Ti-H<sub>2</sub>SO<sub>4</sub> with CR, at first, may seem unfit to this rationale. However, on a closer look at the high % decolorization of Ti-H<sub>2</sub>SO<sub>4</sub> in Fig. 10 it is, in fact, the combined adsorption and photocatalytic effects. Therefore, the difference between the adsorption-only and the combined adsorption + photocatalytic columns should correspond to the true photocatalytic resulting in a small value for photocatalytic effect as expected.

It is doubtful that the rationale for the sulphate anion could be applicable to the phosphate anion since the photocatalytic activity of Ti-H<sub>3</sub>PO<sub>4</sub> was not that low as in the Ti-H<sub>2</sub>SO<sub>4</sub> case. On the contrary, it was quite high, e.g. almost equal to P25 for MB dye, acceptable for CR dye, and only mediocre for CV dye. We feel that more work need to be done to elaborate this strange phenomenon.

#### 4. Conclusions

Six samples of TiO<sub>2</sub> of various amorphous-anatase–rutile contents were prepared by the acid-catalyzed sol–gel method without calcination. Several techniques were used to characterize these samples. Since the calcination was not employed during the preparation, these products mainly composed of an amor-

phous phase with small amount of either mixed anatase–rutile phases or solely anatase phase. The mechanism of crystal growth leading to anatase or rutile phase was proposed. The presence of SO<sub>4</sub><sup>2-</sup> and PO<sub>4</sub><sup>3-</sup> groups was found to inhibit the growth to rutile phase. All samples showed various degrees of photocatalytic activities from almost as good as P25 to mediocre ones. For those with good performances, we feel that they are an inexpensive alternative to the presently available commercial ones due to simple synthesis without the need for calcination.

#### Acknowledgements

Financial supports from the Thailand Research Fund through the Royal Golden Jubilee Ph.D. Program (Grant No. PHD/0126/2546), the Center for Innovation in Chemistry: Postgraduate Education and Research Program in Chemistry (PERCH-CIC), Commission on Higher Education, Ministry of Education, and the Graduate School, Prince of Songkla University are gratefully acknowledged. Sample of Degussa P25 used throughout this work was donated by Degussa AG, Frankfurt, Germany, through its agency in Bangkok, Thailand.

#### References

- [1] A. Fujishima, K. Honda, *Nature* 238 (1972) 37.
- [2] M.R. Hoffman, S.T. Martin, W. Choi, D.W. Bahnemann, *Chem. Rev.* 95 (1995) 69.
- [3] M.A. Fox, M.T. Dulay, *Chem. Rev.* 93 (1993) 341.
- [4] R. Zhang, L. Gao, *Mater. Res. Bull.* 36 (2001) 1957.
- [5] X.-Z. Ding, X.-H. Liu, *Mater. Sci. Eng. A* 224 (1997) 210.
- [6] M. Gopal, W.J.M. Chan, L.C. De Jonghe, *J. Mater. Sci.* 32 (1997) 6001.
- [7] Z.C. Wang, J.F. Chen, X.F. Hu, *Mater. Lett.* 43 (2000) 87.
- [8] Q.-H. Zhang, L. Gao, J.-K. Guo, *Nanostruct. Mater.* 11 (1999) 1293.
- [9] B. Ohtani, Y. Ogawa, S.-I. Nishimoto, *J. Phys. Chem. B* 101 (1997) 3746.
- [10] K.M. Reddy, C.V.G. Reddy, S.V. Manorama, *J. Solid State Chem.* 158 (2001) 180.
- [11] C. Random, S. Wongnawa, P. Boonsin, *ScienceAsia* 30 (2004) 149.
- [12] K.I. Hadjiivanov, D.G. Klissurski, *Chem. Soc. Rev.* (1996) 61.
- [13] S.-J. Kim, S.-D. Park, Y.H. Jeong, *J. Am. Ceram. Soc.* 82 (1999) 927.
- [14] J.-P. Jalava, L. Heikkilä, D. Houi, R. Laiho, E. Hiltunen, A. Hakanen, H. Härma, *Ind. Eng. Chem. Res.* 37 (1998) 1317.
- [15] S.S. Watson, D. Beydoun, J.A. Scott, R. Amal, *Chem. Eng. J.* 95 (2003) 213.
- [16] C. Suresh, V. Biju, P. Mukundan, K.G.K. Warriar, *Polyhedron* 17 (1998) 3131.
- [17] Z. Baolong, C. Baishun, S. Keyu, H. Shangjin, L. Xiadong, D. Zongjie, Y. Kelian, *Appl. Catal. B* 40 (2003) 253.
- [18] S.K. Samantary, P. Mohapatra, K. Parida, *J. Mol. Catal. A: Chem.* 198 (2003) 277.
- [19] A. Zaban, S.T. Aruna, S. Tirosh, B.A. Gregg, Y. Mastai, *J. Phys. Chem. B* 104 (2000) 4130.
- [20] S. Yamazaki, N. Fujinaga, K. Araki, *Appl. Catal. A* 210 (2001) 97.
- [21] B. Zielinska, J. Grzechulska, B. Grzmil, A.W. Morawski, *Appl. Catal. B* 35 (2001) L1.
- [22] G. Sivalingam, K. Nagaveni, M.S. Hegde, G. Madras, *Appl. Catal. B* 45 (2003) 23.
- [23] G.A. Epling, C. Lin, *Chemosphere* 46 (2002) 561.
- [24] C. Hachem, F. Bocquillon, O. Zahraa, M. Bouchy, *Dyes Pigment* 49 (2001) 117.
- [25] A. Sclafani, L. Palmisano, M. Schiavello, *J. Phys. Chem.* 94 (1990) 829.
- [26] M. Styliadi, D.I. Kondarides, S.E. Verykios, *Appl. Catal. B* 47 (2004) 189.

- [27] B. Neppolian, H.C. Choi, S. Sakthivel, B. Arabindoo, V. Murugesan, *Chemosphere* 46 (2002) 1173.
- [28] M.J. Velasco, F. Rubio, J. Rubio, J.L. Oteo, *Thermochim. Acta* 326 (1999) 91.
- [29] K.M.S. Khalil, M.I. Zaki, *Powder Technol.* 92 (1997) 233.
- [30] H.-J. Youn, P.S. Ha, H.S. Jung, K.S. Hong, Y.H. Park, K.H. Ko, *J. Colloid Interface Sci.* 211 (1999) 321.
- [31] K. Nakamoto, *Infrared and Raman Spectra of Inorganic and Coordination Compounds*, 4th ed., Wiley, New York, 1986.
- [32] B. Bazán, J.L. Mesa, J.L. Pizarro, M.I. Arriortua, T. Riojo, *Mater. Res. Bull.* 38 (2003) 1193.
- [33] R. Gómez, T. López, E. Ortiz-Islas, J. Navarrete, E. Sánchez, F. Tzompantzi, X. Bokhimi, *J. Mol. Catal. A: Chem.* 193 (2003) 217.
- [34] Q. Zhang, L. Gao, J. Guo, *J. Eur. Ceram. Soc.* 20 (2000) 2153.
- [35] J. Yu, J.C. Yu, M.K.-P. Leung, W. Ho, B. Cheng, X. Zhao, J. Zhao, *J. Catal.* 217 (2003) 69.
- [36] L. Miao, P. Jin, K. Kaneko, A. Terai, N. Nabatova-Gabain, S. Tanemura, *Appl. Surf. Sci.* 212/213 (2003) 255.
- [37] B. Zielińska, J. Grzechulska, B. Grzmił, A.W. Morawski, *Appl. Catal. B* 45 (2003) 293.
- [38] S.R. Kumar, C. Suresh, A.K. Vasudevan, N.R. Suja, P. Mukundan, *Mater. Lett.* 38 (1999) 161.
- [39] Z. Yanqing, S. Erwei, C. Zhizhan, L. Wenjun, H. Xingfang, *J. Mater. Chem.* 11 (2001) 1547.
- [40] P. Comba, A. Merbach, *Inorg. Chem.* 26 (1987) 1315.
- [41] F.A. Cotton, G. Wilkinson, *Advanced Inorganic Chemistry*, 5th ed., John Wiley & Sons, Inc., New York, 1988, p. 656.
- [42] J.R. Bartlett, J.L. Woolfrey, in: L.L. Hence, J.K. West (Eds.), *Chemical Processing of Advanced Materials*, John Wiley, New York, 1992, p. 247.
- [43] O.J. Wang, S.C. Moss, M.L. Shalz, A.M. Glaeser, H.W. Zandbergen, P. Zschack, in: P. Jena, S.N. Khanna, B.K. Rao (Eds.), *Physics and Chemistry of Finite Systems: From Clusters to Crystals*, vol. II, Kluwer Academic Publishers, Boston, 1992, p. 1287.
- [44] H. Xie, Q. Zhang, T. Xi, J. Wang, Y. Liu, *Thermochim. Acta* 381 (2002) 45.
- [45] A. Houas, H. Lachheb, M. Ksibi, E. Elaloui, C. Guillard, J.-M. Hermann, *Appl. Catal. B* 31 (2001) 145 (and references cited therein).
- [46] M. Abdullah, G.K.-C. Low, R.W. Matthews, *J. Phys. Chem.* 94 (1990) 6820.

## VITAE

**Name** Miss Miki Kanna

**Student ID** 4623015

### Education Attainment

Degree	Name of Institution	Year of Graduation
B. Sc. (Chemistry)	Prince of Songkla University	1999
M.Sc. (Inorganic Chemistry)	Prince of Songkla University	2002

### Scholarship Awards during Enrolment

1. Thailand Research Fund through the Royal Golden Jubilee Ph.D. Program Grant No. PHD/0126/2546
2. Center for Innovation in Chemistry: Postgraduate Education and Research Program in Chemistry (PERCH-CIC), Commission on Higher Education, Ministry of Education

### List of Publication and Proceeding

#### Publications

1. Kanna, M., Wongnawa, S., Sherdshoopongse, P. and Boonsin, P. 2005. Adsorption Behavior of Some Metal Ions on Hydrated Amorphous Titanium Dioxide Surface. *Songklanakarin, J. Sci. Technol.* 27(5): 1017-1026.
2. Hollingsworth, N., Kanna, M., Kociok-Köhn, G., Molloy, K. C. and Wongnawa, S. 2008. Synthesis and Characterisation of New Titanium Amino-Alkoxides: Precursors for the Formation of TiO<sub>2</sub> Materials. *Dalton Transactions.* 631-641.
3. Kanna, M. and Wongnawa, S. 2008. Mixed Amorphous and Nanocrystalline TiO<sub>2</sub> Powders Prepared by Sol-Gel Method: Characterization and Photocatalytic Study. *Materials Chemistry and Physics.* 110: 166-175.

## Proceedings

1. Kanna, M., Wongnawa, S., Sherdshoopongse, and Boonsin, P. 2002. The Adsorption of Metal Ions on Titanium Dioxide Surface. The 1<sup>st</sup> PERCH Annual Scientific Conference. Garden Sea View Resort, Pattaya Chonburi, May 12-15, 2002. pp.124 (Oral presentation)
2. Kanna, M., Wongnawa, S., Sirichote, O., Pakawatchai, C. and Boonsin, P. 2005. Nanoparticle Titanium Dioxide Synthesis via a Sol-Gel Method. The 3<sup>rd</sup> PSU Symposium on Graduated Research. Prince of Songkla University, March 11, 2005. pp.90 (Oral presentation)
3. Kanna, M., Wongnawa, S., Sirichote, O., Pakawatchai, C. and Boonsin, P. 2005. Preparation of Nanoparticle TiO<sub>2</sub> at Temperature below 100°C. The 4<sup>th</sup> PERCH Annual Scientific Conference PERCH Congress IV. Jomthein Plam Beach Resort, Pattaya Chonburi, May 8-11, 2005. pp.92 (Oral presentation)
4. Kanna, M., Wongnawa, S., Sherdshoopongse, and Boonsin, P. 2002. Study of the Adsorption Behavior of Metal Ions on Titanium Dioxide. The 28<sup>th</sup> Congress on Science and Technology of Thailand. Queen Sirikit National Convention Center, Bangkok, October 24-26, 2002. pp. 97 (Poster presentation)
5. Kanna, M., Wongnawa, S., Sirichote, O., Pakawatchai, C. and Boonsin, P. 2004. Preparation of Nanosized Titanium dioxide at Temperature below 100°C. The 30<sup>th</sup> Congress on Science and Technology of Thailand. Impact Exhibition and Convention Center, Muang Thong Thani, Bangkok, October 19-21, 2004. pp.84 (Poster presentation)

6. Kanna, M., Wongnawa, S., Sirichote, O., Pakawatchai, C. and Boonsin, P. 2005. Nanosized Titanium Dioxide Powder Prepared by Sol-Gel Method. RGJ - Ph.D. Congress VI. Jomthein Plam Beach Resort, Pattaya Chonburi, April 28-30, 2005. pp.218 (Poster presentation)
7. Kanna, M., Wongnawa, S., Sirichote, O., Pakawatchai, C. and Boonsin, P. 2005. Photocatalytic Degradation of Methylene Blue Using Nanocrystalline  $\text{TiO}_2$  Prepared by Sol-Gel Method. The 31<sup>th</sup> Congress on Science and Technology of Thailand. Technopolic, Suranaree University of Technology, Nakhon Ratchasima, October 18-20, 2005. pp.131 (Poster presentation)
8. Kanna, M., Wongnawa, S., Sirichote, O., Pakawatchai, C. and Boonsin, P. 2006. Decolourization of Crystal Violet (CV) using Nanocrystalline  $\text{TiO}_2$  Prepared by Sol-Gel Method. The 1<sup>st</sup> Penang International Conferance for Young Chemists. Universiti Sains Malaysia, Pulau Pinang, Malaysia, May 24-27, 2006. pp.189 (Poster presentation)
9. Kanna, M., Wongnawa, S., Sirichote, O., Pakawatchai, C. and Boonsin, P. 2007. Comparison between the Decolourization of Three Dyes (MB, CV, and CR) by Commercial and Hydrated Amorphous  $\text{TiO}_2$ . PERCH-CIC CONGRESS V Theme; Chemistry for Innovation. Jomthein Plam Beach Resort, Pattaya Chonburi, May 6-9, 2007. pp.250 (Poster presentation)